Developing generic and modular approaches to targeted cancer cell therapeutics

Submitted to Cardiff University for the degree of Doctor of Philosophy by:

Emily Margaret Mills

Supervisory team:

Dr Yu-Hsuan Tsai and Prof Arwyn Tomos Jones

For Mum and Dad,
Lots of love,
Favourite Child x

Abstract

The intricacies and complexities of cancer render it a difficult disease to treat, and existing treatments are frequently non-selective. This project investigated two selective cancer therapeutic approaches: organelle-targeted drug delivery, and genetic re-wiring to achieve a switchable CAR-T model.

Cancer mitochondria are different to healthy cells, including a higher mitochondrial membrane potential (MMP) which can be exploited for selective delivery of a therapeutic. Cyanine dyes Cy3 and Cy5, along with a dimer Cy3-Cy5 and a CPP conjugate Cy3-Cy5-R8 were characterised, and all constructs stained the mitochondria of HeLa in an MMP-dependent manner. Staining capacities of Cy3, Cy5 and Cy3-Cy5 were not hindered by serum proteins or endocytosis inhibition. Conversely, serum proteins reduced Cy3-Cy5-R8 staining capacities, and its uptake was endocytosis-dependent. Cy3 was subsequently tested as a mitochondrial-drug delivery vehicle, and Cy3 conjugation to mitochondrial toxins improved EC_{50} values by up to 1000-fold. The Cy3-drug conjugates were more toxic to cancerous (HeLa) vs non-cancerous cells (HEK293), but toxicity was still present in HEK293. Further studies are therefore needed to enhance Cy3-drug selectivity to cancer cells.

Cancers can alternatively be targeted via CAR-T cell immunotherapy; however, CAR-T frequently over-activate and bring unwanted toxicity to the patient. Through genetic code expansion, a new logic gates approach was developed. 11 quadruplet-decoding pyrrolysyl tRNA variants that incorporate BocK were analysed. Unlike their literature representation in *E. coli*, only five variants were functional in HEK293. Increasing tRNA copy number from 1 to 4 improved BocK-incorporation, and PylRS/tRNA was found to function orthogonally alongside a mutant TyrRS/tRNA pair. A split GFP reporter system was subsequently developed, where AND and OR logic operations were successfully generated whereby GFP output can be controlled via the unnatural amino acid makeup of the cellular media. The cell circuits developed here provide a new approach to mammalian cell logic operations, and can potentially be translated into a switchable ON/OFF CAR-T model.

Acknowledgements

Firstly, I would like to thank my supervisor Dr Yu-Hsuan Tsai for his continuous encouragement, support and guidance throughout this project; the experience has been invaluable, and I will forever remain grateful for the opportunity to do a PhD within his research group. Additionally, I would like to extend my thanks to my co-supervisor Professor Arwyn Tomos Jones for continually sharing his knowledge and unparalleled kindness with me throughout the project, while allowing me access to his lab facilities and confocal microscope to perform my studies. Importantly, these thanks are also shared with Dr Edward Sayers, Dr Alexander Nodling and Mr Sanjay Patel for their endless time, patience, assistance and guidance. Importantly, this project would not have existed without the financial support of KESS2 (Knowledge Economy Skills Scholarships), Tenovus Cancer Care and Cardiff University.

Completing this mammoth project would not have been the same without the help and company of my peers; I need to express my sincere gratitude and admiration for each and every past-and-present member of the Luk/Tsai/Jin group. To my co-workers and dear friends Luke (Slukas), Patrick (Patricia) and Simon (Semon), I would like to congratulate you on putting up with me and my terrible nicknames for the entirety of your PhDs! You three have truly made this an unforgettable experience and I can't wait to see where the next chapter takes you. A massive thank you to my dearest friend Slukas however, who effortlessly puts a smile on my face every single day; be it by providing me with coffee and a bacon roll, or being pooped on by birds. Your love, support and friendship is invaluable, and I am infinitely grateful that our paths were fortunate enough to cross.

Lastly, I would like to thank my family and friends. To my best friends Manfy, Ash, Emma, Charl and Coryn, my brothers Alex and James, and my sister-in-law Emma, all your encouragement and support throughout this experience has kept me sane. To my parents Momma and Papa Mills, thank you for holding my hand when times were tough. You are undoubtedly the greatest people in the entire world and I love you more than words could ever convey.

Table of Contents

List of Publications

[1] S. Patel, E. Sayers, L. He, R. Narayan, T. Williams, E. Mills, R. Allemann, L. Luk, A. Jones and Y. Tsai, 2019. Cell-penetrating peptide sequence and modification dependent uptake and subcellular distribution of green florescent protein in different cell lines. *Sci. Rep.*, **9**, DOI: 10.1038/s41598-019-42456-8.

[2] E. Mills, V. Barlow, L. Luk and Y. Tsai, 2019. Applying switchable Cas9 variants to in vivo gene editing for therapeutic applications. *Cell Biol. and Toxicol.*, **36**, 17-29.

[3] A. Nödling, E. Mills, X. Li, D. Cardella, E. Sayers, S. Wu, A. Jones, L. Luk and Y. Tsai, 2020. Cyanine dye mediated mitochondrial targeting enhances the anti-cancer activity of small-molecule cargoes. *Chem. Comm.*, **56**, 4672-4675.

[4] E. Mills, V. Barlow, A. Jones and Y. Tsai, 2021. Development of mammalian cell logic gates controlled by unnatural amino acids. *Cell Rep. Methods*, **in press**, DOI: 10.1016/j.crmeth.2021.100073.

Publications [1] and [2] were used to gain wider context in their respective fields, and contributed to the writing of **Chapter 1**. The data presented in **Chapter 2** is based on the published manuscript [3], with wider context of CPPs obtained from [1]. **Chapter 3** is based on the work presented in [4], and this manuscript is currently in press. All datasets and experimental procedures detailed in this thesis were conducted-by and produced the candidate.

List of Figures

List of Tables

List of Abbreviations

AA	Amino acid	**Cip**	Ciprofloxacin
aaRS	Amino-acyl tRNA synthetase	**DMEM**	Dulbecco's modified Eagle medium
ATCC	American Type Culture Collection	**DNA**	Deoxyribonucleic acid
ATP	Adenosine triphosphate	**DMSO**	Dimethyl sulfoxide
Az	Azido	**dNTP**	Deoxy-ribonucleotide triphosphate
AzF	Azido-phenylalanine	***Ec***	*Escherichia coli*
Boc	Butyloxycarbonyl	**EC_{50}**	Half maximal effective concentration
BocK	Nε-Boc-L-lysine	**EDTA**	Ethylene-diamine-tetra-acetic acid
bp	Base pair	**e.g.**	*Exempli gratia*; for example
BSA	Bovine serum albumin	**eGFP**	Enhanced green fluorescent protein
CPP	Cell-penetrating peptide	**Em**	Emission
CPT	Carboplatin	**Ex**	Excitation
CAR	Chimeric antigen receptor	**ε**	Extinction coefficient
CAR-T	Chimeric antigen receptor T-cell	**FBS**	Foetal bovine serum
CCCP	Carbonyl cyanide m-chlorophenyl hydrazine	**FDA**	Food and drug administration
Fig	Figure	**N°**	Number

FL	Fluorescence	**NA**	Numerical aperture
FRET	Förster resonance energy transfer	**NT**	Not tested
GFP	Green fluorescent protein	**OD**	Optical density
HEK	Human embryonic kidney cells	**OMeY**	3-methoxy-tyrosine
HeLa	Henrietta Lacks cells; human ovarian cancer	**PAGE**	Polyacrylamide gel electrophoresis
KLA	$(KLAKLAK)_2$; toxic peptide	**PBS**	Phosphate-buffered saline
kbp	Kilo-base pair	**PBST**	Phosphate-buffered saline with Tween 20
kDa	Kilo-Dalton	**PCR**	Polymerase chain reaction
l	Path length	**PylRS**	Pyrrolysyl tRNA synthetase
LB	Luria-Bertani	**R8**	Octo-arginine
LDS	Lithium dodecyl sulfate	**RNA**	Ribonucleic acid
LeuRS	Leucyl tRNA synthetase	**RNase**	Ribonuclease
Mito-DNA	Mitochondrial DNA	**RPM**	Revolutions per minute
Mm	*Methanosarcina mazei*	**RPMI**	Rosewell Park Memorial Institute
MMP	Mitochondrial membrane potential	**RT**	Room temperature
mRNA	Messenger RNA	**SDS**	Sodium dodecyl sulphate
N	Number of replicas	**sGFP**	Split green fluorescent protein

sGFP(1-10)	sGFP fragment “1-10”	**TrpRS**	Tryptophyl tRNA synthetase
sGFP(11)	sGFP fragment “11”	**TyrRS**	Tyrosyl tRNA synthetase
siRNA	Small interfering RNA	**UAA**	Unnatural amino acid
stDev	Standard deviation	**v/v**	Volume to volume ratio
TAE	Tris-acetate EDTA	**w/v**	Weight to volume ratio
TAP	Tobacco acid pyrophosphatase	**WT**	Wildtype

CHAPTER 1: Introduction

1.1 Background

To comprehend the fundamental differences between a cancer cell and a healthy cell, it is essential to understand the basics of cellular communication and replication, as disruption of these machineries is responsible for cancer cell generation.[1-3] Cell division contributes to repair, growth and reproduction.[2] During the growth or repair of tissues, cells increase in size as they mature. As a cell grows larger however, its ability to cope with internal metabolic processes is compromised due to a finite limit of intracellular resources.[2] In light of this, when a critical volume threshold is reached, most cells undergo a process of cell division called mitosis. This division process not only enables cells to cope with metabolic needs,[4] it additionally increases the overall surface area of the tissues which improves the efficiency of gas exchange, waste removal, and receipt of extracellular signalling communications.[2, 4]

1.1.1 The cell cycle

There are two types of cell division that occur in the human body. These processes are called mitosis and meiosis. Mitosis is a process that results in two daughter cells that are genetically identical to each other and the original parent cell, and is the form of cell division responsible for tissue growth and repair. On the other hand, meiosis occurs for the purpose of reproduction, in which a germ cell is divided into four genetically unique gametes.[5] The cycle of the cell is integral to sustaining life, and for complex multi-cellular eukaryotes, the phases of the cell cycle enable the generation of vital tissues, organs, and limbs.[6-8] A cell preparing to divide first proceeds through the interphase stage, which is split into 3 distinct phases; G_1 (duplication of cell contents except DNA), S (duplication of DNA), and G_2 (increase in cell size and preparation for cell division).[2-7, 9] Once these stages have been passed at their respective checkpoints, a cell can then move into its designated form of cell division. G_1 is the first growth phase and often the longest,[2, 6] and it is during this stage that a cell can enter G_0 where it becomes dormant or

senescent.[2, 3] A cell typically enters G_0 when it reaches its Hayflick limit, or alternatively when there is no requirement for growth or repair.[4, 9, 10] Notably however, these dormant cells can be reactivated and re-enter G_1 phase upon the receipt of certain growth factors and signals.[4, 6, 7] When a cell has passed through the G_2 checkpoint, it enters the M phase of the cell cycle. For mitotic division, during M phase, cytokinesis occurs which divides the cell contents to opposite poles of the cytoplasm, and a contractile ring cleaves the cell centrally to generate two genetically identical daughter cells (**Figure 1.1**).[2, 3, 7, 8]

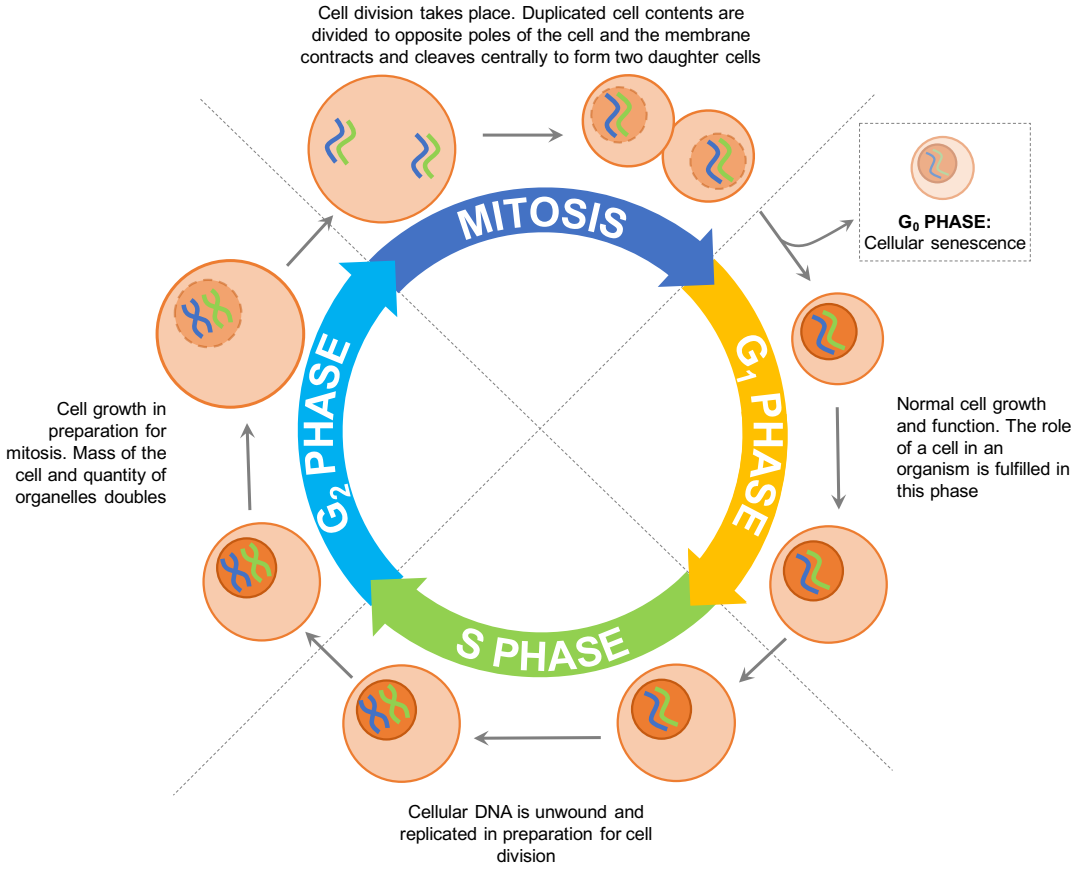

Figure 1.1: The main stages of the cell cycle for the purpose of mitotic cell-division
Diagram to demonstrate the phases of the cell cycle leading to mitosis and what processes occur at each stage. G_1 phase is where a cell matures and performs its designated function in an organism, this is also where a cell enters G_0 phase (cellular senescence). S phase is the process of DNA replication. G_2 phase is the expansion of a cell to duplicate its volume. Mitosis takes place where a parent cell is divided into two genetically identical daughter cells.

Unlike healthy cells that divide in an incredibly controlled manner, cancer cells exhibit an extremely disrupted cell cycle.[11] These unregulated malfunctioning

processes are due to the constant procurement of mutations in the cancer cells genetic code; which alter protein expression, conformation, and function.[11] As a result, these changes modify the speed, activity, and regulation of the core intrinsic pathways designed to prohibit excessive and unrequired cell division, as well as hindering a cancer cells susceptibility to anti-growth signals and entry into G_0.[11] All these factors lead to the uncontrolled cell division which is exhibited in cancerous tumours, and this persistent proliferative activity is one of the main hallmarks of cancer.[12]

1.1.2 Hallmarks of cancer

Cancer, in short, is a disease of a person's self-tissue. Mutations that occur in the genetic information of the cells cause them to proliferate out of control, and ultimately lead to death if left untreated.[1, 3, 13] Although most see the term cancer as one type of disease, it actually is an umbrella term used to describe a group of diseases that all follow the same fundamental hallmarks.[14] The core distinction of cancer from a benign tumour is the ability of cancer cells to spread to other parts of the body, which is referred to as malignancy.[15] There are six core hallmarks that are used to describe any form of cancer (**Figure 1.2**). Coined by Douglas Hanahan and Robert Weinberg in 2000, the hallmarks are (1) evasion of cell death, (2) self-sufficient proliferative signalling, (3) evasion of growth-suppressing signals, (4) the ability to invade other tissues and metastasise, (5) established replicative immortality and (6) the ability to induce and sustain angiogenesis (growth of blood vessels).[12]

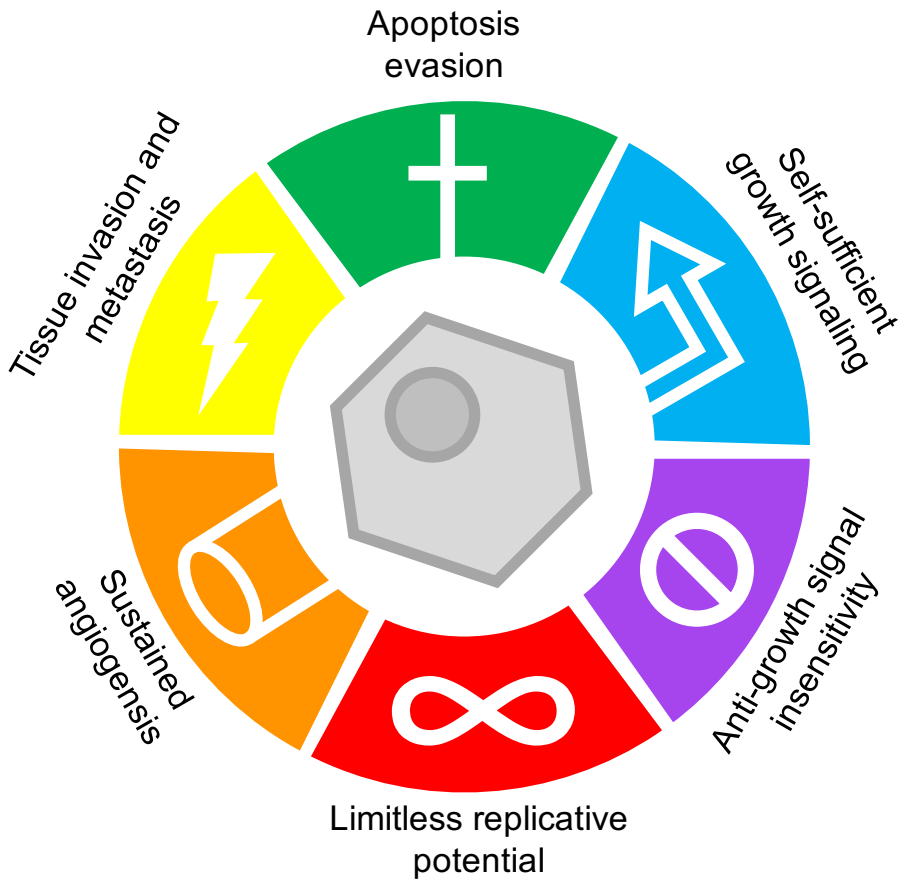

Figure 1.2: The six fundamental characteristics described as the hallmarks of cancer
The hallmarks of cancer are the core cellular characteristics that allow a tumour to persist and can be used to describe cancer cells of any tissue type.

Hallmark 1: Evasion of cell death

All cells have two fundamental programmes hardwired into them; a set of proliferative pathways (which play key roles during tissue growth and repair), and a set of programmed cell death pathways (termed as cellular suicide or apoptosis, amongst other terms).[16-19] Crucially, programmed cell death is a normal process of cellular function during growth, development, infection management, and tissue maintenance.[17, 20] Cancer cells however, through their continuous acquisition of random mutations, often obtain re-wired or malfunctioning apoptotic pathways, and in some instances the systems become completely inactive.[1, 3, 19] There are numerous gain-of-function or loss-of-function mutations that can occur in cancer cells which lead to the end result of death-evasion, however the most prominent is interruption of p53.[21-23] The core function of p53 is DNA surveillance. When damaged DNA is

detected by p53, it either arrests the cell cycle to allow the DNA to be repaired, or alternatively induces apoptosis through upregulation of the pro-apoptotic mitochondrial protein Bax.[19, 24] The purpose of this activity is to prevent incomplete or incorrect genetic material spreading through the tissues.[21-23] When it comes to cancer cells however, they exhibit major disruption apoptotic pathways and, most prominently, p53 activity. Mutations that result in a malfunctioning p53 are typically responsible for evasion of cell death, and uncontrolled proliferative activity.[21, 25] mutations in p53 are represented in approximately 50-60% of all cancers diagnosed globally,[21, 25] and in many cancers, p53 malfunction is unfavourable regarding long-term prognosis.[26-28]

Hallmark 2: Self-sufficient proliferative signalling

In contrast to evasion of cell death, cancer cells additionally exhibit self-proliferative activity. The ability of tissues to promote cell proliferation is critical for growth and development, and this is achieved through changes in the extracellular microenvironment such as upregulation of growth factors.[2-4, 6, 7, 9] However, cancer cells are understood to upregulate their proliferative signalling primarily through excessive growth factor production, and self-stimulation.[1, 3, 11, 29-31] A healthy cell cannot self-stimulate its proliferation, it relies on receiving signals from neighbouring cells. Cancer cells however have been shown to synthesise and release growth factors that bind their own receptors, therefore exhibiting self-proliferative signalling.[29, 30, 32] Additionally, many acquire mutations in their growth factor receptors and their downstream pathways. These mutations create hyper-responsive receptor pathways that carry a lower threshold for successful stimulation, which increases their susceptibility to proliferative signalling significantly.[12, 29, 30, 32]

Hallmark 3: evasion of growth-suppressing signals

Similar to the ability of cancer cells to self-proliferate and become hyper-sensitive to growth signals, they additionally become insensitive to anti-growth signals. Contrary to the mutations procured to enhance proliferative activity, the receptors responsible for receiving anti-growth signals are mutated to

become poorly-functional in cancer cells.[19, 32-34] Typically, they are mutated to an extreme where larger quantities of anti-growth factors are required to successfully stimulate an apoptotic pathway; levels mostly unobtainable within a tissue microenvironment.[17, 19, 21, 35] Secondly, they incur further mutations within the downstream signalling pathways responsible for growth suppression, enabling the cells to avoid destructive processes and continue to unrestrictedly proliferate.[19, 32-34]

Hallmark 4: The ability to invade other tissues and metastasise

When a cancerous tumour grows to a substantial size, a small number of cells in the tumour near blood vessels undergo a series of changes, such as a reduction of surface adhesion proteins which allows them to move freely within the cell mass.[36-38] These mobile cancer cells can then penetrate the blood vessels and travel through the vasculature to a new region where they develop into a new growth.[31, 33, 39] This process is called metastasis, and when metastasis has occurred, cancers are typically much harder to treat.[39, 40] Once in the vasculature, the metastasising cancer cells are vulnerable to patrolling immune cells in the blood, however reports have described metastatic cancer cells evoke various immune-evasion tactics to elude immune-mediated destruction during transport to a new site.[41, 42]

Hallmark 5: Established replicative immortality

During embryogenesis and peak developmental stages, an enzyme called telomerase is expressed to prevent telomere shortening during exponential growth. This prevents a cell from reaching the Hayflick limit during these critical growth stages.[10, 43-45] Normally, in later developmental phases this enzyme is deactivated and no longer expressed; meaning telomeres then function normally to control the replicative lifespan of a health cell. However, approximately 90% of cancer cells commonly incur mutations in this pathway, which ultimately leads to abnormal re-initiation of telomerase expression, production and activation.[46, 47] This is detrimental to the health of the surrounding tissues as the enzyme provides the cancer cells with a limitless

replicative capacity. This leads to an immortal cell-mass and, subsequently, an indefinitely replicating tumour; draining the surrounding healthy tissues of space, nutrients and oxygen. Moreover, cancer cells also sustain the cell cycle by avoiding entrance into the senescent G_0; rendering the cessation of tumour growth unobtainable through natural cellular signalling in the tissue.[1, 3, 11]

Hallmark 6: The ability to induce and sustain angiogenesis

Angiogenesis refers to the process of new blood vessel formation.[36-38] This is an event that naturally occurs throughout our lifespan such as during development, wound healing, and physical changes including puberty and pregnancy.[48] The presence of blood vessels is paramount to the supply of oxygen and nutrients to the tissues, whilst also removing waste and toxic substances such as carbon dioxide. To enable a cell to continuously divide, a constant supply of oxygen and nutrients is crucial to provide the required energy resources.[2, 4] In the case of cancerous tumours, the uncontrolled rapid cellular proliferation described previously causes tissues to become cramped and hypoxic. Without an ample supply of oxygen and nutrients, the cells and tissues would become necrotic. To alleviate this, cancer cells promote the angiogenesis process. They stimulate nearby blood vessels to expand and grow new branches that intertwine through the tumour, enabling cells to receive the nutrients they require for replication and survival.[36, 37, 48] Fascinatingly, within every cancer tumour, residential healthy cells from the original tissue remain. These cells naturally produce angiogenesis-suppressor factors unless new vasculature is required such as for tissue-repair or healing. As these suppressor molecules prevent new vasculature formation through the tumour, malignant cells additionally influence these resident cells through extracellular signalling. The signalling from tumour cells consequently inhibits the production and release of suppressor factors by healthy cells, enhancing vasculature growth through the tumour and thus adequate levels of resources are supplied to the cancer cells.[32, 36-38]

Due to the clear complexities in how a cancer cell functions, it is a notoriously difficult disease to treat. The disease has a major impact on the health and finances of the global population, with an estimated 1 in 2 people having a cancer diagnosis in their lifetime, and treatment often being extensive and costly.[49]

1.1.3 Cancer and global health

Unlike other diseases that have emerged and vanished from the human population over the course of our 7-million-year existence, cancer is a disease that has run side-by-side with us throughout the megaannums of our species. The earliest malignant tumour detected was in a turtle bone fossil dated to approximately 250 million years ago in the Jurassic period.[50] It is without question that as long as there have been complex multi-cellular organisms, there have been cancers. In 2020 alone nearly 20 million new cancer diagnoses were made and, globally, cancer accounts for an average of 10 million deaths per year; a number continuing to rise with increasing life expectancies. With the cost of medical treatments for all cancer patients surmounting to over £555 billion worldwide, cancer forms an economic burden of over £7 billion annually to the United Kingdom alone.[51, 52]

As seen in **Figure 1.3**, the most common form of cancer in the female population is breast and cervical, while for males it is predominantly cancers of the prostate and lung. There are clear geographical trends regarding the predominant form of cancer for each country; this is largely influenced by population genetics, lifestyle, and environmental influences.[49] For example, the countries that have the most diagnoses of lung cancer are typically those that have the highest percentage of smokers in their population, such as Russia, Indonesia, and Eastern European countries. Additionally, forms of breast and lung cancer account for a quarter of all cancers diagnosed globally.[49]

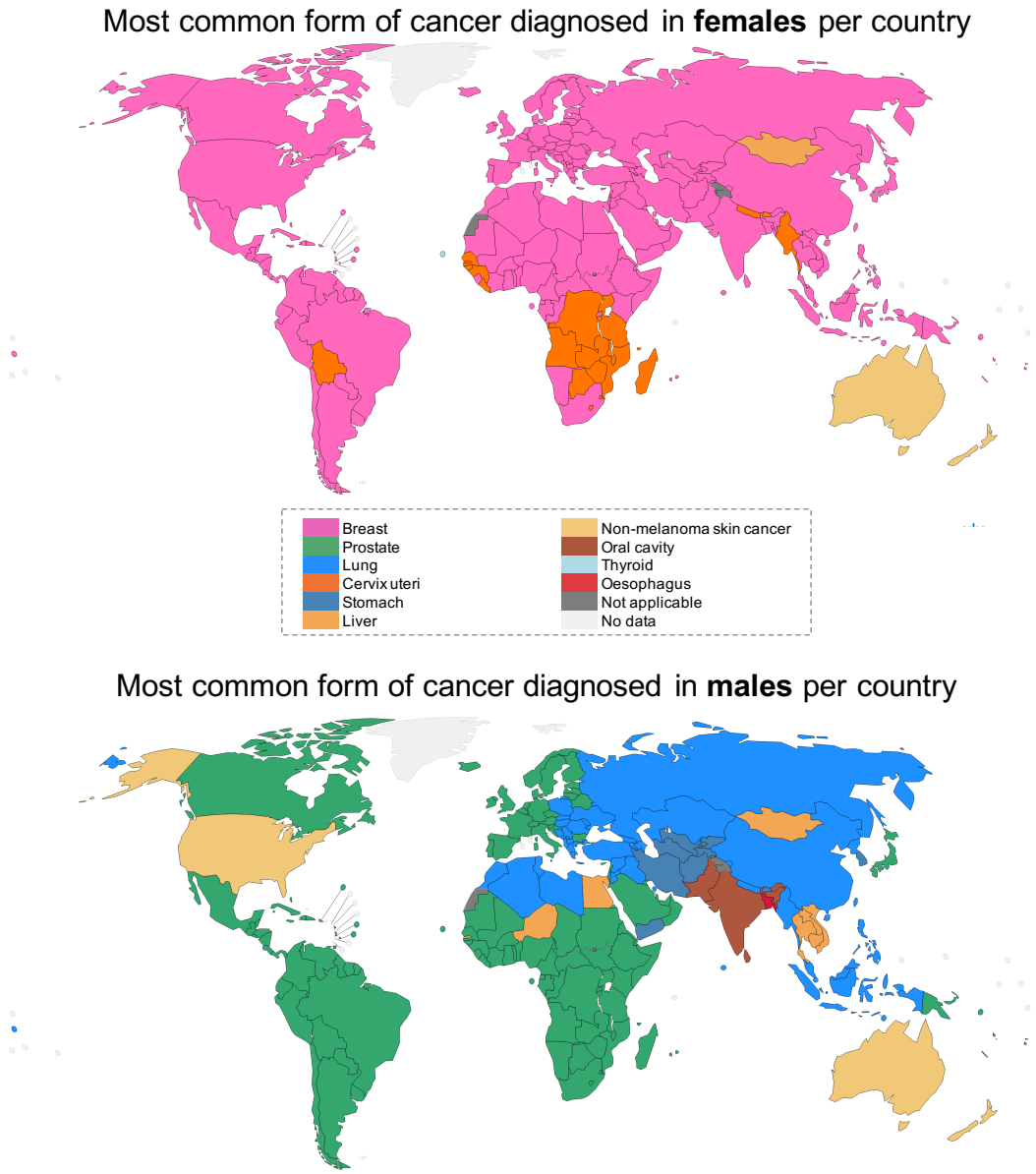

Figure 1.3: Most common cancer diagnoses in males or females per country in 2020
Breakdown of global incidence of cancers diagnosed in 2020. Countries are colour coded to show the most common forms of cancer diagnosed separated by gender. (Chart data generated by the World Health Organisation).

Given the large economic cost of cancer to the global economy, there is demand for cures and new treatments to manage this catastrophic disease. However, the complexities of cancers and their propensity to avoid detection, disruption, and suppression makes them extremely difficult to treat. Moreover, every type of cancer is drastically different, meaning the chance of finding a "magic bullet" cure is incredibly remote, if not impossible. For the best outcome, treatments must be adapted to accommodate for the individual type

of cancer being targeted (i.e. its characteristics, location, forms and functions). As cancer cells are self-tissues, the only way to selectively locate and destroy them is to identify a particular target that distinguishes them from their healthy counterparts.[3, 35, 38, 53, 54] But as our understanding of different cancers continues to broaden with scientific research, we are discovering each cancer to be so unique, that all likely require a tailored treatment to obtain the greatest outcome. However, with over 200 different forms of cancer identified to date, this is becoming an increasingly complex task.

1.1.4 Current treatment approaches

The treatment for cancers that people are most familiar with is a combination of surgical removal, chemotherapy and radiotherapy; officially called adjuvant therapy. The adaptation of adjuvant therapy has vastly improved survival outcomes of cancer patients. Surgical removal allows for the main tumour to be removed with minimal damage to surrounding tissues, while targeted radiotherapy aims to destroy any remaining cancer cells missed by the surgeon, and chemotherapy is responsible for destroying any other cancer cells that may have already metastasised to other regions of the body.

Surgical removal of cancers became increasingly popular as the go-to treatment option during the mid 1800s which coincided with an improved field of anaesthesia techniques, although these treatments were often fatal due to subsequent infection and blood-loss related deaths.[55] However, the first known recording of surgical removal of a cancerous growth incredibly dates back to the Ancient Egyptians in 1500 BC.[56] However, although the improvement in oncological surgery techniques prolonged the lifespan of patients, it was still clear that without a combined therapy to remove all remaining cancer cells left by the surgeon, the rate of patients that went on to develop new tumours remained high.[55]

Radiation therapy (radiotherapy) was first introduced into the field of oncology during the turn of the 20th century. The notion behind radiotherapy was how ionizing radiation damages the cellular DNA during the cell cycle, leading to cell death.[57, 58] The most effective radiation damage occurs when cells are in the M phase of the cell cycle, and because cancer cells divide much quicker than the surrounding tissues, this in turn leads to repeated radiation treatments favourably damaging and destroying malignant cells compared to local healthy tissues. Radiotherapy is a valuable tool to destroy any cancer cells remaining after surgical resection of a tumour, however the treatment requires targeted radiation at a specific site (i.e. the region where the tumour is present), therefore it is only successful in eradicating a patient of their cancer providing the tumour has not already metastasised to any other regions of the body.[57, 58] When there is suspicion or evidence that metastasis has occurred, this is when chemotherapy becomes the preferred option.

Coined from the words chemical (chemo-) and therapeutic (therapy), the first cohort of systemic chemotherapeutics was initially used in the early 20th century during the world wars when nitrogen mustards were used as chemical weapons, but their anti-cancer properties were not attributed to them until the mid 20th century.[59, 60] It is understood that nitrogen mustard drugs react with the nucleotides in DNA. By forming covalent linkages between nucleotides on opposite strands, inter-strand cross links are produced and their accumulation prevents DNA unwinding; blocking translation pathways. As a result, this disables the cell's gene expression and subsequently leads to cellular apoptosis.[61] From this, analogues of the original compounds were synthesised and tested in humanised mouse models with promising results.[59, 60] To this day alkylating drugs based on these compounds are readily used to treat certain forms of cancer but efficacies are varied.[62] Other drug classes soon followed including plant alkyloids (i.e. vinblastine and vincristine), anti-tumour antibiotics (i.e. doxorubicin and epirubicin), topoisomerase inhibitors (i.e. ironectin and amsacrine), and antimetabolite agents (i.e. methotrexate and foxuridine).[63] Antimetabolite agents function by mimicking natural cellular metabolites. They bind-to and compete-for receptors and enzymes alike to

cause cellular disruption. As cancer cells replicate much faster than healthy tissues they require a larger supply of metabolites, therefore this higher demand for nutrient supplies causes these drugs to favour cancer cells, even though they are not technically cancer-specific in their own right.[33, 59, 60]

The process for an oncologist to decide on the best treatment for a patient's cancer is lengthy and complex. Many criteria need to be taken into consideration such as patient factors, likely outcomes, costs, skills and resources, treatment intent, comorbidity and risk of toxicity, as well as the general disease presentation and type of cancer being treated.[64] To put it widely, all therapies carry pros and cons. However, as radiotherapy is typically less invasive and toxic compared to surgery or chemotherapy, it is often used to treat cancers that are not predicted to have metastasised to other regions of the body (especially when surgical removal would be an invasive procedure).[64, 65] Additionally, radiotherapy is also used when a patient is not deemed fit for surgery such as when the procedure required is lengthy and/or high risk i.e. surgical removal of lung cancer.[65, 66] In these circumstances, radiotherapy is commonly employed, sometimes in conjunction with chemotherapy. However, on other occasions, radiotherapy is not deemed as the best option; such as when a tumour can be easily surgically resected, or alternatively when the tumour is suspected to have spread. Under these circumstances the more common approach is surgery or chemotherapy, or a combination of both.[64]

As a whole, there is no set treatment for every cancer patient. The therapy decided upon is typically tailored to each case depending on a unique set of factors, circumstances and criteria. However, even with this in mind most treatments provided to patients will carry a certain degree of side effects or toxicities, especially in the case of chemotherapeutics.[67, 68] This is due to the general non-selective nature of current chemotherapeutics which have adverse effects on other tissues and organs in the body. In general, this non-selectivity is undesirable for the purpose of patient quality of life, and in some

instances the therapies bring a risk of causing damage to vital organs and tissues unrelated to the cancer that is being treated.[69] In short, overcoming this non-selectivity is one of the biggest hurdles to be tackled for the furthering and advancement of current cancer treatments. Notably, there are more-selective treatments becoming available to oncologists, however these therapies are significantly more expensive compared to the pre-established options.[70] As a result of this, these new and improved therapies are scarcely opted for instead of the conventional drugs available due to the incredibly high costs that they incur.[70] An additional hurdle relating to the development of selective treatments is the interface between cancer and the immune system, especially with regards to the emerging field of immunotherapy which aims to treat a patients cancer through manipulation of their own immune system. The processes by which cancer cells hinder or downregulate the immune system is problematic in this field, and there remains many complex stumbling blocks to be addressed in order to improve the overall efficacy of immunotherapeutics.[40, 54, 71-74]

1.1.5 Hurdle 1: non-selective treatments and cost

In order to achieve a new generation of cancer treatments with less side effects and higher potency, one of the major hurdles to overcome is the lack in selectivity of current treatments within the public health system. Developing therapeutics selectively targeted to the cancer cells will significantly increase the success rate of systemic cancer therapeutics because, currently, doses are limited by accompanying toxicities associated with drugs' non-selective interactions.[67, 68] As most drugs have a degree of non-selectivity or indeed non-specificity, side effects generated are the result of the drug affecting other tissues unrelated to the cancer.[69] If a drug could be selectively and reliably delivered to cancer cells with no interaction with neighbouring tissues, a higher dose could be administered without side effects emerging. With that in mind, the patient can receive a higher concentration of drug, subsequently increasing the probability of total malignancy eradication and therefore expanding the likelihood of total disease cure.

Although recent advances have been made in the development and study of selective and targeted cancer therapeutics, these therapies are often expensive, and there remains much to be tested and analysed before they can be transferred into the public health system. There is a clear divide between these two generations of therapeutics, with the earlier generation being non-selective and toxic but much more cost effective, while the newer generation is selective, specific, and significantly less toxic, but carry much higher treatment costs. To benefit the movement of current cancer treatments into a new generation of more targeted and less toxic therapies, it would be beneficial for these new-and-improved treatment options to carry a competitive and more affordable fee.[70]

1.1.6 Hurdle 2: Interface between cancer and immunology

The second hurdle that needs to be overcome is the ability to overcome the intrinsic ability of cancers to evade the immune system.[40-42, 54, 74, 75] The immune system is designed to rid the body of any unhealthy or abnormal cells, and often works hand-in-hand with p53 to ensure malfunctioning or damaged cells are eradicated.[76] As the incidence of mutation in our genetic code during cell division and replication is relatively high compared to other cell types such as bacteria or yeast,[77, 78] it is accepted that a person develops a pre-cancerous mutant cell almost daily, but the immune system is extremely effective in recognising these mutants and destroying them before they spread.[40] However, in some cases, cancer cells can mutate and hijack particular pathways that enables them to avoid the patrolling immune system.[41] In most cases with solid tumours, they create an immunosuppressive microenvironment. This microenvironment acts as a barrier that deactivates and suppresses any patrolling immune cells within the vicinity and prevents the cancer from being detected and destroyed.[30, 32, 35, 53, 58] However, an emerging approach to tackling the failing interface between a patient's immune system and their tumour is re-training the immune system to recognise the cancer cells more readily.

Cancer therapy researchers are now trying to identify treatments that largely overcome these two hurdles of target specificity and immune evasion. Recent developments have identified therapies that can negate non-selectivity, some treatments have been sourced that can suppress the cancer-promoting microenvironment of a tumour, and even treatments that overcome both of these hurdles simultaneously are under development and investigation. With an increasing understanding of the mechanisms and processes tumours adapt and exploit to remain viable, great strides are being made in the negation of these two hurdles. The next section will delve into these further, where a range of methods are being investigated that can establish a new generation of more potent, selective and effective cancer therapies.

1.2 Targeted cancer treatment

As is the case with most non-selective treatment approaches, the use of non-selective cancer agents brings high toxicity to the patient; causing generalised damage to tissues and organs leading to undesirable and often severe side effects.[59, 60, 67, 68] Moreover, the ADME of these drugs can be rather poor, causing a decrease in drug-availability at the tumour site. This lower availability in the target region often is the results of the drugs sequestering elsewhere in the system, reducing the therapeutic output while simultaneously increasing the toxicities of the chemotherapeutics (due to non-selective activities).[79] Moreover, it is noteworthy to mention that a prolonged low concentration of chemotherapeutics can influence the tumours to become multi-drug resistant.[33, 35] This drug resistance is a phenomenon that increases the difficulty of treating cancers, as the cells generate multiple means of drug-evasion including the development of efflux pumps, re-programming pathways, and even changing their metabolic processes entirely.[33, 35] Selective drug delivery is the employment of drugs or vehicles that deliver a therapeutic to a targeted tissue or region. Most common examples are the selective administration of drugs to a particular site, for example the use of local anaesthetics that permits a localised region to be numbed for procedures to be undertaken. In general practice, there is also the administration of steroids via injection to alleviate joint problems, or the topical application of a cream to an affected area of skin. By delivering a drug selectively to the area it is required to treat, the effect of the treatment is improved due to a higher final concentration of drug at the target site. The use of targeted therapies also drastically improves the quality of life for the patient, as it typically leads to a subsidence of side effects and toxicities caused by drug interactions with unrelated tissues and organs. The design and development of a targeted treatment spans multiple scientific disciplines; chemists, biologists, engineers, pharmacists, medics and epidemiologists are typically all required to some degree to take a drug from design to production and medical application.

Regarding targeted cancer therapies, great strides have been achieved in recent decades.[56] An increasing understanding of how cellular pathways and interactions are different between tumour cells and their healthy counterparts has illuminated potential therapeutic targets that would favour the cancer cells against the surrounding tissues. As tumour responses to chemotherapies and cytotoxic compounds are typically brief and unpredictable,[59, 60, 69] by targeting these inherent pathways that are crucial to the cell survival, the overall efficacy of the treatment should increase. Moreover, this selectivity to cancer cells gives oncologists a broader treatment window as residual toxicities are markedly reduced in the patient.

Various opposing approaches have been taken to establish more-selective cancer cell destruction, and a range fields are showing great promise in ascertaining a new generation of targeted cancer therapeutics. The following sections delve into some new and leading fields of cancer treatment research. This ongoing research spans a range of approaches and targets, including therapies focussing on plant-derived therapies, intracellular targets (organelle targeting and kinase inhibitors), nanomedicines such as the use of nanoparticles, residential stem cells, and immunological based therapies (cytokines, antibodies, vaccines and adoptive cell therapy). This section aims to discuss recent the advances in these treatments, along with relevant examples, their impact on the research field, and current limitations.

1.2.1 Plant derived treatments

Many chemotherapies used today were derived from plant molecules, including drugs such as vinblastine, camptothecin, paclitaxel and epipodophylotoxin.[80] Plant-derived drugs are commonly known as plant alkyloids, or by the broader term of phytochemicals (**Figure 1.9**). As efficient as these drugs are in the treatment of cancers, their non-selective activities and toxicities limits their long-term applications.[81-83] As current research is increasing understanding of how cancer cells function (regarding what proteins are upregulated and what signalling pathways are modified) this in

turn has provided a new selection of potential targets for previously disregarded plant-derived molecules.[84-86]

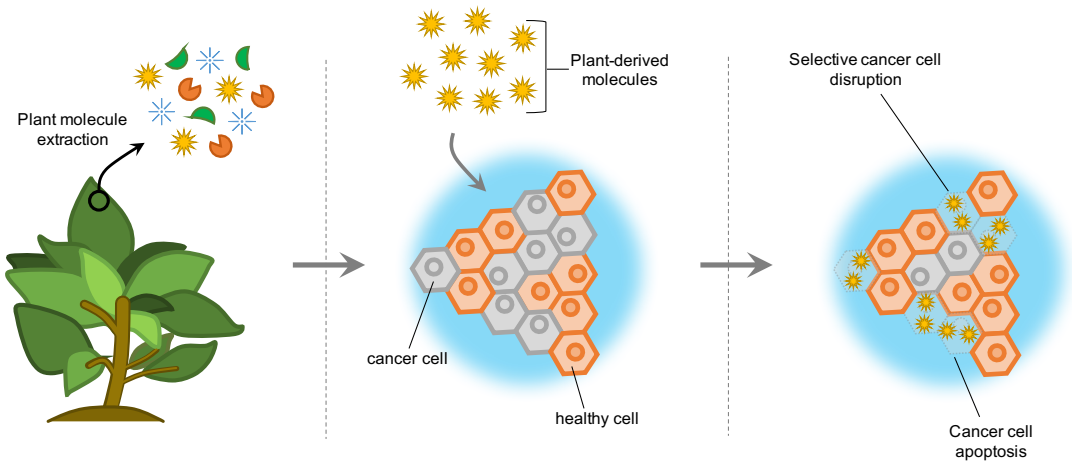

Figure 1.4: Using plant-derived molecules to establish selective cancer cell destruction
Plants are analysed for chemical and biological products. These products are then screened and potential candidates are tested on tumours to assess their potency and selectivity for targeted tumour destruction.

It is estimated that approximately 50% of all anticancer drugs approved between 1940-2014 originated from a plant derived source,[80] however most have exhibited non-selectivity to a certain degree. Their versatility in the field is staggering however, spanning from inhibitors of receptors, kinases, transcriptional factors, microRNAs, cyclins and caspases to name a few.[80-83, 85-87] Additionally, newer treatments have shown promise in early studies including clinical trials. Pre-clinical studies have identified numerous candidates for further exploration, however, and one example includes baicalein. Baicalein was identified as an active component in *Scutellaria baicalensis* (commonly known as the Chinese skullcap), which is a plant that has been used for herbal medicinal purposes for thousands of years.[80, 88] When testing its effects in NSG mice xenograft models of colon cancer, tumour growth was inhibited and apoptosis was readily induced.[89] Further exploration recorded a downregulation in human telomerase reverse transcriptase (hTERT), along with inactivation of MAPK, ERK and p58 signalling pathways.[89] It also repressed expression of C-Myc and oncogenic microRNAs during intraperitoneal administration.[89] Other examples of preclinical trials

include Dercursin, Emodin, and Thymoquinone. All of these drugs however have rather broad modes of action, and many impact the core functions of all living cells, owing to their lack of selectivity.[80] Some drugs have progressed into clinical trials however, including curcumin,[90-93] berberine,[94-96] and lycopene.[80, 97, 98] Curcumin is a product of turmeric, and has shown promise as a highly effective chemopreventative agent such as cancers of the blood, skin, breast, liver, ovary and prostate.[90-93] Early trials have alleviated concerns regarding its safety and efficacy, via representation of safety, tolerability and non-toxicity at respectively high doses.[80, 90-93] It's low bioavailability has been discussed previously however so its use as a sole treatment remains questionable,[80] nevertheless its use in combination with other therapeutics has shown improved cancer regression; namely its combination with gemcitabine in the treatment of metastatic pancreatic cancer.[93, 99, 100] Many other clinical trials are underway using plant-derived treatments, however the results of many remain to be published, and most that have been published lack the selectivity and/or non-toxicity predicted.[80-83, 85-87] This is most likely due to their interactions with core cellular pathways that are not specific to cancer cells, and are alternatively critical for the activity of generalised cell function.

It is well documented that many cancer therapeutics are derived from plant molecules, and more recently a new cohort of plant-derived cancer therapeutics is under investigation to identify treatments with higher cancer antigen selectivity.[80-83, 85-87] Nevertheless, these studies remain in the early stages of investigative development, with many showing less selectivity than that indicated in their pre-clinical studies. In general, most that have shown some efficiency are demonstrating signs of cyclin-dependent kinase inhibition or interference which induces cessation of the cell cycle,[84-86] and some more recently identified drugs include Quercetin and Flavopiridol which have shown evidence of tumour regression *in vitro*.[101] but there remains much to be explored, harnessed and perfected prior to their transfer into a clinical setting, notably due to the discussed frequent lack of bioavailability, reliability and generalised cytotoxicity.

1.2.2 Kinases inhibitors

Kinases are enzymes that use ATP to phosphorylate a protein and in doing so transduce a cellular signal.[13, 53, 102] Kinases are a broad family of proteins, and can be receptor protein kinases, or non-receptor protein kinases. Receptor protein kinases span the cell membrane and translate extracellular signals into cytoplasmic pathways, whereas non-receptor protein kinases relay internal signalling.[4, 102, 103] One family of kinases is the tyrosine kinases which influence a range of biological processes such as DNA synthesis, cell growth, differentiation, migration and death.[104, 105] As they play a key role in a variety of processes significant to cell survival, they have become an increasingly attractive target for cancer therapeutics.[106, 107] One drug example that's widely used is imatinib, which is a derivative of phenylaminepyrimidine. It works by selectively blocking the active site of bcr-abl; a mutant tyrosine kinase commonly present in cancers.[108-110] Bcr-abl is mutated to the point where it is permanently stuck in the "on" position, so continuously transducing and activating signals. Imatinib, by binding to the active site, permanently locks ATP in position on the kinase (therefore it is locked in a closed conformation) and hence prevents subsequent phosphorylation of target residues.[111, 112] Moreover, it can also stimulate the kinase to internalise into the cell, therefore it is unable to transduce its anti-apoptotic signals as normal. Bcr-abl is predominant in a range of tumours, and typically solid tumours are shown to be solely dependent on bcr-abl integrity and activity.[108] Therefore, by default, imatinib is particularly effective in treating these tumours specifically. Overall, Imatinib is reasonably selective to the bcr-abl kinase, however it does continue to have some residual interaction with healthy cellular kinases, but these interactions are largely non-toxic to the healthy tissues as they are more efficiently adapted to accommodating for the loss of signalling through adopting other pathways. Mutations in bcr-abl that can be acquired are a challenge though, as these mutations can change the conformation of the kinase and in turn render imatinib non-functional.[113-115] There are other kinase inhibitors developed that work in a similar manner,[116, 117] including gefitinib and erlotinib. Tamoxifen is also a kinase inhibitor (non-specific), which works by

binding to surface oestrogen receptors and ultimately blocking their oncogenic pathways.[118]

Importantly, unlike cytotoxic drugs, many kinase inhibitors under development have shown low levels of toxicity in clinical trials. Conversely however, some of the leading drugs have been associated with severe side effects, such as pulmonary bleeding (bevacizumab), cardiac damage (trastuzumab), and interstitial lung disease (gefitinib).[119] Moreover, the long-term impact of kinase inhibition therapy is poorly understood. Additionally, in some cases cancer cells develop resistance through further kinase mutations; a common occurrence with imatinib treatment.[113-115] In summary, kinase inhibitors are typically very successful regarding the destruction of cancer cells, however multiple problems remain regarding their safety, treatment longevity, and their long-term impacts on patient health.

1.2.3 Nanotechnologies

Widely referred to as nanomedicine, the adoption of nanomaterials to aid in the delivery and transportation of chemotherapeutics is a continuously advancing field of medicine.[120-122] With a large ratio of surface area to volume, nanocarriers can transport a range of anti-cancer agents such as small-molecule drugs, DNA, RNA and even peptides, while they are capable of carrying fluorescent entities that can be used for imaging purposes to allow the drug localisation within a tumour to be ascertained.[122] The availability of small molecule delivery systems is relatively broad, with the smallest vehicles being the likes of quantum dots and carbon nanotubes, and the larger consisting of protein-based vehicles, micelles and liposomes. One method to increase the delivery and uptake of cancer drugs is their conjugation to albumin. Albumin is a natural protein that is found in a variety of sources such as egg whites, grains and dairy products.[123, 124] As a naturally available substance, albumin has great advantages as a delivery vehicle because it is biocompatible, biodegradable, non-toxic and non-immunogenic, while it advantageously possesses a long half-life in circulating blood plasma.[124]

Furthermore, albumin is cheap to produce, easy to work with and possesses a high binding capacity to a variety of drugs.[125] Drugs can additionally be tethered to albumin through genetic modification. By changing certain amino acid residues in the protein sequence, a functional group can be exposed on the surface of the protein. This presence of a functional group subsequently permits researchers to perform chemical conjugation between a drug and the functional group, resulting in an albumin-drug conjugate.[125, 126] Conjugation of doxorubicin to human serum albumin has been shown to increase anti-tumour activity compared to drug-only,[127, 128] while conjugation of the drug paclitaxel to bovine serum albumin has also shown increased efficacy against prostate cancer.[129] The drug delivery abilities of albumin are widely due to its natural role of transporting and delivering a range of hydrophobic cargos like hormones and vitamins to cells.[130] Importantly, an albumin-conjugated chemotherapeutic is already approved for commercial use and is widely used in the treatment of metastatic breast cancer. The drug, commercially known as abraxane, is a tethered form of paclitaxel and albumin. The albumin is harnessed as a delivery vehicle to transport paclitaxel to the cells, and upon cell delivery, paclitaxel elicits its effects by preventing the normal breakdown of microtubules during cell division.[125] Abraxane has shown significant improvements in treatments of breast, lung and pancreatic cancer since its approval,[123, 125] and other similar drug products are currently undergoing the various phases of clinical trial.[101]

In general, nanoparticles are a new and exciting approach to chemotherapeutics. They have enabled researches to overcome many obstacles with regards to selective and specific drug delivery, and have advanced the field of targeted drug delivery to cancer cells as a whole. Their versatility in cargo is also a great advantage, as they can be adapted to multiple selected fields of drug development such as immunotherapy, gene therapy, and general intracellular disruption. As with all treatments improvements are required, but so far nanoparticle therapies are arguably one of the leading contenders in the new generation of cancer therapeutics.[120-122]

1.2.4 Targeting organelles

Organelles are cellular components that are vital to the survival of a cell; as many therapeutics elicit their end result on particular cellular organelles, generating systems for targeted delivery to cancer organelles has potential for increasing their overall potency. For example, the mode of action of cisplatin is crosslinking with cellular DNA, therefore targeted delivery of cisplatin (or other DNA-targeting drugs) to the cell nucleus is desirable if obtainable.[131] Over the past few decades, developing systems that can target therapeutics to select organelles of cancer cells is gaining traction, with some organelle-homing devices showing great promise, such as the delivery of therapeutics to the nucleus, Golgi body endoplasmic reticulum network, mitochondria and lysosomes (**Figure 1.4**).[132-134] A broad overview of the progress made in each of these fields is provided in this section.

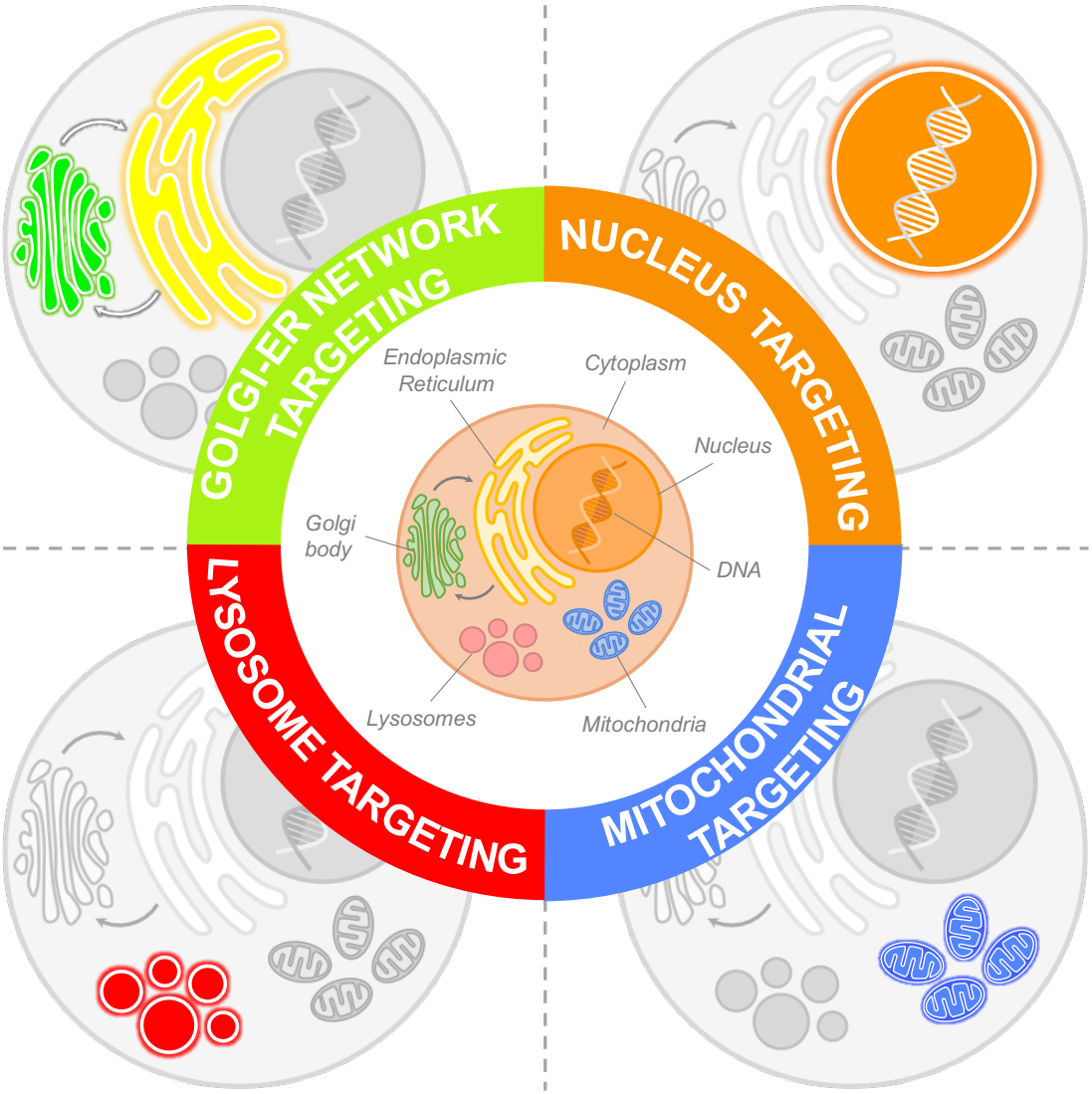

Figure 1.5: The emerging cellular organelles being targeted for cancer drug therapies
Cancer drugs are being developed that selectively deliver to cancer organelles, with some of the most promising including the Golgi-endoplasmic reticulum network, nucleus and DNA, mitochondria and lysosomes.

Nucleus targeting

Many cancer drugs elicit their activities by interaction and disruption of cellular DNA, therefore their overall target is the nucleus of the cell where most endogenous DNA is stored. The nucleus is double-membrane bound and entry is permitted via nuclear pore complexes (NPCs) on the nuclear surface. NPCs are highly complex structures, and their central channel has an approximate diameter of only 5.2 nm in humans.[135] This restrictive channel size of NPCs create a major obstacle with respect to the delivery of DNA-targeting therapeutics, as nuclear-entry of larger drug molecules and

complexes is scarcely successful. Some research has stretched into the use of mesoporous silicone-based nanoparticles (MSNs). These microscopic vehicles are reported to be diverse in the cargoes they can transport, and moreover are small enough to penetrate the nuclear membrane.[132] A comprehensive study was conducted with them relatively recently, where *Pan et al.* described a series of MSNs conjugated to the cell penetrating peptide TAT (MSNs-TAT) that deliver a cargo of the toxic drug doxorubicin (DOX).[136] The MSNs-TAT constructs were made with varying diameter sizes to identify an MSNs-TAT size that was most efficient at penetrating the cellular nuclear membrane. The study concluded that that the general size cut-off for these constructs was a diameter of 50 nm; any MSNs-TAT conjugates with a diameter of 50 nm or larger were unsuccessful at nuclear accumulation and consequently resided around the exterior of the cell nucleus.[136] Importantly, this study was conducted with fixed cells which are metabolically inactive, therefore the nuclear entry of MSNs-TATs described may not be obtainable in a live cell culture. However, the group further developed a very small MSNs-TAT with a diameter of 30 nm which was tested *in vivo*. This 30 nm MSNs-TAT was shown to traffic through extremely small and narrow tumour vasculature, in turn enabling it to localise in hard-to-reach areas of solid tumours. Whether the drug was able to enter the cell nucleus was not clearly documented, nevertheless the 30 nm MSNs-TATs successfully localised in tumour regions and showed a 98% efficiency of tumour-growth inhibition *in vivo*.[137] Other similar methods using cell penetrating peptides and nucleus-localising signal peptides in this fashion of have also been documented.[132] Alternative approaches to targeted nucleus treatments include the re-direction of photothermal agents to the organelle. Put simply, photothermal conversion agents are designed to induce hyperthermia (high temperature) within the cancer cell which causes rapid cell death. Cancer cells however have demonstrated resistance to these treatments, as they typically upregulate certain heat-shock proteins which enhance their thermal resistance and therefore become more thermally stable.[132, 138, 139] Therefore, the idea to target these agents specifically to the nucleus shows promise as the method overpowers the cell's cytoplasmic compensatory strategies.[140, 141]

Lysosome targeting

Lysosomes are vacuolar compartments within the cell cytoplasm that have an acidic content. They play particularly important roles in the degradation, recycling, trafficking and storage of compounds, proteins and molecules of the cell while also being a key contributor to cellular homeostasis and maintenance.[142-144] Importantly, lysosomes have been shown to impact chemotherapy resistance in cancer cells, typically through drug-sequestration.[145] They are also involved in the evasion of immune-surveillance through failure to release immune-checkpoint and –related molecules such as CD200, CD70 and PDL1. They additionally have been shown to degrade MHC class II (preventing antigen presentation), and promote surface expression of the T-cell inhibitory protein CTLA-4.[146-148] As key players in cellular metabolic processes,[144] the changing metabolic pathways observed in cancer cells evoke lysosomal alterations and resultantly compromise their homeostatic properties, consequently impacting the activities and characteristics of malignant tumours.[146] Lysosomes are an interesting target for cancer therapies, as they carry an enzyme called cathepsin. The release of cathepsin into the cellular cytosol initiates apoptosis,[149, 150] therefore if a treatment was designed to break down lysosomal membranes this should subsequently force the cell to enter an apoptotic pathway via cathepsin exposure. Interestingly, some cathepsins are used as extremely reliable diagnostic markers which can depict the likely disease outcome and prognosis.[151-153] Such examples include aspartate cathepsin D and cysteine cathepsins B and L; all of which have direct influences on p53 activation and the cellular apoptotic pathways.[147, 149, 152, 153] Some promising cancer therapeutic targets include the phosphatidylinositol-3'-kinase (PI3K) and HSP70 network. PI3K is commonly overexpressed in cancer cells, and its activity contributes to the promotion of lysosomal surface expression of HSP70, which leads to increased lysosomal stability.[154, 155] Therefore, interrupting the activities of either of both of these proteins would cause lysosomal destabilisation and subsequent membrane permeability leading to content leakage and release of cathepsins into the cytosol. However, this pathway is not cancer-specific; therefore, current research is ongoing to identify a suitable nanocarrier or other delivery system

that can ensure tumour specificity and targeted apoptosis of malignant cells. A promising target for this is peroxidised low density lipoproteins (LDL). LDLs are overexpressed on cancer cell surfaces and are internalised into lysosomes,[133, 156, 157] therefore the conjugation of an inhibitor to an LDL-binding moiety would theoretically ensure more specific tumour delivery of lysosomal drugs.

Endoplasmic reticulum and Golgi body network targeting

The endoplasmic reticulum and Golgi body network is responsible for protein production and folding. After synthesis in ribosomes, proteins are transported to the endoplasmic reticulum for folding and initial *N*- and *O*-glycosylation. Once this is complete, the proteins are then transported to the Golgi body by chaperone proteins for glycan maturation, folding into their final conformation, sorting and trafficking.[158] In cancer cells, there is a significant upregulation of these chaperone proteins in order to accommodate for the high demand for production of upregulated proteins such as surface markers and receptors.[133, 134, 159, 160] Research into the endoplasmic reticulum and Golgi body has identified a link between the network and the activation of pro-survival anti-apoptotic signals.[133, 134] Therefore, targeting the network would not only supress the pro-survival signalling, it would also significantly inhibit the synthesis of proteins crucial for the survival of the cancer cell. Moreover, cancer cells take different production pathways to healthy cells due to the hypoxia-induced stress within solid tumours, therefore there are grounds to identify a cancer-specific target within this network. Treatment of cultures with oxovanadium(IV)-vitamin-B6 showed a selective accumulation in cancer cell endoplasmic reticulums, and moreover the internalisation of the same molecule by healthy cells was significantly slower.[161] Therefore, conjugation of this to drug compounds could prove useful, however it is light-sensitive and easily degradable, therefore the applicability is more challenging.[132, 161] Another approach using cyanine-based pH responsive agents have shown promise; their assembly with bovine serum albumin (BSA) enhanced the selectivity to the site of a tumour, then additionally the pH acidity of the cancer cells allowed for selective intracellular activation of the drug.[162] The study

showed Golgi function to be interrupted as a result, and subsequently the tumour growth was significantly inhibited. Problems with targeting the Golgi body and endoplasmic reticulum network remain however due to their lack of predominance in the organelle-targeting world of research.[133, 163, 164] As such, a big lapse in understanding of the general function of this network makes positive-identification of a cancer-specific target more problematic. Nevertheless, it is anticipated that as knowledge of how the network function grows, discrepancies between the activities of a cancerous-network and a healthy-network will be ascertained and as such more selective treatments can be identified and investigated.

Mitochondria targeting

Mitochondria are organelles that are involved in the survival and death of a cell.[165-167] More importantly however, cancer cell mitochondria are categorically different to those of healthy cells. Such differences include changes to their membrane organisation, metabolism, mitochondrial membrane potential, inactivation of their apoptotic pathways, and promotion of oncogenic activities.[24, 34, 168, 169] These differences largely mediate around the metabolic changes and hypoxia-induced stress of solid tumours (conditions that are resulting of low vasculature and high metabolic demand). A range of mitochondria-targeting drugs have already been approved by governing bodies for the treatment of certain cancers. Lonidamine is a drug that acts as an inhibitor of hexokinases; a key player in the glycolysis of a cell.[170-172] When Lonidamine is administered, the glycolytic flux of cancer cell mitochondria is disrupted which subsequently induces mitochondrial-mediated apoptosis.[133, 170-172] Lonidamine has undergone phase II clinical trials, and 50% of patients treated showed stabilisation of disease following treatment.[173, 174] Moreover, Lonidamine can be used as a combinatory treatment; a cocktail of lonidamine, cisplatin and paclitaxel lead to an 80% response rate in ovarian cancer patients, and 50% of these respondents exhibited complete cessation of disease.[175] Betulinic acid is also extremely effective and has very high selectivity for cancer cells over healthy cells.[176-178] The drug leads to mitochondrial DNA fragmentation, loss of mitochondrial membrane potential

and an increase in ROS production; all triggering activation of the caspase cell death pathway. Additionally, the drug was not successfully blocked when using caspase inhibitors therefore it is highly potent, and importantly it is a p53 independent method of treatment which allows it to be used on p53 negative malignancies, or in conjunction with p53-targeted treatments.[179] Another drug example that targets the mitochondria of cancer cells is GSAO (4-(N-(S-glutathionylacetyl)amino) phenylarsonous acid). GSAO preferentially targets proliferating cells due their naturally higher levels of Ca^{2+} ions in the mitochondria, and elicits its effect through inhibition of adenine nucleotide translocase (ANT) of the mitochondrial inner membrane.[180, 181] As a pro-drug, GSAO relies on cleavage by cell-surface γ-glutamyltranspeptidases to generate GCAO ((4-(N-(S-cysteinylglycylacetyl)amino) phenylarsonous acid), before cell entry and further processing by dipeptidases to generate the active metabolite CAO (4-(N-(S-cysteinylacetyl)amino) phenylarsonous acid) which subsequently elicits its effects in the mitochondria.[182] However, the efficacy of this drug is not great, and is thought to be due to a combination of its bulky size and reliance on multiple metabolic steps for activation. As a result, a second-generation drug has since been generated called PENAO (4-(N-(S-penicillaminylacetyl)amino) phenylarsonous acid), which has an accumulation rate 85% faster than the parent GSAO, and more importantly a 20-fold improvement in tumour specificity.[182] This improvement is theorised to be related to PENAO not having a requirement for metabolic activation, and its smaller size is suggested to increase its success in mitochondrial entry.[182] An intriguing example is the drug Mangafodipir; this dug shows that it is relatively harmless to healthy cells and merely acts as an antioxidant, however in malignant cultures the H_2O_2 pool becomes substantially elevated, increasing intracellular toxicity and leading to cell death.[183] Additionally, co-treatment of mangafodipir with paclitaxel showed an enhanced treatment efficacy in mouse colon cancer models.[133, 183] 2-methoxyestradiol is a drug that induces overproduction of ROS through targeting mitochondrial peroxiredoxins; treatment has shown promising selective toxicity towards leukaemia cells with no effect on healthy residual lymphocytes.[184-187] Other small molecule inhibitors of Bcl-2 proteins show interesting selectivity, including the dugs ABT-737, gossypol, Obatoclax and HA14-1.[133] Overall, great strides have already

been accomplished in identifying treatments that can interrupt malignant cell activity through mitochondrial disruption. However, the specificity of these treatments ranges from poor to highly selective, therefore their investigation with cancer-specific carriers or delivery vehicles is worthwhile of further investigation, as this is likely to simultaneously improve their potency and selectivity.

In general, organelle targeting shows great promise for a new generation of targeted therapeutics, however as with other treatments many drawbacks and unknowns remain. As previously discussed, lysosome targeting has shown promising efficiency in cancer cell destruction, but the current selectivity of the drugs towards cancer cells is limited, and much remains to be overcome and understood to achieve reliable cancer-specific targeting.[131, 133, 145-147] This also applies to the ER-Golgi network; recent research has significantly furthered the understanding of how this network operates and how it differs in cancer cells,[131, 133, 134, 161, 164] however there is still a large void in understanding of its integral pathways and functions, making therapeutic targeting a challenge that carries higher risk of toxicities that may not be immediately explainable.[131, 133, 134, 158] Nucleus targeting has demonstrated great progression in its field, with vast enhancement in treatment potencies and successful improvement in surpassing the nuclear membrane, but similarly penetrating the nuclear membrane is an incredibly complex task which has continuously limited the success of multiple treatment approaches.[131, 138, 188] Out of the four organelles discussed, mitochondrial targeting contestably shows the most promise. As an organelle that is so critical to cellular apoptosis, while exhibiting fundamental differences in cancer cells compared to healthy cells that can easily be targeted (such as an increase in charge), mitochondrial targeting is arguably the most obtainable.[24, 34, 131, 133, 168, 169, 174, 189-193] Furthermore, mitochondria are one of the most researched and understood organelles of the cell, and this comprehensive knowledge and understanding of the intrinsic pathways and functionality of the organelle can only benefit researches and alleviate their plight in the design of new and improved targeted cancer therapeutics.

1.2.5 Cancer stem cells

The emerging subject of cancer stem cells is an important one. Evidence gathered over the last few decades has suggested that most if not all tumours carry residential stem-cell-like cancer cells that permit the growth and persistence of a tumour.[14, 68, 194] Importantly, these cells metabolise at a much slower rate than their tumour counterparts, meaning they commonly lay dormant for a long period of time which subsequently renders chemotherapeutics that destroy fast-dividing cells non-effective.[195, 196] This dormancy means that after the body of the tumour is destroyed by treatments, the stem cell then reactivates itself and produces more cancer cell clones. Cancer stem cells are hence deemed as partially responsible for the high relapse rate in some forms of solid tumours.[195, 196] More critically, some stem cells over time accumulate mutations that render them resistant to treatments, so when they reproduce a new tumour, the following population is then resistant to the initial treatment used to kill the first tumour.[194] An example of this is where stem cells have been identified to acquire mutations in their kinases, which renders kinase inhibitor drugs such as imatinib ineffective, and in-turn an imatinib-resistant tumour of sub-clones from these stem cells then emerges.[197-199] Therefore, in order to improve the longevity of cancer therapeutics, for some forms of cancer the co-treatment of these residential stem cells is crucial to prevent later relapse. To accomplish this, research is needed to identify surface antigens that can distinguish the cancer stem cells from other stem-cell-like tissues of the body, or to identify target metabolic pathways that the stem cells exploit. This identification of target pathways is difficult however, as most pathways used are those of healthy residential stem cells that are crucial for tissue survival.[195, 196] Moreover, the low metabolic rate of stem cells means that even if a treatment is ascertained, its effect will be incredibly slow leading to months or years of prolonged exposure to a therapeutic to achieve a desired effect. Additionally, this requirement for a long treatment time is an obstacle because if the treatments unwittingly lead to loss of residential stem cells in healthy tissues, there is a high risk of severe toxicities.[194] Specifically, the loss of healthy stem cells can lead to tissue and organ failure, and because of the nature of the stem cell functions, these side

effects would not immediately be recognised or surface until much later down the line when permanent damage has occurred.

1.2.6 Monoclonal antibodies

Antibodies are inherently crucial to the immune system. They circulate in the blood and lymphatic vasculature and their role is to bind to foreign antigens on the surface of cells and pathogens, which marks the target for cell destruction by macrophages and complement. Antibodies have been used in targeting cancer cell surfaces, and also as neutralising agents via binding to growth factors and signalling molecules in the tumour microenvironment (**Figure 1.5**).[54, 74, 194, 200] Importantly, antibody therapies can be used as an adjuvant therapy, whereby they can be used in conjunction with other chemotherapeutics simultaneously.[201] Antibodies can induce apoptosis directly, or simply neutralise tissues by binding their receptors and in-turn causing cessation in signalling and growth.

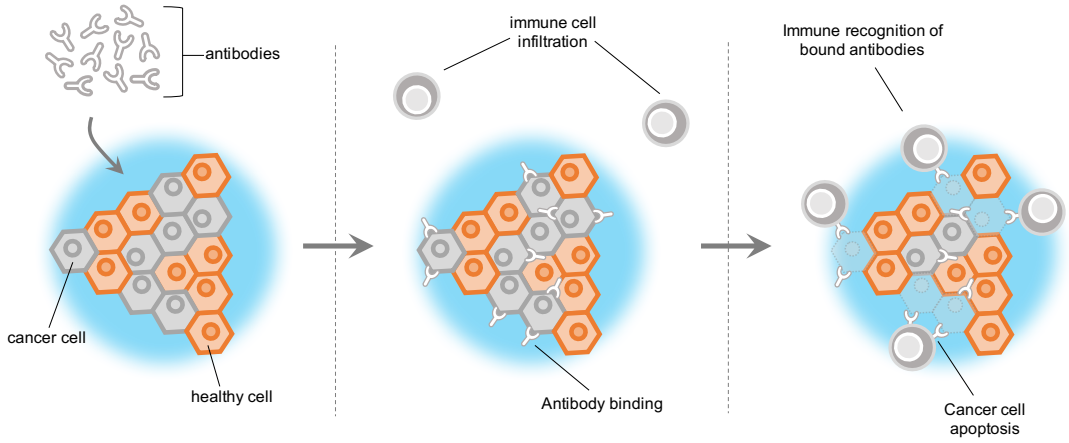

Figure 1.6: Using monoclonal antibodies to selectively destroy cancer cells
Monoclonal antibodies are introduced to the system and exposed to the cancerous tissues. Antibodies bind cancer cells specifically and flag them to be destroyed by complement and immune cells. Antibody-mediated immune destruction of cancer cells is established.

There are a range of antibody therapies that have been developed for cancer treatment, such as Trastuzumab (commercially called Herceptin). This antibody is designed to bind to HER2 (Erb-B2) proteins. These proteins are

responsible for cell growth, survival, adhesion and migration.[202] HER2 positive breast cancer cells have a mutant HER2 receptor that is overexpressed on their surface and locked in an active conformation; causing continuous pro-growth signal transduction and uncontrollable proliferation.[203] Treatment of these cells with Herceptin causes cell arrest at the G_1 phase of the cell cycle, and additionally reduces angiogenesis at the tumour site.[106, 202, 203] There are other antibody treatments available, including Rituximab which is used to target CD antigens expressed on lymphomas, and Alemtuzumab.[194] Unfortunately, alemtuzumab treatment causes depletion of the patient's immune defences and creates an ideal environment for opportunistic infections to flourish,[101, 204] however this is now being trialled as a therapy for autoimmune diseases that exhibit immune system hyper-activation.[101] Another example is Bevacizumab which is designed to target angiogenic pathways used by cancer cells, thus reducing blood vessel production at the tumour site and starving the cells of nutrients and oxygen (subsequently reducing their growth capacity).[205] As these antibodies are ready-made before delivery into the patient, the treatment is categorised as 'passive immunotherapy'. This means that the immunotherapy will only have an effect for as long as the antibodies are present in the circulation (as the patient's immune system is not being trained to make replacements), therefore treatment efficacy time windows are limited. Additionally, multiple phase I trials using antibody therapy have exhibited extensive toxicities and undesired immunological effects in patients,[106, 194, 202, 203] therefore much remains to be researched to improve the safety and reliability of these therapies.

1.2.7 Cytokines

Cytokines are a large family of small proteins that are commonly referred to as the messengers of the immune system. Their role is to relay conversational signals between immune cells and environmental tissues; rendering them as regulators of both innate and adaptive immune responses.[206] Cytokines work as an interconnected signalling network, therefore for a desired output or activity a simultaneous presence of multiple cytokines is required.[206] Their central role in activating and stimulating the immune system is a desirable field

to exploit for targeted cancer therapy in the means that they can stimulate the immune system to identify and destroy residential tumour cells in tissues.[207, 208] Moreover, they can be administered directly to the tissues to alleviate the immuno-suppressive microenvironment of the tumour, enabling patrolling immune cells to infiltrate the tissues more effectively; leading to immune-mediated identification and destruction the cancer cells (**Figure 1.6**).[101, 206, 207]

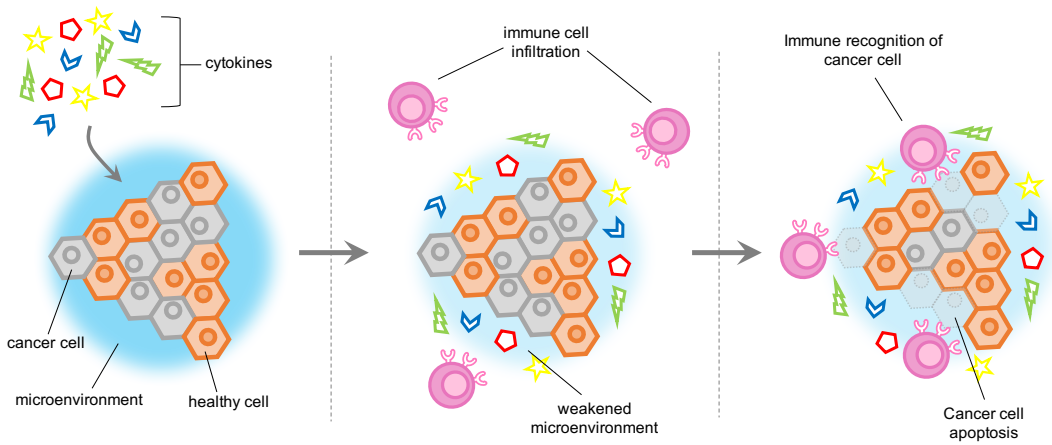

Figure 1.7: Principles of using cytokines to establish selective cancer cell destruction
Cytokines are introduced to the site of the tumour and subsequently disrupt the microenvironment. The immunosuppressive qualities of these treatments permit natural immune infiltration and targeted tumour destruction.

Despite these strong theories and hypotheses, vast investigations have been conducted using cytokines to treat cancerous tumours, however few have exhibited an observable tumour regression, and heightened toxicity is common.[101] Some examples include the administration of IL-6, which was shown to ultimately act as a growth factor for myeloma cells and promote tumour growth.[209] Other studies looked into IL-2 which showed great efficacy in tumour regression, however its administration proved extremely toxic to the patient with side effects with the subsequent development of septic shock syndrome.[210, 211] However, modification of the IL-2 sequence has shown some promise, where two amino acid substitutions from the WT sequence (named BAY 50-4798) substantially alleviated toxicity while retaining a high potency in mouse models.[101, 212, 213] Additionally, the potency of IL-2 is not always a hindrance, as lower doses have been suggested to be immuno-restorative;

benefitting other methods of combinatory therapies.[101, 214] Given the low efficacy or applicability of single-cytokine use in cancer treatment, the field has more recently spread into using a cocktail of cytokines with hopes of a more desirable output, and some combinations are showing promise. IL-1β alone was unsuccessful in improving cancer regression, but combining it with IL-2 alleviated any IL-2 toxicity while retaining its mediated tumour destruction.[101, 210, 215] Another cocktail of IL-2 and IFN-α2b has shown selective tumour eradication in patients, and has been approved by the FDA for the treatment of renal cancers, blood cancers such as lymphoma and leukaemia, and certain forms of melanoma.[200, 216] Cytokines are additionally being tested as adjuvants for other therapies, such as cancer vaccinations. IL-12 alone is non-functional, however when used in the adjuvant of a peptide vaccine for cancer, an increased immunisation and immune response was observed, leading to an improved tumour regression.[217-219] The IFN-α family of cytokines broadly promotes immune responses, such as upregulating the surface expression of MHC class one and adhesion molecules on immune cells.[220] They further promote the activities of B-cells and T-cells, and have anti-angiogenic activities. This leads to improved immune cell interaction with cancer cells, and therefore a higher ability of immune cells to recognise and destroy tumours.[207, 208]

As a whole, cytokine therapies have shown a great improvement over recent years, and overall have furthered the understanding of the cytokine networks that are present in the interface between cancers and immunology.[101, 206, 207] At present however, progression in cytokine treatment is slow, and this is particularly impacted by the inherent complexities and intricacies of cytokine networks that are yet to be fully comprehended, or understood.[210, 211] Nevertheless, the inclusion of cytokines as part of adjuvant therapies has been immeasurable, as it has greatly improved the overall efficacy of countless drugs and treatments that were prior relatively unsuccessful.[207, 208, 217-220]

1.2.8 Vaccination

Employing of vaccination as a treatment for cancer is categorised as 'active immunotherapy' because, unlike passive immunotherapy, the patient's immune system is promoted to initiate its own intrinsic responses.[221] As the immune system is stimulated to target the residential tumours and their antigens favourably, the use of vaccination is classed as a selective therapeutic to treat cancers.[222] As vaccinations induce a broad stimulation of the immune system, they are widely accepted to be more specific and more effective than cytokine therapies. The method of using vaccinations to treat patients with cancer is not a new one; initial efforts in the mid 1900s involved isolating cancer cells, irradiating them to prevent them from multiplying into a tumour, and injecting them into a patient.[73] The principle was the same in the sense that the patient's immune system would be trained to believe that the cancer cell is a foreign entity, therefore leading to immune-mediated eradication. Most modern approaches to cancer vaccination therapies centre around the use of peptides alone, or as part of a viral vector system (**Figure 1.7**).[221, 223]

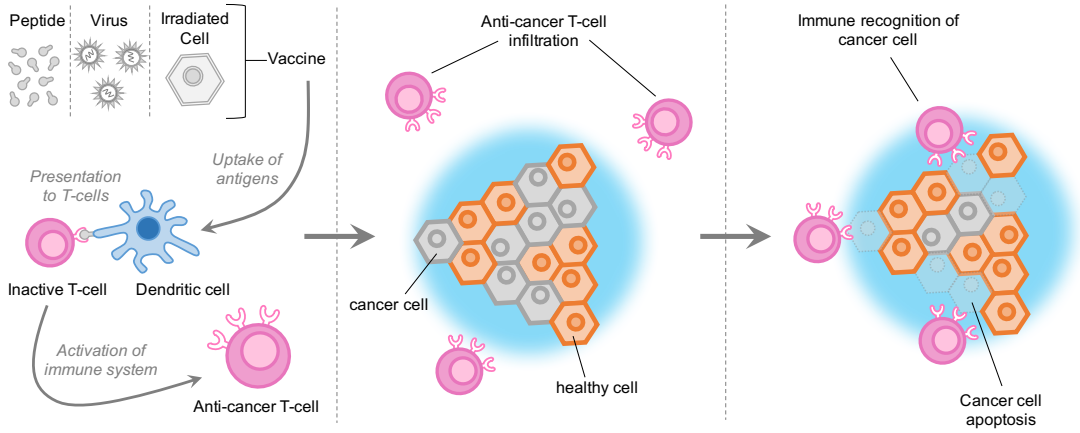

Figure 1.8: Principles of vaccination use as a targeted cancer therapeutic approach
Delivery of cancer vaccines in varying forms aims to train the immune system to recognise cancer antigens as targets. Immune cells subsequently infiltrate the tumour environment to selectively destroy the cancerous growth.

When peptides are used solely, they have an accompanying adjuvant that contains fragments of virus or bacterial cell wall in order to stimulate an

inflammatory reaction and hence initiate immune-recognition.[74, 101, 222, 223] Another interesting technique that evolved from initial efforts of using entire irradiated cancer cells is where a biopsied tumour cell is infected with a virus and then deactivated prior to re-introduction into the patient.[101, 222, 224] The principle of this is when the virus has infected the cell, viral proteins are expressed on the cell surface. This expression of viral molecules on the surface of the cell heightens its immunogenicity, creating a higher inflammatory response.[101] As a result, once the cell has been destroyed by the immune system after inoculation into the patient, it is theorised that antigens from the cancer cell are spilled into the vicinity and picked up by immune cells and recognised as antigens. Immune-recognition of the antigen follows, and subsequently the immune system destroys the cancer cells presenting the antigen on their surface. Viral vectors have also shown promise as cancer-vaccine vehicles. They have been modified to present to the immune system in a range of ways, including expression of surface cancer antigens, carrying DNA encoding tumour antigens, and even having a cargo of therapeutic cytokines that enhance the immune reaction.[223]

Vaccination for cancer remains in its infancy, but the potential to use vaccination to immunise a patient against their own cancer is a potentially groundbreaking approach, providing it can successfully be developed into a fully reliable and effective system.[74, 222-224] Much remains to be discovered in order to make these approaches more reliable, more specific, and more effective. Nevertheless, with the momentum that vaccination is progressing through modern day research in regard to cancer therapy, if these stumbling blocks can be overcome it would present with an astonishing new take on modern day cancer therapeutics.

1.2.9 Gene therapies

Gene therapy is an approach that has become of increasing interest in the field of cancer treatment over recent years.[225-229] The technique involves the delivery of gene-silencing material for oncogenes or pathogenic genes, or

alternatively can be used to deliver therapeutic genes into the cells. The field of gene therapy is a large one, but it is generally split into two disciplines; transcriptional control (DNA level interference) and post transcriptional control (mRNA level interference). Targeting a therapy to the nucleus is preferential because DNA strand degradation in the cytoplasm is common.[230] Adding to the previously described methods of CPP and nanocarriers (pores/micells), these have also been adapted to deliver therapeutic genetic material to cancer cell nuclei. One group described a complex of MSNs-TAT that can successfully deliver therapeutic DNA and mRNA to the nucleus with a reasonably high efficacy.[136, 137] siRNA has been delivered using similar means, with the ultimate target being the disruption of oncogenic kinase expression which leads to marked reduction in tumorigenesis.[231] Alternative approaches to gene therapy includes CRISPR-Cas9 which can effectively replace mutated and malfunctioning genes with the correct sequence leading to an alleviation of disease.[225] Delivery of CRISPR-Cas9 remains a difficulty however, especially given the size of Cas9.[232] Typically, virus particles are required to enable Cas9 delivery to the cell, and therefore the use of viruses adds an additional complexity to the system. Moreover, the regulation of transgene expression is highly important to obtain a desired effect and negate any potential side effects from overexpression or overproduction of the therapeutic sequence.[225, 232, 233] Given these obstacles, Cas9 treatments are in need of a switchable expression system, where if toxicity is observed or the treatment is no longer required, the gene can be switched off. Some studies obtain this by the use of inducible gene promotors which can be induced by small molecules or hormones, with such examples including Lac or IPTG.[227, 234, 235] Another obstacle with viral gene delivery is the immune system. In order for the gene to be delivered to the cancer cells, it is important that the virus vehicles don't evoke too-strong an immune response because in the event of an immune reaction, most will be destroyed prior to reaching the target tumour. To negate this, some have researched the inclusion of polyethylene glycol (PEG) in the viral capsid. Commonly referred to as a "magic cap", inclusion of hydrophobic polymers such as PEG leads to a stable water shell around the viral capsid when in solution. This in turn shields the virus from unwanted host-vector interactions (such as antibody binding) by steric hindrance, and subsequently

permits immune-evasion.[236] Put simply, this method reduces the ability of immune cells to detect and destroy the virus, leading to a larger load of virus evading immune destruction and successfully reaching the tumour site. Additionally, including proteins specific to the patient in the viral membrane has shown improvement to a similar end, as the overall immunogenicity of the virus is reduced as it is more frequently recognised as self.[74, 223, 227] Some viral carriers are natively less immunogenic such as lentivirus and adeno-associated virus, so using these as gene therapy carriers typically comes with less immune interruption and improved delivery.

Regardless of evading the immune system, viral particles carrying gene therapies also need to be selective to their target. Viral proteins for these delivery vehicles are commonly modified to increase their specificity to cancer cell surface antigens, which in turn reduces the risk of infecting non-malignant tissues which would understandably lead to toxicity and a reduced treatment potency. Another problem with viral delivery is the accumulation of viral load in the liver. Studies have shown that up to 90% of therapeutic viral loads are sequestered in the residential immune cells of the liver, which substantially depletes the availability of the treatment for tumour infiltration.[227] To enhance the selective infectivity of the viral carriers, an alternative method is to ensure that the therapeutic virus is only produced and/or functional in cancer cells; leading to a high concentration of therapeutic viral load within a solid tumour.[237] The method is an interesting one if it works, but understandably is fraught with complexities and unknowns. It concentrates on designing a therapeutic gene-therapy virus that can only replicate within cancer cells via exploitation of cancer-selective gene promotors such as PSA, hTERT, E1A and AFP.[227, 237] This selective reproduction thus means that the virus is exclusively reproduced at the site of the tumour and therefore more particles can then go on to infect neighbouring cancer cells. But the health and safety concerns of administering an active and replicative virus to a person is understandably concerning, and therefore without intrinsically precise and understood mechanisms and modes of action to ensure acute selectivity and 100% reliability, the likelihood of this method of gene therapy being approved

for general practice remains remote. Additionally, some studies have used gene therapy viruses in conjunction with therapeutic agents which is a technique broadly termed as Cancer Terminator Virus (CTV) therapy.[227] Asides from viral delivery of gene therapies, other methods of gene delivery include chemicals, liposomes, albumin and gold nanoparticles.

A very interesting approach under investigation is the use of genetically modified mesenchymal stem cells. These cells when administered naturally home to the tumour microenvironment due to the concoction of stimulatory signals present within the region.[195, 237-239] Some researchers have modified these cells to highly express certain cytokines that promote the integral immune response.[227] Therefore, when administered, these genetically modified cells track to the tumour site and then highly stimulate the patrolling immune system, leading to tumour immune infiltration and initiation of an adaptive immune response that destroys the cells. On the subject of cytokines, one highly promising gene target is MDA-7/IL-4; termed by some as a potential magic bullet for cancer therapies.[240-244] The gene is naturally tumour suppressive, and most importantly, incredibly potent as it only harms cancer cells with ultra-specificity. Moreover, abnormally low levels of this cytokine have been identified in a wide range of solid tumours such as breast, liver, prostate, colon, lung and ovary.[245] Crucially, injection of terminal patients with an adenovirus expressing this cytokine showed a significant response in 44% of patients treated.[241]

Overall, the field of gene therapy for cancer treatment is relatively new, and it has already exhibited great promise through a range of techniques, however researchers still need to prove that it can be accurately controlled, targeted and regulated.[56, 227] Most gene therapies can be used as part of a combinatory treatment in tandem with other drugs. Nevertheless, many obstacles remain to ensure selectivity, and of course the restrictions of genetic modification use for general practice, and generalised public trepidation about the method remains a problem.[246] However, it is anticipated that gene therapy could be

the new leading form of targeted treatment for a range of diseases, however this can only be achieved when all the outstanding unknowns can be addressed to obtain a high degree of safety and reliability.[56, 227]

1.2.10 Cell based therapy (adoptive therapy)

Cell based therapy (also referred to as Adoptive Therapy) is a technique that exploits the immune system of a patient to achieve cancer cell destruction.[247] The method uses varying techniques that can involve increasing the population of a patient's natural immune cells, or more complex models using genetic modification to achieve enhanced cancer targeting and destruction.[247] Adoptive therapy has three major classifications; Tumour-Infiltrating Lymphocyte (TIL) therapy, engineered T-Cell Receptor (TCR) therapy, or Chimeric Antigen Receptor (CAR) cell therapy (**Figure 1.8**). An up and coming additional classification is Natural Killer Cell (NKC) therapy, but many hurdles remain to be overcome for this treatment approach to be a viable option.[248]

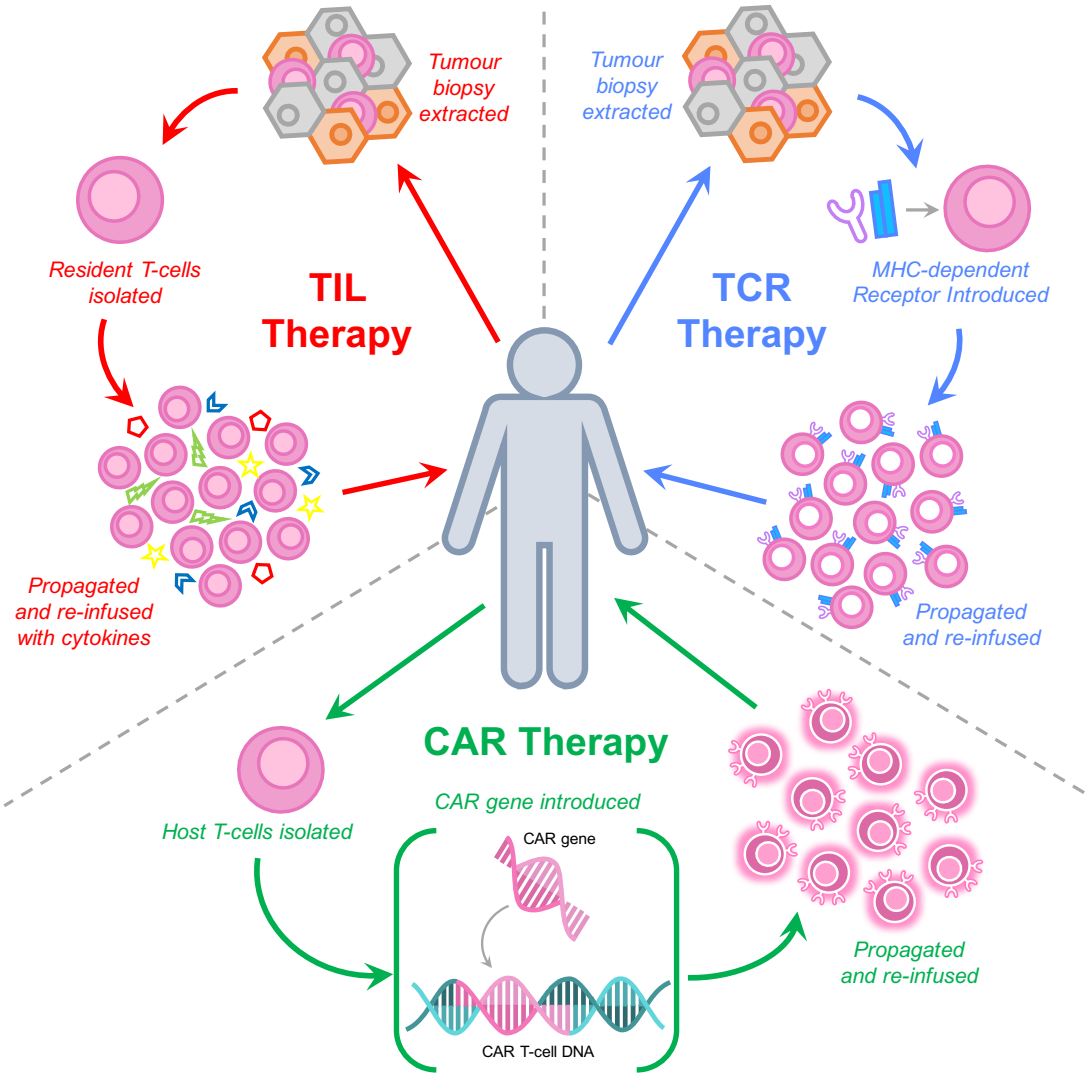

Figure 1.8: The three principle approaches to Adoptive Cell Therapy; TIL, TCR and CAR
Varied immune cell modification techniques used to achieve targeted cancer cell destruction.

Tumour-Infiltrating Lymphocyte therapies (TIL)

TIL therapy works by isolating T-cells that have already successfully infiltrated a patient's tumour, then manually proliferating and activating them prior to re-infusion into the patient. These T-cells are commonly called killer T-cells, as they are extremely effective at recognising cancer cells and eliminating them in a targeted manner. Moreover, their presence in a tumour is commonly used as a biomarker to predict positive outcomes from a cancer diagnosis.[249, 250] They were first reported to be effective against tumours by *Spiess et al.*,[251] and since then Phase I-II clinical trials are ongoing against a range of cancers which have reported mixed results[72, 252-257] Typically, the treatments were most

effective against melanoma and easily accessible superficial tumours, but some recent studies have shown promise in pancreatic, gastrointestinal and ovarian cancers which are typically harder to treat with common therapies.[258-261] Although relatively successful, TIL therapy has setbacks. Difficulties in obtaining prolonged activation and proliferation are common, and these characteristics are required to achieve effective anti-tumour activity. Co-treatment with IL-2 supplementation has been reported to improve this, however frequent infusion of IL-2 is typically required to achieve a noticeable improvement.[247] Moreover, TIL therapy relies on the cancer cells to present the target antigens via MHC; a hurdle in the case of tumours that have hijacked the MHC presentation pathway and thus do not present it on their surface.[262]

Engineered T cell receptor (TCR) therapy

Using TCR therapy is an adaptation of TIL therapy, however the T-cells harvested from the tumour site of additionally modified to express a mutated T-cell receptor that has enhanced tumour homing capabilities.[247] The use of these engineered receptors provides oncologists with the opportunity to personalise patient treatments, as an individual's cells can have a specialised TCR introduced that would enable selective and effective tumour destruction. Moreover, the treatments are typically more effective than TIL as the cells are modified to have a higher activity.[247] Examples of TCR therapy have shown promising results, especially when targeting MART-1 antigens in melanomas.[263, 264] One study promoted the targeting of gp100 which is a common antigen present on metastatic melanomas, and tumour reduction was observed in up to 30% of candidates in clinical trial.[228] Some groups have investigated the targeting of Cancer/Testis antigens (C/T). This population of genes are expressed during normal embryogenesis then later silenced in all tissues except the testis for spermatogenesis. However, C/T genes are commonly reactivated in cancers to promote growth and survival with a high incidence in melanomas.[247] C/T antigens such as SSX, NY-ESO-1 and the MAGE gene group have been targeted with TCRs and generally show an effective tumour regression when treating cancers such as neuroblastoma, liposarcomas and ovarian cancers.[265-267] Although a potential improvement

compared to TIL therapies due to the heightened activation and targeting, TCR therapy still relies on MHC presentation of antigens which is a hazard that can limit the efficacy of the treatment.[247, 262]

CAR-T cell therapy

As previously stated, the limitations of TIL and TCR therapies are the requirement of MHC presentation and cytokines to enable prolonged and effective tumour destruction. An exciting approach to evade this requirement is the use of chimeric antigen receptor (CAR) therapies. Unlike TIL or TCR, CAR can bind to raw antigens on the cell surface, bypassing the MHC pathway.[247] The first generation of CARs was in the 1980s,[268, 269] and in October 2017 a CAR modified T-cell (CAR-T) therapy was approved by the FDA for treatment of B-cell lymphoma.[71] CAR therapies are most frequently effective with haematological based cancers, such as forms of lymphoma and leukaemia, where CD-19 has been most explored as a target antigen given its overexpression on the surface of the cancer cells.[270-274] Newer generations of CAR have since been developed after the first in 1980, with these second and third generations focussing on inclusion of intracellular domains to promote co-stimulation, survival and proliferation once the cells are infused into the patient.[247] Such domains used most widely include CD28, 4-1BB, OX-40, IL-12 and 4-1BBL.[275-280] The inclusion of an intracellular CD3ζ domain on the CAR structure creates efficient and constant promotion of IL-2 production; removing the requirement for IL-2 co-administration in the infusion cocktail.[247] However, this heightened activity of CAR treatments has its complications as their rapid destruction of cancer cells often leads to adverse toxicity in the form of cytokine storms.[207, 281, 282]

Overall, the technique of adoptive cell therapy shows promise, however many hurdles need to be addressed, such as immune cytokine over-activation in the case of CAR and the restriction of MHC presentation requirement for TIL and TCR.[71, 247, 283-285] Additionally, introduction of genetically modified cells to patients is wrought with trepidation within the general public, alongside

extensive regulation and health and safety concerns; which will undoubtedly impact the approval of the therapies within a public health service.[246]

1.2.11: Insights

Great strides have been made in the development of new and improved targeted cancer therapeutics, spanning a vast range of disciplines and techniques adopted.[47, 53, 101, 121, 133, 140, 168, 191, 226, 227] As with most new approaches under development, difficulties remain regarding the overall efficacy and reliability of the treatments. Additionally, adverse side effects and toxicities remain a concern, which is a common observation the case of plant-derived therapeutics,[80-83, 85-87] stem cell targeting,[194-196] and antibody therapies.[106, 194, 202, 203] Other approaches additionally demonstrate a degree of unreliability with regard to their therapeutic output, and longevity. For example, due to the key roles of kinases in the propagation and sustenance of cancer cells, kinase inhibition is a rational approach.[13, 53, 102] However, the frequent acquisition of mutations in the kinases of a cancer cell often impacts the durability of these treatments; whereby these gain-of-function kinase mutations have been attributed to the development of kinase-inhibitor resistance in tumours after prolonged treatment.[113-115] Cytokine treatment has also improved over recent decades and expanded the knowledge of the interface between cancer and immunology,[101, 206, 207] but progression in cytokine treatment remains slow. The inherent complexities and intricacies of cytokine networks is not fully understood, and this in turn can lead to unpredictable results.[210, 211] Nevertheless, the inclusion of cytokines in tandem with other treatment approaches has been immeasurable, as it has greatly improved the overall efficacy of countless therapeutic approaches including antibody therapies, vaccination, and even drugs.[207, 208, 217-220]

More reliable and promising fields include organelle targeting,[131, 133] gene therapies,[227, 286] and adoptive cell therapy.[247, 283, 285] Organelle targeting has greatly improved the efficacies of drugs, and can be obtained through a variety of means such as the use of nanotechnologies, delivery vectors and charged

molecules.[131, 133] Arguably the development of mitochondrial targeting treatments is advancing the fastest, as the mitochondria of cancer cells harbour multiple characteristics that are inherently different to health cells which can be exploited with relative ease.[24, 34, 131, 133, 168, 169, 193] Moreover, the exploitation of these characteristics has not only improved the mitochondrial toxicity of therapeutics, it has additionally improved their cancer cell selectivity; reducing toxicities and side effects. [24, 34, 131, 133, 168, 169, 174, 189-193] Moreover, the use of fluorescent dyes can also be harnessed as vehicles for selective mitochondrial delivery, and their ability to be visualised within a cell can only benefit researches in gaining understanding of their localisation and modes of action when conjugated to toxins.[191, 193, 287-292]

Gene therapies have additionally contributed to, and enhanced cancer therapies. [227, 286] The technique has expanded multiple research fields, and its versatility has been harnessed in numerous ways; including incorporation of therapeutic genes, gene silencing techniques, enhanced viral particles for vaccination procedures, and the development of adoptive cell therapies through the use of engineered TCR and CAR receptors.[227, 236, 247, 283, 285, 286] Gene based therapies in the field of immunology have greatly advanced the field, with the use of CAR-T arguably showing the most promise as a new immunotherapy technique.[71, 226, 229, 273, 293, 294] The limitations of these cells, however, is the immune response generated when they are infused into the patient. While the CAR-T cells successfully target and kill the cancer cells with a high affinity, their rapid reaction often results in an overwhelming immune response, with non-selective cell destruction and flooding the system with inflammatory cytokines which is extremely toxic to a patient.[281, 282, 284, 295] Nevertheless, further genetic modification of CAR-T is within reach, and more recent studies are focussing on methods to modulate the activity of these cells with aims to alleviate the toxicities they bring to patients.[285, 296-299]

1.3 Summary, Aims and Objectives

1.3.1 Summary and outlook

Although large leaps have been achieved in the treatment of cancer over the last few decades, the disease continues to be one of the biggest contributors to global mortality. Moreover, the economic burden of cancer continues to increase, with an annual predicted global economic cost of over £7.2 billion to the United Kingdom alone.[51, 52, 64, 70] The focus of cancer therapeutics has been turned to a new generation of treatment approaches that aim to be simultaneously more effective and less toxic. The use of delivery vehicles to improve therapeutic selectivity and potency has shown promise, with major progress being made in the development of new mitochondrial-targeting therapies.[131, 133, 168, 193, 300] Alternatively, the combination of gene therapy with immunotherapy is also an advancing field of research.[227, 236, 247, 283, 285, 286] The ability to genetically modify a patient's immune system to generate cancer-destructive CAR-T cells has not only shown effective cancer remission in patients, it also enables long term immunity towards certain forms of cancer, namely cancers of the blood.[71, 226, 229, 273, 293, 294] Many hurdles remain between the current status of cancer therapies and the end-goal aim of disease eradication. However, the continuous expansion of knowledge concerning the functionality of different cancers, and the relentless efforts of scientists to push the boundaries of modern science means this end-goal remains a potential reality that is not out of reach.

1.3.2 Project aims

The aim of this project was to develop two opposing systems that contribute to the field of selective cancer therapies. The project explores mitochondrial drug targeting through the use of cyanine dye molecules, and improved cancer immunotherapy through the proposed development of a switchable CAR-T model.

As the relationship between cyanine dyes and cellular mitochondria is not entirely understood with contradictory reports in the literature, the project here provides an in-depth categorisation of the simple cyanine dyes in HeLa cells, and assesses their capacity as a mitochondrial-targeting delivery vehicle. It was crucial to identify their dependencies such as mitochondrial membrane potential, presence of serum and reliance on endocytosis; as these criteria will influence their applicability as a delivery vehicle. The project then applied the knowledge gained from these studies to investigate the dyes as drug delivery vehicles when transporting a range of cargo, and comparing the toxicities of these conjugates when compared to their native drug alone, and similarly in the non-cancerous cell line HEK293.

Regarding a new approach to a switchable CAR-T, the project aimed to determine whether unnatural amino acid incorporation can be modified into a logic gate design, which can then be transferred into a switchable CAR-T model. It focuses on uses the technique known as genetic code expansion which can permit the expression of multiple proteins simultaneously within a cell via the unnatural amino acid makeup within the culture. The main objectives for this project include identification and testing of a quadruplet decoding system that is active in mammalian cells, and subsequently combining it with an amber-decoding system and transferring the two into a switchable GFP reporter design. Building on this, if found to be successful, this proposed switch system could then be transferred to a switchable CAR-T model whereby the cells can be activated or deactivated depending on the unnatural amino acid makeup in the cellular media.

As a whole, with one part of the project focussing on targeted and selective delivery of therapeutic agents to cancer cells, and the other exploring methods to generate a new stimulus-responsive CAR-T model, it is anticipated that this project will simultaneously contribute new techniques to the fields of mitochondrial drug delivery, and CAR-T therapies.

CHAPTER 2:
Cyanine dyes as cancer drug delivery vehicles

Preface

Cellular mitochondria are the core regulators of energy production and cell fate. Moreover, there are many distinct differences that have been identified between mitochondria of healthy cells and their cancerous derivatives. Additionally, mitochondrial drug targeting has shown promise in the treatment of cancer as interruption of mitochondrial function is detrimental to cell health, leaving mitochondria-targeting drugs of interest to researches developing new and improved chemotherapeutics. Fluorescent dyes that specifically bind to cellular organelles and entities are an incredibly valuable tool for cell imaging and understanding cellular processes. With their organelle specificity in mind, it was decided to investigate whether conjugation of mitochondrial-toxic drugs to fluorescent mitochondrial-seeking dyes would improve their overall toxicity. In this chapter, cyanine dyes Cy3 and Cy5 were investigated as drug delivery vehicles. Due to an inconsistent representation across the literature, it was important to conduct a full assessment of their mitochondrial-targeting activities and dependencies; such as the influence of mitochondrial membrane potential, or presence of serum. Two conjugates were also included; a Cy3-Cy5 dimer with hopes of increased staining potency, and a CPP conjugate to ascertain whether CPPs can alter the entry mechanism of the construct. When these characteristics were deciphered, there were no detectable improvements between Cy3-Cy5 and Cy3 or Cy5 individually, and inclusion of a CPP sequence hindered overall staining of the dyes. With this in mind, the simple Cy3 was conjugated to three different forms of mitochondrial drug (a toxic peptide, a small molecule, and a metallocomplex) and in each case toxicity was significantly improved compared to drug alone, or an unconjugated mix of dye and drug. Confocal imaging showed clear disruption of mitochondrial structure, and the potency of the drugs was improved up to 1000-fold with Cy3 conjugation. Notably, the toxicity was significantly higher in cancer cells compared to non-cancerous cells, however toxicity was still exhibited in the non-cancerous models, therefore improvements are required to further-enhance the selectivity of the constructs.

2.1 Background

Mitochondria are central to most key mechanisms of cell survival, including oxidative phosphorylation, central carbon metabolism and biosynthesis of intermediates critical to cell growth and proliferation.[301] They play crucial roles in almost all aspects of cellular activity (**Figure 2.1**), spanning from metabolic signalling, inflammation, cell death, cell transformation and cell fate.[167, 300, 301] They contribute to the immune system, hormone homeostasis and even the aging process. Given their participation in almost all aspects of cell fate and functionality, it comes without surprise that they are often central to the development and persistence of chronic diseases and cancers.[24, 34, 168, 169, 190, 192, 300, 302]

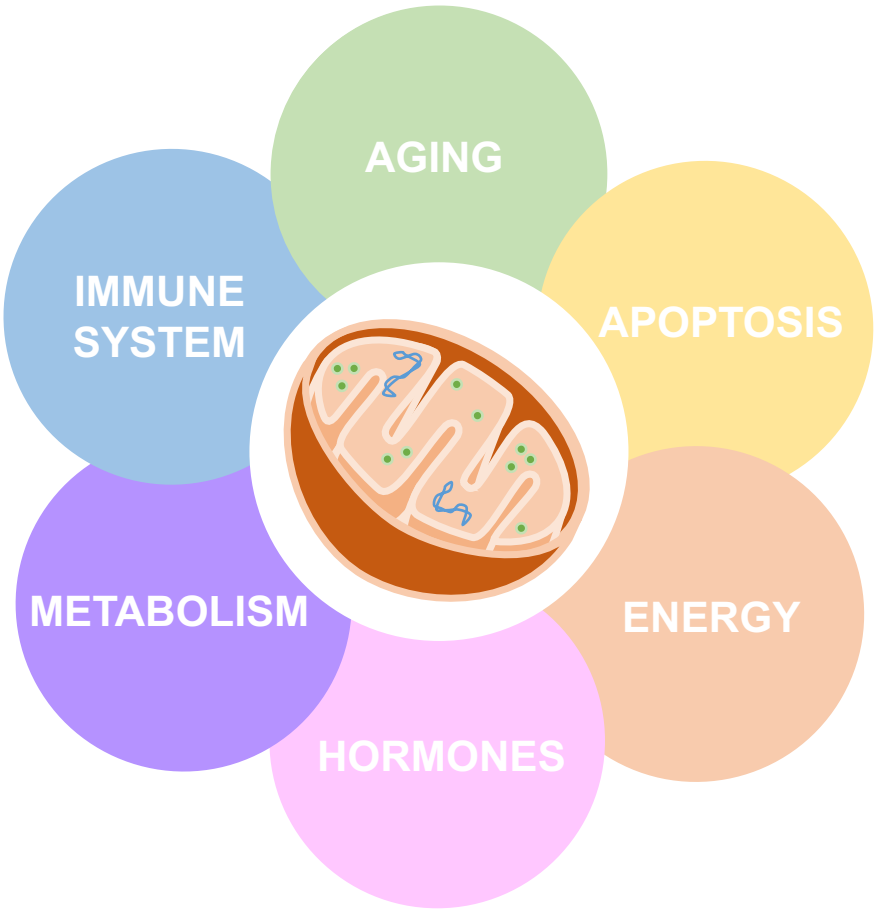

Figure 2.1: Mitochondria at the centre of most aspects of cellular survival and lifespan
Mitochondria maintain metabolic processes, hormonal balances, energy production, apoptotic pathways, immuno-regulation and the aging process.

2.1.1 History of mitochondria

Mitochondria were first extensively reported in the literature in the late 19th century, but were not associated with cellular respiration until the 20th century. Their history of evolution is debateable; however, the *Endosymbiotic Theory* is the most widely accepted.[303-305] As double-membrane bound organelles with their own genome, the theory states that mitochondria originated as an oxidative bacterium holding a symbiotic relationship with a methionagen cell; a relationship influenced by external pressures and environmental changes.[303, 305] The bacteria provided chemical energy to the methionagen, and in exchange the methionagen stored most of the bacteria's genetic material and synthesised its proteins. By making less of its own materials, the bacteria's energy production rate increased; creating an efficient and constant supply of chemical energy to the methionagen. Eventually, this dependence on each other resulted in the methionagen phagocytosing the bacteria and forming a eukaryote (**Figure 2.2**). Eukaryotes produce approximately 80% of mitochondrial proteins, however a small portion of genetic material, known as mito-DNA, is retained and transcribed by mitochondrial ribosomes.[167, 303, 305, 306]

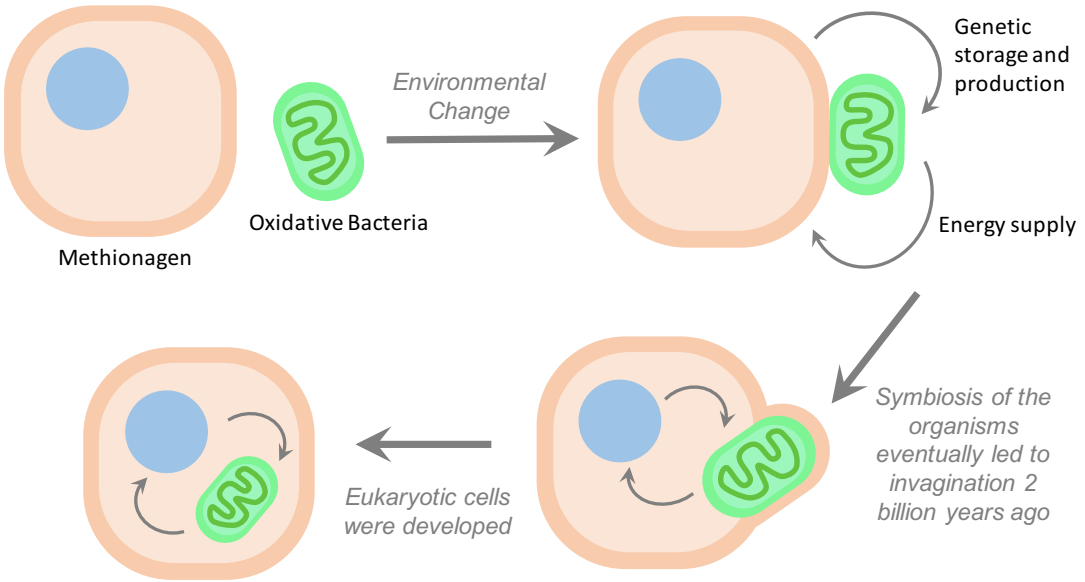

Figure 2.2: The symbiotic theory of mitochondrial evolution from oxidative bacteria
Environmental changes and pressures influence the formation of a symbiotic relationship between a methionagen and oxidative bacteria, exchanging energy supplies for genetic storage and production. Over an extensive period, the oxidative bacteria is invaginated and the eukaryote precursor cell is formed.

2.1.2 Structure and function of mitochondria

The mitochondria (singular, mitochondrion) are double membrane bound organelles found in most eukaryotic cells.[167] Named from the Greek “mitos” (thread) and “chondrion” (granule or grain-like), they provide the largest supply of chemical energy to the cell in the form of ATP (adenosine triphosphate).[167, 301] Commonly within the region of 0.5 – 1.0 μm in length, they can vary tremendously in size and structure, depending on external pressures, metabolic signals, and cell cycle stages.[301, 307]

Structurally, mitochondria are complex organelles. Their central matrix is where the Krebs Cycle is located, and is encompassed by two distinctive membranes, the outer mitochondrial membrane and the inner mitochondrial membrane (**Figure 2.3**). Although both are formed of a phospholipid bilayer, the two membranes are categorised by distinctly diverse compositions and functions.[167] The outer membrane is relatively uniform and smooth, where its permeability typically permits diffusion of molecules up to approximately 5 kDa in size. It acts as a cell signalling platform, enabling the merging of signalling cascades that are read, translated, and transmitted into the mitochondrial space. In contrast, the inner membrane is pleated to form an arrangement of cristae: these deeply convoluted and pleomorphic invaginations dramatically expand the surface area of the inner membrane, while harbouring machinery required for mitochondrial respiration.[308] Adding to their complex structure, mitochondria can also morph their appearances depending on cell type, incoming metabolic signals, or even deviate their appearance relative to the stages of the cell cycle; these morphological changes (known as mitochondrial fusion and fission) are paramount to sustain the function of the mitochondria under various external stimulus and environments.[167, 307, 308] Mitochondria can be found as single organelles, but most frequently converge into large interconnected networks through a cell, frequently transported throughout the cytoplasm to match the local energy needs of an intracellular region.[309] Moreover, the interactions of mitochondria with neighbouring cellular organelles are critical for signalling and overall mitochondrial function. They engage in complex membrane dynamics with the endoplasmic reticulum, the

plasma membrane, lysosomes, endosomes and peroxisomes to name a few examples.[308] These relationships are critical for the maintenance of cellular health, and the translation of signalling pathways where mitochondria act as a central hub for signal input and output.[166, 189]

Of all the important functions of mitochondria that have been identified, their ability to provide chemical energy in the form of ATP has always been their central and most important role in the cell.[310] Decades of research through the mid 20th century slowly characterised and identified how this is achieved, and it is by the electron transport chain (often referred to as the ETC). By a series of proton pumps across the inner mitochondrial membrane, protons (H^+) are pumped into the intermembrane space in an irreversible direction. This one-way trafficking of protons into the intermembrane space results in a high concentration of protons locked in the inter membrane space, subsequently generating a proton gradient across the inner membrane.[310] As the mitochondrial matrix is consequently rendered negatively charged, the protons will naturally seek transport back into the matrix to balance the opposing charges. This transport of protons back into the matrix can only occur through a specialised transmembrane pump called ATPase. By harnessing the energy generated from the electron transport chain complexes, ATPase subsequently transfers protons through to the negatively charged mitochondrial matrix, and this passage of protons through ATPase simultaneously fuels the phosphorylation of ADP to form ATP (**Figure 2.3**).[310]

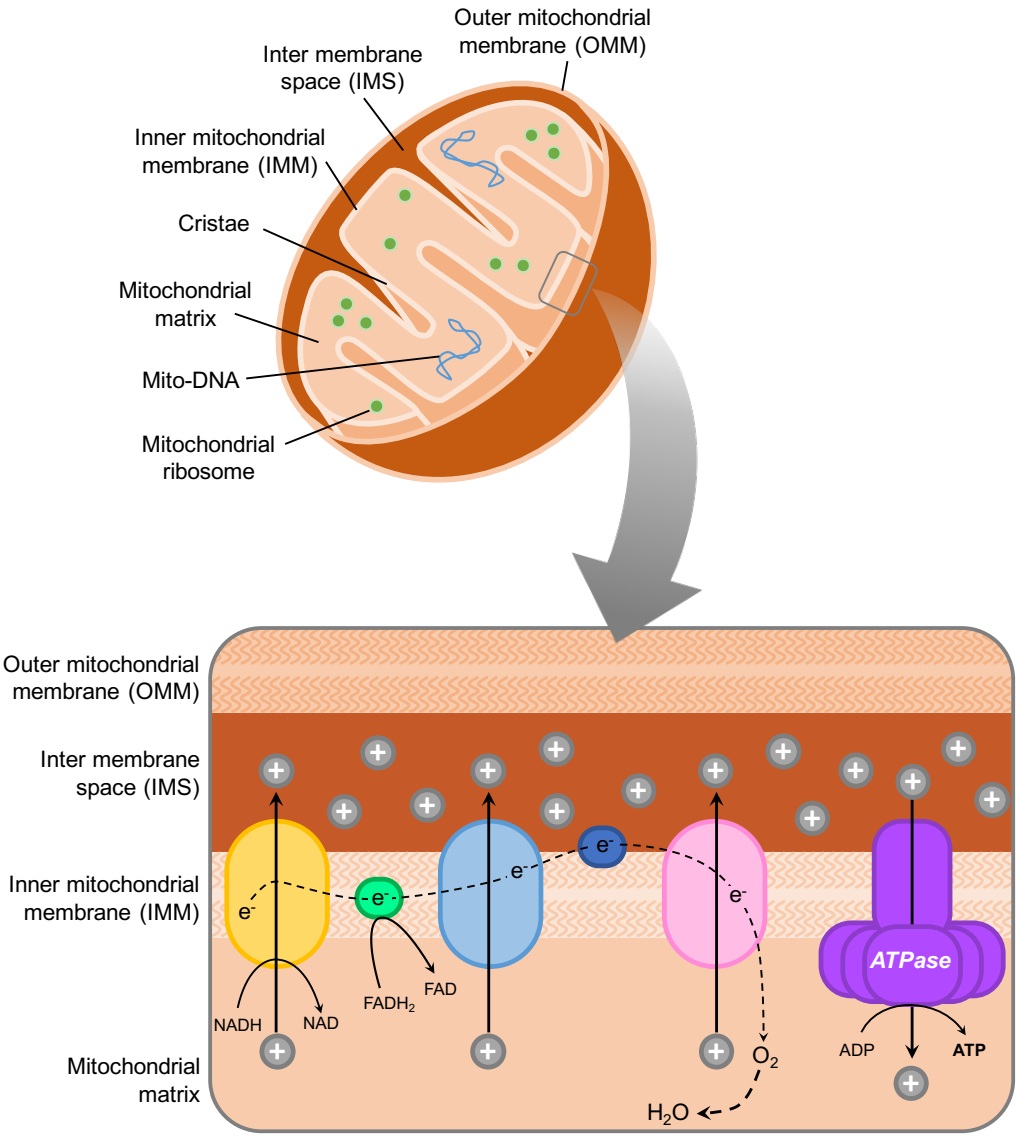

Figure 2.3: Mitochondria structure and mechanism of the electron transport chain (ETC) *Mitochondria are double-membrane bound organelles with invagination of the inner mitochondrial membrane increasing surface area. Mitochondria have their own DNA and ribosomes for protein production. The intermembrane space is where the electron transport chain is located, which produces energy for the cell in the form of ATP via the trafficking of protons across the inner mitochondrial membrane.*

2.1.3 Mitochondria: cellular disease and cancer

As the indispensable energy supply for the cell, the central regulator of intrinsic apoptotic pathways, and puppeteer of a plethora of metabolic and signalling processes, mitochondria are crucial to the survival of a cell, and therefore their mutation or malfunction can subsequently lead to a range of diseases that span from mild to life-limiting.[24, 34, 166, 168, 169, 190, 192, 300, 302, 307] Typically, mitochondrial diseases are more severe when they affect cells of the muscles,

cerebrum, or nerves. This is the case as these tissues contain cells that use much more energy than other cells in the human body, therefore a lack of mitochondrial function and energy production is more detrimental to the sustainability and maintenance of these tissues. Nevertheless, diseases that manifest from mitochondrial dysfunction cover a vast range of medicinal disciplines including diseases in the fields of psychology,[311-313] endocrinology,[314-317] neurology,[318-321] developmental biology,[165, 322-324] and optometry.[325, 326]

Given the central control of mitochondria to determine cell survival, proliferation and death, they can consequently be utilised as a lethal weapon by cancer cells to maintain tumour survival and growth. As mitochondria house many pro-apoptotic proteins in their intermembrane space, they dictate the onset of intrinsic apoptotic pathways by controlling the release of these proteins into the cell cytosol.[24, 34, 300] There has been an onslaught of research into the functionality of mitochondria in cancer cells compared to their normal counterparts, and there is ample evidence that they are categorically different,[24, 34, 168, 300] directly contributing to tumorigenesis and its progression. Cancer cell mitochondria typically have modified levels of reactive oxygen species, which has been linked to cancer cell resistance to some chemotherapies.[169, 192, 302] Mutations developed in the mito-DNA can cause a malfunctioned electron transport chain, leading to inefficient ATP production and overproduction of reactive oxygen species. This overproduction of reactive oxygen species in turn results in oxidative damage to DNA and surrounding tissues, favouring chromosomal instability and furthering carcinogenesis. Mutation in mito-DNA has also been linked to a significant increase of developing cancers of the breast, thyroid and prostate,[190] alongside development of a plethora of other diseases.[190] Notably, many of the cancer hallmarks such as excessive proliferation, resistance to death or anti-growth signals, impaired apoptosis and enhanced anabolic activity have all been connected to mitochondrial dysfunction.[24, 34, 168, 190, 192, 302] Interestingly, tumour cells exhibit an extensive reprogramming of their

metabolic pathways, resulting in an increased susceptibility to mitochondrial perturbations.

To acquire the amount of carbon needed to enable tumour progression and growth, remarkably cancer mitochondria can interchangeably use glycolysis, oxidative phosphorylation, or fatty acid oxidation as the source of energy to compensate and adapt to local micro-environmental conditions and pressures (such as acidosis).[34] This consistently provides the cell with the carbon source and energy it requires, enabling tumour growth, proliferation and metastasis. The changeable diversity and adaptability of cancer cells and their mitochondria is a challenge to therapeutics. Not only can cancer cell mitochondria employ a range of drug evasion and cell survival mechanisms, the cell itself can also adapt to therapeutics – using them as a selective pressure to generate a new method or approach to gain the desired outcome. Cancer mitochondria most distinctively have a higher mitochondrial membrane potential, and this is due to their deviating mechanisms of energy production.[24, 168] This variation in charge alongside production of different metabolites, make them relatively distinctive targets for cancer therapy. Moreover, mitochondrial destruction results in the release of pro-apoptotic peptides which can override the death-evasion mechanisms and cause the cell to die.

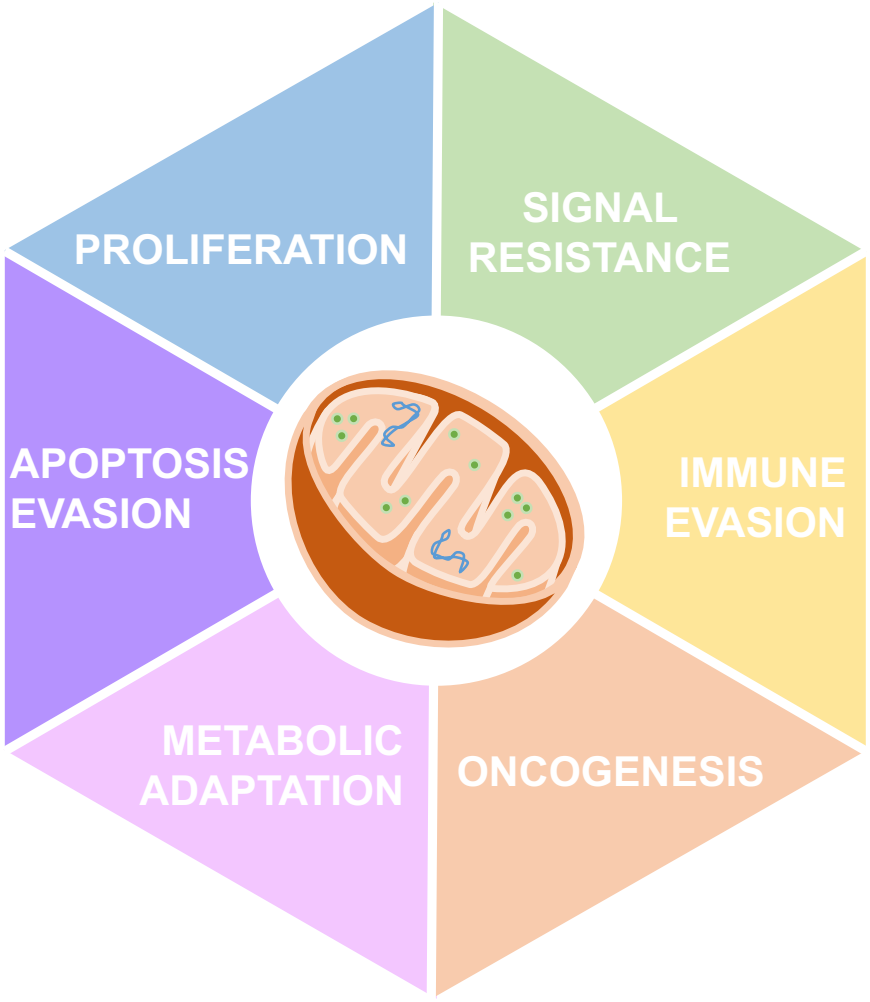

Figure 2.4: The influence of mitochondrial processes on the hallmarks of cancer
Cellular changes occurring in cancer cells that are purely or partly related to, or caused by changes of pathways and signalling of the residential mitochondria.

2.1.4 The revolution of mitochondria-targeted drugs

Direct drug targeting to mitochondria is applicable to a wide range of primary or secondary mitochondrial diseases (diseases directly or indirectly caused by mitochondrial dysfunction).[327] As mitochondria are responsible for numerous vital cellular processes, mitochondrial drug targeting is arguably the most efficient method of inducing controlled and targeted cellular senescence and apoptosis. Mitochondrial drug targeting can be applied to numerous highly prevalent diseases and pathological processes, all with important social, medical and economic impacts.[24, 165] This makes mitochondria attractive targets regarding cancer therapy specifically, as cancer cells have been shown

numerously to develop (multi-)drug resistance, particularly by adapting alternative cellular pathways in order to sustain survival.[33-35, 42]

The negative charge of mitochondrial membranes is the most commonly exploited factor used for construct mitochondrial localisation, and as cancer mitochondria have hyperpolarised membranes (approximately -220 mV) compared to healthy equivalents (-160 mV), positively charged compounds tend to favour the mitochondria of cancers.[24, 34, 168] The most common cationic compound studied for this purpose is arguably the biologically stable triphenylphosphonium ion (TPP) which has been widely used as a mitochondrial targeting vector.[191, 328] Attributed to its charge and hydrophobicity, TPP readily penetrates cells and accumulates in the mitochondria, obtaining a mitochondrial concentration 100-500 times higher than that in the cell cytosol.[191, 193] Moreover, cancer-drug delivery to mitochondria using TPP-modified vesicles or liposomes has been reported.[329, 330] Nevertheless, other small cationic molecules have been shown to exhibit mitochondrial-penetrating traits, such as rhodamine, pyridinium and cyanine dyes.[287-292] The additional fluorescent properties of these compounds mean they are frequently employed as fluorescent probes, imaging reagents, and photodynamic therapy agents.[191, 288] In light of this, as mitochondria have found attention as drug targets for a variety of diseases, employment of mitochondria-targeting dyes as theranostic delivery systems is worthy of further exploration. Drug-targeting with cationic lipophilic dyes is within reach, as the Nernst equation shows that for every 60 mV increase in membrane potential, the concentration of lipophilic compounds increases 10-fold.[300, 331] Further, these dyes successfully function after oral or intravenous administration and are reported to be safe in the long term for human trials, therefore therapeutic applications are possible.[332, 333]

2.1.5 Cyanine dyes as fluorescent imaging probes

Organelle-specific fluorescent labelling by small molecular dyes is an established and fundamental technique in any discipline working with

mammalian cell imaging.[188, 334, 335] It facilitates the assessment of cell structure, cytoplasmic changes and can be employed as a tool to determine the specificity of labelled compounds by co-localisation assessment.

Cationic, poly-aromatic dyes have been developed as mitochondria-selective stains previously,[288, 290, 291, 328, 336, 337] and due to their hydrophobicity, the dyes can passively diffuse through the cell membrane, while their positive charge leads to mitochondrial accumulation (mediated via negative mitochondrial membrane potential). The most commonly employed dyes are structurally based on rhodamines or heteroatom doped cyanines.

Cyanine dyes come in a range of structures and indeed the most established mitochondrial fluorescent stains are cyanine-derived, such as the MitoTracker family (**Figure 2.5a**). By maintaining an array of conjugated hydrocarbon chains (alternating single and double C-C bonds), the amount of conjugation determines the emission wavelength of the molecule, and therefore determines its fluorescent colour (**Figure 2.5b**). The lesser conjugation, the lower the emission wavelength (ranging in blues and greens), but as the conjugation increases, the emission wavelength increases – leading to fluorescence within the oranges, reds and far-reds region.[338] So far, the simplest cyanine dyes Cy3 and Cy5 are structurally similar to benzoxazolium dyes, and have found wide use as fluorescent labels or FRET pairs to study a variety of cellular processes including protein-protein interactions.[337, 339-341] The literature surrounding the use of cyanine dyes for mitochondrial targeting is contradictory, and papers can rarely be directly compared due to discrepancies in techniques used between research groups. The major differences include variations in the cells used (mesenchymal stem cells, macrophages, or canine kidney cells), construct design (inclusion of additional ring structures, or tethering to esters and use of succinamide) and contradictions in the results reported.[291, 337, 339, 342] Due to this plethora of inconsistencies in pre-established published results and methods, a full categorisation of a range of cyanine dye compounds is worthwhile to provide

a more consistent and comprehensive overview of their modes of action and potential limitations as fluorescent probes.

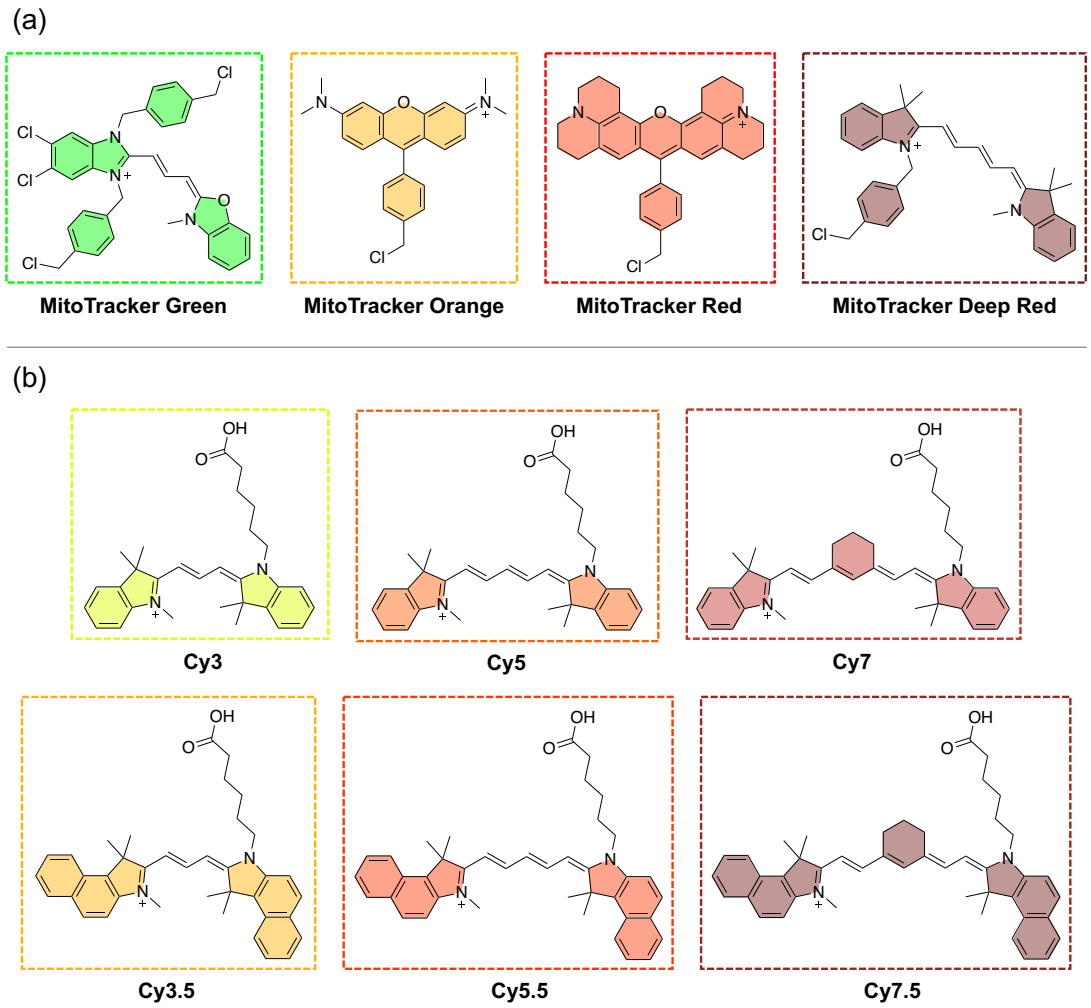

Figure 2.5: Chemical structures and fluorescence of MitoTracker and cyanine dyes. *(**a**) Structure of MitoTracker dyes MitoTracker Green, Orange, Red and Deep Red. (**b**) Structure of simple cyanine dyes Cy3, Cy5, Cy7, Cy3.5, Cy5.5 and Cy7.5. All constructs are coloured to symbolise their colour of fluorescence.*

2.1.6 Aims and objectives

The aim of this chapter was to determine whether mitochondrial targeting cyanine dyes can be harnessed as cancer drug delivery vehicles.

This aim is built on the premise that mitochondria are impressive targets for cancer therapeutics under development, with many reporting a high efficiency and efficacy. With cancer mitochondria being inherently different to healthy cell mitochondria, this provides the possibility of targeting them more specifically, and hence favourably destroying cancer cells. One of the crucial differences in cancer cell mitochondria that can be targeted is their mitochondrial membrane potential, which is significantly more negatively charged. As a result, using positively charged moieties as a vehicle would theoretically deliver therapeutics to the cancer cells more favourably, and the use of charged materials to deliver cancer therapeutics has been widely discussed in recent literature. Moreover, the use of fluorescently charged entities could enable a greater understanding of how the therapeutic functions via fluorescent imaging. With this in mind, cyanine dyes were selected as drug-delivery vehicle candidates as they have been described to locate in cellular mitochondria previously, and exhibit fluorescence which is beneficial for imaging purposes with regard to their characterisation. With this in mind, it was decided to investigate conjugation of cyanine dyes to mitochondrial drugs of varying characteristics (a small molecule, a metallocomplex and a toxic peptide) to investigate both the drug delivery capacities of cyanine dyes, and the versatilities in cargo they can transport.

As the literature representation of cyanine dyes in mammalian cells is contradictory, this project aimed to analyse the intrinsic behaviours of Cy3 and Cy5 in HeLa cells, and to assess their capacity as a delivery vehicle. It was crucial to identify their dependencies such as mitochondrial membrane potential, presence of serum, and reliance on endocytosis, as these criteria will influence their applicability as a delivery vehicle. The project then applied the knowledge gained from these studies to investigate the dyes as drug delivery vehicles and their capability in transporting a range of cargo; comparing the toxicities of these dye-drug conjugates to their native drug alone, and testing their toxicity in the non-cancerous cell line HEK293.

2.2 Construct localisation in cancer cells

Prior to assessing the capability of cyanine dyes to act as drug delivery vehicles, it was important to characterise their habitual activity in mammalian cells. The compounds in this chapter were tested in Henrietta Lacks cells (HeLa). HeLa are an aggressive cervical cancer cell line frequently used in cancer research studies throughout the biochemistry and pharmaceutical sciences.[343] The localisation studies performed here create a broader understanding and characterisation of the compounds employed; giving a more uniform comprehension of the intracellular behaviours which may influence their employability as delivery vehicles.

2.2.1 Structure and designs of cyanine dye constructs

The construct designs used throughout this project are detailed in **Figure 2.6**. All constructs detailed were kindly synthesised by Dr. Alexander Nödling, Mr. Davide Cardella and Dr. Xufei Li for the purpose of these experiments.

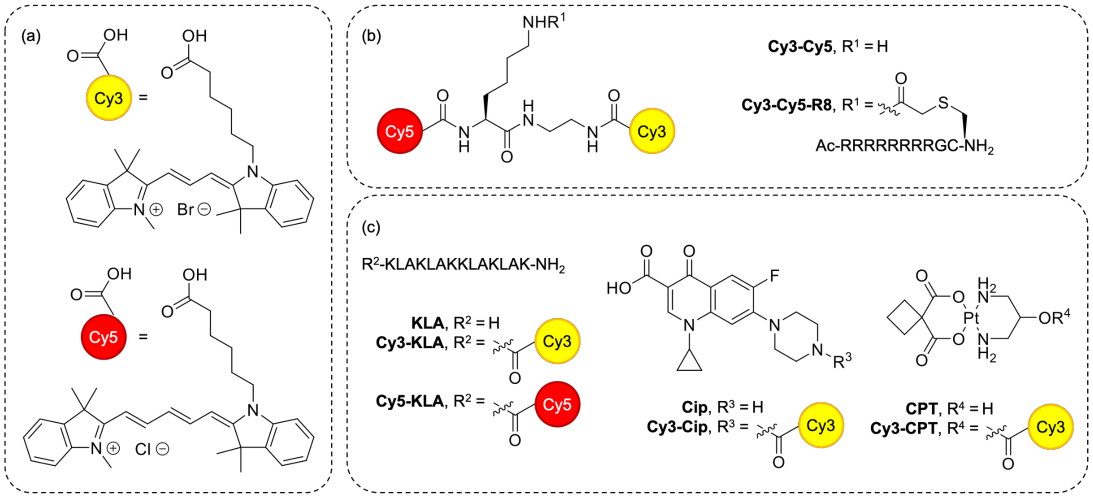

Figure 2.6: Chemical structure of cyanine dye and drug compounds used in this project *(**a**) **Cy3** and **Cy5**. (**b**) **Cy3-Cy5** and **Cy3-Cy5-R8.** (**c**) Dye-drug conjugates **Cy3-KLA**, **Cy5-KLA**, **Cy3-Cip** and **Cy3-CPT**.*

The constructs described were chosen for a range of reasons. As the simplest and smallest cyanine dye molecules, **Cy3** and **Cy5** were the leading candidates as drug delivery vehicles, and their full characterisation was required prior to drug conjugation. It was also noteworthy to investigate whether conjugation of the two dyes together (**Cy3-Cy5**) could improve potency, as the presence of two cyanine dyes in a single molecule increases the molecular charge (so theoretically the efficiency of the molecules would improve). Regarding **Cy3-Cy5-R8**, conjugation of a cell-penetrating peptide (CPP) to a cyanine dye has been reported to inhibit mitochondrial localisation,[344] so it was worthwhile to determine whether conjugation of a CPP to a double-cyanine dye molecule (increased charge) would permit mitochondrial targeting. Additionally, this could ascertain whether the presence of a CPP entity could alter the entry pathway of the construct into a cell. Referring to the drug conjugates (**Figure 2.6c**), three distinctive drug molecules; a mitochondrial toxic peptide $(KLAKLAK)_2$ (**KLA**), a small chemical mitochondrial drug Ciprofloxicin (**Cip**) and a metallocomplex mitochondrial drug Carboplatin (**CPT**) were conjugated to **Cy3** or **Cy5** respectively. These represent three important classes of drugs in clinical application and the molecular targets of all these drugs are believed to be the mitochondria.[345-351] **KLA** is a pro-apoptotic, antimicrobial peptide that is understood to engage in disruption of the mitochondrial membrane.[345, 346] **Cip**, a fluoroquinolone with antibiotic activity, has previously exhibited cytotoxicity in eukaryotes due to damage caused to mitochondrial DNA.[347-350] **CPT** is a derivative of Cisplatin (a widely established cancer drug) that impairs mitochondrial function, inducing apoptosis.[351] The diverse properties of these candidates would indicate whether the drug-delivery capacity of the dyes is affected by the size and molecular makeup of the transported cargo.

2.2.2 Mitochondrial localisation:

The first set of experiments were conducted to characterise the mitochondrial localisation of the dye constructs. The activities and dependencies of the dyes alone needed to be established prior to investigating drug conjugation; a necessary step as the presence of a drug-cargo could alter the natural cellular

activities and subsequently hinder the ability to determine the mitochondrial-homing capacity of the constructs. To assess this, HeLa cells were treated with 10 μM **Cy3**, **Cy5**, **Cy3-Cy5** or **Cy3-Cy5-R8** respectively in serum free media at 37 °C 5% CO_2 atmosphere for 1 h. Prior to imaging, cells were washed with PBS and incubated with Hoechst 33258 nuclear stain for 10 minutes. Confocal assessment of construct localisation revealed clear fluorescent staining patterns reminiscent of mitochondrial structures (**Figure 2.7**), represented by filamentous architectures located within the cell cytoplasm. Cellular staining patterns of mitochondria is distinctive, with numerous examples in the literature.[287, 288, 336, 352]

For all four compounds, **Cy3** and/or **Cy5** fluorescence was observed to be of equal intensity, while Hoechst nuclear stain visualised the cell nucleus. Regarding **Cy3-Cy5** and **Cy3-Cy5-R8**, it was anticipated that **Cy3** fluorescence would be weaker due to a FRET (Försters Resonance Energy Transfer) interaction with **Cy5**. FRET occurs when the emission wavelength of one compound falls within the excitation range of the other, so when molecules are within close proximity, the energy from compound-1's fluorescence is transferred to excite compound-2. In this case, **Cy3**'s emission of 575 falls within the range of **Cy5**'s excitation spectra, leading to **Cy5** fluorescence. The reasons for the equal imaging intensity is unclear, but for efficient FRET to occur, molecules need to be precisely positioned and arranged. It is possible that the lack of reduced **Cy3** fluorescence as anticipated is related to discrepancies in compound solubility, stacking, or potentially self-quenching.[340] These can all manifest into a weak FRET efficiency, resulting in an inability to visualise the difference via imaging alone.

Importantly, the absence of co-localisation between the constructs and Hoechst nuclear stain is clear, and calculated Pearson's coefficients between the cyanine compounds and Hoechst stain respectively range between -0.055 to 0.145. Pearson's coefficient scores range from 0 to 1, 0 being no co-localisation and 1 being absolute co-localisation.[353] These low scores illustrate

the compounds inabilities to cross the intact nuclear membrane to bind to negatively charged DNA; findings that are consistent with the literature.[291, 337, 344]

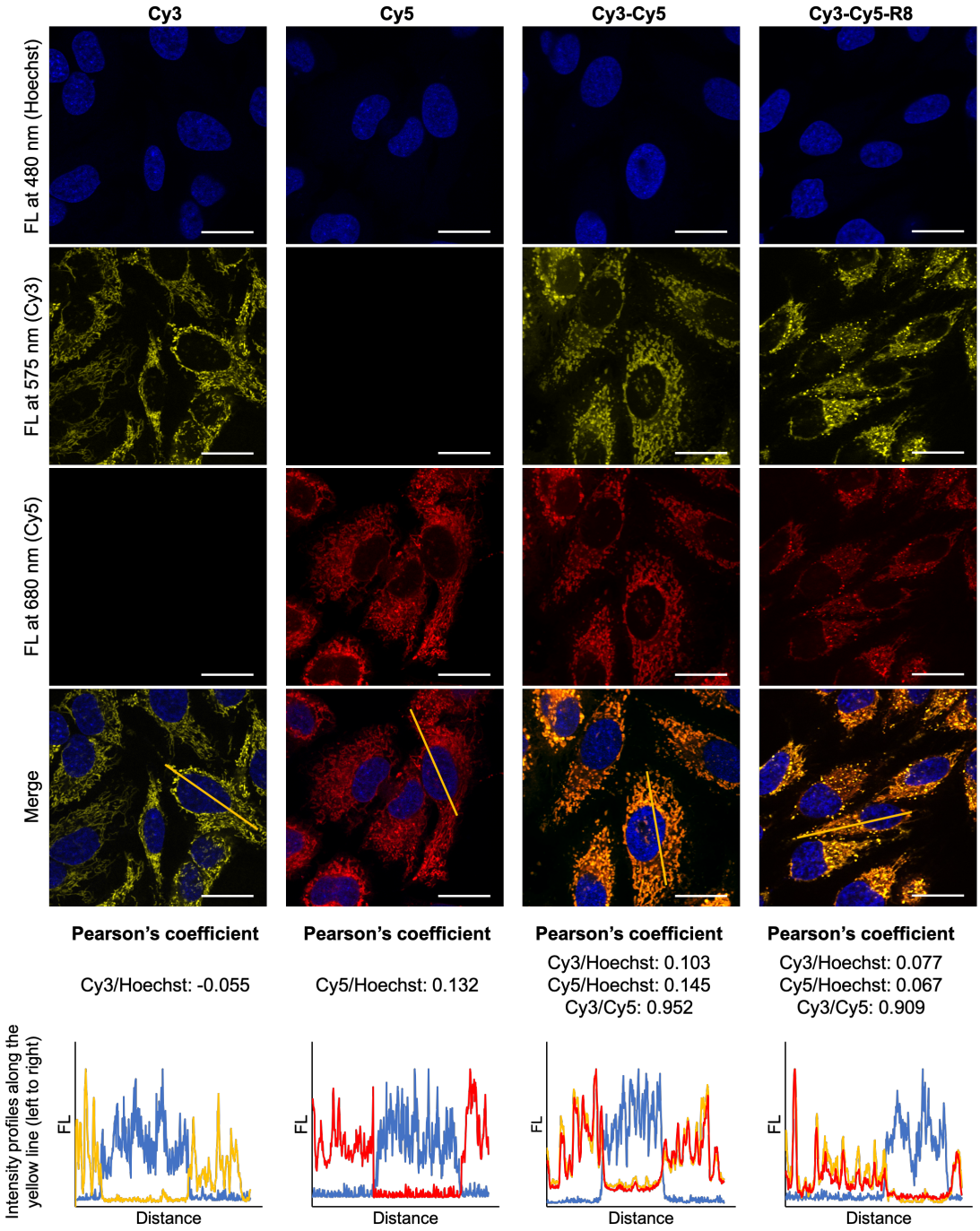

Figure 2.7: Cellular localisation of the cyanine dye constructs described *HeLa cells were treated with 10 μM **Cy3**, **Cy5**, **Cy3-Cy5** or **Cy3-Cy5-R8** at 37 °C for 1 h before staining the nucleus with Hoechst and imaging. Pearson's correlation coefficients for **Cy3** or **Cy5** with Hoechst are detailed and fluorescence profiles show fluorescence readings across the drawn yellow line profile. Scale bars denote 25 μm. Representative (N = 10) confocal microscopy images are shown here.*

For the two conjugate compounds **Cy3-Cy5** and **Cy3-Cy5-R8**, Pearson's co-localisation co-efficient between **Cy3** and **Cy5** fluorescence were 0.952 and 0.909 respectively, and fluorescence intensity graphs show a consistent fluorescence pattern between the two channels, corroborating the Pearson's colocalisation readings. The **Cy3-Cy5-R8** observations are a counteraction of *Ross et al.*'s findings which stated that cell penetrating peptides are incapable of crossing the mitochondrial membrane regardless of conjugation to a lipophilic cation.[344] Indeed, the study was conducted using CPPs Tat (HIV-1 derivative), and Penetratin (Antennapedia homo-protein derivative) which have relatively similar amino acid sequences compared to R8 and nearly identical charged states.[354] However, using TPP (triphenolphosphonium) as a lipophilic cation is a noteable discrepancy. Comparing this to **Figure 2.7**, there remains the suggestion that results cannot be directly compared to *Ross et al.*, therefore the accuracy of the statement should be determined by the combination of lipophilic cation and CPP employed. Another report concluded that **Cy5** conjugation alone to R8 is not capable of tracking to the mitochondria,[342] but the conjugated cationic molecules used in **Figure 2.7** have a higher charge with the addition of **Cy3**, which potentially permits mitochondrial delivery.

Along with mitochondrial staining patterns with **Cy3-Cy5-R8** treatment, notably there was further staining reminiscent of endosomes (small vesicular structures in the cytoplasm). As an endocytosis-dependent moiety,[354] it is plausible that R8 may divert the mode of entry from the dyes favoured transduction pathway, engaging in an R8-mediated endocytosis pathway.

To confirm the suggested mitochondrial-selective staining, co-localisation studies of the constructs with MitoTracker Green were performed (**Figure 2.8**). **Cy3** and **Cy5** had Pearson's coefficients with MitoTracker Green of 0.863 and 0.877 respectively, supporting the understanding that these dyes selectively stain cellular mitochondria. However, performing the same experimental procedure with the conjugated **Cy3-Cy5** or **Cy-Cy5-R8** was less informative.

Cy3-Cy5-R8 had Pearson's coefficients with MitoTracker of 0.418 and 0.601 for **Cy3** or **Cy5** fluorescence, values much lower than that of the unconjugated **Cy3** or **Cy5** compounds. Moreover, it is clear from the imaging that the mitochondrial structures remain intact, however they are mostly either stained with **Cy3-Cy5-R8**, or MitoTracker Green with minimal evidence of co-staining. It is noteworthy to highlight the likely deviation in cell-entry mechanisms used by MitoTracker Green or **Cy3-Cy5-R8**. With MitoTracker Green entering a cell by endocytosis-independent transduction, and **Cy3-Cy5-R8** suggested to be endocytosis-dependent, the colocalisation values will be impacted by the presence of endosomes solely containing **Cy3-Cy5-R8**.

Interestingly, **Cy3-Cy5** co-treatment with MitoTracker Green showed dye aggregation and no mitochondrial staining; with low Pearson's coefficients of 0.449 and 0.593 for **Cy3** or **Cy5** fluorescence with MitoTracker. As this was unexpected, it was worthy to alter the procedure to test different processes of compound treatment (**Figure 2.9a-b**). The rearrangement of treatment-order aimed to resolve this observation, however negligible improvement in staining pattern and Pearson's coefficients were detected. As a control, cells were co-stained with unconjugated **Cy3** + **Cy5** and MitoTracker Green. This lead to an increased Pearson's co-efficient of 0.758 and 0.837, and distinctive mitochondrial staining patterns were observed (**Figure 2.9c**). This control demonstrated that the three dyes are capable of co-localising within a single cell, therefore the observed aggregation and poor co-localisation between **Cy3-Cy5** and MitoTracker is unclear. It could potentially be caused by an exposed amine group on the **Cy3-Cy5** conjugating link reacting with Cl groups on MitoTracker, however this was not investigated further as it exceeded the scope of the project.

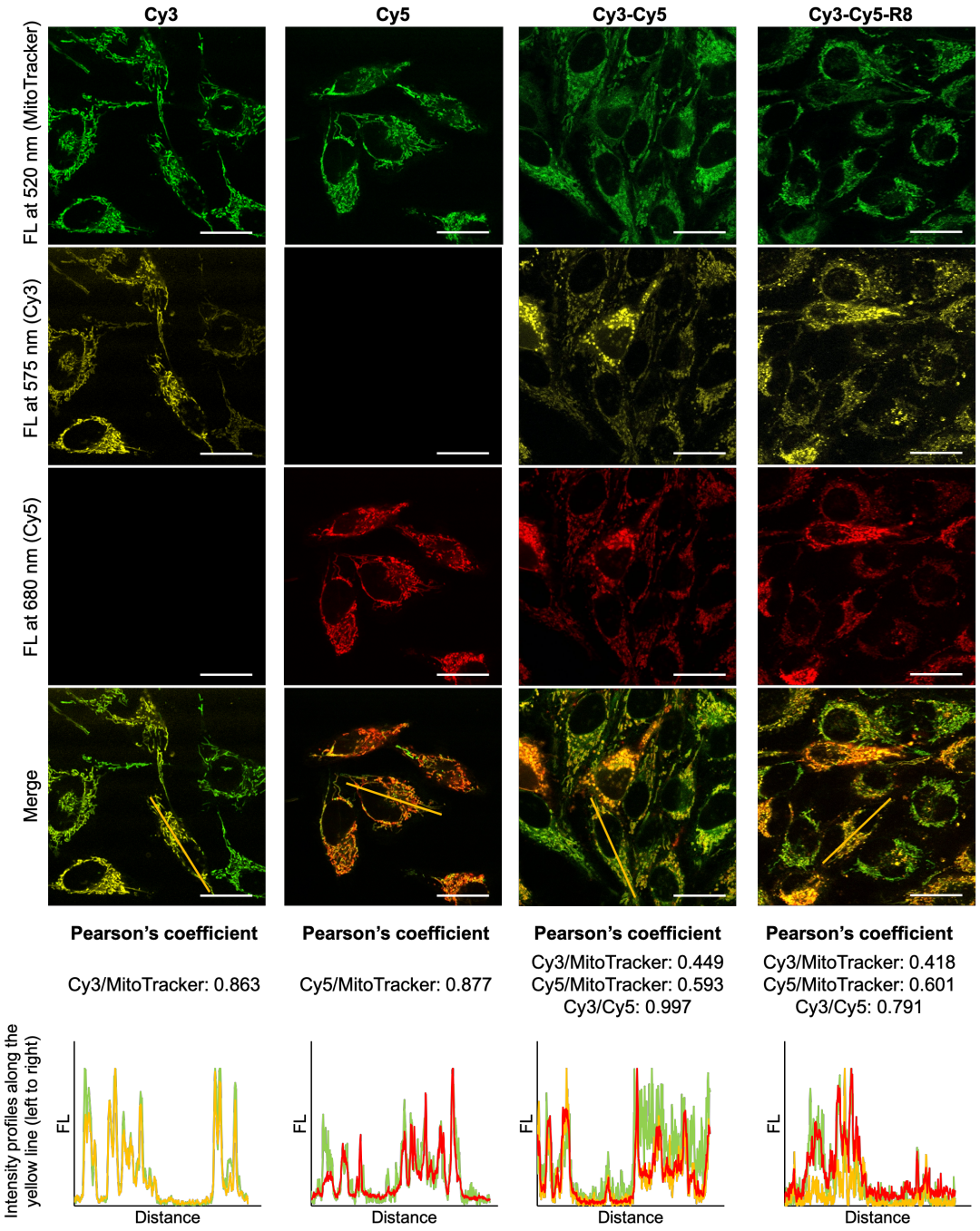

Figure 2.8: Mitochondrial localization of Cy3 and Cy5 with MitoTracker Green
*HeLa cells were treated with 10 μM **Cy3** or **Cy5** at 37 °C for 1 h before staining the mitochondria with 20 nM MitoTracker Green and imaging. Pearson's correlation coefficients for **Cy3** or **Cy5** with MitoTracker are 0.863 and 0.877, respectively. Excitation wavelength for MitoTracker Green, Cy3, and Cy5 is 488, 543, and 633 nm, respectively. Scale bars denote 25 μm. Representative (N = 10) confocal microscopy images are shown here.*

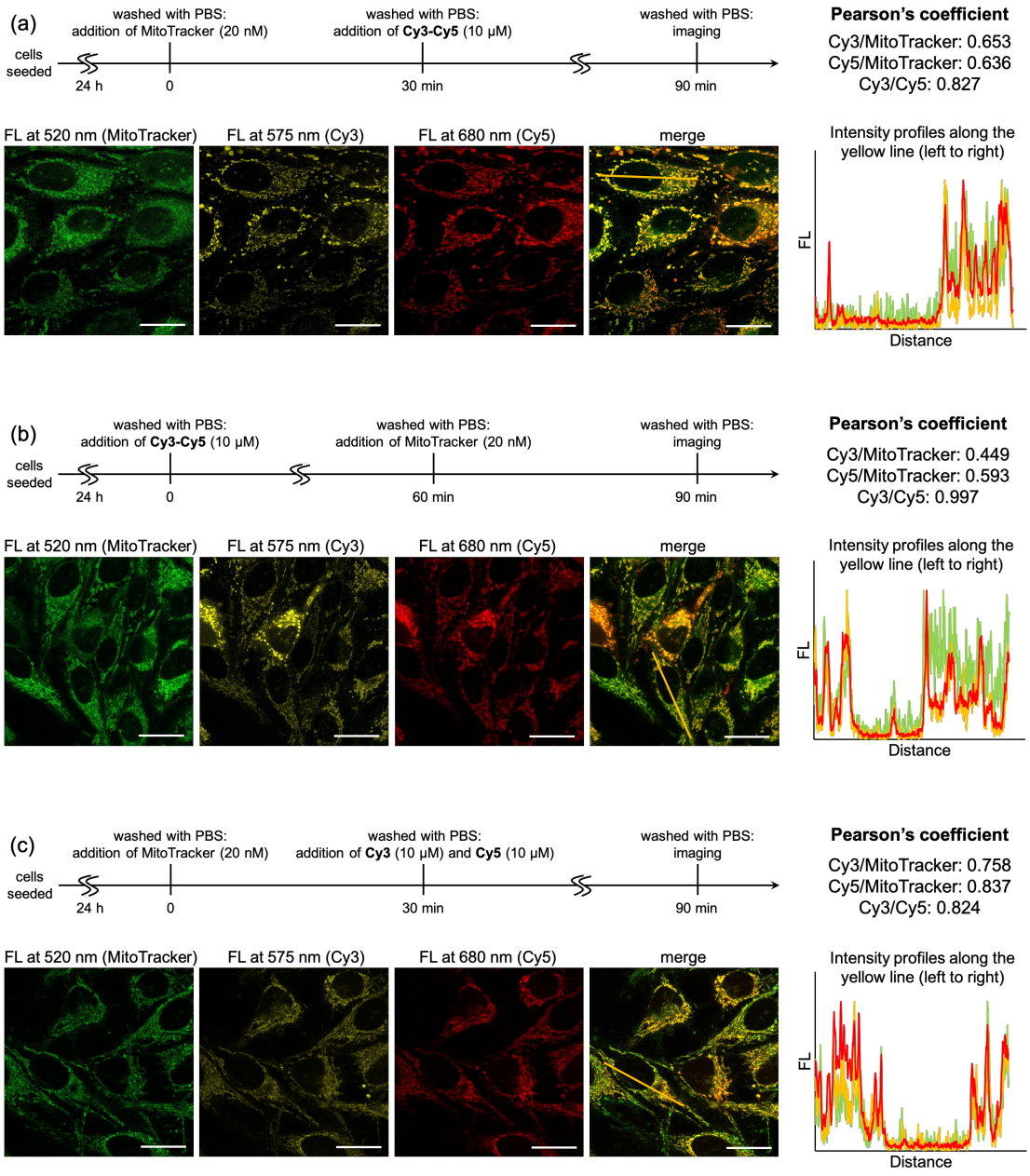

Figure 2.9: Colocalization of Cy3-Cy5 or Cy3-Cy5-R8 with MitoTracker Green in HeLa *(**a**) Cells were treated with 20 nM MitoTracker for 30 min in serum free DMEM, followed by incubation with 10 μM **Cy3-Cy5** in serum free DMEM for 1 h before imaging. (**b**) Same as (**a**) except cells were incubated with **Cy3-Cy5** first, followed by treatment with MitoTracker. (**c**) Same as (**b**) except a mixture of **Cy3** and **Cy5** was used instead of **Cy3-Cy5**. (**d**) Same as (**b**) except **Cy3-Cy5-R8** was used instead of **Cy3-Cy5**. Excitation wavelength for MitoTracker Green, Cy3, and Cy5 is 488, 543, and 633 nm, respectively. Scale bars denote 25 μm. Representative (N = 10) confocal microscopy images are shown here.*

2.3 Construct uptake mechanisms

After characterising the mitochondrial targeting of **Cy3**, **Cy5**, **Cy3-Cy5** and **Cy3-Cy5-R8**, identifying crucial external factors that may influence the habitual activities of the dyes was a necessity. Deciphering the dependencies of the constructs and external influential factors required for mitochondrial staining is critical to understanding their mode of action, and identifying limitations that could hinder their use as mitochondrial drug-delivery vehicles. This section explores a range of important fundamental conditions and establishes the construct behaviours within each. It investigates mitochondrial staining efficiencies across treatment-concentration variation, the influence of serum presence, staining characteristics during mitochondrial membrane potential disruption, and construct mitochondrial staining patterns during endocytosis inhibition.

2.3.1 Concentration dependent uptake

Concentration dependence is a beneficial aspect of pharmaceutical drugs as it enables tailored treatments and temporal control to aid alleviation of side effects. For example, if a patient receiving drug treatment begins to exhibit symptoms of non-selective drug activity, or the side effects are presenting at a high severity, the ability to reduce the treatment concentration of that drug and it still retain its function facilitates the omission of symptoms, while retaining a level of drug effect. Therefore, it was important to determine whether the mitochondrial targeting specificity of the constructs can be retained across a range of concentrations, as this in turn supports their feasibility as mitochondrial drug delivery entities.

To investigate this, HeLa cells were treated with 10 μM, 2.5 μM or 1 μM **Cy3**, **Cy5**, **Cy3-Cy5** or **Cy3-Cy5-R8** respectively in serum free media at 37 °C 5% CO_2 atmosphere for 1 h. Prior to imaging, cells were washed with PBS and incubated with Hoechst 33258 nuclear stain for 10 minutes. Confocal

assessment of construct localisation revealed clear concentration-dependent fluorescent staining (**Figures 2.10** and **2.11**). All four constructs displayed a clear positive correlation between fluorescence intensity and concentration of treatment, with 10 μM the clearest for detailed fluorescent imaging. These results are consistent with previous research.[291, 342, 344, 355]

Interestingly, when the concentration of **Cy3-Cy5-R8** specifically is reduced from 10 μM to 2.5 μM, there is a marked reduction in mitochondrial staining pattern, with the most prominent fluorescent entities appearing to be endosomal structures. Endosomes are cytosolic membrane-bound vesicles which are involved in intracellular transport, and are described as small rounded entities approximately 0.5 μm in diameter.[143] The fluorescence pattern of **Cy3-Cy5-R8** at 2.5 μM gives potential insight into its mode of entry, suggesting the construct is endocytosis dependent. It is unclear however, whether **Cy3-Cy5-R8** is capable of using its **Cy3-Cy5** moieties as an endosomal escape unit once inside the cell cytoplasm, or whether the **Cy3-Cy5** moiety promotes endocytosis-independent uptake of the conjugated CPP at higher concentrations.

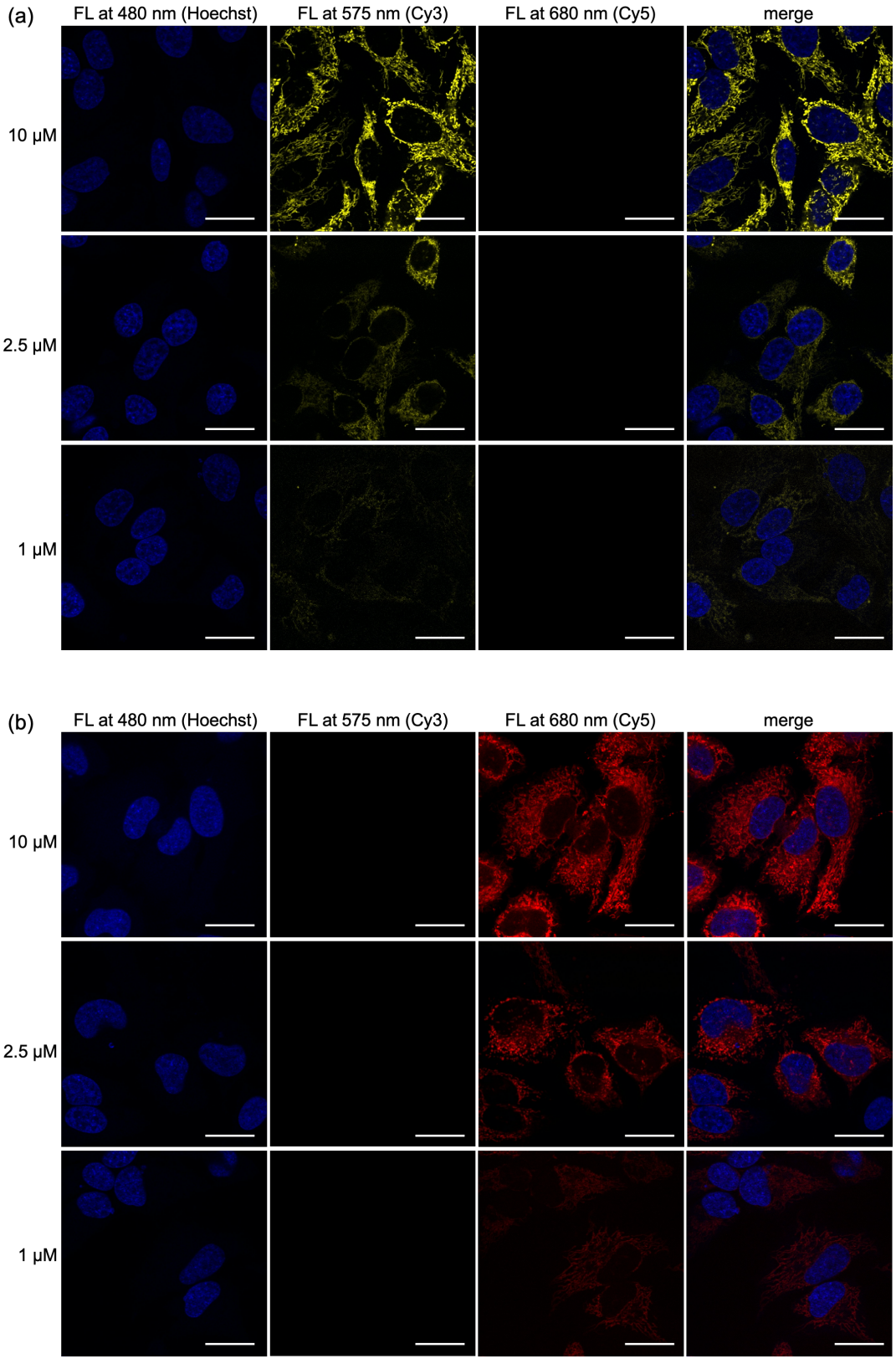

Figure 2.10: Concentration-dependent cellular uptake of Cy3 and Cy5
*(**a**) **Cy3** concentration-dependent uptake. (**b**) **Cy5** concentration-dependent uptake. Scale bars denote 25 µm. Representative (N = 10) confocal microscopy images are shown here.*

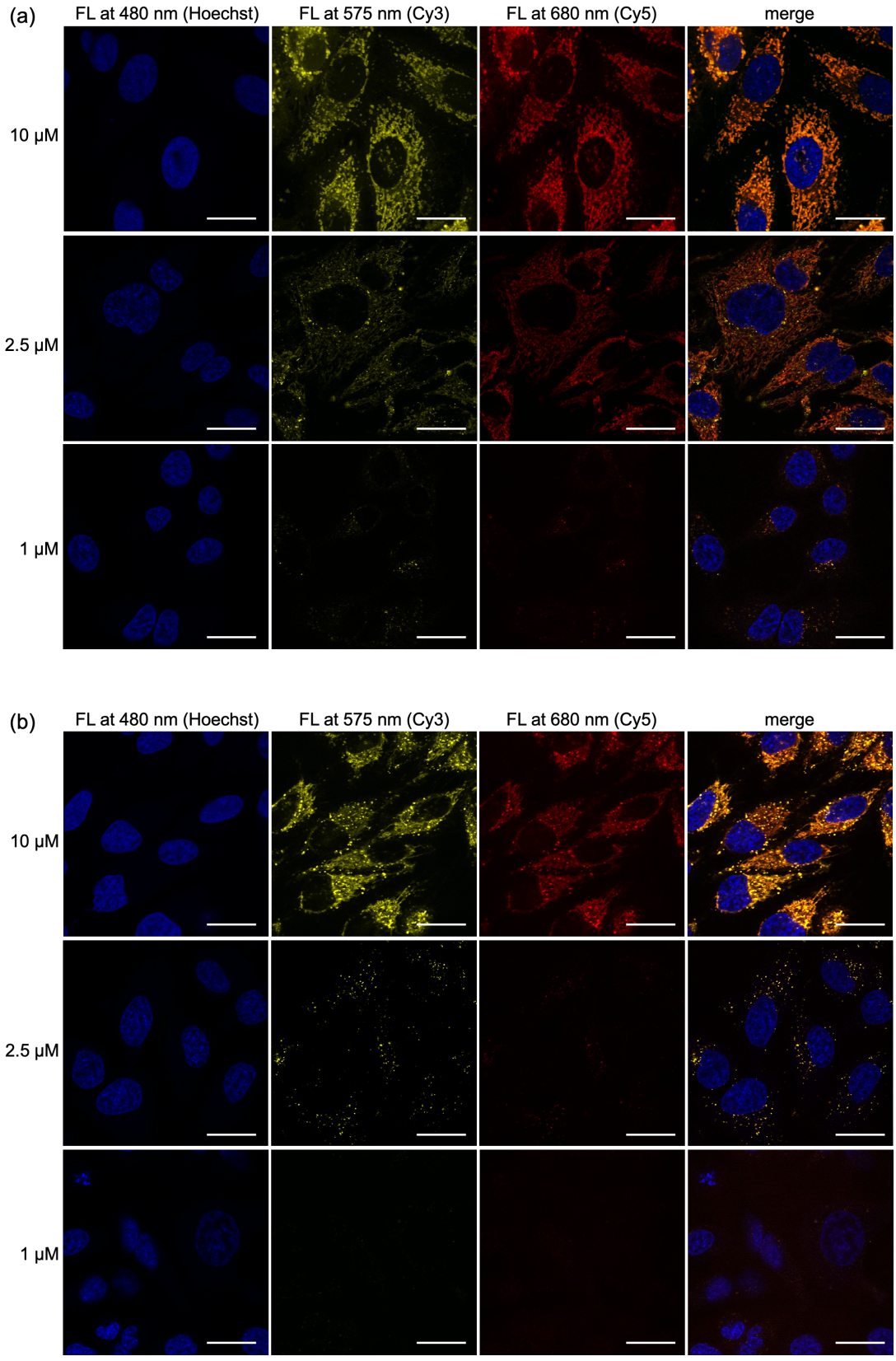

Figure 2.11: Concentration-dependent cellular uptake of Cy3-Cy5 and Cy3-Cy5-R8
*(**a**) **Cy3-Cy5** concentration dependent uptake. (**b**) **Cy3-Cy5-R8** concentration dependent uptake. Scale bars 25 μm. Representative (N = 10) confocal microscopy images are shown here.*

2.3.2 Serum dependent uptake

To be used as drug cargo delivery vehicles, it is necessary that the compound's behaviours are not hindered by the presence of serum. Foetal Bovine Serum (FBS) is a commonly employed supplement to recreate the natural extracellular environment within *in vitro* settings.[356] Containing a mixture of nutrient molecules, natural proteins and amino acids, a 10% v/v supplementation of FBS is commonly used to assess the potential behaviours of a compound *in vivo*. HeLa cells were treated with 10 μM **Cy3**, **Cy5**, **Cy3-Cy5**, or **Cy3-Cy5-R8** respectively in media supplemented with 10% v/v FBS at 37 °C 5% CO_2 atmosphere for 1 h. Prior to imaging, cells were washed with PBS and incubated with Hoechst 33258 nuclear stain for 10 minutes (**Figure 2.12**). The fluorescence of **Cy3**, **Cy5** and **Cy3-Cy5** were found to be unaffected by 10% FBS media supplementation during treatment, with no visible deviation in the staining pattern or fluorescence intensity compared to those observed in **Figure 2.7**. However, there is a clear decrease in the fluorescence intensity of **Cy3-Cy5-R8** under 10% FBS media conditions compared to that observed in a serum-free environment.

Serum proteins have been shown to hinder the efficiencies of CPP molecules,[354, 357] mostly linked to the presence of serum albumin and enzymes. Serum albumin is the most abundant protein found in blood plasma, accounting for approximately 50% of all serum proteins. Albumin is responsible for transportation of hormones, fatty acids, and a plethora of other compounds due to its monomeric design.[123, 358] As a charged peptide, it is not surprising that R8 has "sticky tendencies". It is clear from **Figure 2.12** that serum in the media during treatment reduces **Cy3-Cy5-R8** uptake, and it is plausible that electrostatic interactions occurring between the conjugate and albumin or other serum proteins caused a reduced delivery of **Cy3-Cy5-R8** to the cells.

The propensity for **Cy3-Cy5-R8** to have a markedly reduced efficiency in the presence of serum is a concern for its translation into a pharmaceutical setting.

It could consequently entail a demand for higher treatment concentration to establish a comparable availability of treatment to the tissues. Additionally, given its suggested interactions with serum proteins that are not comprehensively understood, a substantial risk of side effects developing is presented. An interesting murine study using Cy7-derivatives as cancer targeting entities suggested albumin as a critical component for cancer cell retention, however the structures of the molecules used in the report carried many discrepancies compared to the molecules in this study, and the authors deemed the presence of a Cl residue responsible for the interaction with albumin;[359] a residue that is not included in the structures used here. Moreover, an explanation for the specific interactions of serum with R8 and not the other dye molecules is unclear as all are positively charged. Nevertheless, the interactivity may be dependent on the charged arginine residues on **Cy3-Cy5-R8** specifically.

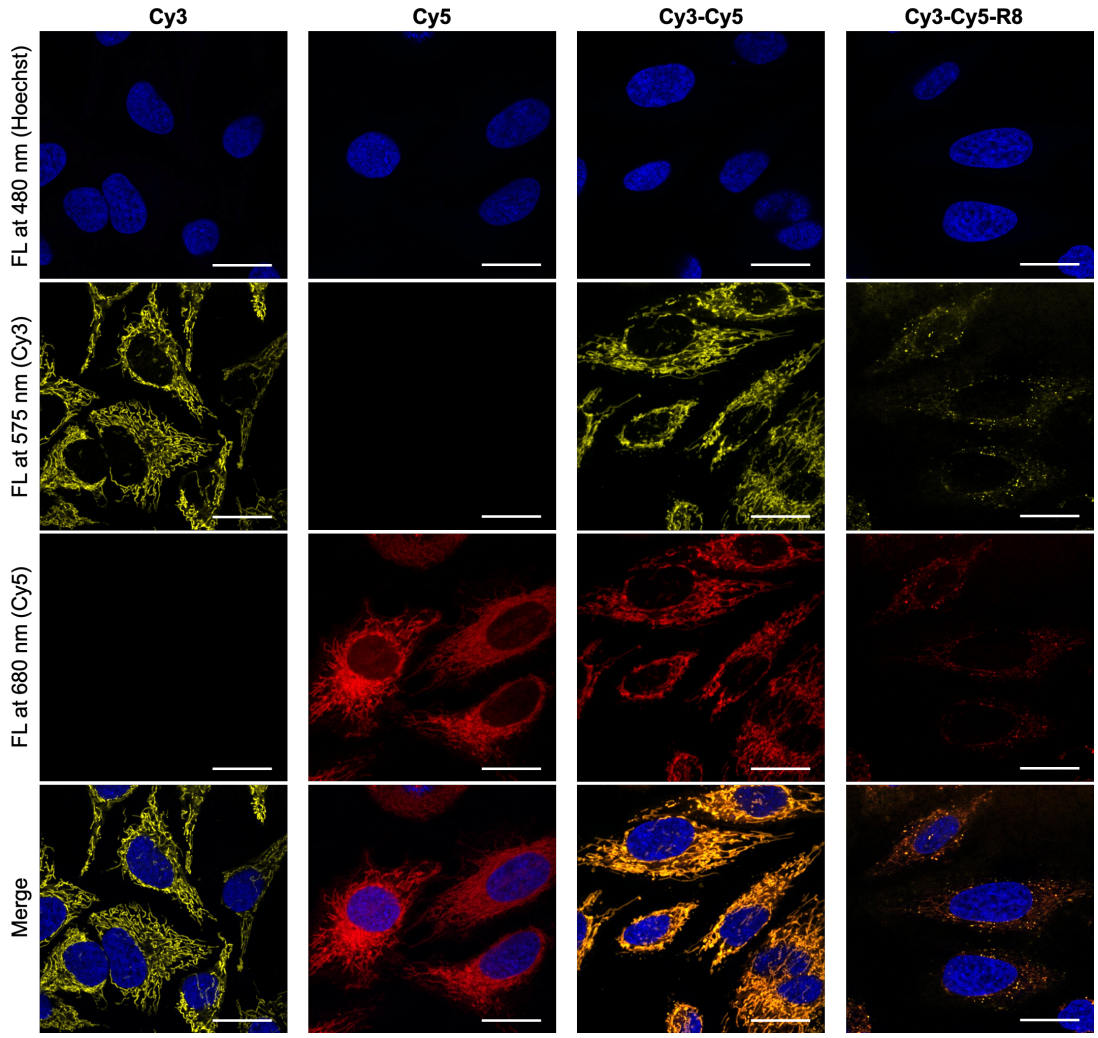

Figure 2.12: Presence of serum in growth media and its impact on uptake of constructs *Representative (N = 10) confocal microscopy images of HeLa cells treated with 10 μM of* ***Cy3****,* ***Cy5****,* ***Cy3-Cy5*** *or* ***Cy3-Cy5-R8*** *in presence of 10% serum at 37 °C for 1 h before imaging. Scale bars denote 25 μm.*

2.3.3 Mitochondrial membrane potential dependence

Mitochondrial membrane potential (MMP) is a charge generated by proton pumps along the mitochondrial membrane.[287, 292] MMP is crucial for the storage and generation of cellular energy, where the production of a proton gradient facilitates the production of ATP. Changes in the MMP of mitochondria can be linked to cell death, homeostatic dysfunction, and is a common observation in cancer cells.[34, 168, 300] Cancer cells typically have a higher MMP than their healthy counterparts, and this has been linked to their alternative approach to energy production and storage to promote cell survival under hypoxic conditions.[24, 34, 168, 169] It is subsequently crucial to characterise

the cyanine dye constructs' dependability on MMP, and identify whether MMP disruption has an effect on their targeting behaviours. It has been shown previously that cyanine dyes are typically MMP dependent,[328] but other compounds studied have structural differences compared to the compounds used here, so it was deduced as important to establish whether this statement applies to the compounds being investigated in this project specifically.

For this proof of principle approach, the experiments were focussed on the activity of **Cy3** specifically. As the simplest molecule of the compounds used, and the main investigative vehicle for drug delivery cargo in later studies, it was deemed the most important molecule to investigate MMP dependence. The MMP disruption agent used was CCCP (Carbonyl cyanide m-chlorophenyl hydrazine) which is an established MMP-disruption inducing drug.[287] CCCP causes uncoupling of the proton gradient present across the mitochondrial membrane by inhibition of the electron transport chain. Acting as an ionophore, it inhibits the proton gradient and reduces the functionality of ATP synthetase. HeLa cells were treated with 10 μM **Cy3** in serum-free media at 37 °C 5% CO_2 atmosphere for 1 h. Cells were then washed with PBS and incubated with Hoechst 33258 nuclear stain for 10 minutes as an imaging control prior to treatment with 20 μM CCCP. **Cy3** staining was evaluated over a 6-minute period of CCCP treatment, then a 10 minute and 60-minute interval after CCCP removal (**Figure 2.13a**).

Upon CCCP treatment, a clear loss of mitochondrial filamentous staining was observed, where the dye appeared to "bleed" into the cellular cytoplasm and overall staining pattern represented a smudged appearance. This deduces that **Cy3** used here is dependent on MMP, as the mitochondria specific staining is lost once the MMP is disrupted. CCCP was then removed and cells washed to assess whether the dye would track back to the mitochondria once MMP is re-established. Cells were imaged at 10 minutes and 60 minutes post-CCCP removal. At 10 minutes, there is a definitive staining pattern reminiscent

of what was observed during CCCP treatment. This is likely due to the inability for a membrane potential to be re-established within the 10-minute timeframe.

Interestingly however, after 60 minutes of incubation post-CCCP removal, MMP has had sufficient time to recover and mitochondrial staining is re-established. This is in line with previous studies using similar molecules, and corroborates the literature representation. Overall this supports the understanding of the dependence of cyanine dyes on mitochondrial membrane potential, but has also highlighted that the mitochondrial staining can be re-established once the MMP has returned.

The evidence in **Figure 2.13b** is supportive of the theory that simple cyanine dyes do not irreversibly bind to the mitochondria, a process that is common in most commercial mitochondria stains.[287, 288] As a result, it was important to perform cell fixing studies on cells treated with **Cy3**, as it would help determine whether the dyes form a permanent or semi-permanent interaction with the mitochondria themselves. Cell fixation is a process involving the treatment of cells with a fixing agent, typically paraformaldehyde. The process kills the cells, but importantly retains all cellular structures. Cell fixing importantly removes all membrane potentials in the cells (as they are no longer living). MitoTracker has been widely understood to bond covalently to mitochondrial membrane proteins,[287, 336] therefore fixing cells after MitoTracker treatments does not alter the staining pattern as the dyes are permanently bound to the structures.

HeLa cells were treated with MitoTracker, and then co-treated with **Cy3** at 10 μM. Cells were imaged before and after fixing, and Pearson's coefficients calculated under both conditions (**Figure 2.13b**). Prior to cell fixing, MitoTracker and **Cy3** co-localised as expected, with clear mitochondrial staining and a Pearson's coefficient of 0.863. After fixation, however, there is an evident shift in staining pattern of **Cy3**. Resembling staining observed during CCCP treatment, **Cy3** appears to bleed into the surrounding cellular

space and distinctive mitochondrial staining patterns are lost (**Figure 2.13b**). This resulted in a substantial reduction in the Pearson's co-efficient value that came to 0.379 after cell fixing. Overall these experiments have determined the importance and reversible dependence of cyanine dyes on MMP.

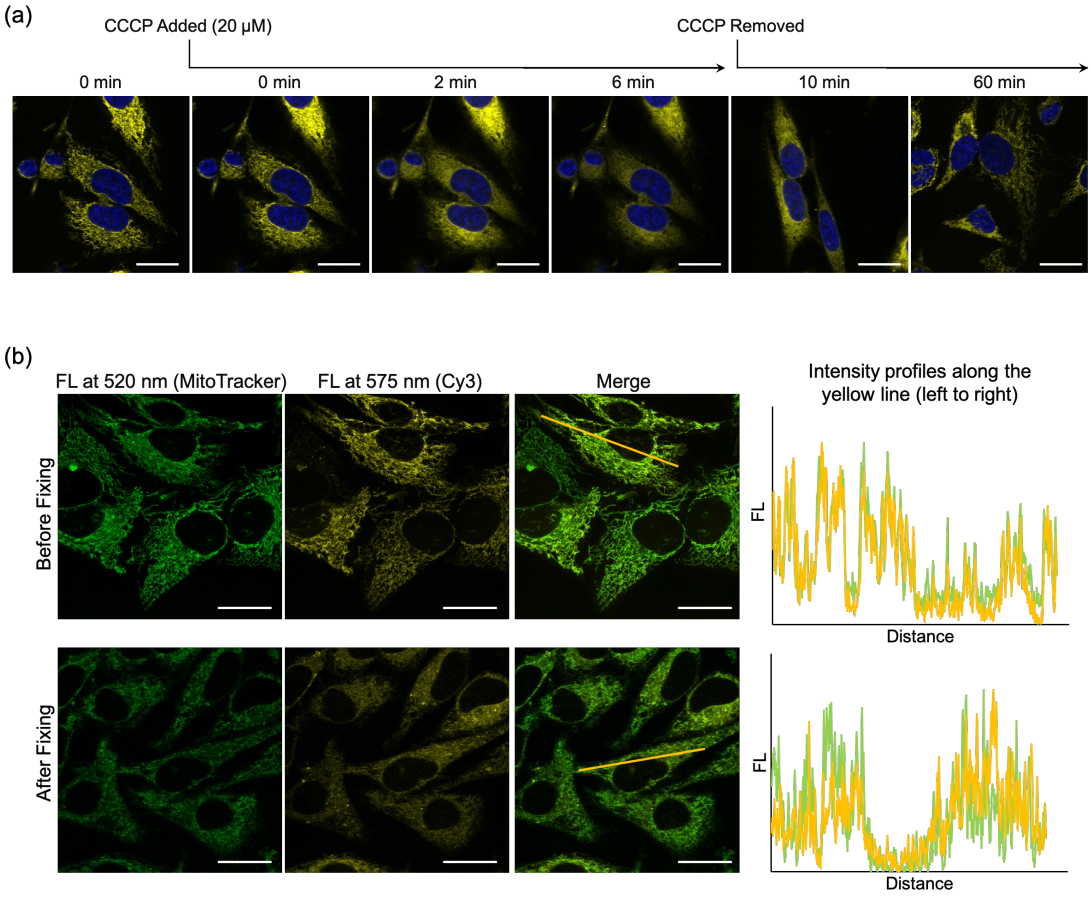

Figure 2.13: Influence of mitochondrial membrane potential on construct localisation
*(**a**) Confocal analysis of HeLa cells stained with **Cy3** during mitochondrial depolarisation with 20 µM CCCP treatment over a 6-minute period. Further imaging of HeLa cells 10 and 60 minutes after CCCP removal. (**b**) Before and after cell fixing with paraformaldyhide treatment. Scale bars denote 25 µm.*

2.3.4 Endocytosis dependent uptake

Endocytosis is a process by which cells take up molecules from their extracellular environment. The term endocytosis is broad, encompassing a wide range of mechanisms, but the general process involves invagination of a cargo via the cell membrane and subsequent generation of membrane-bound vesicles (**Figure 2.14**). The entry of a molecule into a cell can be strictly

endocytosis-dependent, strictly endocytosis-independent, or a mixture of both; attributed to their biological properties, size and charge. Smaller charged molecules tend to be directly transduced across the membrane due to interactions-with and the biochemical-properties-of the lipid bilayer, whereas larger or uncharged compounds rely on endocytosis pathways to enter a cell. CPPs are designed to promote endocytosis by interacting with cell surface proteins and thus promoting internalisation in an endocytosis dependent manner.

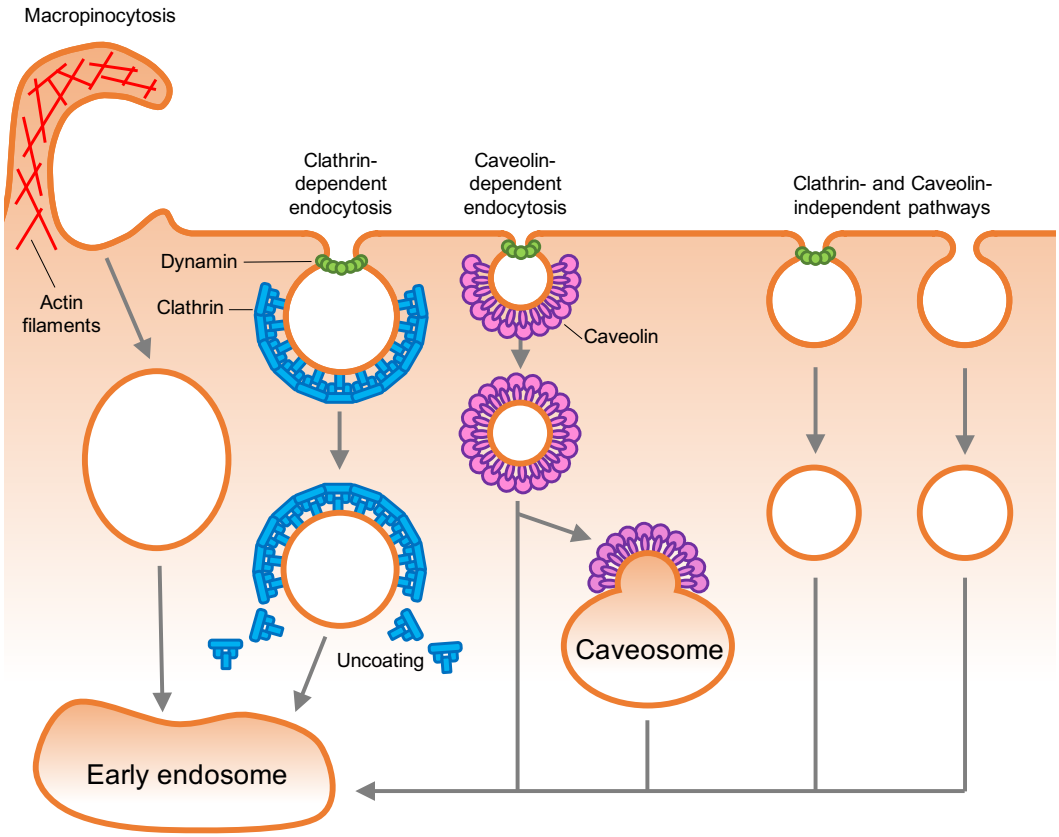

Figure 2.14: Various mechanisms of how mammalian cells endocytose molecules
Mechanisms can be dependent or independent of clathrin or caveolin proteins, and enter various phases of maturation once in the intracellular environment.

Regarding the potential mechanism of **Cy3-Cy5-R8** cell-entry, the observations so far not been clear-cut, and it was crucial to identify the effects of endocytosis inhibition on the constructs in this project. Cancer cells have been known to be selective about what molecules they intake, with an

astonishing ability to fine-tune their endocytic pathways to avoid delivery of drugs and other toxic substances.[142] Drugs that are not reliant on endocytic pathways and enter via passive diffusion (transcellular or paracellular) are typically more effective in the treatment of cancers as the cells are limited in the mechanisms or approaches they can adapt to evade drug delivery and uptake.

There are many drugs that are used to disrupt endocytosis, but they typically inhibit a particular branch of endocytic pathways, and have a plethora of underlying influences on general cellular behaviour. Considering this, the results cannot be accurately representative of a selective endocytosis halt. A common approach that is arguably the most accurate in specifically inhibiting all endocytic pathways is incubation of cells at 4 °C for a short period of time. This cold shock therapy slows the metabolic rate of the cells, and prevents temperature-dependent mechanisms from occurring. As vesicle-fusion events are temperature-dependent processes, they cannot occur at cold temperatures, therefore endosomes cannot be formed during 4 °C incubation.[360] Of course, cells are unable to survive at 4 °C for a prolonged period of time, but cold shock therapy is a commonly-used and effective method to inhibit endocytosis for a short period of time, while maintaining live cells.[361]

HeLa cells were pre-chilled to 4 °C for 10 minutes prior to treatment with 10 μM or 2.5 μM of **Cy3, Cy5, Cy3-Cy5** or **Cy3-Cy5-R8** respectively for a further 10 minutes prior to imaging. Confocal imaging concluded the prediction that **Cy3**, **Cy5** and **Cy3-Cy5** were all capable of staining mitochondrial structures at 10 μM or 2.5 μM (**Figure 2.15**), with fluorescence intensity and pattern indistinguishable from that of incubation at 37 °C (**Figure 2.16**).

The staining observed for **Cy3-Cy5-R8** however was interesting. At the higher concentration of 10 μM, cells display intracellular mitochondria-like staining, but presented with large aggregates around the cell membrane (**Figure 2.15**).

However, at the lower concentration of 2.5 μM, no fluorescence is detected at all. Intriguingly, this points to the possibility of **Cy3-Cy5-R8** being able to undergo endocytosis-dependent and endocytosis-independent uptake. The presence of aggregates around the cell membrane suggests binding of **Cy3-Cy5-R8** to lipid rafts on the cell surface, but inhibition of endocytosis results in a halt of transport at the outer membrane after binding. Nonetheless, it is interesting that a lower concentration sees no staining at all, and there are a few potential explanations for these findings. It is possible that, under higher concentrations, the conjugate is at a concentration where it can over-saturate the cell's lipid bilayer, forcing transduction of some **Cy3-Cy5-R8** through the membrane into the cytoplasm where it subsequently engages with mitochondria. But this explanation would predictably result in a weakened fluorescence of **Cy3** or **Cy5** compared to the other compounds, which is not the case. Therefore, it may suggest that at lower concentrations the compound is solely dependent on endocytosis, but at higher concentrations it can enforce both endocytosis-dependent and endocytosis-independent pathways. This theory is corroborated by the results in **Figure 2.11**, where treatment of cells with **Cy3-Cy5-R8** at 2.5 μM saw only endosomal structures, and treatment at 10 μM saw mitochondrial staining alongside endosomes. Nevertheless, the results in **Figure 2.15** and **Figure 2.16** clearly demonstrate that **Cy3**, **Cy5**, and **Cy3-Cy5** are strictly endocytosis-independent, whereas **Cy3-Cy5-R8** remains dependent on a combination of the two; depending on the level of construct crowding at the cellular membrane.

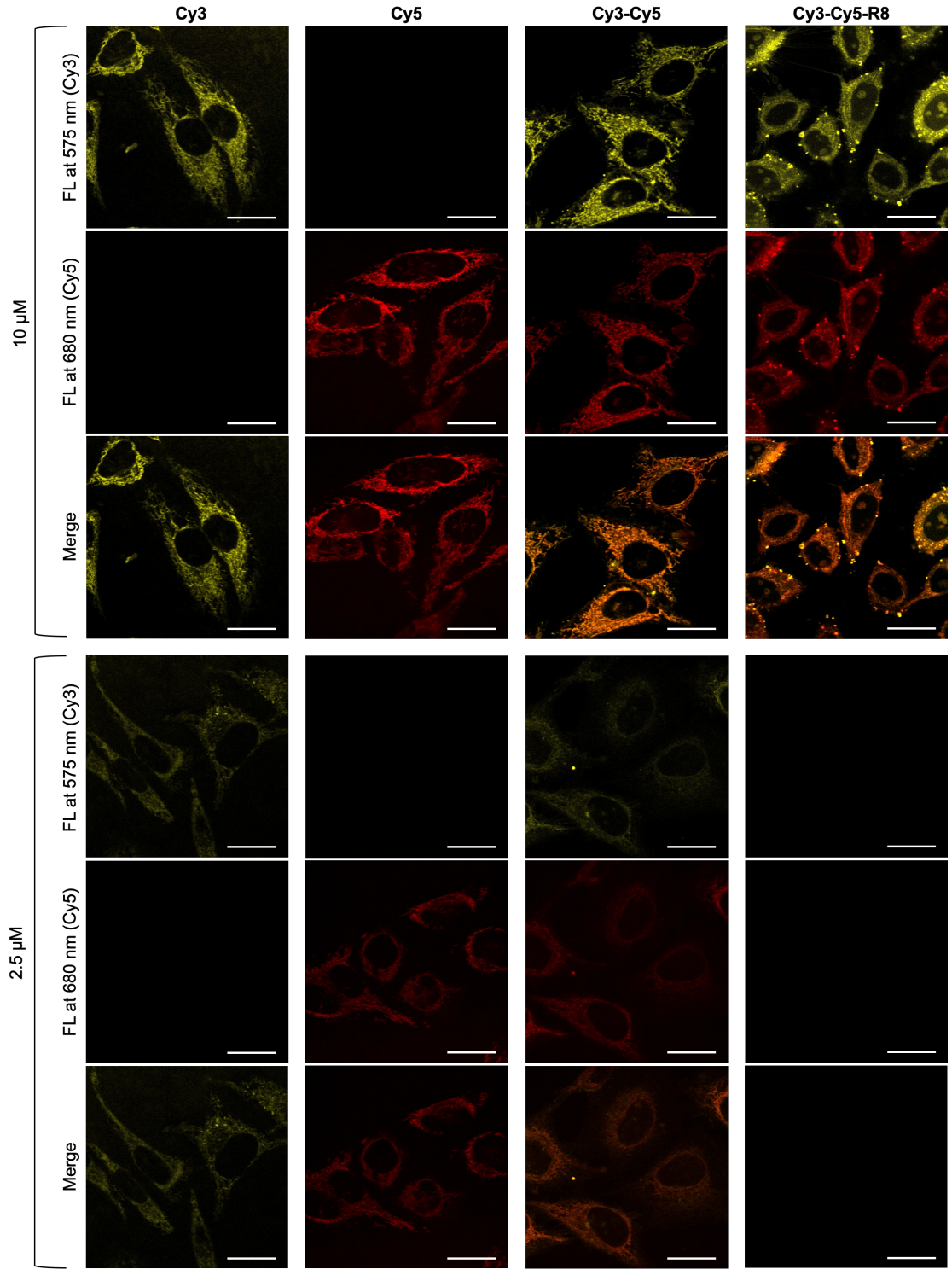

Figure 2.15: Concentration-dependent cellular uptake of constructs at 4 °C incubation
HeLa cells were incubated in pre-chilled media at 4 °C for 10 min before addition of the indicated compound at either 10 µM or 2.5 µM. Cells were incubated at 4 °C for another 10 min before imaging. Scale bars denote 25 µm. Representative (N = 10) confocal microscopy images are shown here.

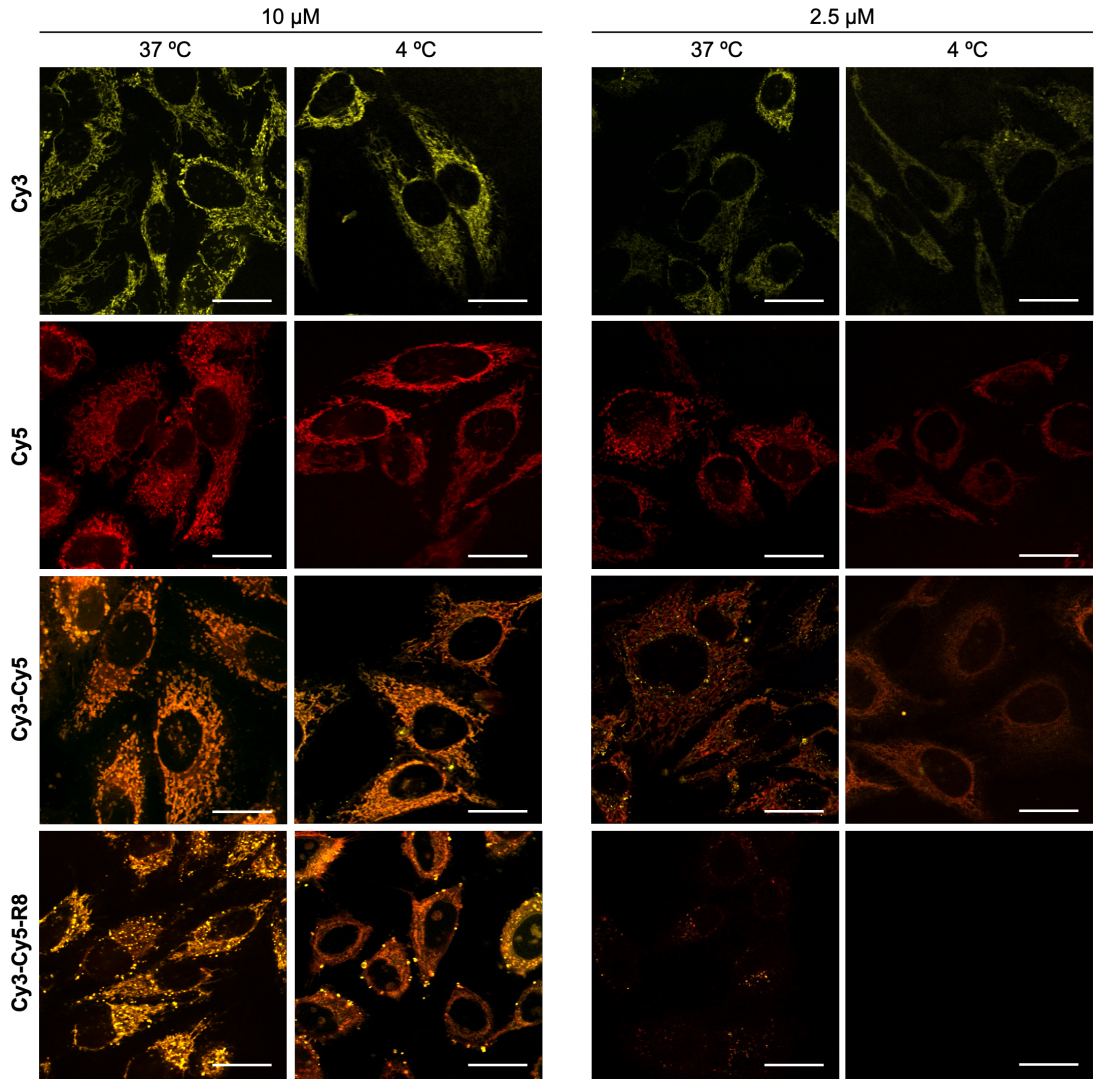

Figure 2.16: Concentration-dependent cellular uptake of constructs at 4 °C and 37 °C. *HeLa cells were incubated in pre-chilled media at 4 °C for 10 min before addition of the indicated compound at either 10 μM or 2.5 μM for 10 min incubation before imaging. For 37 °C, HeLa cells were incubated with the indicated compound for 1 h before imaging. All images merges of Cy3 and Cy5 recorded fluorescence. Scale bars denote 25 μm.*

2.4 Cyanine Dyes as drug delivery systems

Prior to testing cyanine dyes as drug delivery vehicles, characterisation of their activities was crucial to establish their sustainability and viability for such a role. From the experiments detailed so far, it was clear that the simplest cyanine dyes **Cy3** and **Cy5** were able to consistently track to mitochondria under most external pressures (excluding MMP disruption). The theory was that the conjugated **Cy3-Cy5** or **Cy3-Cy5-R8** would result in a higher targeting ability due to their increased charge, however this didn't appear to be the case with negligible improvement in fluorescence intensity (**Figure 2.7**). Moreover, the use of multiple dyes in a single molecule may entail a higher propensity for aggregation, therefore, it was deduced to focus on the simple **Cy3** and **Cy5** as targeted delivery vehicles for mitochondrial-toxic cargoes. Mitochondria serve as the powerhouse as the cell, being the central dogma for cellular metabolism, energy production and survival. It is well understood that mitochondrial drug targeting is one of the most efficient ways to treat cells, and moreover cancer cell mitochondria are relatively different to their healthy counterparts,[34, 168, 300] suggesting an opportunity to target them preferentially. It remains the question as to whether cyanine dyes can be exploited as drug delivery moieties, so it was time to investigate this theory. Alongside toxicity testing of cells treated with drugs conjugated to **Cy3**, imaging was conducted to establish whether the dyes were preferentially tracking the drugs to the cellular mitochondria.

2.4.1 Confocal imaging of drug treatments

To assess both the mitochondrial-delivery capacity of **Cy3** and its cargo diversity, the dye was conjugated to three distinctive drug molecules; a mitochondrial toxic peptide $(KLAKLAK)_2$ (**KLA**), a small chemical mitochondrial drug Ciprofloxicin (**Cip**) and a metallocomplex mitochondrial drug Carboplatin (**CPT**). These represent three important classes of drugs in clinical application and the molecular targets of all these drugs are believed to be the mitochondria.[345-351] **KLA** is a pro-apoptotic, antimicrobial peptide that is

understood to engage in disruption of the mitochondrial membrane.[345, 346] **Cip**, a fluoroquinolone with antibiotic activity, has previously exhibited cytotoxicity in eukaryotes due to damage caused to mitochondrial DNA.[347-350] **CPT** is a derivative of Cisplatin (a widely established cancer drug) that impairs mitochondrial function, inducing apoptosis.[351]

Confirmation of the drug conjugates tracking to the mitochondria specifically would aid in understanding their interactions in the cell, and **Cy3** fluorescence serves as a visualisation tool to track cargo localisation. Co-localisation analysis of **Cy3** and MitoTracker fluorescence was conducted from confocal imaging. HeLa cells were pre-treated with MitoTracker and Hoechst and washed with PBS prior to treatment with 10 μM **Cy3-KLA**, **Cy3-Cip** or **Cy3-CPT** respectively for 10 minutes. To enable clear fluorescent imaging of the **Cy3** moieties, 10 μM drug concentration was used. Co-localisation analysis between **Cy3** and MitoTracker fluorescence revealed **Cy3-Cip** to have a Pearson's coefficient of 0.927, whereas **Cy3-CPT** had a Pearson's coefficient of 0.873, and **Cy3-KLA** had a coefficient of 0.830, confirming high co-localisation of the dyes (**Figure 2.17**).

It is clear from the imaging results that mitochondrial structures are lost after 10 minutes incubation with the drug conjugates. For **Cy3-KLA**, the cells nuclei became abnormal in structure, with the DNA appearing to coil up (resulting in intermittent blue fluorescence of Hoechst). Further, pockets of dye fluorescence can be seen in the nucleus of the cells, showing that the toxic activity of **Cy3-KLA** likely has interactions with the nuclear membrane, permitting drug entry into the organelle. Notably, alongside the observed **Cy3** fluorescence present in the nucleus after treatment with **Cy3-KLA**, there is a faint presence of Mitotracker green fluorescence evident within these pockets which is markedly less than that observed in cytoplasmic regions. As MitoTracker is described to covalently bond within the mitochondria,[287] the reasons for this presentation are unclear. Additionally, there is no presence of MitoTracker within the nucleus when cells were treated with **Cy3-Cip**, or **Cy3-**

CPT. It is difficult to find a concrete explanation for this presentation with regards to **Cy3-KLA**, but it is plausible that an excess of MitoTracker was present within the cells at the time of **Cy3-KLA** treatment. As the cells were treated with **Cy3-KLA** within 20 minutes of MitoTracker staining, potentially an excess of MitoTracker meant that although the dye had associated with the mitochondria via charge, not all of the dye had covalently bonded with its target prior to the addition of **Cy3-KLA**. This circumstance would have subsequently lead to MitoTracker nuclear localisation upon **Cy3-KLA**'s predicted interruption of the nuclear membrane, as the remainder of un-bound MitoTracker present would subsequently be available to interact with the exposed negatively charged DNA. This theory is also supported by the fact that the MitoTracker fluorescence within the nucleus is observably less when compared to the cytoplasmic regions of the cells; illustrating the potential that only the leftover and unbound dye was available to subsequently relocate to the nucleus. As previously stated however, explanations for these findings are unclear; without further experimental exploration, the reasons behind the finding can only be hypothesised. Treatment with **Cy3-CPT** resulted in rounding and disassembly of mitochondrial structures, and evident blebbing of the cell membrane (seen as green-edged circular structures expanding from the cell surface). Treatment with **Cy3-Cip** caused cells to round up; there was no evident fluorescence in the nucleus, therefore Ciprofloxacin isn't likely to have direct interaction with nuclear integrity at the 10-minute interval. With **Cy3-Cip** treatment, mitochondrial structures appear to coil up within the cytoplasm with a different phenotype to the bleeding of staining seen with **Cy3-KLA**, or the breakdown of filamentous structures with **Cy3-CPT** treatment.

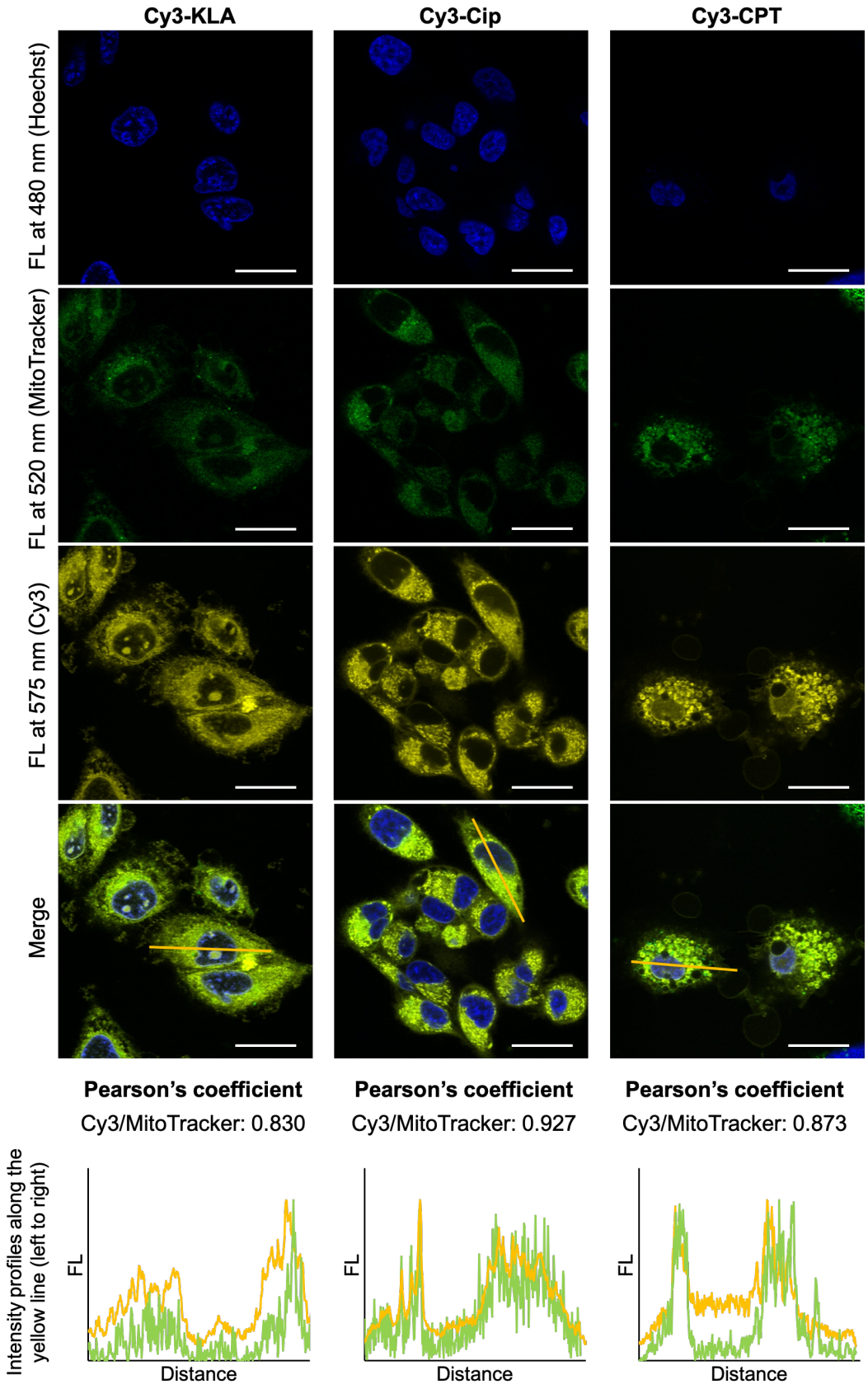

Figure 2.17: Co-localisation of Cy3 conjugates with MitoTracker Green in HeLa at 37 °C. *Pearson's correlation coefficients for **Cy3-KLA**, **Cy3-Cip** or **Cy3-CPT** with MitoTracker are 0.830, 0.927 and 0.873, respectively. All incubations with **Cy3-drug** were 10 min. Scale bars denote 25 μm. Representative (N = 10) confocal microscopy images are shown here.*

2.4.2 Toxicity analysis

To accurately assess mitochondrial targeting by **Cy3-*drug*** conjugation, for each drug HeLa cell viabilities were assessed under 4 conditions for each conjugate: **Cy3-*drug***, **Cy3** + ***drug***, **Cy3** alone and ***drug*** alone. The additional control of **Cy3** + ***drug*** was used to provide insight into whether the conjugation to **Cy3** is necessary to achieve an increase in toxicity if one is observed, and not simply due to the combination of molecules regardless of conjugation. The toxicity of **Cy3** alone is also crucial to understand any background toxicity that may occur during fluorescent imaging. Standard dose-response curve fitting was performed for each condition to establish individual EC_{50} values. Cell viability testing was conducted using CellTiter-Blue; a commercially available assay that provides a homogeneous fluorescent method to monitor cell viability. The assay is based on a live cell's ability to convert the non-fluorescent redox dye resazurin into the highly fluorescent pink dye resorufin (excitation/emission 571/584 nm). Therefore, high pink fluorescent values are representative of the reduced product resorufin, and thus are indicative of the viability of a culture.

Across all three **Cy3-*drug*** conjugates, an increase in toxicity was observed when covalently conjugated to **Cy3** (**Figure 2.18a-c**). Comparing the toxicity of covalent conjugation to **Cy3** with the toxicity of the lone cargo, toxicity increases from 100-fold (EC_{50} = 0.8 μM vs 85 μM for **Cy3-CPT** vs **CPT**) to 1000-fold (EC_{50} = 4 μM vs 4020 μM for **Cy3-KLA** vs **KLA**) were obtained. **Cy3** alone exhibits a cytotoxicity EC_{50} value of 26 μM, however a 5- to 30-fold enhancement was nonetheless observed across all covalently conjugated constructs (**Figure 2.18**).

As these toxicity results were promising, a further conjugate was tested, **Cy5-KLA**. This was to evaluate whether the results can be replicated using **Cy5** as a delivery vessel and to determine whether the results in **Figure 2.18** are specific to **Cy3,** or can be transferable across the cyanine dye range. Indeed,

Cy5-KLA presented the same way as **Cy3-KLA**, with an EC_{50} of 5 μM vs 4020 μM for **Cy5-KLA** vs **KLA** (**Figure 2.18d**).

Crucially, the **Cy3-*drug*** conjugates were all shown to be more toxic in cancer cells than non-cancer cells when comparing their toxicities in HeLa to HEK293. The EC_{50} value of **Cy3-KLA** is significantly lower ($p > 0.01$) in HeLa (4.0 μM) compared to HEK293 (11.1 μM). Furthermore, a 10-fold increase in EC_{50} (and therefore potency) was observed with **Cy3-CPT** (0.8 μM vs 11.1 μM) while a 2-fold increase was observed for **Cy3-Cip** (3.9 μM vs 6.7 μM). Their selectivity in different cell lines may be derived from the MMP being more negative in cancer cells compared to non-cancer cells.[34, 168, 300] However, it needs to be considered that the cell lines used here are immortalised so cannot be considered as a clear representation of how the conjugates would behave in an *in vivo* model. A natural mammalian system carries a plethora of additional complexities that cannot be assessed *in vitro*; therefore, testing these conjugates *in vivo* is crucial to ascertain whether the promising results obtained here are transferable to a clinical setting.

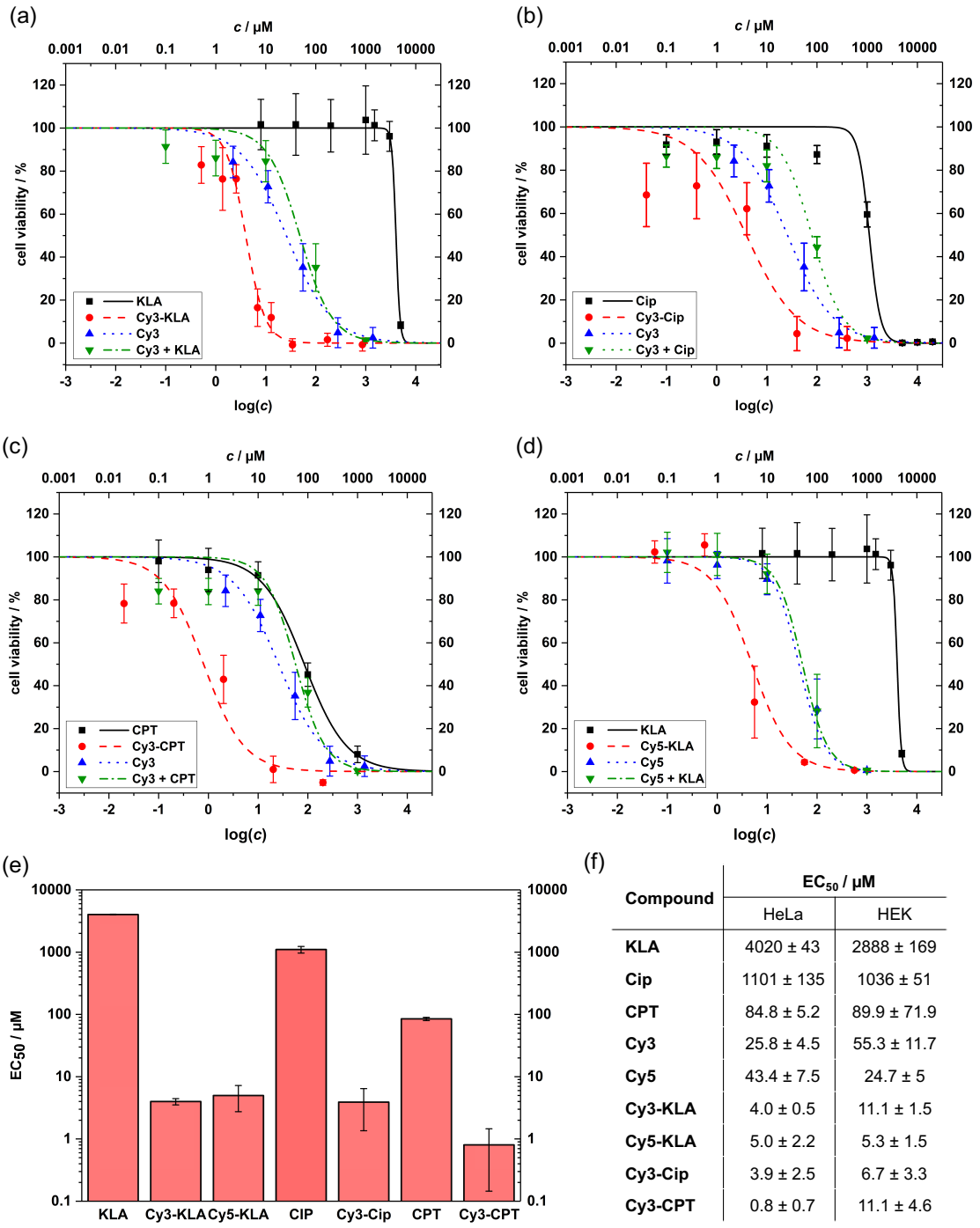

(f)

Compound	EC_{50} / µM	
	HeLa	HEK
KLA	4020 ± 43	2888 ± 169
Cip	1101 ± 135	1036 ± 51
CPT	84.8 ± 5.2	89.9 ± 71.9
Cy3	25.8 ± 4.5	55.3 ± 11.7
Cy5	43.4 ± 7.5	24.7 ± 5
Cy3-KLA	4.0 ± 0.5	11.1 ± 1.5
Cy5-KLA	5.0 ± 2.2	5.3 ± 1.5
Cy3-Cip	3.9 ± 2.5	6.7 ± 3.3
Cy3-CPT	0.8 ± 0.7	11.1 ± 4.6

Figure 2.18: Cytotoxicity and EC_{50} values of Cy3-drug conjugates in HeLa and HEK293 *(**a–d**) Effects of covalent conjugation of small molecules to cyanine dyes on HeLa cell viability: (**a**) **Cy3-KLA**, (**b**) **Cy3-Cip**, (**c**) **Cy3-CPT**, (**d**) **Cy5-KLA**. HeLa cells were treated with the indicated compounds at the indicated concentration for 48 h before the quantification of cell viability using CellTiter-Blue. (**e**, **f**) Comparison of EC_{50} values of small molecules and their cyanine dye conjugates. HeLa cells were treated with the indicated compounds at the indicated concentration for 48 h before the quantification of cell viability using CellTiter-Blue.*

2.5 Conclusions

To summarise, the work depicted in these studies has characterised the mitochondrial-homing capacity of simple cyanine dyes, and represented their capability for exploitation as an anti-cancer drug delivery vehicle. The compounds detailed can effectively localise at the mitochondria at relatively low concentrations, and **Cy3**, **Cy5** and **Cy3-Cy5** are not dependent on endocytic pathways to enter a cell. **Cy3-Cy5-R8** was generated and tested to analyse whether the addition of a CPP can alter the pathway in which the dyes enter a cell, and moreover to test previously reported behaviours of cyanine dyes in cell entry when conjugated to a CPP entity. The dyes were found to be dependent on the mitochondrial membrane potential, and conjugation of simple cyanine dyes **Cy3** or **Cy5** dramatically increased the toxicity of a cytotoxic peptide, small molecule and a metallocomplex drug. Strong evidence was gathered to determine the mode of entry **Cy3-Cy5-R8** adapts, concluding that it is endocytosis-dependent at lower concentrations until a particular concentration threshold where direct membrane transduction can be achieved. The dyes do not irreversibly bind to the mitochondria, but their targeted staining behaviours can be restored when MMP is re-established.

Although the results show a clear toxicity to cancer cells, determining their specificity was crucial to address their future applications as cancer drug delivery entities. Although an increased toxicity was observed in cancer cell lines compared to non-cancer cell lines, there was still a marked toxicity in non-cancer cell lines, illustrating a minimal level of specificity. To translate these findings into a clinical setting, it would be necessary to test on a wider range of cancer and non-cancer cell lines, alongside a range of primary cancer and non-cancer cells. These results will be required to determine whether the results found here can be converted into a clinical setting. Specificity of the compounds could possibly be improved via addition of a receptor-targeting entity to specifically bind to cancer cell surface markers, however this approach is complex and lengthy with no promise of success. The conjugation

to a receptor-targeting molecule will make the compound much larger, likely more complex, and risks the retention of molecular stability. Moreover, in targeting receptors or surface proteins, a release-mechanism will also be required to facilitate drug conjugate release into the cell once the membrane has been targeted. This cell-homing moiety may also restrict the efficiency of cyanine dye entry into the cell, bringing the risk of a reduced toxicity or efficacy. There are many hurdles to be addressed before these findings can potentially be transcribed into a therapeutic setting, however the findings to this point are promising – the next stage of research will need to focus on improving specificity, whilst not detrimentally damaging the toxicities or efficacies of the constructs.

2.6 Experimental Section

2.6.1 Measuring dye-containing molecule concentration.

Dye-containing constructs were dissolved in dH_2O and concentrations were calculated from the Beer–Lambert law [A = ε c l] where A is the absorbance value, l is the path length and ε is the extinction coefficient. For **Cy3**-containing constructs, concentration was determined using ε of **Cy3** (150,000 $L \cdot mol^{-1} \cdot cm^{-1}$ at the excitation wavelength of 555 nm), and for the dual dyes using ε of **Cy5** (250,000 $L \cdot mol^{-1} \cdot cm^{-1}$ at the excitation wavelength of 646 nm). 10 Measurements were conducted using a ThermoFisher NanoDrop ND-ONE-W spectrophotometer and an average taken to calculate the concentration. Absorbance values were measured in 10 mm path-length cuvettes (Fisher Scientific, #11847832).

2.6.2 Cell culture

HeLa and HEK293 cells were obtained from ATCC and routinely tested for mycoplasma infection. HeLa and HEK293 were maintained in T75 flasks at 37 °C in a 5% CO_2 atmosphere in DMEM (Fisher Scientific, #11574516) supplemented with 10% (v/v) FBS (Fisher Scientific, #11573397). Cells were maintained at a sub-confluent monolayer, and split at 80-85% confluency. For splitting, cells were washed with PBS, trypsinised in 1 mL of trypsin (Fisher Scientific, #11560626) and 200 µL of the 1000 µL trypsin cell suspension is re-suspended in 12 mL fresh DMEM containing 10% (v/v) FBS in a new T75 flask.

2.6.3 Confocal microscopy

HeLa cells were seeded at a density of 3×10^5 cells per imaging dish (MatTek, #P35G-1.5-10-C) and grown at 37 °C in a 5% CO_2 atmosphere in DMEM (ThermoFisher, #61965026) supplemented with 10% (v/v) FBS

(ThermoFisher, #10270106) for 24 h. Cells were washed twice with 1X PBS (pH 7.4) and once with the imaging medium, i.e. serum free RPMI (ThermoFisher, #32404014) containing 1% (w/v) BSA (Fisher Scientific, #11493823) prior to undertaking the relevant staining procedures. For nuclear staining, cells were incubated with Hoechst 33258 (10 mg/mL; Invitrogen, #H3569) at 10 µg/mL in the imaging medium at 37 °C for 5 min. For mitochondrial staining, cells were washed with PBS and incubated with MitoTracker Green (Invitrogen, #M7514) at 20 nM in imaging medium at 37 °C for 30 min and washed twice with PBS before imaging in imaging media. For the constructs, concentrations and procedures are detailed in each protocol listed.

Cell analysis was conducted using a Leica TCS SP5 confocal laser-scanning microscope using 488 nm Argon laser, and 543 nm, 633 nm HeNe lasers. Images were collected using a 63 x 1.4 NA objective at 2.5 times zoom. Images were 16bit depth, 98.6 x 98.6 microns with 5.192 pixels per micron resolution gathered through a 95.5 µm pinhole. Excitation/emission used for Hoechst 33258, MitoTracker Green, **Cy3**, and **Cy5** were 405/480 nm, 488/520 nm, 543/575 nm, and 633/680 nm respectively. Line-by-line generated images were acquired via sequential scanning between the fluorophores. To permit accurate comparability across all data sets presented, microscope settings (including offset, gain and laser power) remained constant. For each representative image displayed, 5 to 10 distinct fields of view were imaged. All imaging was performed on live cells unless otherwise stated.

2.6.4 Cell uptake experiments at 37 °C

HeLa cells were seeded at a density of 3×10^5 cells per imaging dish and grown at 37 °C in a 5% CO_2 atmosphere in DMEM supplemented with 10% (v/v) FBS for 24 h. Cells were then washed twice with 1X PBS (pH 7.4) and once with the imaging medium. Cells were treated with a compound at the indicative concentration for 1 h at 37 °C in imaging medium with or without 10% FBS (for serum dependent uptake). Media was removed, cells washed

twice with PBS and once with serum free RPMI. For nuclear stain, cells were incubated with Hoechst nuclear stain (Fisher Scientific, #10778843) following the procedure previously described, and then imaged. When nuclear stain was not used, cells were washed after compound treatment three times with PBS and incubated in serum free RPMI prior to imaging.

2.6.5 Cell uptake experiments at 4 °C

HeLa cells were seeded at a density of 3×10^5 cells per imaging dish and grown at 37 °C in a 5% CO_2 atmosphere in DMEM supplemented with 10% (v/v) FBS for 24 h. Cells were then washed twice with 1X PBS (pH 7.4) and once with the imaging medium. Cells were chilled to 4 °C for 5 minutes before washing with chilled PBS and 10 minutes treatment with the constructs at indicated concentrations at 4 °C. They were washed with chilled PBS and incubated in pre-chilled RPMI for imaging.

2.6.6 Pre/post fixed cell imaging

HeLa cells were seeded at a density of 3×10^5 cells per imaging dish and grown at 37 °C in a 5% CO_2 atmosphere in DMEM supplemented with 10% (v/v) FBS for 24 h. Cells were then washed twice with 1X PBS (pH 7.4) and once with the imaging medium. Cells were washed with PBS and incubated with MitoTracker (20 nM) for 20 minutes, washed with PBS and then incubated with **Cy3** (10 μM) in serum free DMEM for a further 20 minutes. Cells were washed with PBS and incubated in serum free DMEM when imaged on the microscope, prior to fixation. Fixation was conducted via media removal, cells washed with PBS and then incubated at the room temperature with 3% paraformaldehyde in PBS for 20 minutes. Cells were further washed with PBS and incubated with 10 mM NH_4Cl for 5 minutes prior to imaging again on the confocal microscope.

2.6.7 Depolarization experiments

HeLa cells were seeded at a density of 3 × 10^5 cells per imaging dish and grown at 37 °C in a 5% CO_2 atmosphere in DMEM supplemented with 10% (v/v) FBS for 24 h. Cells were then washed twice with 1X PBS (pH 7.4) and once with the imaging medium. Cells were washed with PBS, and **Cy3** (10 μM) was added and incubated for 10 minutes in 10% v/v FBS DMEM. Cells were washed and incubated in 500 μL of the aforementioned DMEM for imaging 0 minutes, then a further 500 μL of carbonyl cyanide m-chlorophenyl hydrazine in 10% FBS DMEM (CCCP, Fisher Scientific, 10175140) at 40 μM was added to the cells (final concentration in well of 20 μM CCCP, 10% FBS). Cells were imaged at 0, 2 and 6 minutes of CCCP treatment. CCCP media was then removed and cells washed 3 times with PBS prior to incubation in aforementioned 10% FBS DMEM. Cells were incubated at 37°C 5% CO_2 atmosphere, and imaged at 10 minutes and 60 minutes after CCCP removal.

2.6.8 Imaging Cy3 conjugates

HeLa cells were seeded at a density of 3 × 10^5 cells per imaging dish and grown at 37 °C in a 5% CO_2 atmosphere in DMEM supplemented with 10% (v/v) FBS for 24 h. Cells were then washed twice with 1X PBS (pH 7.4) and once with the imaging medium. Media was removed, and cells washed three times with PBS prior to staining with MitoTracker at 20 nM in serum free DMEM for 20 minutes. Cells were washed again twice with PBS and incubated with Hoechst stain (at concentrations previously described) in serum free DMEM for 5 minutes. Cells were washed twice with PBS and treated with the appropriate conjugates at 10 μM for 10 minutes under tissue culture conditions prior to washing with PBS and imaging.

2.6.9 Image analysis

All images were processed equally and analyzed using the software program Fiji (version 1.0) as part of the ImageJ suite. For co-localization graphs, guides of 45-52 μm were drawn on the image and profile plots generated for each

channel along the guide from left to right. Data sets generated from this were collected and processed in Microsoft Excel. Pearson's coefficient values were calculated with Fiji using the "Coloc 2" function. Ten images were analysed to calculate the mean Pearson's coefficient.

2.6.10 Cell viability assays

Cells were seeded at a density of 2×10^4 cells per well in a Corning 96-well plate (Fisher Scientific, #10357891) and grown at 37 °C in a 5% CO_2 atmosphere in DMEM supplemented with 10% (v/v) FBS for 24 h. Constructs were diluted into DMEM supplemented with 10% FBS to the appropriate concentration, and cells in each well were incubated with 100 µL of the suspension. After 24 h at 37 °C, 20 µL of CellTiter-Blue (Promega, #G8080) was added to each well. The plate was incubated for another 4 h at 37 °C before analysis on a Perkin Elmer Victor X plate reader (excitation 531 nm; emission 595 nm). Each data point is calculated from three biological replicates (i.e. cells split from three different passages), and each biological replicate is calculated from three technical replicates (i.e. cells split from the same passage). Values from cell-only (i.e. non-treated) wells with CellTiter-Blue in each biological replicate were set as 100% viability. For treatments containing **Cy3**, blanks were generated with cell-free wells containing the compounds and not adding CellTiter-Blue. The fluorescent reading for these wells depicted background **Cy3** fluorescence, and values were deducted from the treatment readings. A $\log_5$ or $\log_{10}$ scale of treatment concentration was used throughout toxicity analysis of the various conditions (**Table 2.1**). Concentrations used for each condition remained the same across HEK and HeLa analysis.

Table 2.1: List of concentrations used to analyse construct toxicity

Treatment	Concentration (μM)								
KLA	0	1	8	40	200	1000	1500	3000	5000
Cy3	0	2.2	11.1	55.3	276.7	1383.3			
Cy3 + KLA	0	0.1	1	10	100	1000			
Cy3-KLA	0	0.5	1.4	2.6	6.9	12.9	34.3	171.7	858.3
KLA	0	1	8	40	200	1000	1500	3000	5000
Cy5	0	0.1	1	10	100	1000			
Cy5 + KLA	0	0.1	1	10	100	1000			
Cy5-KLA	0	0.056	0.56	5.6	56	560			
Cip	0	0.1	1	10	100	1000	5000	10000	20000
Cy3	0	2.2	11.1	55.3	276.7	1383.3			
Cy3 + Cip	0	0.1	1	10	100	1000			
Cy3-Cip	0	0.04	0.4	40	400				
CPT	0	0.1	1	10	100	1000			
Cy3	0	0.1	1	10	100	1000			
Cy3 + CPT	0	0.1	1	10	100	1000			
Cy3-CPT	0	0.02	0.2	2.0	20	200			

2.6.11 Statistical analysis

For all statistical analysis, data for each condition was obtained from three independent biological replicates, each formed of a minimum of 2 technical replicates, and significance values were calculated using a paired Student's t-test. For curve fitting (**Figure 2.18a-d**), data was plotted in OriginLab® (version 9.4) and a standard "dose response curve" was fitted: $y = A1 + \frac{A2-A1}{1+10^{(LOGx0-x)p}}$. Data analysis for **Figure 2.18** was completed with the assistance of Dr Alexander Nödling.

Table 2.2: Pearson's coefficient values for Figure 2.7

	Cy3	Cy5	Cy3-Cy5			Cy3-Cy5-R8		
Replicate	Cy3:Hoechst	Cy5:Hoechst	Cy3:Hoechst	Cy5:Hoechst	Cy3:Cy5	Cy3:Hoechst	Cy5:Hoechst	Cy3:Cy5
1	-0.085	0.132	0.074	0.114	0.987	0.069	0.117	0.915
2	-0.070	0.129	0.320	0.137	0.860	0.108	0.052	0.817
3	-0.010	0.227	0.080	0.180	0.992	0.099	0.062	0.949
4	-0.120	0.205	0.099	0.320	0.940	0.112	0.075	0.877
5	-0.040	0.134	0.215	0.211	0.889	0.052	0.059	0.993
6	-0.030	0.081	0.116	0.218	0.912	0.089	0.106	0.831
7	-0.042	0.118	0.087	0.085	0.983	0.130	0.145	0.994
8	-0.010	0.152	-0.020	0.120	0.986	-0.030	-0.050	0.984
9	-0.032	0.090	0.016	0.007	0.992	0.071	0.021	0.785
10	-0.110	0.050	0.046	0.058	0.975	0.068	0.087	0.949
Average	**-0.055**	**0.132**	**0.103**	**0.145**	**0.952**	**0.077**	**0.067**	**0.909**
StDev	*0.039*	*0.054*	*0.099*	*0.090*	*0.049*	*0.045*	*0.054*	*0.078*

Table 2.3: Pearson's coefficient values for Figure 2.8

	Cy3	Cy5	Cy3-Cy5			Cy3-Cy5-R8		
Replicate	Cy3:MT	Cy5:MT	Cy3:MT	Cy5:MT	Cy3:Cy5	Cy3:MT	Cy5:MT	Cy3:Cy5
1	0.966	0.987	0.330	0.438	0.732	0.324	0.575	0.903
2	0.896	0.738	0.449	0.593	0.997	0.355	0.484	0.797
3	0.947	0.786	0.462	0.302	0.905	0.622	0.601	0.879
4	0.738	0.899	0.184	0.329	0.852	0.397	0.482	0.779
5	0.979	0.739	0.177	0.120	0.761	0.274	0.342	0.735
6	0.870	0.891	0.385	0.299	0.784	0.259	0.328	0.712
7	0.864	0.993	0.582	0.272	0.976	0.668	0.782	0.979
8	0.721	0.815	0.195	0.253	0.762	0.418	0.601	0.891
9	0.851	0.984	0.170	0.318	0.847	0.556	0.350	0.766
10	0.796	0.939	0.254	0.448	0.987	0.428	0.436	0.818
Average	**0.863**	**0.877**	**0.319**	**0.337**	**0.860**	**0.430**	**0.498**	**0.826**
StDev	*0.090*	*0.101*	*0.146*	*0.129*	*0.101*	*0.142*	*0.144*	*0.085*

Table 2.4: Pearson's coefficient values for Figure 2.9

	Cy3-Cy5 + MitoTracker			MitoTracker + Cy3-Cy5			Cy3/Cy5 + MitoTracker		
Replicate	Cy3:MT	Cy5:MT	Cy3:Cy5	Cy3:MT	Cy5:MT	Cy3:Cy5	Cy3:MT	Cy5:MT	Cy3:Cy5
1	0.330	0.438	0.732	0.549	0.543	0.862	0.782	0.754	0.945
2	0.449	0.593	0.997	0.539	0.538	0.832	0.617	0.654	0.780
3	0.462	0.302	0.905	0.723	0.567	0.963	0.760	0.756	0.851
4	0.184	0.329	0.852	0.765	0.524	0.991	0.744	0.748	0.842
5	0.177	0.120	0.761	0.653	0.636	0.827	0.730	0.765	0.856
6	0.385	0.299	0.784	0.595	0.527	0.953	0.651	0.631	0.824
7	0.582	0.272	0.976	0.569	0.652	0.888	0.746	0.753	0.877
8	0.195	0.253	0.762	0.732	0.638	0.938	0.766	0.799	0.879
9	0.170	0.318	0.847	0.391	0.479	0.749	0.742	0.810	0.905
10	0.254	0.448	0.987	0.719	0.576	0.992	0.801	0.659	0.896
Average	**0.319**	**0.337**	**0.860**	**0.624**	**0.568**	**0.900**	**0.734**	**0.733**	**0.866**
StDev	*0.146*	*0.129*	*0.101*	*0.117*	*0.057*	*0.081*	*0.057*	*0.062*	*0.046*

Table 2.5: Pearson's coefficient values for Figure 2.17

	Cy3-KLA	Cy3-Cip	Cy3-CPT
Replicate	Cy3:MT	Cy3:MT	Cy3:MT
1	0.730	0.876	0.747
2	0.736	0.991	0.923
3	0.932	0.996	0.931
4	0.917	0.942	0.853
5	0.838	0.994	0.914
6	0.769	0.782	0.980
7	0.897	0.914	0.934
8	0.889	0.859	0.899
9	0.879	0.923	0.792
10	0.712	0.991	0.759
Average	**0.830**	**0.927**	**0.873**
StDev	*0.085*	*0.072*	*0.081*

CHAPTER 3:
Genetic code expansion as therapeutic switches

Preface

Although the approach to drug delivery in **Chapter 2** was successful and demonstrated efficient delivery of toxic compounds to cancer cells, limitations remained regarding cancer cell specificity as the compounds continued to show toxicity (albeit significantly lesser) to non-cancerous cells. The next objective was to investigate an alternative approach to cancer therapeutics. By manipulating the immune system with internal cellular control of genetic processes, non-selective activity and generalised toxicity commonly observed in drug-mediated cancer treatments can be negated. Opposed to external drug delivery, the aim of this chapter was to introduce a mammalian cell logic gate system to allow the temporal control of engineered cancer-homing T-cells via targeted incorporation of unnatural amino acids. As a whole, mammalian cell logic gates hold great potential for wide ranging applications, but most currently available use drug molecules or their derivatives that carry intrinsic biological activities. To construct truly orthogonal circuits and artificial regulatory cellular pathways, biologically inert molecules are ideal as molecular switches, such as unnatural amino acids. A technique known as 'genetic code expansion' is used to incorporate an unnatural amino acid. An aminoacyl-tRNA synthetase and tRNA pair that decodes a blank codon is engineered and introduced into a cell to incorporate a designated unnatural amino acid at a targeted site during protein production. In mammalian cells, genetic code expansion remains highly restricted to incorporation of a single unnatural amino acid due to a lack of blank codons. Therefore, this work focussed on the emerging field known as quadruplet decoding, where a quadruplet codon is used to increase the availability of blank codons. 11 pyrrolysyl tRNA variants that decode quadruplet codons were screened, and the most efficient quadruplet was put through a series of optimisation prior to transfer into a mammalian cell logic gate design. Using a quadruplet-decoding orthogonal pair with an amber (UAG)-decoding pair, novel logic gates that can be efficiently controlled by two different unnatural amino acids were constructed and achieved; projected to be applied to a switchable cancer-targeting CAR-T design.

3.1 Background

3.1.1 From DNA sequence to protein

The central dogma to molecular biology is the conversion of DNA coded sequences to functional proteins.[362] All living organisms carry a genetic code; a double helix sequence made entirely out of 4 distinct nucleotides (adenine (A), guanine (G), cytosine (C) and thymine (T)) (**Figure 3.1a**). Arranged in a precise sequence and held in place by two adjacent sugar phosphate backbones, the nucleotide sequences throughout the DNA encodes every fundamental aspect of a living organism.[362] The DNA double helix is formed of a "sense" strand, and an "anti-sense" strand (**Figure 3.1b**), held together by hydrogen bond interactions between adjacent bases. As adenine always pairs with thymine (A-T) and cytosine always pairs with guanine (C-G), the anti-sense strand encodes a perfect complementary replica of the sense strand.

Within the DNA of a cell there are sections known as genes; the coding regions that are converted into proteins.[363] Within the genes, each triplet of nucleotides on the DNA sequence is called a codon and each codon encodes for a particular amino acid; the building blocks of proteins.[363] There are 64 distinct A/C/T/G combinations, resulting in 64 codons. Of the 64 triplet codons, 61 are responsible for all of the 20 canonical amino acids (naturally occurring) and the remaining three (TAG, TAA and TGA) are used as stop codons. These stop codons only appear at the end of a gene, and signal the termination of a gene sequence,[364] consequently evoking the cessation of protein production. However, to convert a gene into a protein, a sequence of events occur that can be simplified to two distinct steps; transcription and translation.

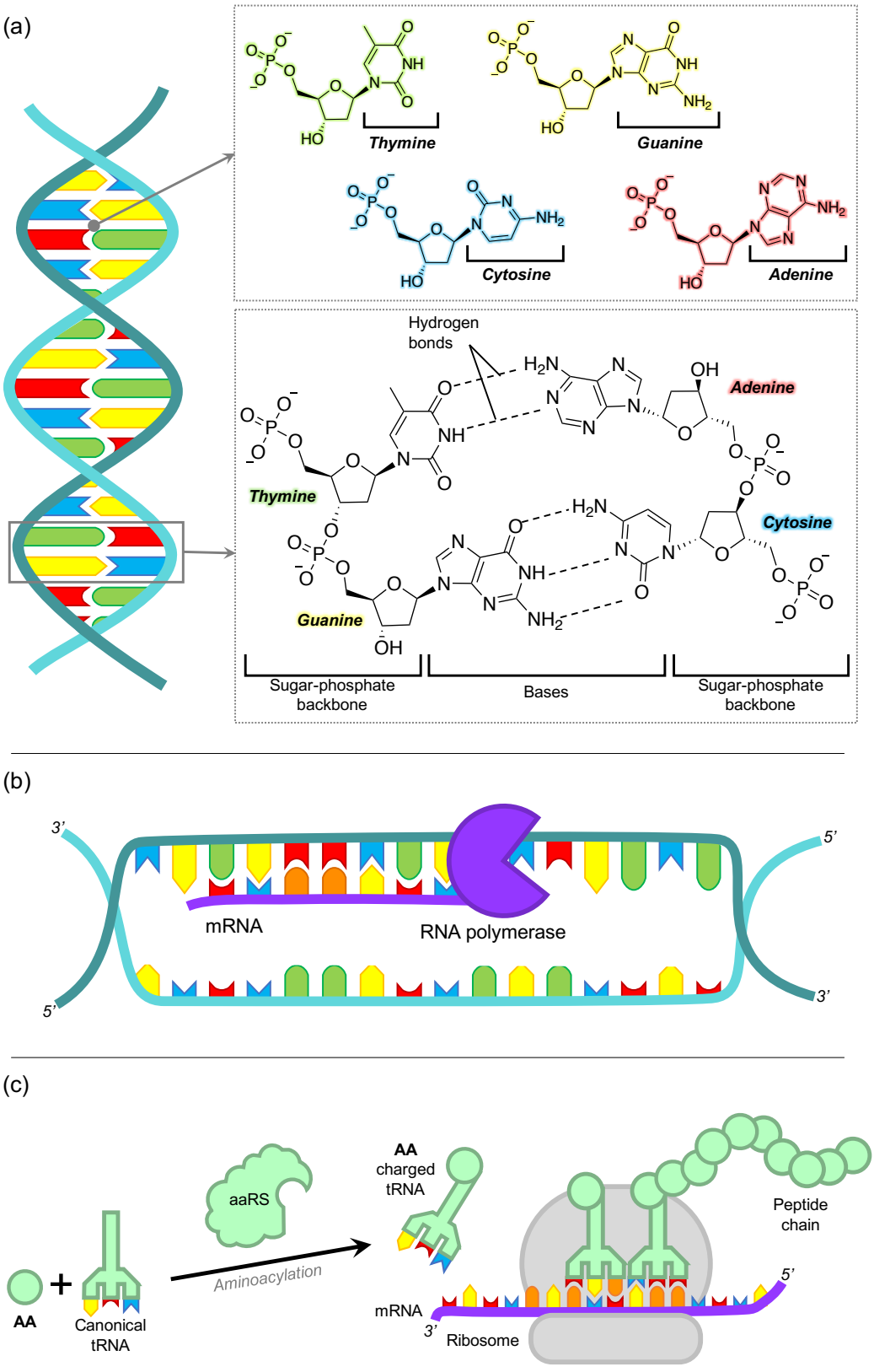

Figure 3.1: DNA structure and processes of protein production from a DNA sequence *(**a**) Double-helix structure of DNA and chemical structures of A/T/C/G nucleotides and how they form base pairs. (**b**) Process of transcription; converting a DNA sequence to mRNA. (**c**) process of translation; converting an mRNA sequence to protein (AA = amino acid, aaRS = aminoacyl tRNA synthetase).*

The first stage is transcription, where a single stranded messenger RNA (mRNA) is generated from the gene sequence (**Figure 3.1b**). mRNA is also formed of 4 nucleotides like DNA, but in mRNA the thymine (T) is replaced with uracil (U). It is widely accepted that cellular production of uracil is more energy efficient than thymine production, and as RNA is constantly being produced for various purposes unlike DNA, the substitution of thymine for uracil renders RNA production is understood to be more energy efficient as a whole.[365] Moreover, the distinct difference between RNA and DNA via thymine substitution facilitates the intracellular distinction between DNA and RNA, enabling targeted DNA recognition for a variety of purposes, such as mutation detection, DNA folding and transcription. The mRNA of a gene is made by forming a complimentary strand to the anti-sense strand (in other words, replicating the sequence of the sense strand as a single stranded RNA).

Once transcription has occurred, the mRNA is trafficked to the cellular ribosome (in eukaryotes, it is trafficked out of the cell nucleus prior to locating at the ribosome). Ribosomes are specialised cellular macromolecules distributed throughout the cytoplasm and facilitate the translation of mRNA into proteins.[366] Once the mRNA binds the ribosome, tRNA is employed to permit translation (**Figure 3.1c**). tRNA (transfer RNA) are cloverleaf shaped single-stranded RNA structures that decode the mRNA sequence and facilitate the formation of the peptide chain.[367] Each tRNA is specific to its amino acid, and has a designated tRNA synthetase to aminoacylate them together.[368] tRNA carry an anticodon at the bottom of their stem loop which is complimentary to the mRNA codons, therefore they permit the assignment of the 20 canonical amino acids to a designated codon (**Figure 3.2**). With the mRNA within the ribosome, the anticodon of the charged tRNA interacts with the complimentary codon on the mRNA sequence, in-turn bringing their amino acid within close proximity of the neighbouring amino acid and provoking hydrolysis and creating a covalent amide bond between the two residues.[366, 367] This process results in a chain of amino acids, which then undergoes a series of folding to generate the final functional protein.[363, 364, 366, 367]

(a)

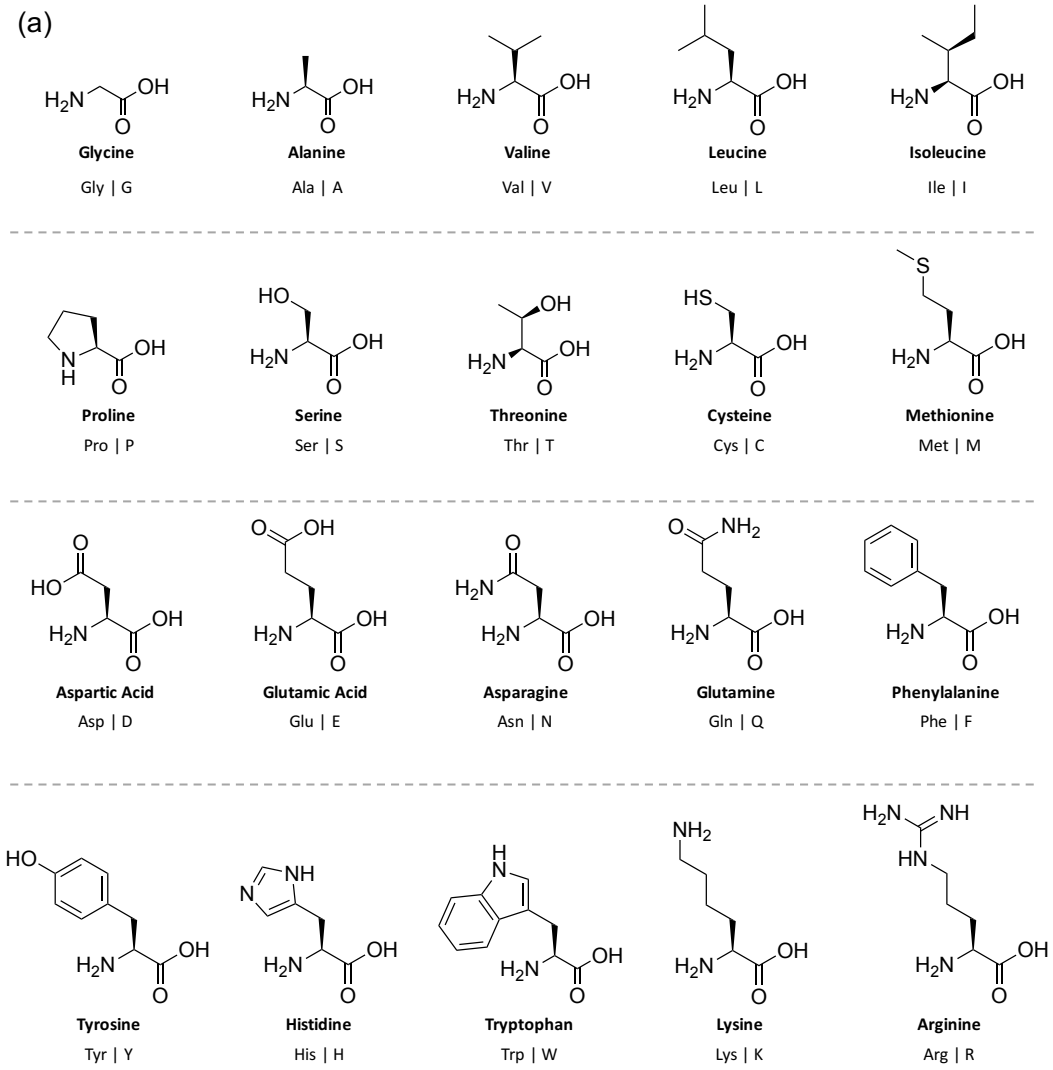

(b)

Second base of codon

First base of codon	U		C		A		G		Third base of codon
U	UUU	Phenylalanine	UCU	Serine	UAU	Tyrosine	UGU	Cysteine	U
	UUC		UCC		UAC		UGC		C
	UUA	Leucine	UCA		UAA	***STOP***	UGA	***STOP***	A
	UUG		UCG		UAG		UGG	Tryptophan	G
C	CUU	Leucine	CCU	Proline	CAU	Histidine	CGU	Arginine	U
	CUC		CCC		CAC		CGC		C
	CUA		CCA		CAA	Glutamine	CGA		A
	CUG		CCG		CAG		CGG		G
A	AUU	Isoleucine	ACU	Threonine	AAU	Asparagine	AGU	Serine	U
	AUC		ACC		AAC		AGC		C
	AUA		ACA		AAA	Lysine	AGA	Arginine	A
	AUG	Methionine	ACG		AAG		AGG		G
G	GUU	Valine	GCU	Alanine	GAU	Aspartic Acid	GGU	Glycine	U
	GUC		GCC		GAC		GGC		C
	GUA		GCA		GAA	Glutamic Acid	GGA		A
	GUG		GCG		GAG		GGG		G

Figure 3.2: Amino acid structures and their codon-assignment in mammalian cells
*(**a**) Canonical amino acid structures, names and abbreviations. (**b**) Genetic code amino acid codon-assignment table.*

3.1.2 Genetic code expansion

Genetic code expansion is a process that has been used to improve protein investigation over the past 20 years, and relates to incorporation of unnatural amino acids into polypeptide chains. The technique has advanced understanding of protein structure, enzyme active site functionality, and facilitated studies on intracellular protein trafficking and localisation via the use of targeted probes.[369-372] Genetic code expansion is a powerful technique with wide-ranging applications in protein research.[372-377] By repurposing the innate cellular translation machinery, the method enables site-specific unnatural amino acid incorporation into a target protein. To incorporate an unnatural amino acid, an orthogonal aminoacyl-tRNA synthetase (aaRS) and tRNA pair that decodes a blank codon is required.[372-377] The amber (UAG) codon is typically used as the blank codon in genetic code expansion (**Figure 3.3**) because it is typically the least-frequently employed stop codon in most organisms, and does not encode an amino acid.[378] An orthogonal pair refers to a set that functions independently of its surrounding cellular machinery, therefore it theoretically has no interaction with naturally occurring tRNA/aaRS pairs. Thus far, a multitude of orthogonal pairs have been developed and optimized for unnatural amino acid incorporation in response to the amber codon (i.e. amber suppression) in various organisms.[372-375, 377] Arguably, pyrrolysyl (Pyl)-tRNA synthetase (PylRS) and its cognate tRNA from the archaeal *Methanosarcina* species is the most widely utilized orthogonal pair in prokaryotic and eukaryotic systems.[372-375, 377] This is particularly so because PylRS does not recognise the anticodon step loop of the cognate tRNA during amino-acylation unlike other tRNA/aaRS pairs. Nevertheless, various *Escherichia coli* aaRS (e.g. *Ec*LeuRS, *Ec*TyrRS, *Ec*TrpRS) and their cognate tRNAs have also been exploited, and specifically engineered to function as orthogonal pairs to incorporate unnatural amino acids with diverse chemical and physical properties in mammalian cells.[372] Theoretically, it is possible to employ multiple orthogonal pairs concurrently in mammalian cells,[372, 379, 380] however such applications are often thwarted as these pairs are all originally engineered for amber suppression. Advances in targeted UAA incorporation are becoming increasingly inhibited by the limitations of the natural genetic

code. As all triplet base combinations are occupied by naturally occurring tRNA and amino acids throughout all organism genomes, the expansion and incorporation of multiple unnatural amino acids into a single protein is extremely limited, restricting its employment in more complex biochemical studies.

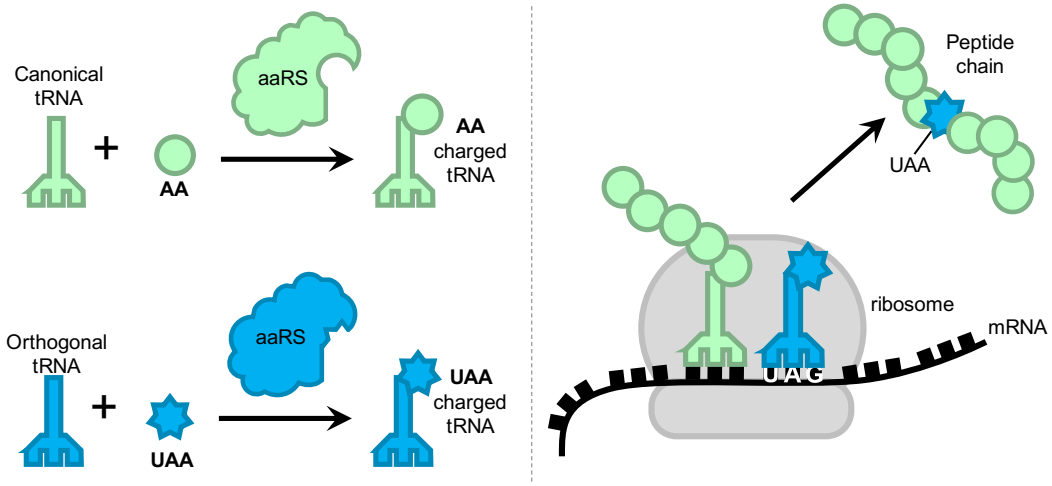

Figure 3.3: The process of unnatural amino acid incorporation using amber decoding
Employing orthogonal tRNA/aaRS pairs for selective unnatural amino acid incorporation into proteins using amber codon (UAG) suppression. (AA = amino acid, UAA = unnatural amino acid).

3.1.3 The realm of quadruplets

Genetic code expansion is required to investigate protein activity in a more in-depth and comprehensive manner, and a potential resolution for the triplet restriction is the use of quadruplet codons. This concept involves the addition of an extra base at the target codon for UAA employment, and generating a tRNA with a complementary quadruplet anti-codon that can be selectively amino-acylated (**Figure 3.4**). Quadruplet decoding has been applied to a range of studies in bacterial culture using various orthogonal aaRS/tRNA pairs.[341, 381, 382] If quadruplets were employed into the modern-day approaches to UAA protein studies, there is a potential for 256 blank codons to be made available, thus it would theoretically be achievable to introduce multiple distinct amino acids within a single cell for more complex and in-depth biochemical studies. However, there are a multitude of complications when employing

quadruplet tRNA, such as off-target interference with translation inducing frame shifts in natural peptide sequences. Quadruplet-decoding incorporation of unnatural amino acid studies have predominantly been in bacterial strains,[341, 373-376, 378, 382] while mammalian research remains in its infancy.[378-381, 383, 384] Unnatural amino acid incorporation in mammalian studies carry a large potential in medicinal research, and has many applications into pharmaceutical sciences, protein activity, active site activity and catalysis in a mammalian environment. Thus, the need for an expanded genetic code is also relevant to mammalian studies, as these have the same limitations as those of bacteria regarding amber codon usage.

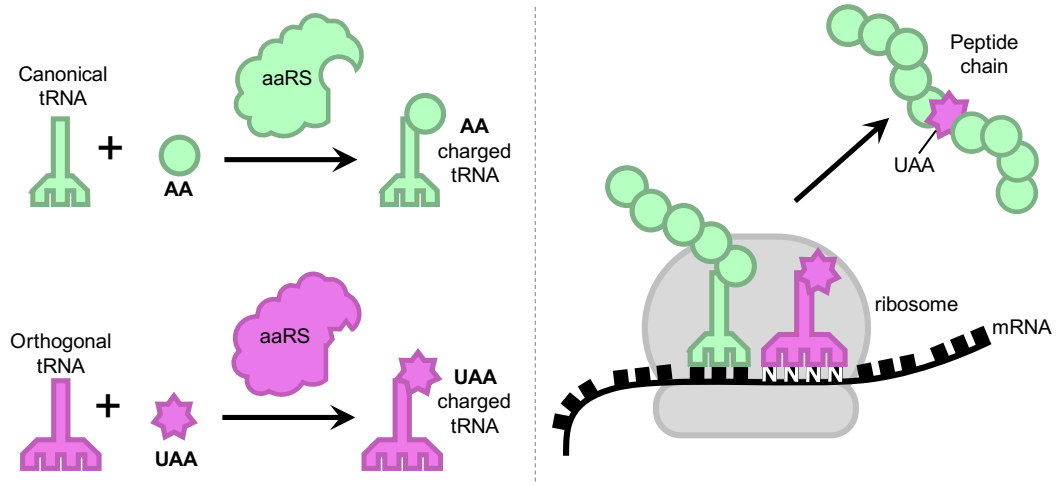

Figure 3.4: Process of unnatural amino acid incorporation using quadruplet decoding
Employing orthogonal tRN/aaRS pairs for targeted unnatural amino acid incorporation into proteins using quadruplet codons. (AA = amino acid, UAA = unnatural amino acid).

As unnatural amino acids generated for genetic code expansion are artificial synthetic molecules (no existence in nature), they are widely considered to be biologically inert as observable changes in cellular phenotypes are yet to be described.[383, 385-388] This is advantageous when investigating their potential applications in cancer therapies, as theoretically their administration would not produce any undesirable phenotypes. As such, it is interesting to consider their translation into a cancer treatment design, whereby their ability to obtain genetic control could be manipulated into activation of genetically modified anti-cancer entities. The dual operation of a quadruplet-decoding aaRS/tRNA

paired with an amber-decoding aaRS/tRNA within the same cell holds the potential to be adapted as genetic switch systems; for example, the supplementation of one amino acid induces activation of a protein or cell, and supplementation of an opposing amino acid evokes their deactivation. As a whole, this approach to controlling a desired output via two inputs is termed as a biological logic gate.

3.1.4 Logic gates as biological therapies

Put simply, the term biological logic gates refer to integrated cellular systems where a particular input is used to control a desired output. The engineering of mammalian cell logic gates has revolutionized synthetic biology, enabling the development of sensors, diagnostics and therapeutics.[286, 389-392] The employment of environmental or synthetic switches is a fast developing next-generation technique for intricate cellular phenotype control, with exponential biotechnological and biomedical applications.[233, 299, 393-396]

Regarding environmental stimuli, over the past decade a plethora of new methods have entered the literature ranging from chemical-logic gates, to gene logic gates, and even post translational protein dimerization methods. *Soheili et al.* recently expanded their use into a new method of investigating cellular activities for therapeutic gain.[397] An ongoing problem of cancer treatments is the development of multi-drug resistance, which is commonly achieved via overexpression of a glycoprotein called MDR1. In order to investigate whether the use of a targeted MDR1 shRNA could indeed reduce the expression of the gene, the group developed a logic operating system with hopes to gain more accurate and informative data sets. They created a modified synthetic breast cancer cell line (MCF7) via transduction of lentivirus materials. By placing the expression of a synthetic MDR1 gene under a promotor that requires DOX for activation, and similarly an shRNA construct that requires IPTG supplementation for expression, they were able to accurately investigate the effects of the targeted shRNA. They demonstrated that MDR1 was only expressed in the cells when supplemented with DOX, and

moreover if DOX and IPTG are simultaneously supplemented, the expression of MDR1 reduced significantly by 75% through IPTG-mediated shRNA interference with MDR1.[397] Although a relatively simple design, this technique is a useful one for investigation of genetic therapies, as the expression of a target cancer gene can be induced by the user, and therefore the actual specificity of the designated treatment can be more accurately ascertained.

Another promising environmental stimulus-responsive cancer therapeutic is the use of modified nanoparticles.[120-122, 132] By generating nanoparticles that release their chemotherapeutic cargo upon a particular signal at the tumour site, side effects of non-selectivity can be largely negated due to the switchable nature of the treatment. Many nanoparticles that respond to external or internal stimuli have been developed over recent years, and most take advantage of the natural environmental differences between a tumour and a healthy tissue. One such difference is the pH of the tumour microenvironment. It has been noted that a gradient of pH is present between tumour intra- and extracellular regions caused by the tumour having a higher metabolic demand than what is supplied to it.[1, 120-122, 162] By receiving less nutrients and oxygen than is required, cancers tend to accumulate large volumes of lactic acid within their near proximity. Given this increase in acidity, pH-responsive nanoparticles are a great example of a stimulus-responsive treatment option, as they selectively release large volumes of chemotherapeutic cargo to tumours only when receiving a dedicated acidic input.[162] Typically, these constructs remain in a stable form at physiological pH, but acidic environments induce hydrolysis and protonation of the structures, causing to structural breakdown and subsequent release of the drug. Moreover, these nanoparticles can further be used to transport other means of therapy such as siRNA to interrupt the transcriptome of the cancer cells with aims to disrupt their function. Prior to development of nanoparticles, the use of siRNA was broadly unsuccessful due to its poor systemic stability and vulnerability to circulating degrading enzymes.[230] Moreover, siRNA is a useful tool when treating multi-drug resistant cancers, as it can disrupt the pathways adopted to cause drug resistance, subsequently reassigning the cells as chemotherapeutic-sensitive. Additionally, siRNA can

also be used to downregulate anti-apoptotic enzymes and proteins, making the cell more vulnerable to destruction.[231] Other stimulus-responsive nanoparticles have been developed in recent years, including ones that respond to redox conditions, or can be degraded by enzymes that are highly expressed in certain tumours.[101, 120-122]

Particularly, switchable treatments have been formed to respond to external stimulus issued by the vender, allowing temporal control and user-mediated manipulation of a desired phenotype. One field of this is designing therapeutics that respond to light.[139, 162, 396] Stimulus such as light are particularly useful when treating very solid tumours, as they are commonly extremely hard to penetrate with bulky treatments. Due to their dense arrangement, thick extracellular matrix and lack of extensive vasculature, solid tumours have a reduced uptake of nanoparticles and other large drug complexes. The employment of light treatments like infrared light has shown promise in early studies of light-activated cancer therapeutic designs. By using particles small enough to surpass the dense infrastructure of the tumour, infrared light is then directed at the tumour site, and absorbed by the molecules. As a result, these particles generate large amounts of heat, substantially increasing the temperature of the tumour and consequently burning and destroying the tumour tissues.[138, 139] However, the low penetration of light through skin is an enormous obstacle for these therapies to overcome, therefore at present these treatments only remain potentially suitable for the treatment of superficial, surface and exposed cancers, such as tumours of the oral cavity and skin.

Although many such logic gates have been developed to function in mammalian cells, commonly employed switch-input molecules such as rapamycin and its derivatives carry intrinsic biological activities and bring risk of toxicity.[286, 390, 398, 399] To construct truly orthogonal circuits and artificial regulatory pathways in cells, biologically inert molecules, such as unnatural (non-canonical) amino acids, are ideal as control switches. Being inert, they cannot interfere with natural cellular processes so can selectively serve as

input signals, making them a practical choice to control logic gates within a pharmaceutical setting.

The use of logic gate switches is in the early stages of revolutionising cancer immunotherapy.[296-299] The natural immune system is designed to relegate the body of pathogens and mutant cells, such as cancers.[40, 75] Interestingly, cancers are renowned for their ability to effortlessly evade the immune system through a variety of mechanisms.[40, 75] It is also very difficult for the immune system to recognise cancers as threats, as they display self-antigens on their surface, posing as healthy tissues.[42] Cancer immunotherapy is a growing field, where different techniques are employed to train the patient's immune system into overriding the cancer immune evasion tactics and successfully destroying the tumours.[54, 74, 200] One of the most promising emerging techniques is the use of Chimeric Antigen Receptor T-cells (CAR-T).[226, 229, 283, 293] These cells are engineered T-cells, where they are extracted from the patient and modified to express chimeric antigen receptors (CARs) (**Figure 3.5a**). These receptors are targeted to antigens overexpressed on cancer surfaces, such as CD19, and have shown great promise in the revolution of immunotherapy cancer treatment. The limitations of these receptors, however, is the immune response generated when they are infused into the patient. While the CAR-T cells successfully target and kill the cancer cells with a high affinity, their rapid reaction often results in an overwhelming immune response, with non-selective cell destruction and flooding the system with inflammatory signalling molecules called cytokines (known as a cytokine storm) which is extremely toxic to a patient (**Figure 3.5b**).[281, 282, 284, 295] Recent projects have been attempting to generate ways to temporally control or mediate the activity of CAR-T,[285, 296-299] with hopes of reducing the immuno-toxicity they bring.

Acquiring the ability to control the activity of cancer immune-therapeutics would undoubtedly aid the achievement of efficient anti-tumour activity with reduced side effects. Recent advances have focussed on the development of CAR-T cells that respond to particular stimulus. One approach is the use of a

split receptor design whereby dimerization of two complementary parts is required to activate the receptor.[294, 298, 299] By using a split receptor, the anti-tumour activity of the CAR-T is determined by the dimerising of the split receptor complex. Such dimerising receptors have been made using entities such as leucine zippers, as the zippers can be modified to tailor their binding affinity to each other, in turn modulating the efficiency of the receptor. Moreover, addition of another competing zipper with a stronger binding affinity can be administered to dislodge the active zipper, therefore deactivating the CAR-T. This approach enables users to fine-tune the strength of a CAR-T response, and also allows them to effectively deactivate the CAR-T if adverse side effects are exhibited in the patient, improving the overall safety of the treatment. Other similar approaches have been developed to achieve the same goal, with dimerising pairs such as biotin and avidin, and neo-epitope tags being used. More successful takes on dimerising CAR receptors have been achieved by the use of switch molecule inputs. A research group in 2015 demonstrated how the activities of CAR-T can be controlled remotely by the simple administration of either rapalog (an analogue of rapamycin) and gibberellin.[299] When mice were injected with these modified CAR-T, the group successfully showed that CAR-T anti-tumour activity can be specifically tailored by the concentration of drug administered. The field of switchable immunology remains in its infancy however, and each approach brings limitations. For example, systemic delivery of a leucine zipper to compete for the active zipper site is fraught with difficulties due to the tendency of leucine zippers to be degraded in the system prior to arriving at the CAR-T site. Moreover, the use of drug molecules as a dimerising entity also brings additional toxicities and complications, and there appears to be very little studies that exhibit both an ON and OFF switch procedure, both of which are necessary to establish complete control of the CAR-T functional activity.

Giving the pharmaceutical applications and treatment options CAR-T provide the cancer field, adapting a logic gate system to these receptors is a potential gold mine for targeted control and activation of CAR-T to minimise side effects. Multiple studies have investigated the use of split receptor systems, where a

dimerising molecule is employed to enable receptor assembly and downstream immune activation.[229, 296, 298, 299] However, these switch molecules are not without their complications, as they are typically drug molecules known to have adverse non-selective toxicities and effects in their own right.[286, 390, 398, 399] Moreover, studies so far have simply focused on either an ON or an OFF CAR-T switch, and have not developed an interchangeable control. The use of genetic code expansion as logic switches for CAR-T activity is a promising approach that can mitigate the toxicity of switch drug molecules, can evoke regional CAR-T activation via targeted administration (i.e. unnatural amino acid infusion into the tissues surrounding the tumour), and theoretically would have no adverse side effects in the patient as the translational machinery is specific to the modified CAR-T, and the unnatural amino acids are biologically innate.

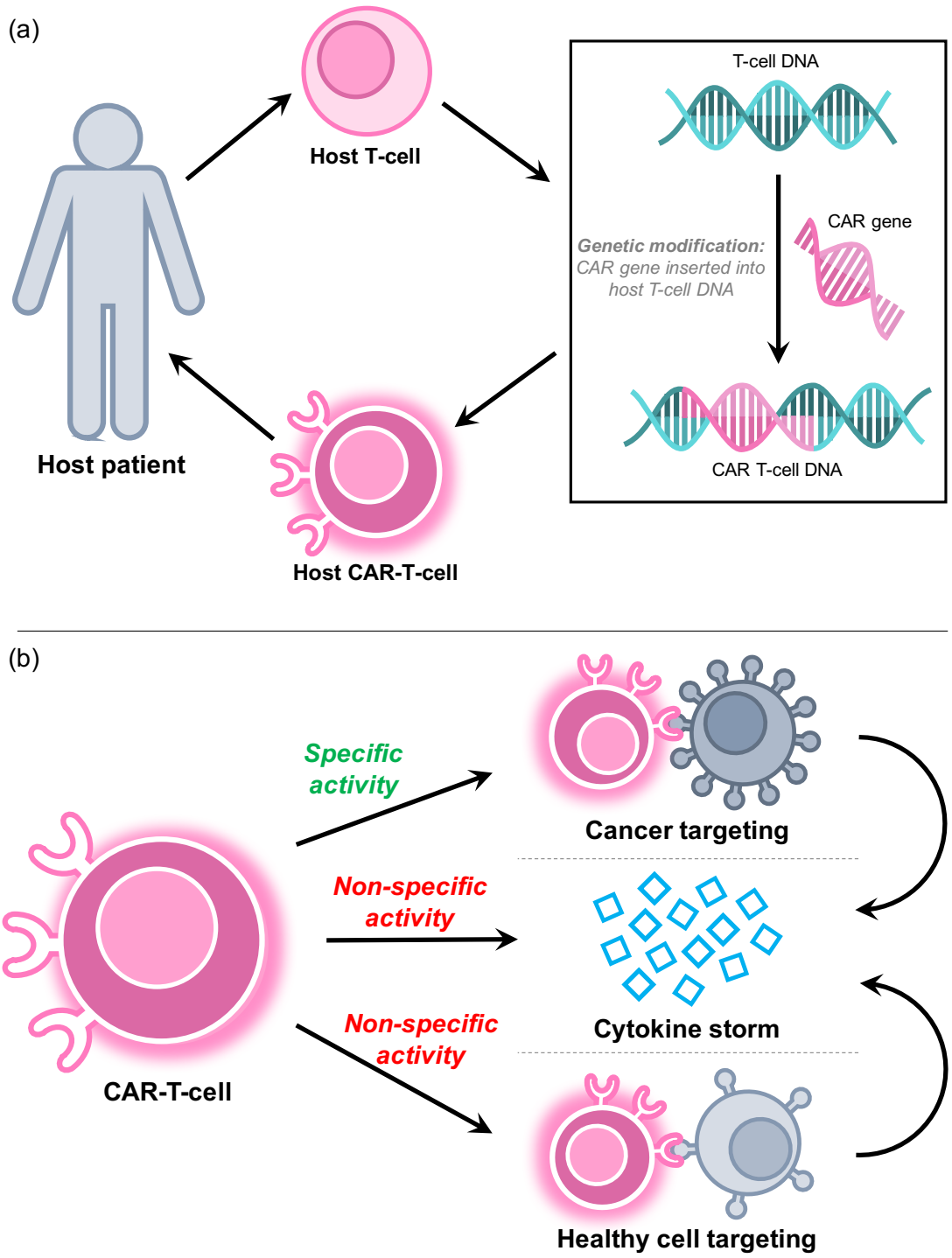

Figure 3.5: Principles of CAR-T cell therapy for cancer and the current downfalls
*(**a**) Process of patient T-cell modification to make self-CAR-T cells. T-Cells are extracted from the patient and genetically modified to enable CAR expression. These CAR-T cells are then propagated and infused back into the patient for cancer therapy. (**b**) Activities of CAR-T cells; specific targeting and killing of cancer cells, however non-selective activities include cytokine storms and healthy tissue destruction. Destruction of cancer and healthy tissues contributes to cytokine storm.*

3.1.5 Aims and objectives

The aim of this project was to determine whether unnatural amino acid incorporation can be modified into a logic gate design, which can then be transferred into a switchable CAR-T model.

The premise of this proposal was on the basis that only in the presence of an unnatural amino acid can a reporter protein form. When an unnatural amino acid is not present, its cognate tRNA cannot be aminoacylated so does not interact with the blank codon, and subsequently the translational process will terminate at that residue.[375, 376, 388, 389] Building on this knowledge, the expression of a full length and active protein can be controlled via supplementation of an unnatural amino acid within the cellular media.[376, 388] Moreover, when combining multiple independent aaRS/tRNA pairs that incorporate different unnatural amino acids, the expression of multiple target proteins within a cell can theoretically be modulated by supplementation of their cognate unnatural amino acids into the cellular media.[372, 379, 380] In short, the expression of multiple proteins can be simultaneously influenced by the unnatural amino acid makeup within the culture. Building on this, if found to be successful, the switch model could be transferred to a switchable CAR-T design. CAR-T have shown great promise in the field of cancer immunology, however their lack of control once in a patient can be a complication, with cytotoxicity arising from their over-activation.[74, 226, 293] However, through the development of a switch system via the use of unnatural amino acid supplementation, it is hypothesised that the activity of CAR-T can be controlled via two unnatural amino acids; one for an activation switch such as permitting receptor expression, and the other for inactivation such as expression of a cytotoxic protein.

The main objectives for this project include identification and testing of a quadruplet decoding aaRS/tRNA pair that is active in mammalian cells, testing its orthogonality with an amber decoding aaRS/tRNA pair, development of a switchable GFP reporter design, and finally transfer of the system into a switchable CAR-T model.

3.2 Mammalian genetic code expansion

Prior to analysing the applicability of genetic code expansion for mammalian cell logic gates, it was necessary to identify two orthogonal tRNA/aaRS pairs to be exploited as logic operation systems. The unnatural amino acids (UAAs) used throughout this chapter are detailed in **Figure 3.6**. These UAAs were chosen due to their wide commercial availability, and commonality within the field of genetic code expansion.[372]

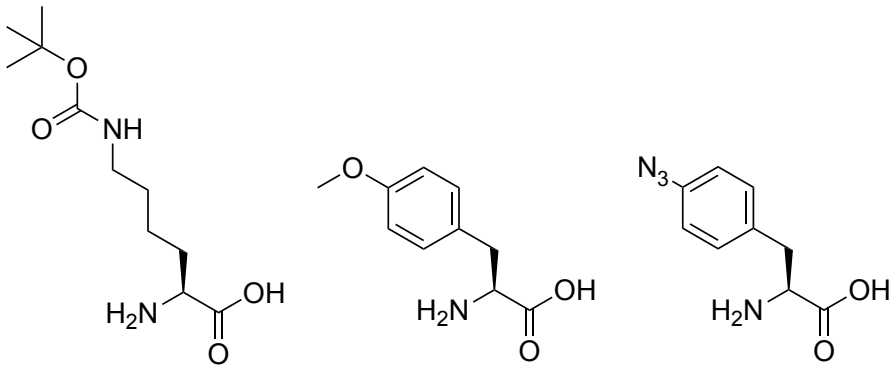

Abbreviation	BocK	OMeY	AzF
Full name	*(Nε-Boc-L-lysine)*	*(Methoxy-L-tyrosine)*	*(4-azido-L-phenylalanine)*
aaRS	*Mm*PylRS	*Ec*TyrRS	*Ec*TyrRS
aaRS mutations	WT	Y37V, D182S, F183M, G265R	Y37V, D182S, F183M, G265R

Figure 3.6: Unnatural amino acid structures, names and their paired tRNA synthetases
Structures and names of unnatural amino acids used in this chapter, alongside the aminoacyl tRNA synthetase (aaRS) used for their incorporation, and synthetase mutations if applicable (WT refers to wild type sequence).

3.2.1 Identifying Pyl tRNA variants for quadruplet decoding

Pyrrolysyl tRNA synthetase (PylRS) and its cognate tRNA are arguably the most versatile and evaluated pair for unnatural amino acid incorporation into peptide chains.[372-375, 377] As PylRS does not recognise the anticodon stem loop of its cognate tRNA, mutations of the nucleotides within this region (25-39) are commonly investigated as they are theoretically tolerated by the synthetase. These mutations have been largely exploited in *E. coli* for incorporation of the unnatural amino acid Nε-Boc-L-lysine (BocK) (**Figure 3.6**), and some have utilised this PylRS versatility to engineer quadruplet-decoding tRNA, however these studies exhibited varying degrees of efficiency (**Table 3.1**).

Table 3.1: Pyl tRNA quadruplets described in the literature for BocK incorporation

Nº	Nucleotide position				Target Codon	Efficiency	Reference
	25-28	29-30	31-33	34-39			
1	UGGA	CU	**UCUA**	AAUCCG	***TAGA***	++	*Wang et al. 2014* [341]
2	UGGG	CU	**UCUA**	AUCUCG	***TAGA***	+++	*Wang et al. 2014* [341]
3	UUGG	AU	**UCUA**	ACCUUG	***TAGA***	+++++	*Wang et al. 2016* [382]
4	UGGG	CU	**UCUA**	AUCCUG	***TAGA***	++++	*Wang et al. 2016* [382]
5	UCGG	AU	**UCUA**	ACCUUG	***TAGA***	+++	*Wang et al. 2016* [382]
6	UGGA	CU	**ACUA**	AAUCCG	***TAGT***	+	*Wang et al. 2016* [382]
7	UGGG	CU	**ACUA**	AUCUUG	***TAGT***	++	*Wang et al. 2016* [382]
8	UAGG	CU	**ACUA**	AUCUUG	***TAGT***	++	*Wang et al. 2016* [382]
9	UUGG	AU	**ACUA**	ACCUUG	***TAGT***	++	*Wang et al. 2016* [382]
10	UGGA	CU	**CCUA**	AAUCCG	***TAGG***	+	*Wang et al. 2016* [382]
11	UUGG	CU	**CCUA**	AUCUUG	***TAGG***	+++	*Wang et al. 2016* [382]
12	UGGG	CU	**CCUA**	AUCUUG	***TAGG***	+++	*Wang et al. 2016* [382]
13	UAGG	CU	**CCUA**	AUCUUG	***TAGG***	+++	*Wang et al. 2016* [382]
14	UGGA	CU	**GCUA**	AAUCCG	***TAGC***		*Wang et al. 2016* [382]
15	UGGA	CU	**UCCU**	AAUCCG	***AGGA***	+	*Niu et al. 2013* [381]
16	UGGA	AU	**UCCU**	ACUCCG	***AGGA***	++	*Niu et al. 2013* [381]
17	UGGA	CU	**UCCU**	AUUCCG	***AGGA***	++	*Niu et al. 2013* [381]
18	UCGG	AU	**UCCU**	ACCCUA	***AGGA***		*Niu et al. 2013* [381]
19	UGGG	AU	**UCCU**	ACCCUA	***AGGA***	++++	*Niu et al. 2013* [381]
20	AGGG	CU	**UCCU**	AUCCGU	***AGGA***		*Niu et al. 2013* [381]
21	UGGG	CU	**UCCU**	AUCCUA	***AGGA***		*Niu et al. 2013* [381]
22	GGGG	CU	**UCCU**	AUCCGC	***AGGA***	+++++	*Niu et al. 2013* [381]
23	UCCU	CU	**UCCU**	AAUAGG	***AGGA***	+++++	*Wang et al. 2014* [341]
24	UGGA	CU	**UACU**	AAUCCG	***AGTA***		*Wang et al. 2014* [341]
25	UUGG	CU	**UACU**	AUCCUG	***AGTA***	+++	*Wang et al. 2014* [341]
26	UGGA	CU	**CUAG**	AAUCCG	***CTAG***	++	*Wang et al. 2014* [341]
27	UGGC	CU	**CUAG**	AACCCG	***CTAG***	+++	*Wang et al. 2014* [341]

Black: WT sequence bases; blue: mutated bases; red: anticodon. Efficiency scores were decided by visual results presented in each paper: the best quadruplet for each article is scored as +++++, the least efficient as + and non-functional left blank.

Taking a range of *Mm* pyrrolysyl tRNA quadruplets developed in *E. coli* to incorporate BocK, a library of 11 pyrrolysyl tRNA mutants was designed to test their translated efficiency in mammalian cells. (**Table 3.2**) For the purpose of continuity and comparison, the mutants were renamed (**Table 3.2**, **column 1**), however their relative number to **Table 3.1** is detailed in the second column. Pyrrolysyl tRNA variants chosen for analysis were to decode UAGN (N = A/U/C/G), CUAG and AGGA codons and all were to incorporate the unnatural amino acid BocK. Although they have been shown to be effective in *E. coli*, the translation machineries in *E. coli* and mammalian cells are different,[400] therefore tRNA optimized in one system may not be suitable for the other.

Table 3.2: Pyl tRNA quadruplets chosen from Table 3.1 for testing in HEK293

Designated Name	Nº	Nucleotide position				Target Codon
		25-28	29-30	31-33	34-39	
UCUA	**1**	UGGA	CU	**UCUA**	AAUCCG	***TAGA***
UCUA(Ev1)	**4**	UGGG	CU	**UCUA**	AUCCUG	***TAGA***
UCUA(Ev2)	**2**	UGGG	CU	**UCUA**	AUCUCG	***TAGA***
CUAG	**26**	UGGA	CU	**CUAG**	AAUCCG	***CTAG***
CUAG(Ev1)	**27**	UGGC	CU	**CUAG**	AAUCCG	***CTAG***
UCCU	**15**	UGGA	CU	**UCCU**	AAUCCG	***AGGA***
UCCU(Ev1)	**23**	UCCU	CU	**UCCU**	AAUAGG	***AGGA***
UCCU(Ev2)	**22**	GGGG	CU	**UCCU**	AUCCGC	***AGGA***
GCUA	**14**	UGGA	CU	**GCUA**	AAUCCG	***TAGC***
ACUA	**6**	UGGA	CU	**ACUA**	AAUCCG	***TAGT***
CCUA	**10**	UGGA	CU	**CCUA**	AAUCCG	***TAGG***

Black: WT sequence bases; blue: mutated bases; red: anticodon.

3.2.2 Cloning of Pyl tRNA variants

To enable a systematic and consistent comparison of the 11 quadruplet variants, an evaluation plasmid was required (**Figure 3.7b**). The plasmid design consists of a single copy of tRNA, pyrrolysyl tRNA synthetase, and an eGFP reporter with the appropriate codon at the 150th residue. In order for the genes to express, promotor regions are required at the 5' to the gene sequence, and promotor regions are typically specific to the cell type (i.e. bacterial promotors cannot function in mammalian cells, and vice versa). The promotors chosen for the evaluation plasmid were U6 for tRNA, EF1α for the synthetase, and CAG for the reporter eGFP. U6 is a natural type III RNA polymerase promotor, that is commonly used for driving the expression of small RNA sequences, commonly small hairpin RNA (shRNA) or small interfering RNA (siRNA).[401] The benefit of U6 is that repeating "U6 > gene" units can be arranged in close proximity in a nucleic acid sequence, facilitating the simultaneous expression of multiple gene copies from a single DNA string and achieving a higher yield.[401, 402] Therefore, if desired, multiple "U6 > tRNA" units can be added and expressed on a single plasmid, yielding larger quantities of tRNA. The eukaryotic translation Elongation Factor 1 alpha promotor (EF1α) is commonly used for mammalian cell transfections and has been used for synthetase expression in mammalian systems previously. Naturally, it controls the expression of the *EEF1A1* gene, that encodes a small peptide that is responsible for the enzymatic delivery of aminoacyl tRNAs to the ribosome in most tissues.[403] As the function of this gene naturally is essential for cell translation and survival, it is constitutively expressed at high levels, therefore EF1α promotor exploitation for synthetase expression results in high yields of the pyrrolysyl tRNA synthetase. Crucially, to obtain a clear indication of the quadruplet decoding efficiency of each tRNA mutant, it was paramount that the amount of reporter eGFP expression was extremely high, as full saturation of reporter eGFP ensures a correct representation of decoding efficiency, so eGFP fluorescence is accurately representative of quadruplet decoding, not the limitation of available eGFP mRNA. Therefore, the CAG promotor was used for reporter eGFP expression as it is frequently used to drive high levels of gene expression in mammalian cells. Generated

by the lab of Dr Jun-ichi Miyazaki,[404] it is a synthetic promotor formed via combination of a cytomegalovirus enhancer element, the first exon and intron of the chicken beta-lactamase gene, and a splice acceptor from the rabbit beta-globin gene. All three of the promotors in the evaluation plasmid design have been utilised previously for unnatural amino acid incorporation.[381, 383, 405-408]

If decoding of the reporter quadruplet codon at the 150th residue is successful it will result in the production of full-length eGFP, however, if the first three bases of a quadruplet codon are decoded as a triplet codon, a translational frameshift will occur. A further silent point mutation downstream to the 150th residue was introduced into the eGFP sequence. This point mutation ensured that, if the quadruplet is decoded then the overall peptide sequence will not be altered, however if the first three bases are decoded by cognate triplet tRNA, the frameshift will encounter a stop codon within a few residues, leading to premature termination (**Figure 3.7a**). This point mutation was crucial to ensure that full-length and fluorescent eGFP is only produced upon successful quadruplet codon decoding, therefore enabling accurate comparison.

All evaluation plasmid clones were generated by a series of cloning. tRNA (**Figure 3.7d**) and eGFP mutants were generated by PCR mutagenesis of carrier plasmids. The plasmids carrying the desired mutations were then purified and confirmed via sanger sequencing. To form evaluation plasmids, these mutant eGFP and tRNA fragments were cut from their carrier plasmids and T4 ligated into the evaluation vector.

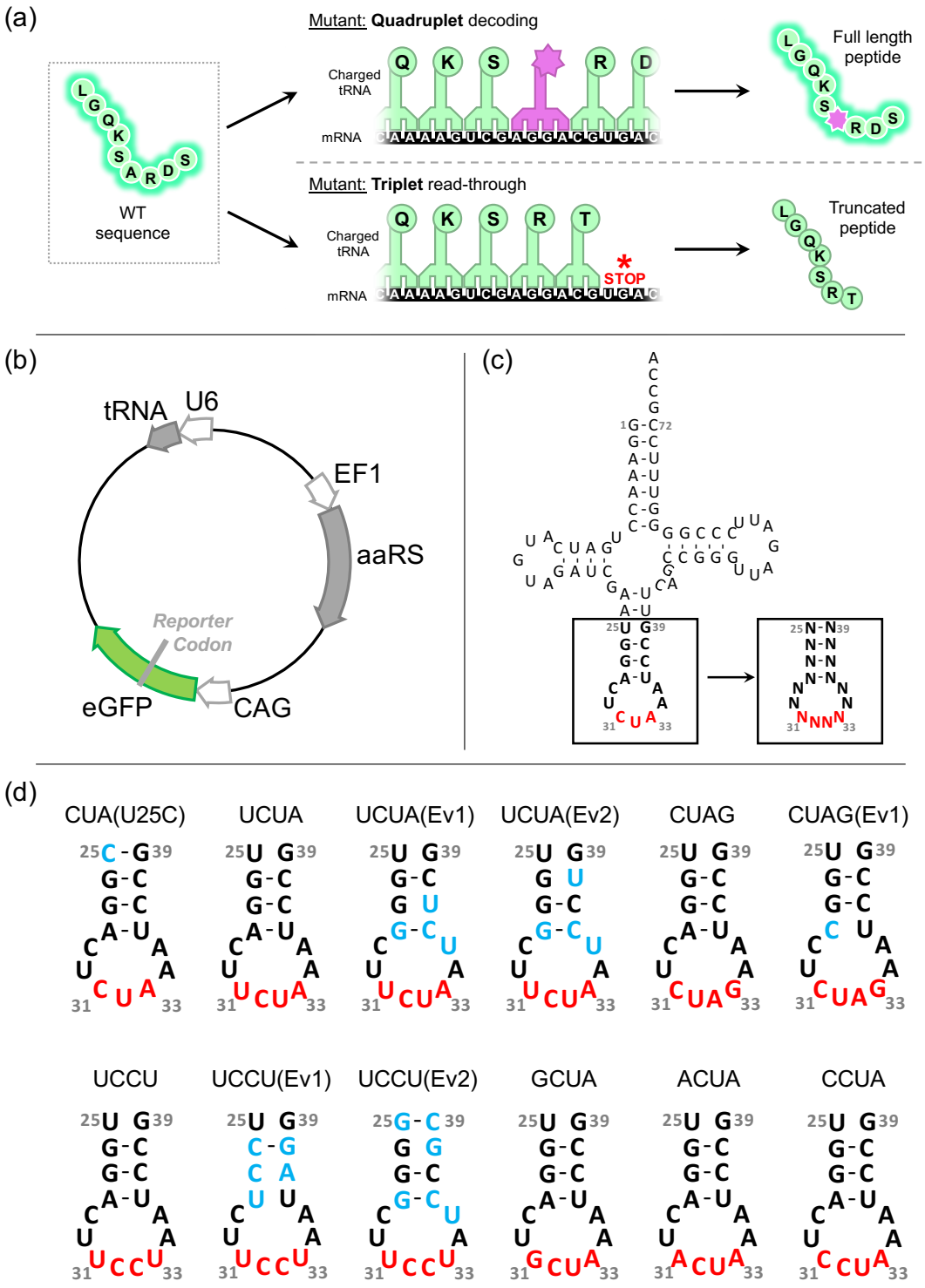

Figure 3.7: Design of evaluation plasmid and tRNAs for quadruplet decoding analysis
*(**a**) Graphic representation of premature termination if triplet read-through of mutant sequence occurs. (**b**) Evaluation plasmid design. (**c**) Structure of pyrrolysyl tRNA and anticodon stem loop that is modified in each mutant. (**d**) Sequence structure of tRNA mutants to be tested. Red bases denote anticodon, black bases show bases retained from WT sequence, blue bases show those mutated from the WT sequence.*

3.2.3 Analysis of quadruplet decoding efficiency

Human Embryonic Kidney cells (HEK293) were transiently transfected with an evaluation plasmid (**Figure 3.7b**) and cultured for 24 hours in DMEM supplemented 10% v/v FBS supplemented with 1 mM BocK, a substrate of the wild-type PylRS. In contrast to the observations in *E. coli* where all variants were functional,[341, 381, 382] only five Pyl tRNA variants led to BocK-dependent production of eGFP detected by fluorescence microscopy (**Figure 3.8** and **3.9**) and immunoblotting (**Figure 3.10**). Intriguingly, negligible eGFP production was observed with either Pyl $tRNA_{UCUA}$ or Pyl $tRNA_{UCUA(Ev2)}$, which have previously been shown to function in HEK293T cells with 5 mM BocK.[384] Nonetheless, it is possible that deviations in the cell line tested (HEK293 vs HEK293T) and concentration of BocK used (1 mM vs 5 mM) could be responsible for this discrepancy. Nevertheless, it is evident from the two CUAG- and three AGGA-decoding variants that the nucleic acid sequence in the anticodon stem loop has significant influence on the incorporation, where base mutations can either improve ($tRNA_{UCCU}$ vs $tRNA_{UCCU(Ev2)}$) or reduce ($tRNA_{CUAG}$ vs $tRNA_{CUAG(Ev1)}$) the incorporation efficiency. Importantly, the functional Pyl tRNA variants remain orthogonal in mammalian cells, as neither fluorescence nor eGFP was detectable in the absence of BocK (**Figure 3.9**). Particularly, Pyl $tRNA_{CUAG}$ and Pyl $tRNA_{UCCU(Ev2)}$ showed efficiency comparable to that of Pyl $tRNA_{CUA(U25C)}$, a variant with improved amber suppression efficiency in mammalian cells (**Figure 3.10c**).

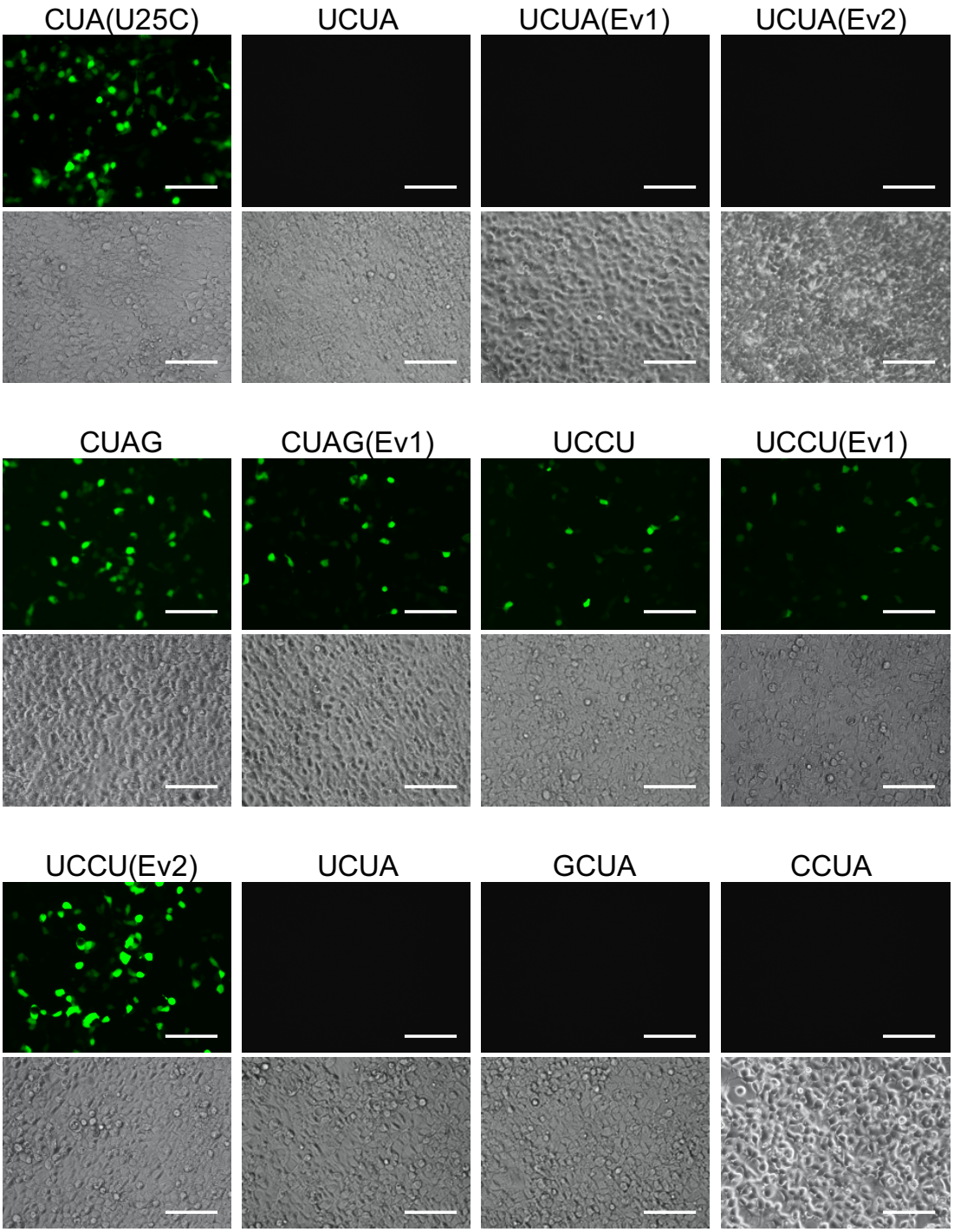

Figure 3.8: Decoding-efficiency fluorescent imaging of evaluation plasmids with BocK
HEK293 cells transiently transfected with each plasmid and incubated in the presence of 1 mM BocK for 48 hours. eGFP fluorescence represents successful quadruplet decoding and BocK incorporation, bright field images provided as an imaging control and representative of equal cell confluency across conditions. CUA(U25C) used as a decoding control. All images are 223 µm × 167 µm, scale bars denote 50 µm.

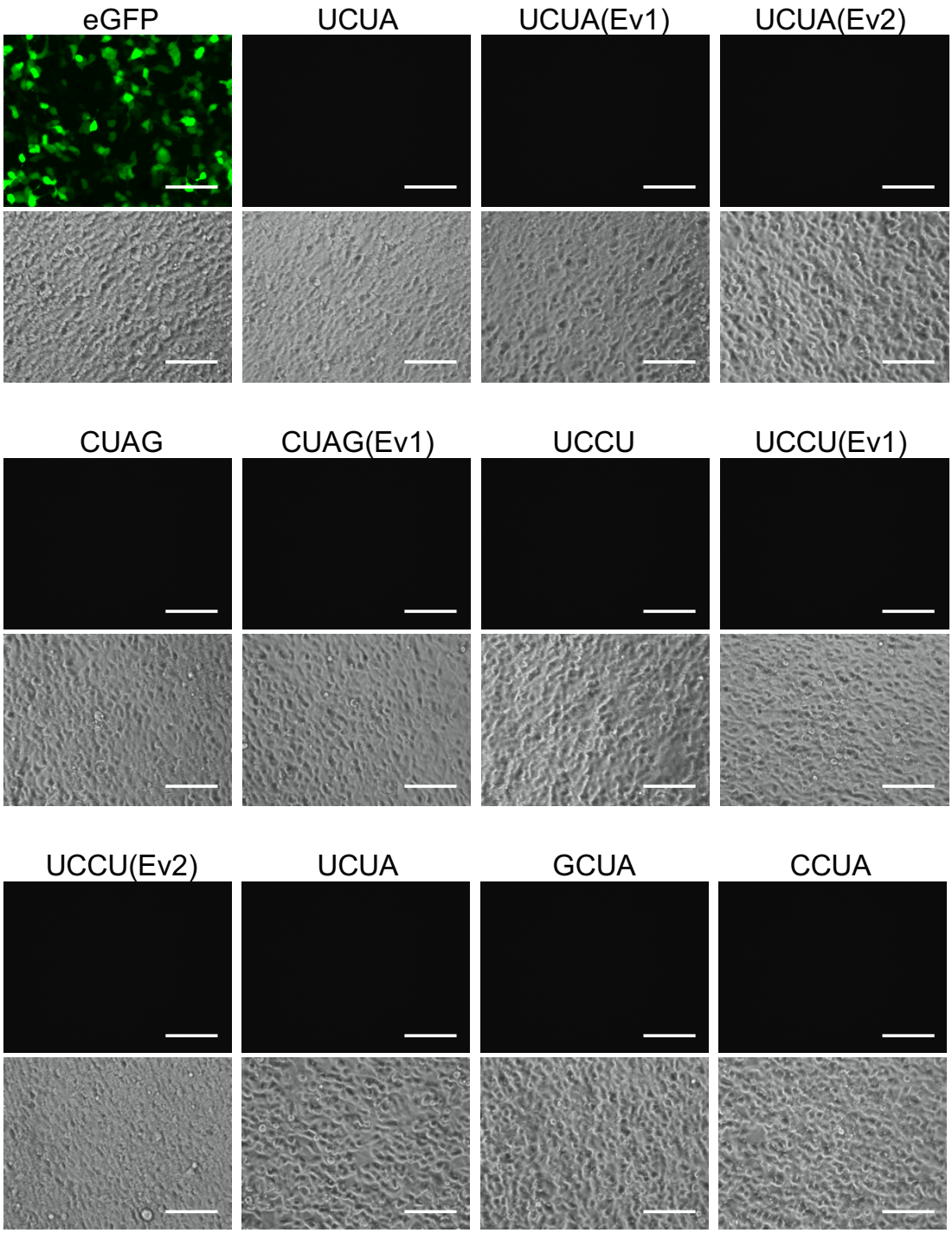

Figure 3.9: Imaging of BocK dependent eGFP fluorescence for each evaluation plasmid
HEK293 cells transiently transfected with each plasmid and incubated for 48 hours with no BocK supplementation. No eGFP fluorescence was detected demonstrating BocK specificity, bright field images provided as an imaging control and representative of equal cell confluency across conditions. Transfection with an eGFP plasmid used as a fluorescence control. All images are 223 μm × 167 μm, scale bars denote 50 μm.

(a)

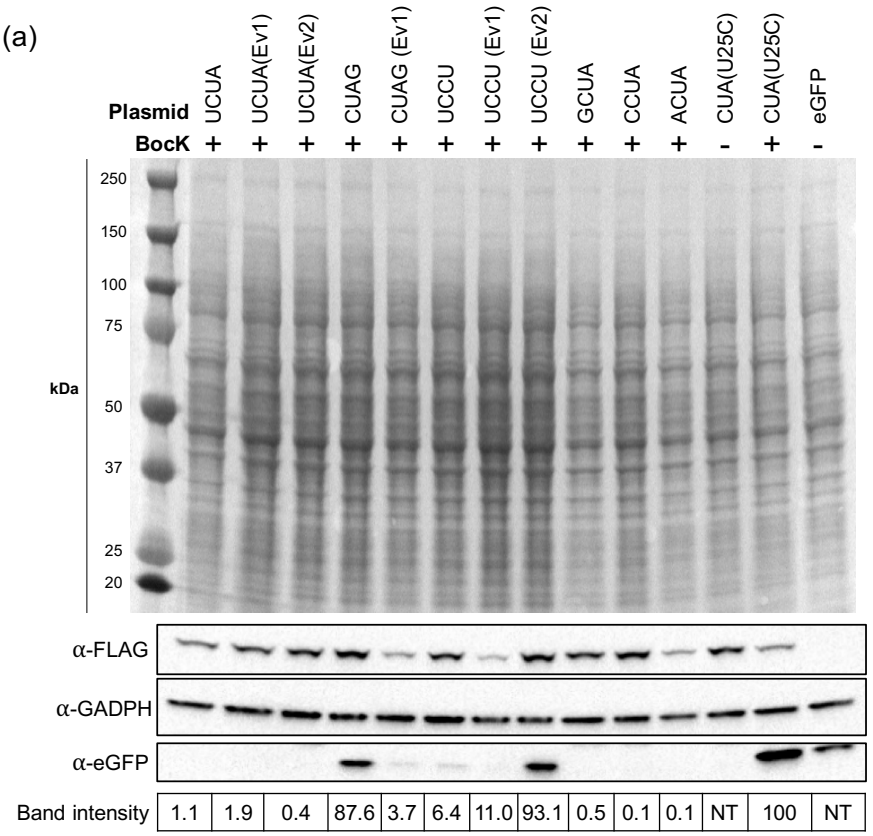

(b)

Plasmid	Test 1	Test 2	Test 3	Average (%)	StDev
UCUA	1.1	0.3	0.2	**0.6**	0.5
UCUA(Ev1)	1.9	0.3	0.1	**0.8**	1.0
UCUA(Ev2)	0.4	0.1	0.2	**0.2**	0.2
CUAG	87.6	31.7		**59.6**	39.5
CUAG(Ev1)	3.7	1.8	0.3	**1.9**	1.7
UCCU	6.4	2.1	0.2	**2.9**	3.2
UCCU(Ev1)	11.0	0.9	0.1	**4.0**	6.1
UCCU(Ev2)	93.1	52.3	84.0	**76.4**	21.4
ACUA	0.5	0.2	0.2	**0.3**	0.2
CCUA	0.1	0.1	0.2	**0.2**	0.0
GCUA	0.1	0.3	0.9	**0.5**	0.4
CUA(U25C) (+)	100	100	100	**100**	0

(c)

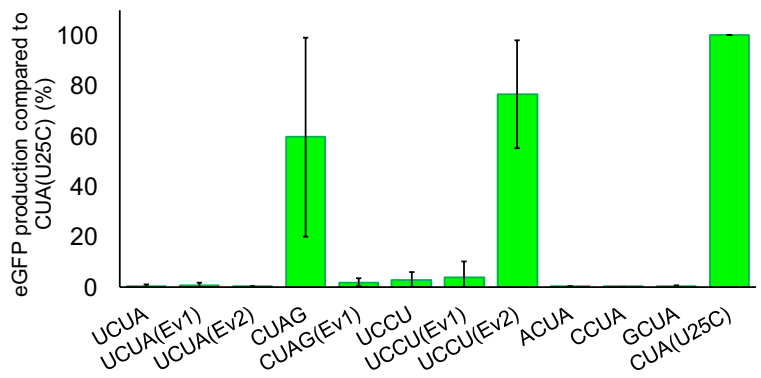

Figure 3.10: Western blot analysis of decoding efficiency for each quadruplet mutant
*(**a**) Representative blot of transfection samples; α-GAPDH used for control, α-FLAG for PylRS detection and α-eGFP depicts full length eGFP. Band intensities of eGFP deduced by setting Pyl $tRNA_{CUA(U25C)}$ (+BocK) as 100%, NT = not tested. (**b**) table of combined band intensity analysis of biological replicas, including average values for each quadruplet and standard deviation (**c**) Graph of data in (**b**) to show amount of full-length eGFP produced by quadruplet BocK incorporation, error bars denote standard deviation from three biological replicates.*

3.2.4 Cloning and testing of an orthogonal pair

To exploit genetic code expansion as molecular switches, an orthogonal tRNA/aaRS pair that does not cross-react with quadruplet Pyl tRNA/PylRS is required. Several *E. coli* aaRS (e.g. *Ec*TyrRS, *Ec*LeuRS etc) and their cognate tRNA have been engineered as orthogonal pairs for amber suppression in mammalian cells to incorporate unnatural amino acids.[372] The *Ec*TyrRS has been engineered to incorporate a range of synthetic tyrosine or phenylalanine analogs, including 3-methoxytyrosine (OMeY) or 4-Azido-phenylalanine (AzF).[372] As PylRS/tRNA has previously been identified to function orthogonally in *E. coli*, it should remain orthogonal in mammalian cells to an engineered *Ec*TyrRS/$tRNA_{CUA}$ pair. To verify this, an *Ec*TyrRS variant containing 4 residual mutations (Y37V, D182S, F183M and G265R) (called TyrRS* here) was selected.[409] The $tRNA_{CUA}$/TyrRS* pair was cloned into the same evaluation plasmid design as the pyrrolysyl pairs for accurate comparison of efficiency (**Figure 3.11a**). All components were generated via PCR and cloned into the evaluation plasmid vector, ensuring the only deviation in plasmid sequence between the pyrrolysyl plasmids and tyrosyl plasmids was the eGFP reporter codon, and the tRNA and synthetase genes.

HEK293 cells were transiently transfected with the evaluation plasmid and cultured for 24 hours in DMEM 10% v/v FBS supplemented with 1 mM OMeY or AzF respectively, both substrates of the TyrRS* mutant.[409, 410] The observations by *Italia et al.* saw for this TyrRS* mutant that OMeY incorporation was stronger than AzF,[410] however in contrast to those findings, the opposite was observed in this case. Fluorescent eGFP was clearly presented to be of greater intensity when cells were incubated with 1 mM AzF compared to 1 mM OMeY (**Figure 3.11b**).

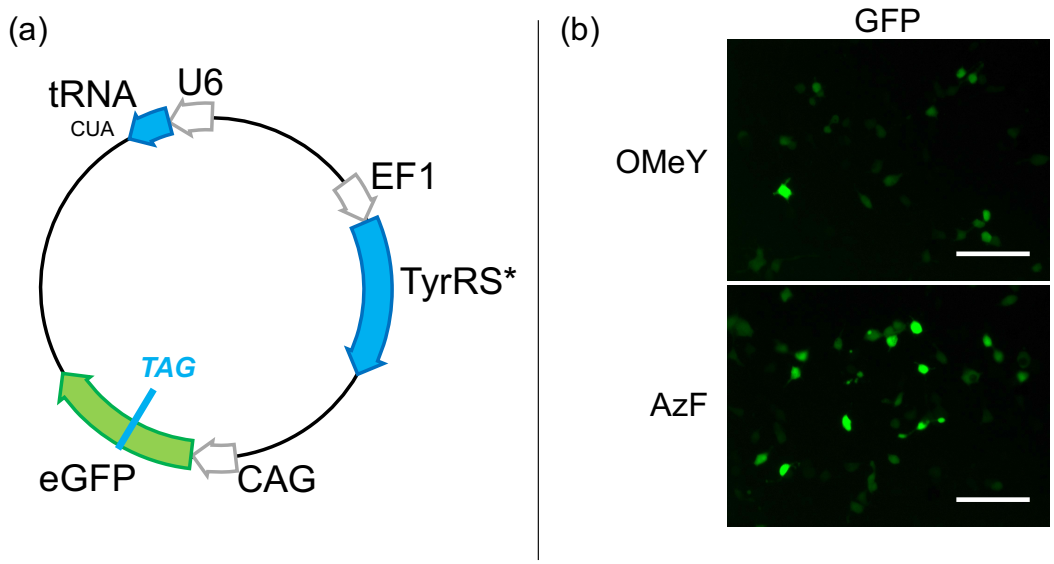

Figure 3.11: TyrRS*/tRNA$_{CUA}$ pair decoding efficiency in presence of OMeY or AzF
*(**a**) structure of evaluation plasmid generated to measure TyrRS*/tRNA$_{CUA}$ mediated amber suppression. (**b**) eGFP fluorescent imaging of HEK293 cells transfected with the evaluation plasmid in (**a**) and incubated with either OMeY or AzF at 1 mM concentration for 48 hours. All images are 223 µm × 167 µm, scale bars denote 50 µm.*

To successfully exploit the PylRS/tRNA$_{UCCU(Ev2)}$ and TyrRS*/tRNA$_{CUA}$ as molecular switches, it was paramount to deduce their orthogonality to each other. If cross reactivity occurs between the pairs (i.e. Tyr tRNA$_{CUA}$ incorporating BocK, or Pyl tRNA$_{UCCU(Ev2)}$ incorporating AzF) then the end result would be unwanted background activity when performing logic operations which is not desired as it can hinder the applicability of the design. To examine this, HEK293 were transiently transfected with either the PylRS/tRNA$_{UCCU(Ev2)}$ or TyrRS*/tRNA$_{CUA}$ evaluation plasmids and cultured for 24 hours in the presence of either 1 mM BocK or 1 mM AzF media. Indeed, eGFP fluorescence was only detected when a pair was in the presence of its cognate unnatural amino acid, confirming the absence of promiscuity between the pairs (**Figure 3.12a**). The results confirm the orthogonality of the two pairs and their use for independent logic operations. Therefore, they are promising candidates for molecular switch models, as they selectively incorporate their cognate unnatural amino acids with no observable cross-reactivity.

Furthermore, as the pairs have been identified to function with a reasonable efficiency, it was noteworthy to assess their ability to perform a double

incorporation into a single eGFP reporter as this has seldom been accomplished in mammalian cells. To assess their ability to double incorporate, a two-plasmid transfection model was designed (**Figure 3.12b**). The reporter eGFP on the Pyl evaluation plasmid was mutated via PCR to introduce an amber codon at the 40th residue ($eGFP_{40TAG\text{-}150AGGA}$), while the original reporter eGFP in the Tyr evaluation plasmid was removed. This design ensured full length eGFP would only be accomplished when OMeY or AzF and BocK are concurrently incorporated into the same amino acid chain. Unfortunately, low levels of eGFP fluorescence was detected by light microscopy (**Figure 3.12c**), however controls were performed to determine selectivity, and under 4 conditions ((1) no unnatural amino acids, (2) BocK only, (3) AzF only and (4) BocK and AzF) eGFP fluorescence was only detected when in the presence of both BocK and AzF (**Figure 3.12d**). Although double incorporation was not as efficient as hoped, this data remains crucial when considering mammalian cell logic gate designs, as it demonstrates that an effective result is unlikely to occur if incorporation is required to be within the same protein sequence. This is not to be unexpected however, as incorporating both amino acids into a single chain means the output has an accumulative dependence on both pairs. For example, if TyrRS*/$tRNA_{CUA}$ has an overall incorporation efficiency of 50% compared to endogenous aaRS/tRNA pairs, then only 50% of the reporter peptide that was initiated for translation is available for BocK incorporation. Then, if PylRS/$tRNA_{UCCU(Ev2)}$ also has an efficiency of 50%, then the total yield of full length protein carrying both amino acids would be approximately 25%. However, if logic gates are designed where two independent peptides are employed for each amino acid, then the overall output would be 50% yield as the pairs are not reliant on the efficiency of each other.

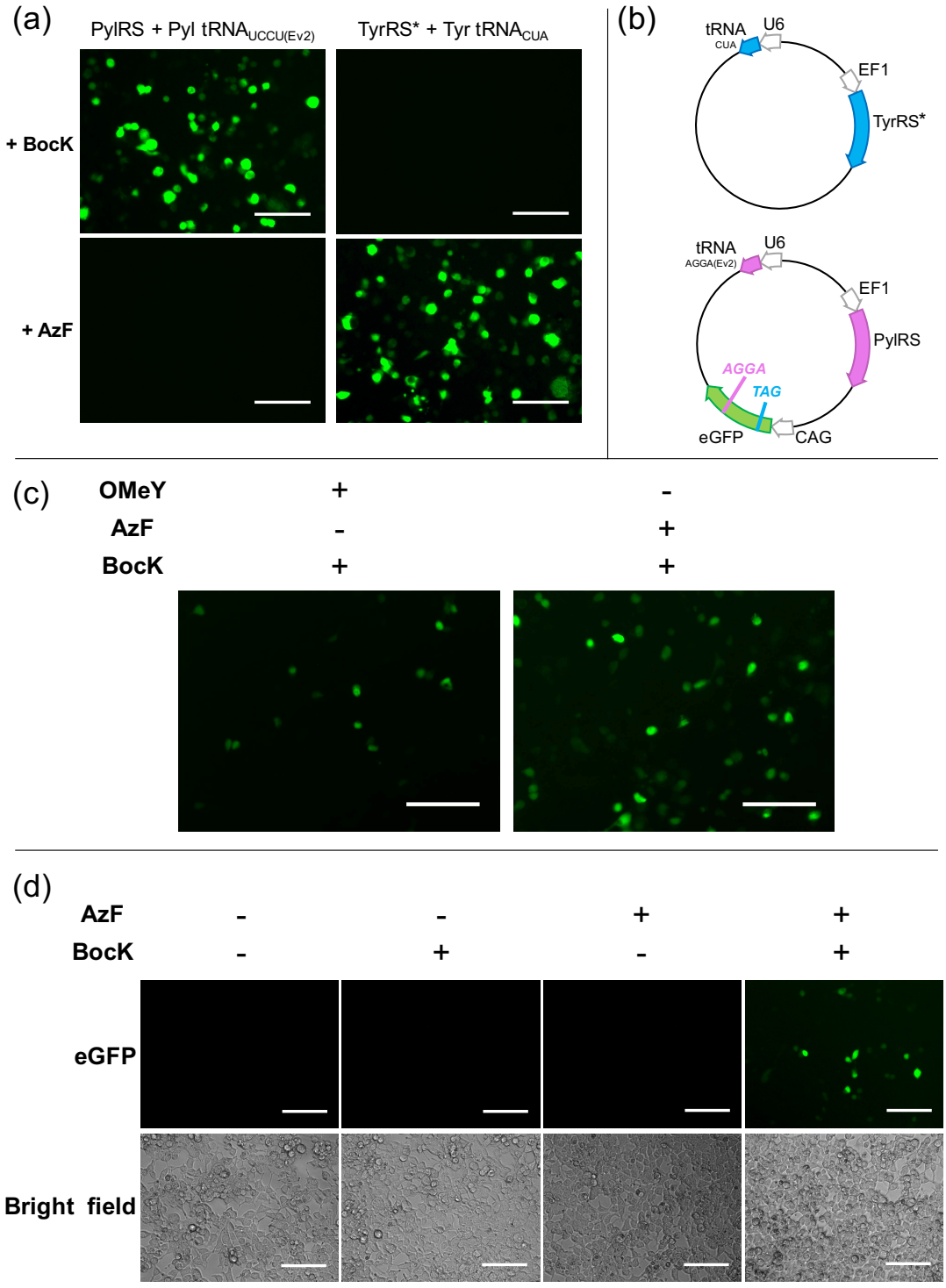

Figure 3.12: PylRS/tRNA and TyrRS*/tRNA orthogonality and dual operation in HEK293
*(**a**) Fluorescent imaging representation of the orthogonality of the two tRNA/aaRS pairs. When incubated in the presence of either 1 mM BocK or 1 mM AzF, eGFP fluorescence was only detected when aaRS/tRNA pair was in the presence of their cognate amino acid, confirming no cross-reactivity. (**b**) Plasmid design for co-transfection to determine the efficiency of double-incorporation. (**c**) Fluorescent imaging of HEK293 cells production of eGFP via double incorporation in the presence of BocK and either OMeY or AzF. (**d**) Double incorporation specificity testing; transfected HEK293 in presence of no amino acid, AzF only, BocK only, or both AzF and BocK. eGFP fluorescence only detected when cells are in the presence of both AzF and BocK. All images are 223 μm × 167 μm, scale bars denote 50 μm.*

3.3 Optimising mammalian quadruplets

Once the two incorporation systems had been cloned and tested, the next stage was to try and improve their incorporation efficiencies.

3.3.1 eRF1(E55D) factor testing

A previous research article discussed the use of a mutated eukaryotic release factor (eRF1) to increase the incorporation efficiency of aaRS/tRNA for amber suppression.[406] eRF1 is a native protein to mammalian cells, where it facilitates the enzymatic shipment of aminoacylated tRNA to the ribosomes. It was demonstrated that a simple mutation of the 55th residue from glutamic acid to aspartic acid (E55D) gave a significantly higher yield of unnatural amino acid incorporation. As this factor was already available as part of the lab plasmid library, it was noteworthy to investigate whether the presence of this eRF1 variant (eRF1(E55D)) improved the activity of PylRS/tRNA$_{UCCU(Ev2)}$ or TyrRS*/tRNA$_{CUA}$. HEK293 cells were transiently transfected with either the pyrrolysyl or tyrosyl evaluation plasmid and co-transfected with a plasmid encoding eRF1(E55D) under a CAG promotor system. As a control, a plasmid encoding native eGFP was co-transfected with the eRF1(E55D) plasmid. Unfortunately, no improvement in eGFP fluorescence was detected (**Figure 3.13a**). However, the paper that developed this eRF1 variant noticed improved incorporation when there are multiple UAA incorporation sites in a single gene sequence. Therefore, the presence of the eRF1(E55D) for double incorporation was also tested. Unfortunately, this was also unsuccessful, and no distinguishable improvement could be detected between cells in the presence or absence of eRF1(E55D) (**Figure 3.13b**). Again, these results cannot be directly compared to the paper that reported this variant, as they used a PylRS mutant for amber incorporation, and they had not tested a Tyr variant. Moreover, the PylRS/tRNA pair used for double incorporation in **Figure 3.13b** was a quadruplet mutant, not an amber suppressing variant like the research article which may influence the transferability.

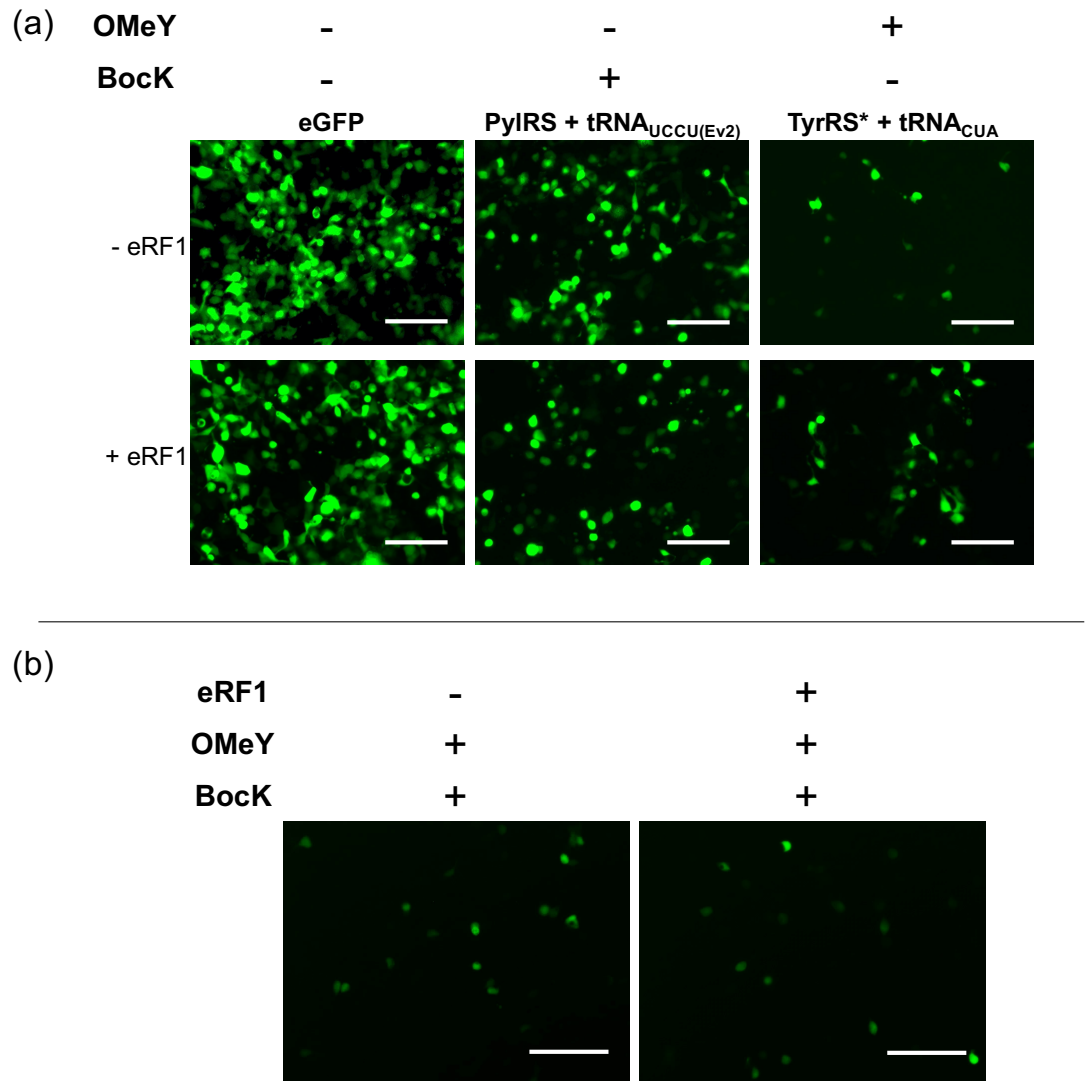

Figure 3.13: Determining impact of eRF1(E55D) on unnatural amino acid incorporation
*(**a**) HEK293 cells transfected with either PylRS/tRNA$_{UCCU(Ev2)}$ or TyrRS*/tRNA$_{CUA}$ evaluation plasmids and incubated for 48 hours in the presence of their cognate unnatural amino acid at 1 mM in the presence or absence of eRF1(E55D). Transfection of a plasmid encoding eGFP was used as a fluorescence control. (**b**) Double incorporation efficiency in the presence or absence of eRF1(E55D). All images are 223 µm × 167 µm, scale bars denote 50 µm.*

3.3.2 1x vs 4x tRNA design and cloning

Most research into mammalian genetic code expansion uses a cassette of tRNA genes. It is thought that this would improve the overall efficiency,[377, 381, 383, 385, 408, 409] as more tRNA is transcribed resulting in a higher availability of tRNA for amino-acylation and hence unnatural amino acid incorporation. As the evaluation plasmids that have been used up to this point carry a single copy of tRNA, it was deemed worthy to assess whether quadrupling the

amount of tRNA on each plasmid would increase the amount of full length eGFP produced.

To clone a 4x tRNA cassette, a series of PCR reactions were performed and assembled into a cassette. The resulting plasmids were only different to their parents by having 4 copies of tRNA each under a U6 promotor (**Figure 3.14**). As previously discussed, the benefit of U6 is that repeating "U6 > gene" units can be arranged in close proximity in a nucleic acid sequence, facilitating the simultaneous expression of multiple gene copies from a single DNA string enabling higher yield.[401, 402] Therefore, this could be exploited when multiplying the copy number of tRNA genes in a single plasmid. HEK293 were transiently transfected with evaluation plasmids encoding a single copy or 4 copies of their cognate tRNA. Cells were incubated with 1 mM BocK or AzF respectively for 24 hours prior to fluorescent imaging. For both PylRS/$tRNA_{UCCU(Ev2)}$ and TyrRS*/$tRNA_{CUA}$, a marked increase in fluorescent eGFP was detected when multiple copies of tRNA were used (**Figure 3.15**). Moreover, western blot analysis revealed an average 2.5-fold increase in eGFP for PylRS/$tRNA_{UCCU(Ev2)}$ (**Figure 3.15a**), and an average 6.5-fold increase in eGFP for TyrRS*/$tRNA_{CUA}$ (**Figure 3.15b**). Students paired t-test statistical analysis revealed p values of $p < 0.05$ and $p < 0.03$ respectively for PylRS/$tRNA_{UCCU(Ev2)}$ or TyrRS*/$tRNA_{CUA}$ when comparing 1x tRNA to 4x tRNA. Moreover, the multiplication of tRNA copies for TyrRS*/$tRNA_{CUA}$ saw an eGFP yield more comparable to PylRS/$tRNA_{UCCU(Ev2)}$ overall, which is beneficial to logic operation construction as comparable levels of output are desired for an equal level of control between switches.

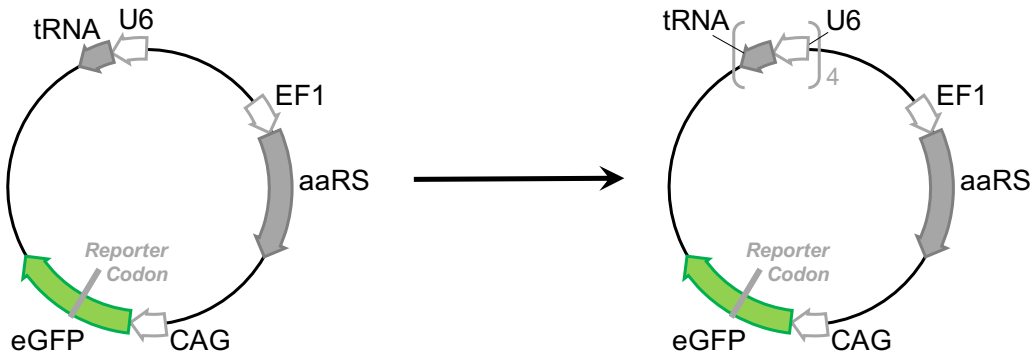

Figure 3.14*:* Graphical representation of modifications made to evaluation plasmids to increase tRNA copy number from n = 1 to n = 4.

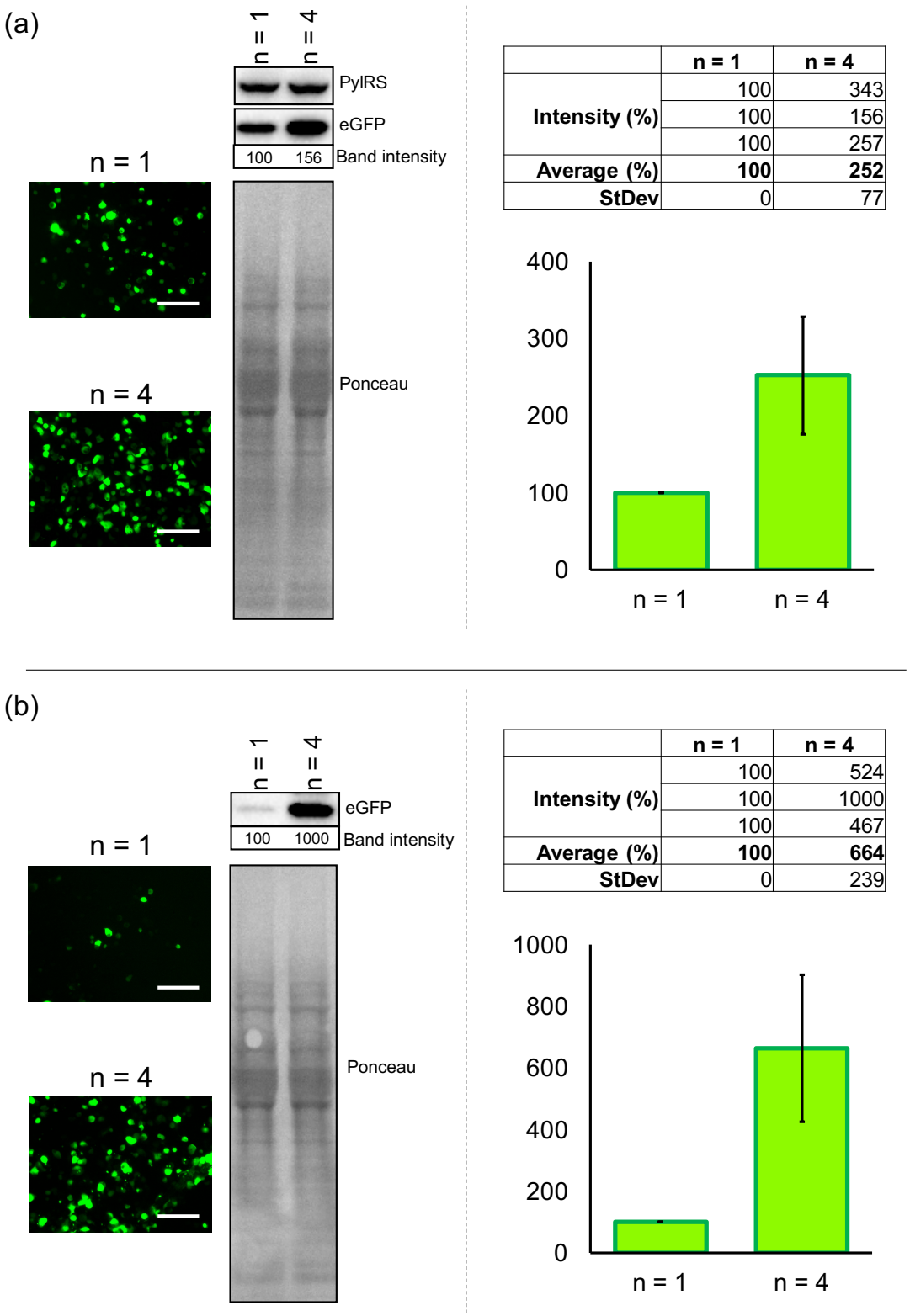

Figure 3.15: Efficiency of PylRS and TyrRS* decoding compared to tRNA copy number
*(**a**) Representative fluorescent imaging and western blot analysis of BocK incorporation when copy number of $tRNA_{UCCU(Ev2)}$ is increased from n = 1 to n = 4. Band intensities across 3 biological replicas averaged and plotted on a graph, error bars denote standard deviation. (**b**) Representative fluorescent imaging and western blot analysis of AzF incorporation when copy number of $tRNA_{CUA}$ is increased from n = 1 to n = 4. Band intensities across 3 biological replicas averaged and plotted on a graph, error bars denote standard deviation. All images are 223 µm × 167 µm, scale bars denote 50 µm.*

As increasing the number of tRNA from n = 1 to n = 4 provided a valuable improvement in eGFP production for both aaRS/tRNA pairs, it was seen to be worthwhile to assess whether increasing tRNA copy number could improve double-incorporation into a single eGFP. As shown, double incorporation into eGFP using a single reporter and one copy of each tRNA was not particularly efficient with TyrRS*/$tRNA_{CUA}$ and PylRS/$tRNA_{UCCU(Ev2)}$ (**Figure 3.12**), and testing alongside the eRF1(E55D) factor also failed to improve the incorporation (**Figure 3.13**). In theory, increasing the copy number of tRNA and the reporter gene would increase overall output, as there is more target mRNA being produced due to the reporter gene being duplicated, and there is more tRNA available for aminoacylation and subsequent UAA incorporation.

To test whether increasing tRNA and reporter genes would improve eGFP output in a double-incorporation design, the plasmids detailed in **Figure 3.12b** were modified to generate two evaluation plasmids that carry the reporter eGFP, PylRS or TyrRS* and 4 copies of their respective tRNA (**Fig 3.16a**). These plasmids were then co-transfected into HEK293 and examined under the same 4 conditions of UAA supplementation as previously stated. Direct comparison of the original design (Design A) to the optimised design (Design B) showed a clear improvement in eGFP production which was visualised by fluorescent microscopy and western blotting (**Figure 3.16b**). Moreover, eGFP fluorescence continued to be selective to only be present when cells were incubated with AzF and BocK concurrently. Importantly, these results show that even under conditions where tRNA copies are increased, the pairs continue to selectively incorporate their cognate unnatural amino acids with no observable cross-reactivity.

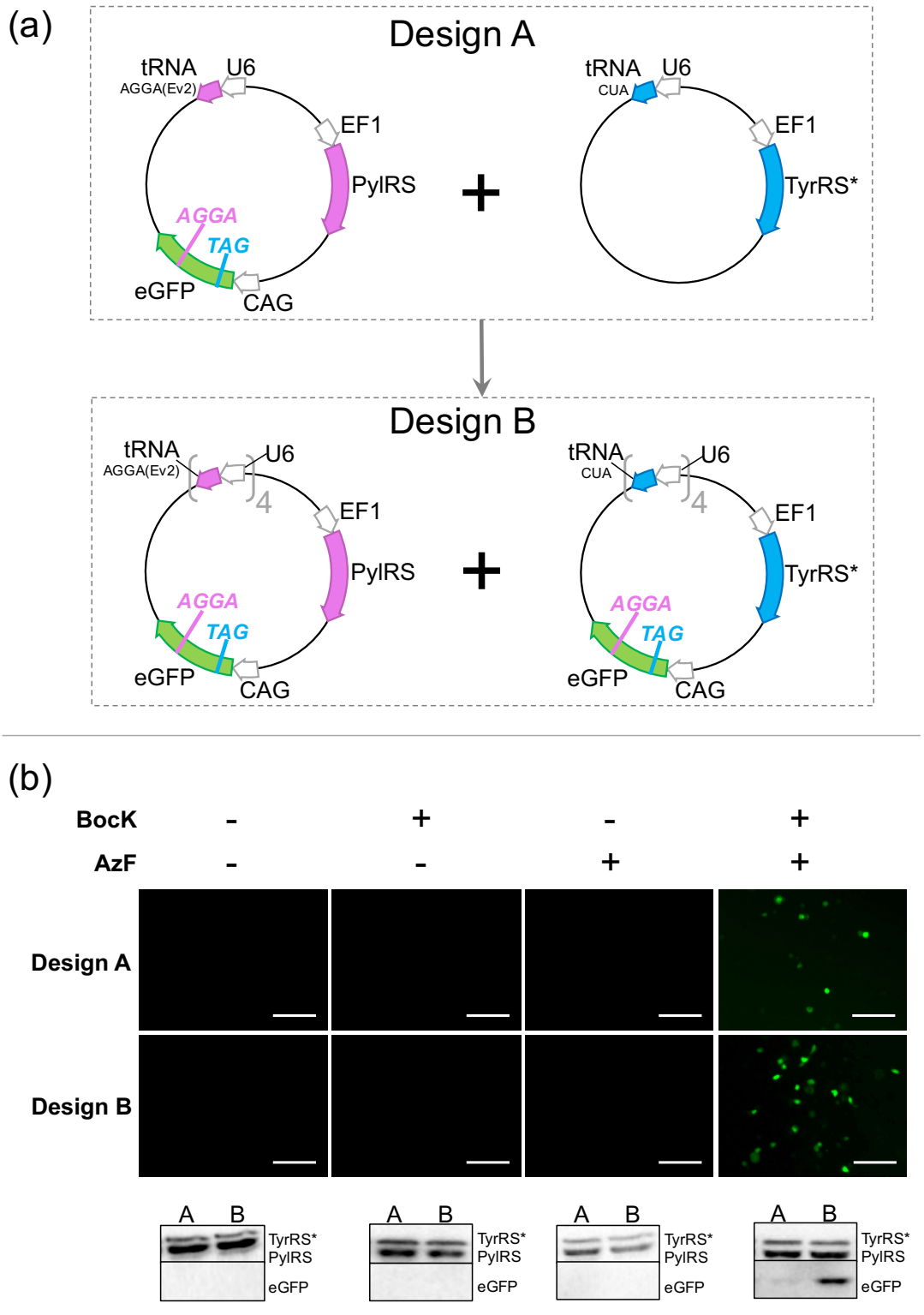

Figure 3.16: Double-incorporation with increased copy numbers of tRNA and reporter
*(**a**) Change in plasmid designs used to increase copy numbers of reporter gene and tRNA copy numbers; named "Design A" and "Design B". (**b**) Fluorescent imaging of cells under 4 conditions of UAA supplementation and corroborating western blots. All images are 223 µm × 167 µm, scale bars denote 50 µm.*

3.4 Mammalian cell logic gates

3.4.1 Design and testing of split GFP

To assess the applicability of genetic code expansion as therapeutic logic gate switches, it was first essential to design simple logic gates with fluorescent reporters. These experiments would provide visual representation of whether unnatural amino acids can be adapted as switch molecules, confirm whether the backbone design is suitable for therapeutic control and moreover represent how efficient the system design is as a whole. It was important to perform these experiments for general troubleshooting prior to the conversion into a therapeutic design. For these visual reporter logic gates, systems were designed using the split GFP system (sGFP). sGFP is a derivative of the native fluorescent GFP protein, developed by *Cabantous et al.* and optimised in mammalian cells by *Kamiyama et al.*[411, 412] The split protein relies on the concurrent presence of two polypeptides to form a fluorescent complex; a larger subunit called sGFP(1-10), and a smaller subunit called sGFP(11). The sGFP fluorescent chromophore can only develop and mature upon complex assembly, therefore sGFP(1-10) and sGFP(11) are not fluorescent in their individual forms (**Figure 3.17a**). As the logic gates would benefit from a transfection control, a design that employs mCherry (red fluorescent protein) as a constitutive reporter was constructed. Prior to testing BocK and AzF as switch molecules however, ensuring that the native design works was a necessity. Using a CAG promotor, mCherry was positioned 5' and in-frame to the split GFP peptide sequences, with a P2A self-cleavable peptide sequence between the C-terminus of mCherry and the N-terminus of sGFP(1-10) or sGFP(11) respectively. P2A is an 18 amino-acid sequence that undergoes spontaneous proteolysis during peptide folding that leaves a single proline residue at the N-terminus of the 3' peptide and the remaining residues on the C-terminus of the 5' peptide. It is derived from the porcine teschovirus-1, and has been widely utilised in mammalian studies.[413] For these logic gates, the inclusion of a P2A cleavable linker would ensure separation of the sGFP fragments from the constitutive mCherry during protein folding, reducing the

risk of mCherry blocking or hindering the sGFP(1-10) and sGFP(11) complex formation (**Figure 3.17b**).

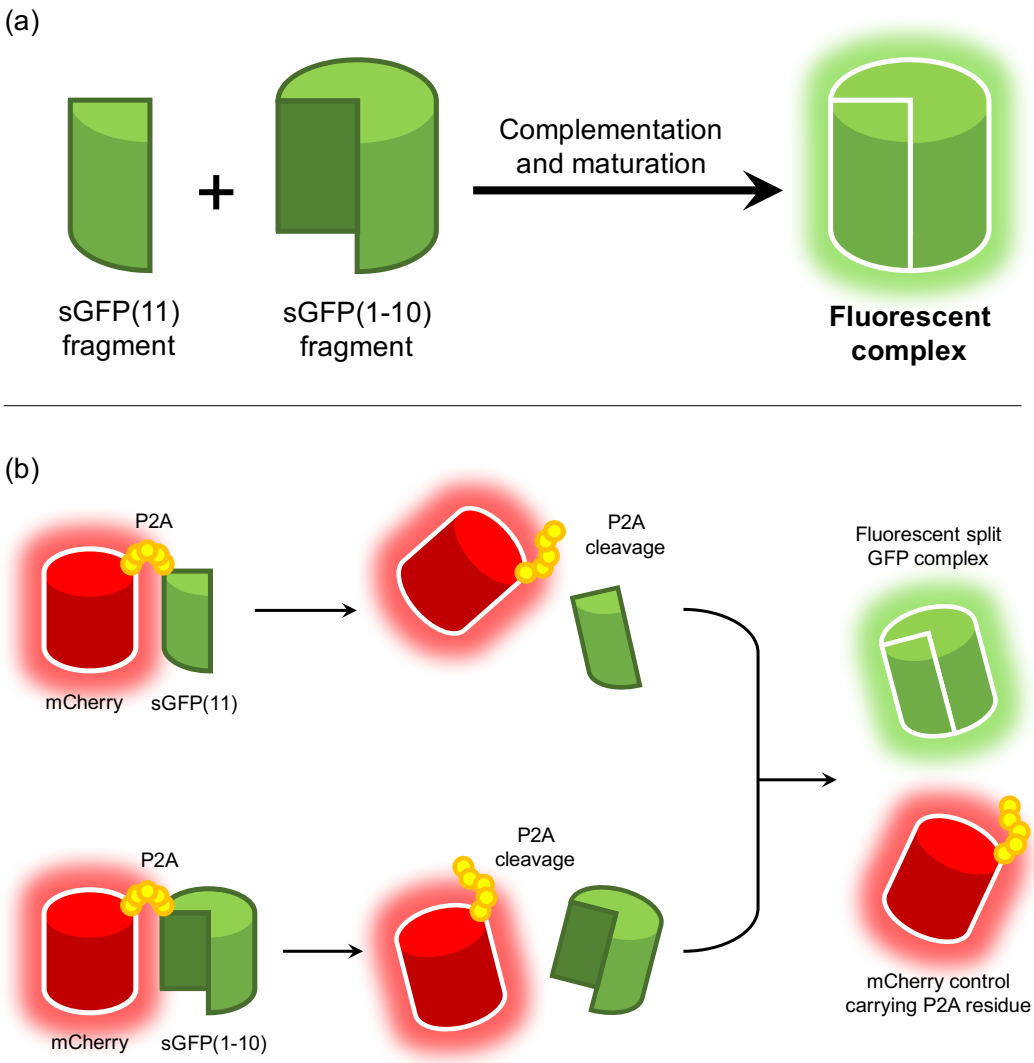

Figure 3.17: Proposed approach to acquire UAA-dependent mammalian cell logic gates
*(**a**) Split GFP complex; GFP fluorescence dependent on self-complementation of sGFP(1-10) with sGFP(11). (**b**) General backbone design for adaptation to enable BocK and AzF dependent logic operation.*

DNA fragments optimised for mammalian expression systems encoding sGFP(1-10) and sGFP(11) were purchased and cloned via PCR and Gibson assembly into a vector carrying mCherry with a C-terminal P2A sequence (**Figure 3.18a**). HEK293 cells were transiently transfected with either plasmids or co-transfected with both plasmids and incubated for 24 hours prior to imaging. Wells were imaged using a light microscope and mCherry and GFP fluorescence recorded for each condition. As predicted, GFP fluorescence

was only detected when cells were co-transfected with both plasmids, and no GFP was visualised when cells were only transfected with each plasmid individually. (**Figure 3.18b**).

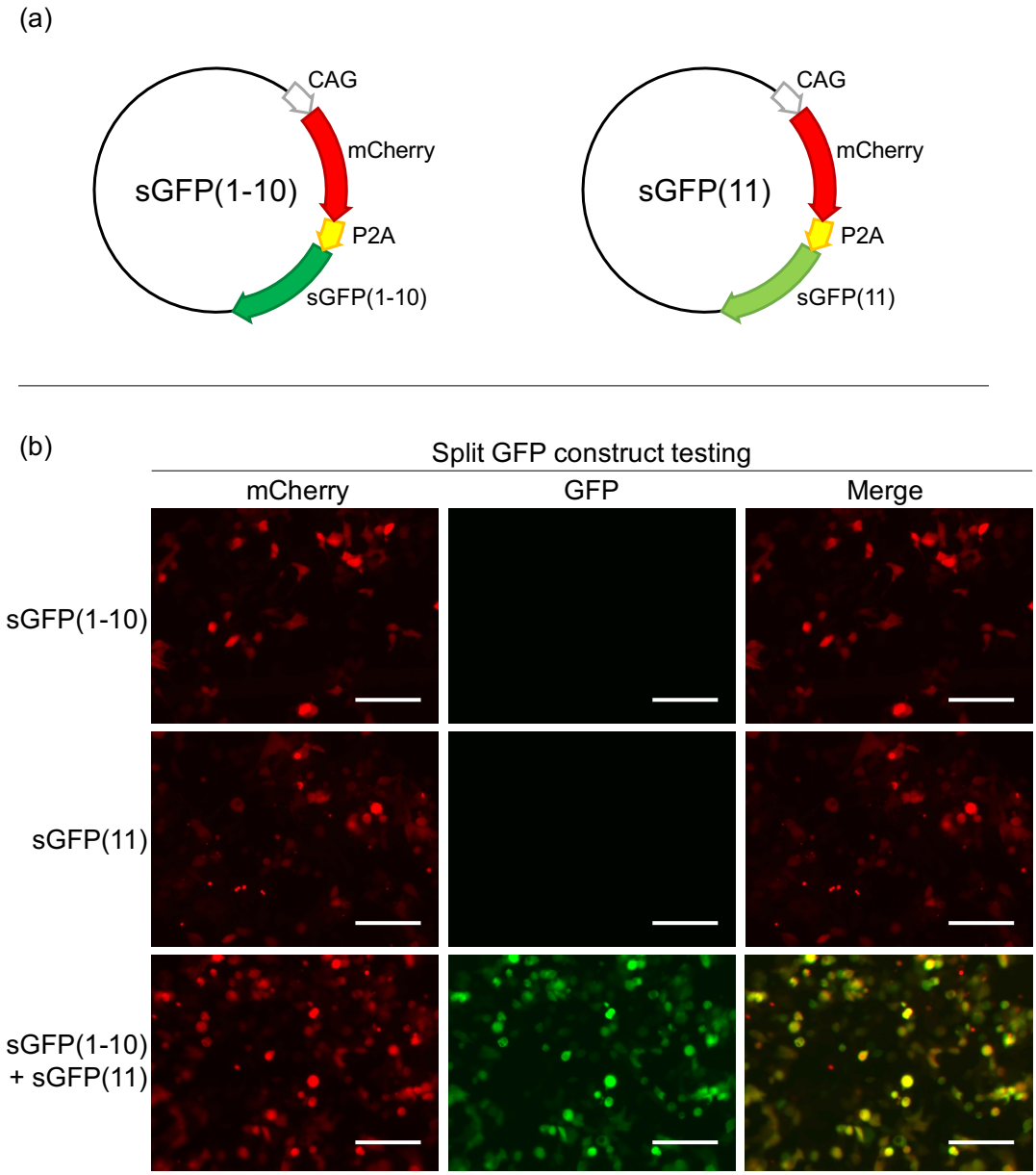

Figure 3.18: Split GFP complementation testing in HEK293 with mCherry control.
*(**a**) plasmids designed for co-transfection as illustrated in **Figure 3.16b**. (**b**) Fluorescent imaging of HEK293 transfected with either or both plasmids. mCherry used as a transfection control. All images are 223 µm × 167 µm, scale bars denote 50 µm.*

The observations made in **Figure 3.18** confirm the functionality of the design in **Figure 3.17b**, therefore the experimental plasmids could now be modified

where the expression of sGFP(1-10) or sGFP(11) fragments would be strictly dependent on the presence or absence of BocK and AzF.

3.4.2 AND split GFP logic gates

Logic gates with an AND operation require the presence of both inputs to achieve the desired output.[414] To generate an AND logic gate with unnatural amino acid incorporation, split GFP complex formation needed to be dependent on the presence of both AzF and BocK. To achieve this, the system detailed in **Figure 3.17b** was modified to ensure sGFP(1-10) and sGFP(11) production was dependent on AzF or BocK incorporation respectively (**Figure 3.19**). Introduction of a TAG codon or an AGGA codon at the junction between the P2A linker and sGFP fragments should hypothetically ensure translation of the split GFP peptides could only take place if AzF or BocK were concurrently incorporated (**Figure 3.19a**). Moreover, as sGFP fluorescence is dependent on the mutual presence of sGFP(1-10) and sGFP(11) for chromophore maturation, This design would ensure that GFP fluorescence was dependent on the presence of AzF and BocK as the sGFP fragments could only be produced upon their incorporation into the sequence (**Figure 3.19b**). Similar to the design in **Figure 3.17b**, it was important to retain mCherry fluorescence as a transfection control. By comparing mCherry fluorescence to GFP fluorescence, the efficiency of the logic gates could be visually ascertained. To achieve the experimental design denoted in **Figure 3.19**, two plasmids were cloned. Previous optimisation studies proved multiple repeats of U6>tRNA increased overall output, and generated a more comparable output efficiency between BocK and AzF incorporation. To ensure the unnatural amino acids incorporated would not interfere with the P2A splicing or the split GFP complex formation, a spacer was introduced between C-terminal P2A and N-terminal sGFP(1-10) or sGFP(11) respectively. This spacer of three amino acid residues (G-K-S) would help to ensure that BocK or AzF would have no structural hindrance on the P2A cleavage or split GFP fragment activities. The two plasmids cloned carried the respective UAA incorporation machinery (TyrRS*/$tRNA_{CUA}$ or PylRS/$tRNA_{UCCU(Ev2)}$), and their complementary reporter system (i.e. *mCherry-P2A-TAG-sGFP(1-10)*, or

mCherry-P2A-AGGA-sGFP(11)) (**Figure 3.19a**). The plasmids detailed were cloned through a series of PCR and Gibson assembly procedures.

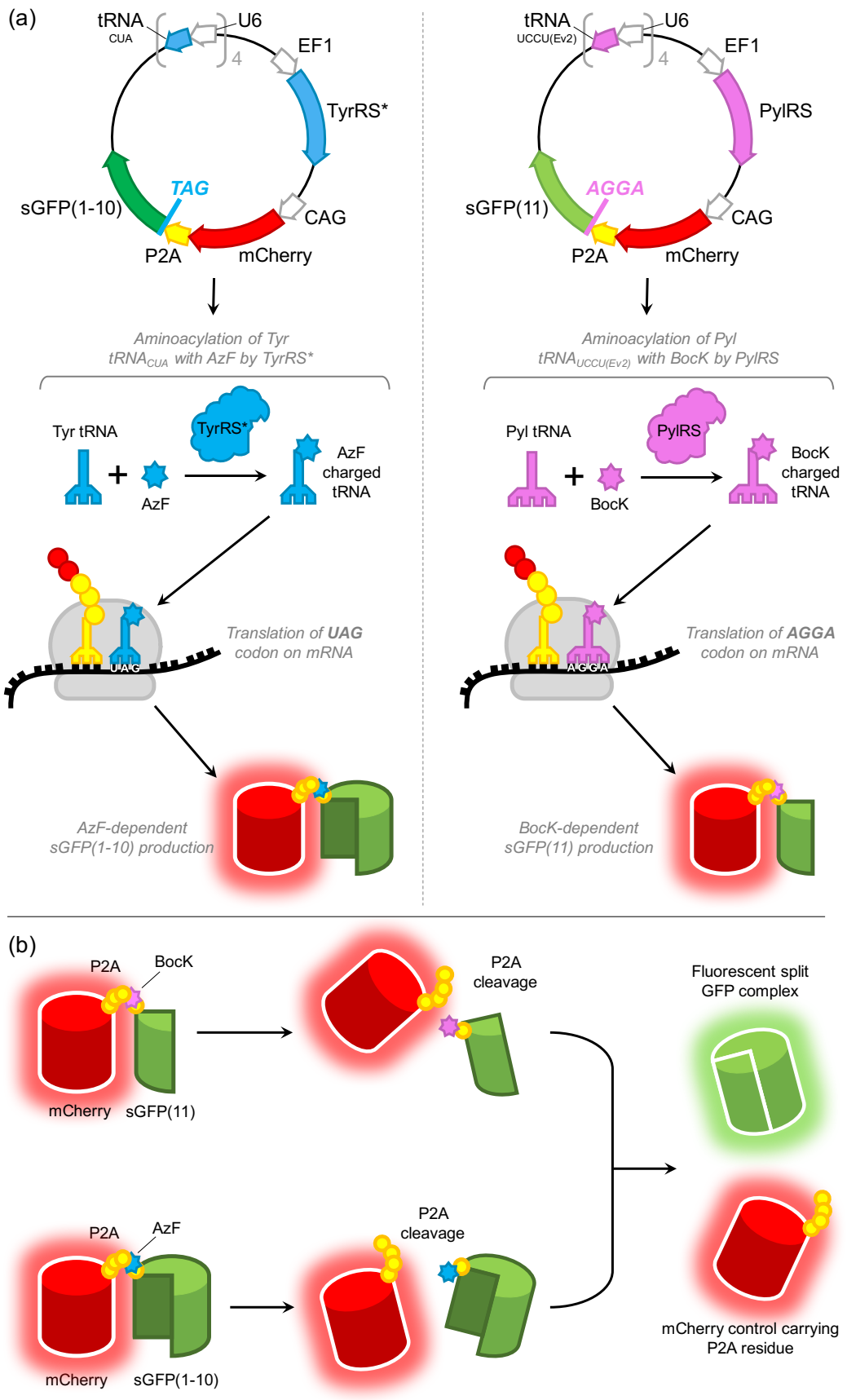

Figure 3.19: Design to obtain UAA dependent AND logic operation with BocK and AzF
*(**a**) Plasmids for AND logic operation; sGFP(1-10) and sGFP(11) production dependent on BocK and AzF. (**b**) schematic principle of AND logic sGFP complementation.*

HEK293 cells were transiently co-transfected with both of the plasmids (**Figure 3.19a**) and incubated for 48 hours in four different conditions; (1) no UAAs, (2) BocK only, (3) AzF only and (4) AzF and BocK. For all conditions, BocK and AzF were at a final concentration of 1 mM in the cell growth media. As predicted, GFP fluorescence could only be detected when cells were incubated in the presence of both AzF and BocK (**Figure 3.20**), and mCherry fluorescence was of equal intensity across all 4 conditions. GFP fluorescence was observed to be of a relatively high level, demonstrating a reasonably high efficiency of the system.

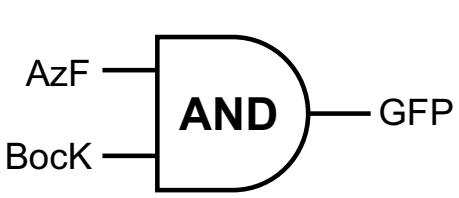

AzF	BocK	GFP
0	0	0
1	0	0
0	1	0
1	1	1

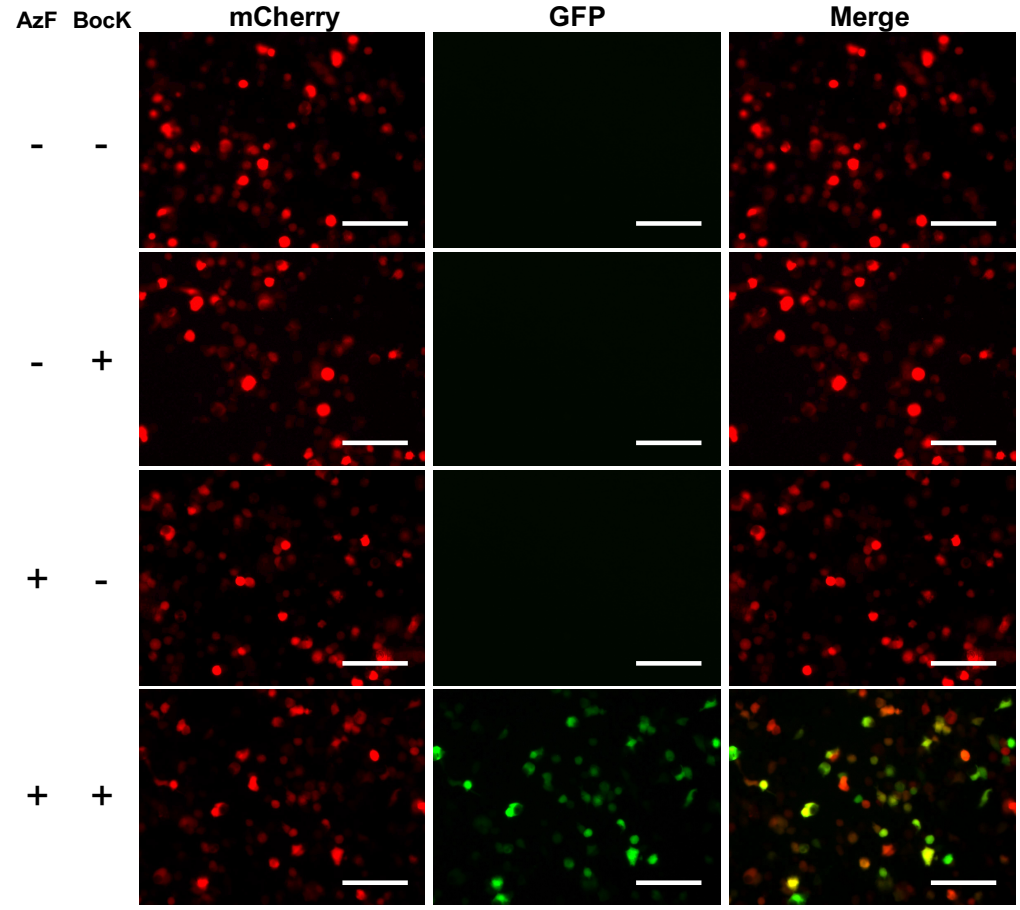

Figure 3.20: Fluorescent imaging of HEK293 cells transfected with AND logic plasmids
Cells were transfected and incubated under 4 conditions: (1) No BocK or AzF, (2) BocK only, (3) AzF only and (4) BocK and AzF. All amino acids were supplemented at 1 mM concentration and cells incubated for 48 hours. mCherry fluorescence used as a transfection control. All images are 223 µm × 167 µm, , scale bars denote 50 µm.

To confirm the specificity of BocK/AzF dependence and continuation of orthogonality, the plasmids were individually transfected into HEK293 cells and incubated in the presence or absence of their cognate amino acid for 48 hours. Cells were then imaged for mCherry and GFP fluorescence. As expected, there was no green fluorescence detected regardless of unnatural amino acid supplementation (**Figure 3.21**), however mCherry fluorescence

was detected, confirming its constitutive expression and successful transfection.

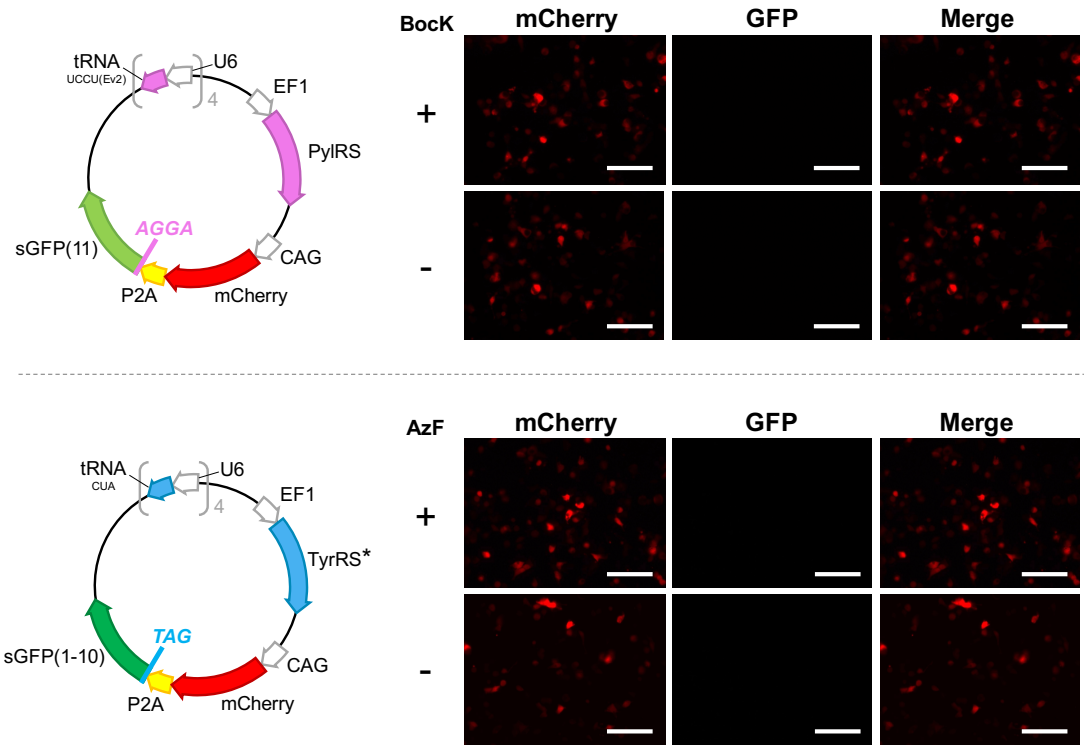

Figure 3.21: Transfection of HEK293 with individual plasmids from AND logic operation
Cells were incubated in the presence and absence of their cognate unnatural amino acid (BocK or AzF). All images are 223 µm × 167 µm, scale bars denote 50 µm.

3.4.3 OR split GFP logic gates

Logic gates with an OR operation require the presence of either inputs to achieve the desired output.[414] To generate an OR logic gate with unnatural amino acid incorporation, split GFP complex formation needed to be dependent on the presence of either or both AzF and BocK. To achieve this, the mCherry and split GFP coupled system was modified to ensure sGFP(1-10) was constitutively expressed, and sGFP(11) production was dependent on the incorporation of either AzF, BocK or both (**Figure 3.22**). By replacing one of the mCherry genes with sGFP(1-10), this ensured constitutive expression of sGFP(1-10). Furthermore, ensuring both plasmids have the sGFP(11) gene downstream of the P2A linker, the introduction of a TAG codon or an AGGA codon at the junction between the P2A linker and sGFP(11) sequences would

theoretically ensure production of the complementary fragment when cells are in the presence of either or both AzF and BocK. Similar to the design in **Figure 3.20**, it was important to retain mCherry fluorescence as a transfection control, so it was retained on one of the plasmids. By comparing mCherry fluorescence to GFP fluorescence, the efficiency of the logic gates could be visually ascertained.

To achieve the experimental design denoted in **Figure 3.22b**, a similar plasmid construction to the AND logic gate was used, however the TyrRS*/$tRNA_{CUA}$ plasmid had its mCherry gene replaced with sGFP(1-10), and the original sGFP(1-10) exchanged for sGFP(11) (i.e. *mCherry-P2A-TAG-sGFP(1-10)* was exchanged for *sGFP(1-10)-P2A-TAG-sGFP(11)*). The pyrrolysyl plasmid remained the same as used in the AND logic gate. Again, to ensure BocK or AzF incorporation would not interfere with P2A splicing or split GFP complex formation, a spacer was used between C-terminal P2A and N-terminal sGFP(11) to ensure the unnatural amino acids incorporated would have no structural hindrance on the P2A cleavage or split GFP fragment activities. The plasmids detailed were cloned through a series of PCR and Gibson assembly procedures.

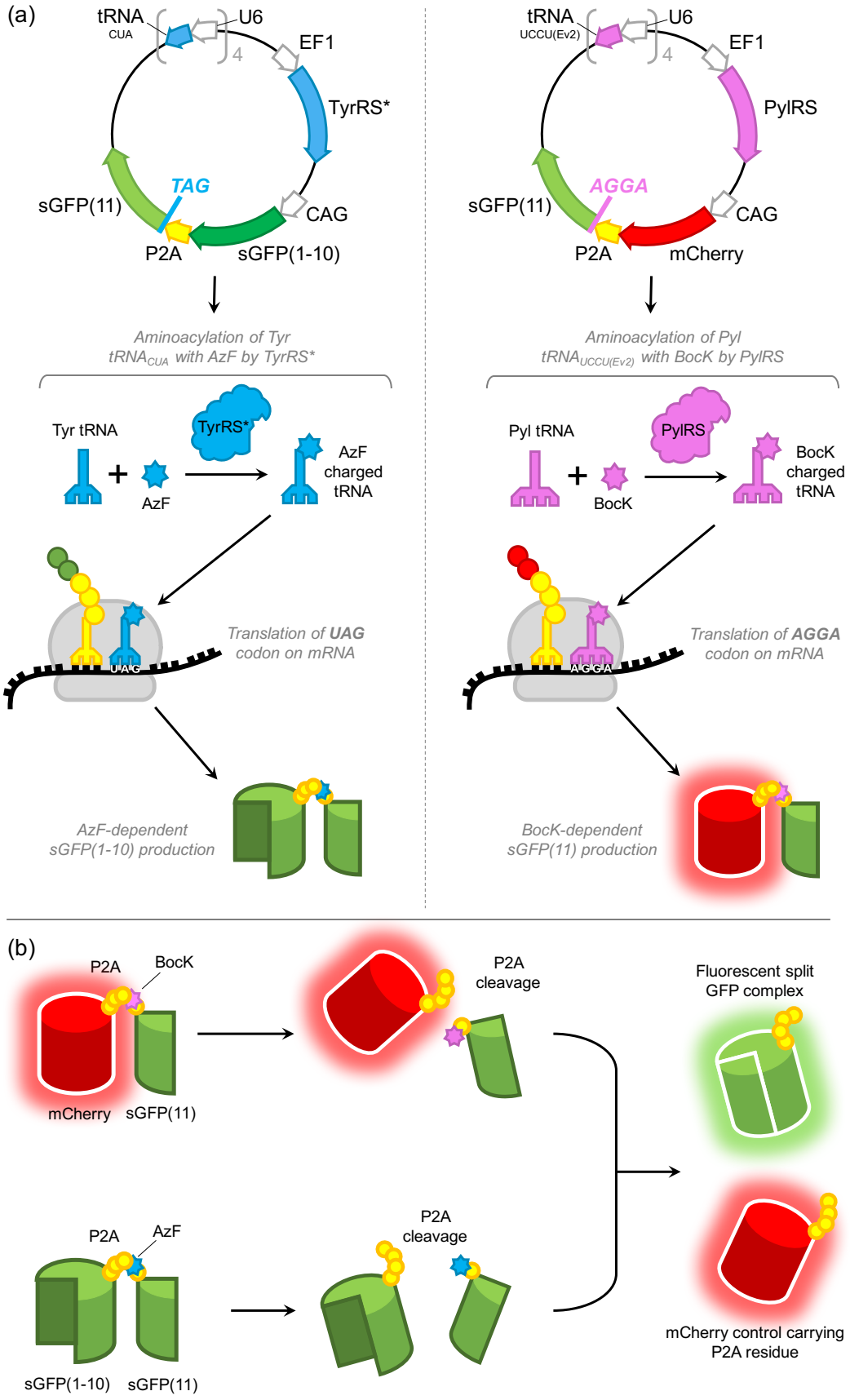

Figure 3.22: Design to obtain UAA dependent OR logic operation with BocK and AzF
*(**a**) Plasmids for OR logic operation; constitutive sGFP(1-10) expression and BocK / AzF dependent sGFP(11). (**b**) schematic principle of OR logic sGFP complementation.*

HEK293 cells were transiently co-transfected with both of the plasmids (**Figure 3.22a**) and incubated for 48 hours in four different conditions; (1) no UAAs, (2) BocK only, (3) AzF only and (4) AzF and BocK. For all conditions, UAAs were at a final concentration of 1 mM in the cell growth media. As predicted, GFP fluorescence could be detected when cells were incubated in the presence of either or both AzF and BocK (**Figure 3.23**), and mCherry fluorescence was of equal intensity across all 4 conditions. GFP fluorescence was observed to be of a relatively high level, demonstrating a reasonably high efficiency of the system.

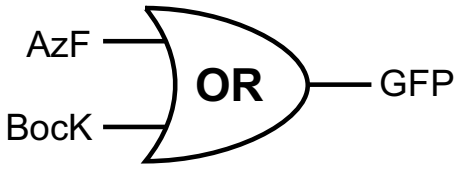

AzF	BocK	GFP
0	0	0
1	0	1
0	1	1
1	1	1

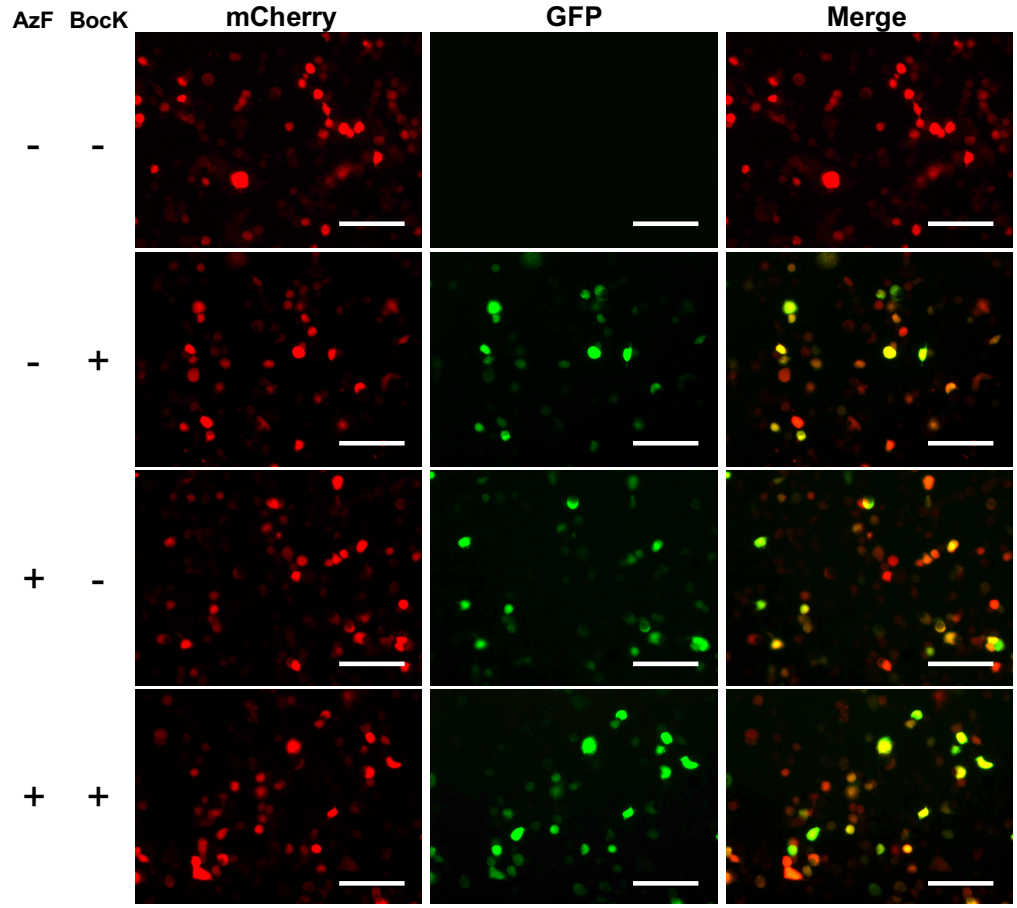

Figure 3.23*: Fluorescent imaging of HEK293 cells transfected with OR logic plasmids*
Cells were incubated under 4 conditions: (1) No BocK or AzF, (2) BocK only, (3) AzF only and (4) BocK and AzF. All amino acids were supplemented at 1 mM concentration and cells incubated for 48 hours. mCherry fluorescence used as a transfection control. All images are 223 µm × 167 µm, scale bars denote 50 µm.

To confirm the specificity of AzF dependence and continuation of orthogonality, the new TyrRS* plasmid was individually transfected into HEK293 cells and incubated in the presence or absence of AzF for 48 hours. Cells were then imaged for mCherry and GFP fluorescence. As expected, green fluorescence was dependent on the presence of the cognate unnatural amino acid AzF (**Figure 3.24**).

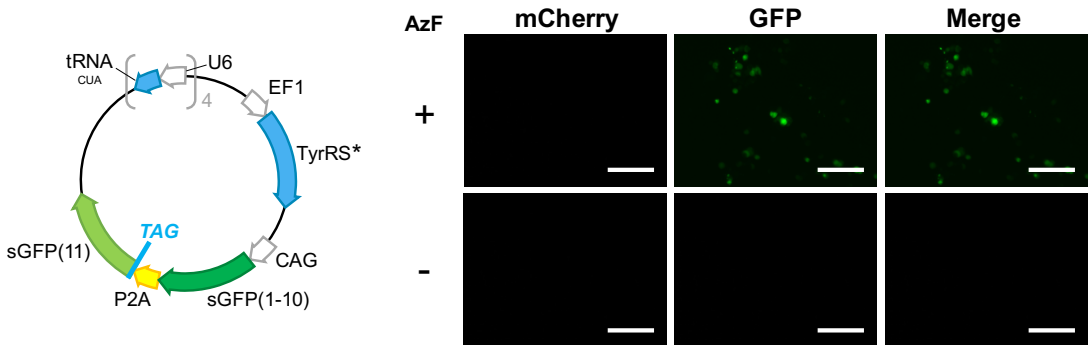

Figure 3.24: Transfection of HEK293 with individual plasmid for OR logic operation
Cells were incubated in the presence and absence of the cognate unnatural amino acid AzF. All images are 223 µm × 167 µm, scale bars denote 50 µm.

3.5 Controlling CAR-T cell function

3.5.1 Design and development of CAR-T cell logic gates

The intention of this research project was to generate a logic gate where cancer targeting T-cells can be temporally controlled by unnatural amino acid supplementation. Chimeric antigen receptor T-cells (CAR-T) are an emerging therapy in cancer treatment, where the patients T-cells are harvested, genetically modified to express receptors targeted to an antigen on their cancer cell surface, and then re-instated into the patient.[74, 226, 283, 293] From literature research as discussed in **section 3.1.4**, there is a shortfall in the ability to control CAR-T cells once they are introduced to a patient. Patients experience undesirable side effects, including the common occurrence of cytokine storms which can be fatal. It is crucial in this line of research to develop CAR-T that can be intrinsically controlled, and it is believed that the adaptation of unnatural amino acid incorporation as orthogonal and innate molecular switches can enable a titrated activation and temporal control of CAR-T (**Figure 3.25**).

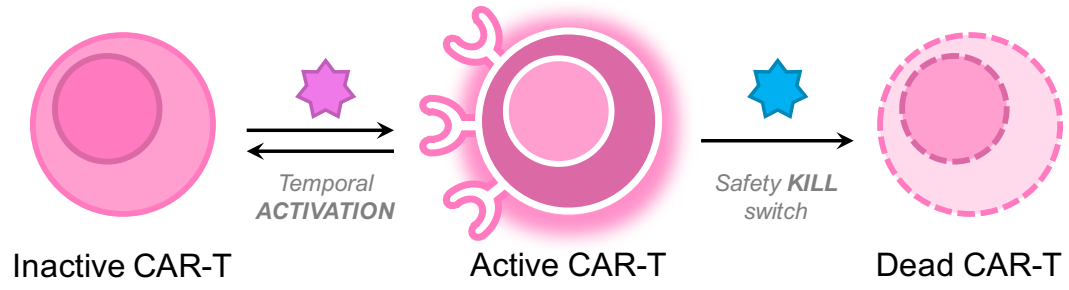

Figure 3.25: Proposed design for temporal control of CAR-T via UAA supplementation
Schematic representation of the design for CAR-T cell temporal activation and safety kill switch control via supplementation of either BocK or AzF respectively.

To assess the applicability of genetic code expansion as molecular cancer therapeutic switches, a series of experiments were designed. It was first necessary to design a CAR-T cell receptor that can only be activated in the presence of one unnatural amino acid, and a safety kill switch that can only be

activated in the presence of another orthogonal unnatural amino acid. The CAR targeting CD19+ cells has been reported in the literature previously, and has shown promising results through clinical trials.[226, 293, 294, 415] CD19 is a surface antigen that is predominantly overexpressed in many cancer cell lines, notably B-cell lymphoma cancers.[416] As a receptor designed to target CD19 antigens has already been established and widely analysed, it was deemed the most sensible chimeric antigen receptor to adapt for genetic code expansion logic gates. Moreover, for a safety kill switch, studies have been conducted previously, but so far, the literature primarily focuses on a single switch, be it activation, inactivation, or cell destruction.[54, 226, 296-299] The aim of this research project was to assess the ability to incorporate two molecular switches into a single system, whereby a titre supplementation of one unnatural amino acid can determine the basal activity of CAR-T (i.e. CD19 targeting), providing more temporal and theoretically reversible control over CAR-T activity, while also incorporating a safety kill switch that can enable fast degradation and inactivation of the CAR-T if adverse toxicity is observed and cannot be controlled. (**Figure 3.26**) The kill switch employed for this purpose is barnase; a cytotoxic peptide that has previously been shown to be an effective inducer of cellular apoptosis in cancer.[417]

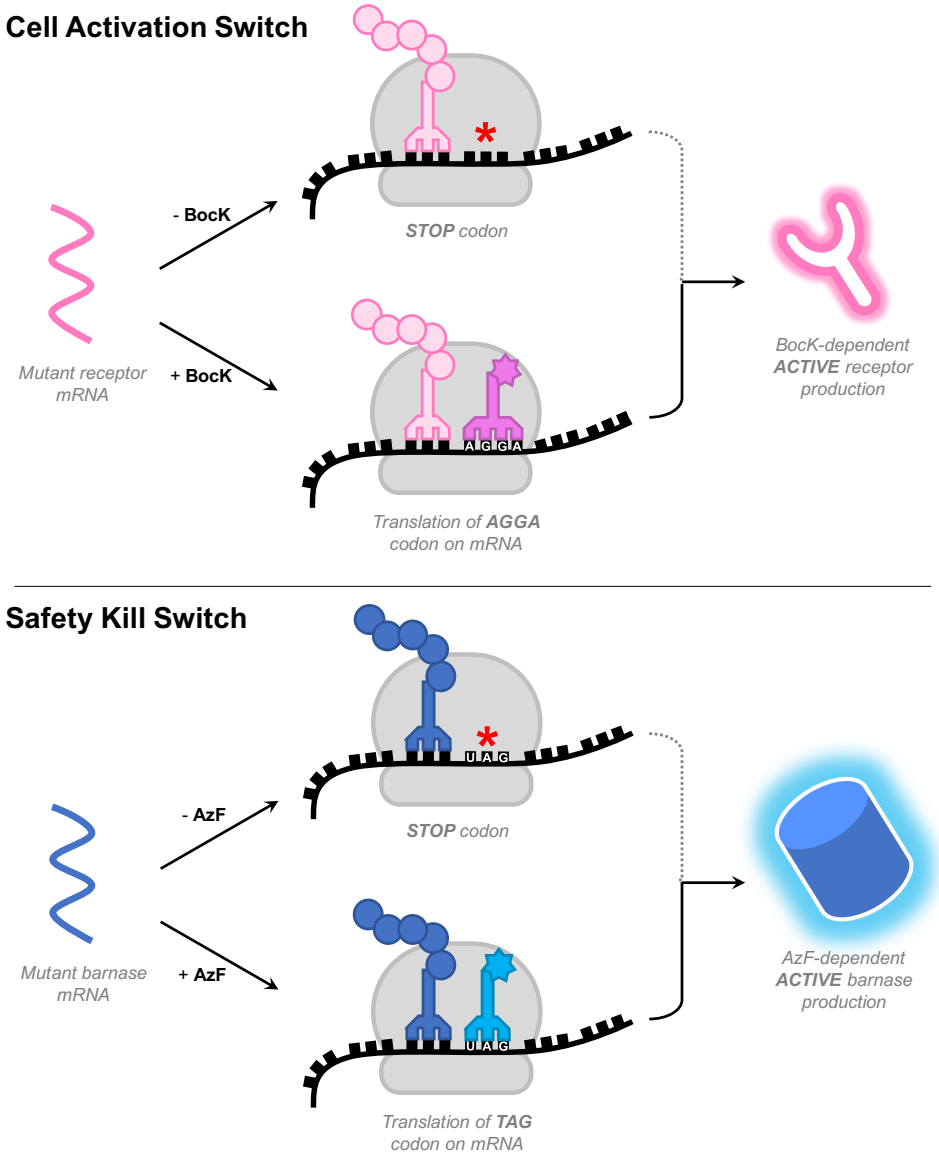

Figure 3.26: Principle approach to obtain UAA-mediated receptor activation/apoptosis
Illustration of the principles of enabling BocK-dependent receptor activation (Cell Activation Switch) and AzF dependent barnase production (Safety Kill Switch).

As T-cells are devoid of endocytosis pathways, the method of transfection as used up to this point with HEK293 cells would not be successful. As a result, the DNA constructs require delivery by a recombinant virus. For safety purposes, the viral proteins are separated across 3 plasmids; one for "envelope", one for "packaging", and one carrying the model DNA as a "transfer plasmid".[418] Furthermore, as a transduction control, fluorescent proteins will be used to visibly distinguish whether cells have successfully integrated the packaged DNA, and cells carrying both fluorescent reporters can be isolated via Fluorescent Activated Cell Sorting (FACS). The

experimental design consists of two phases of viral transduction, to enable the incorporation of both switch systems to the T-cells to generate switchable CAR-T (**Figure 3.27**).

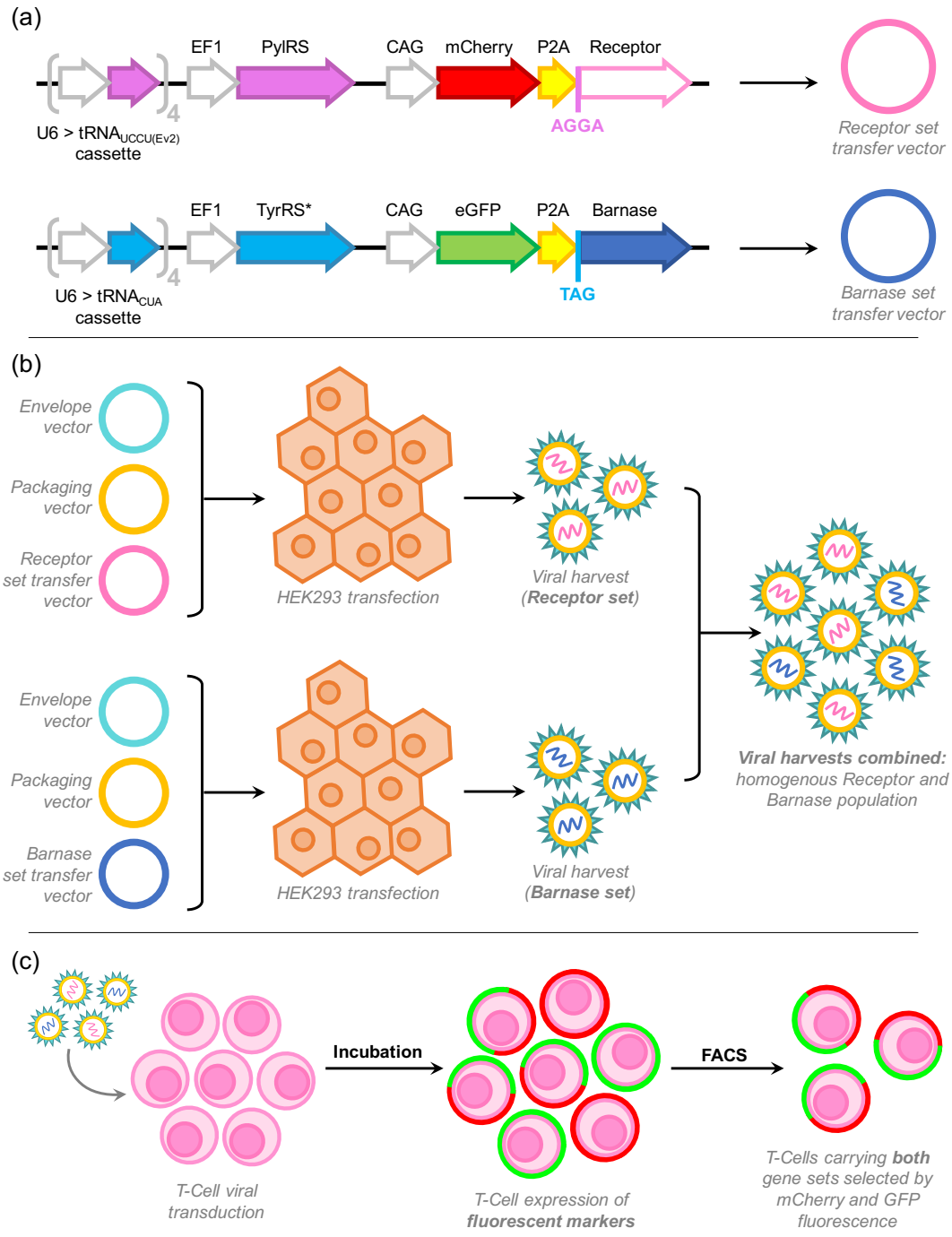

Figure 3.27: Laboratory process for generation and isolation of switchable CAR-T cells *(**a**) gene construct designs for BocK-dependent receptor production and AzF dependent barnase production. (**b**) process of producing viral load carrying receptor or barnase genetic material. (**c**) transduction of Jurkat cells with viral harvest and isolation via FACS through fluorescent markers.*

3.5.2 Plan to test CAR-T logic gates

After FACS sorting of the CAR-T via their fluorescent GFP and mCherry reporters, it is predicted that approximately 30% of all cells will have taken both DNA sets (displaying mCherry and GFP fluorescence) (**Figure 3.27c**). Once these cells have been isolated, they will be propagated to obtain a homogenous culture and maintained accordingly. To assess their switchable activity, their viability in reaction to AzF supplementation will be analysed. It is predicted that upon increasing concentrations of BocK, an increase in active receptor is produced, leading to an increase in overall volume of active CAR-T (**Figure 3.28a** and **3.28c**). Similarly, upon increasing AzF concentration, a sharp drop in cell viability will be detected, due to TAG read-through generating full length apoptotic barnase and therefore inducing apoptosis (**Figure 3.28b** and **3.28d**). Moreover, it is hypothesised that this decrease in cell viability will be significantly greater than that of cells treated with AzF that are not carrying the mutant barnase sequence. It would be noteworthy to analyse these results using FACS with Annexin V staining, as this is a commonly employed technique to detect apoptotic bodies.[419] It is crucial that the cells undergo an apoptotic cell death, as necrosis will result in a large release of inflammatory markers,[420] therefore necrosis is sub-optimal when attempting to rectify a cytokine storm. Barnase has been demonstrated as an effective apoptotic peptide in mammalian cells,[417] however if there are substantial volumes of necrotic cell death detected, the design could be altered to use alternative apoptotic peptides, such as saporin.[421, 422]

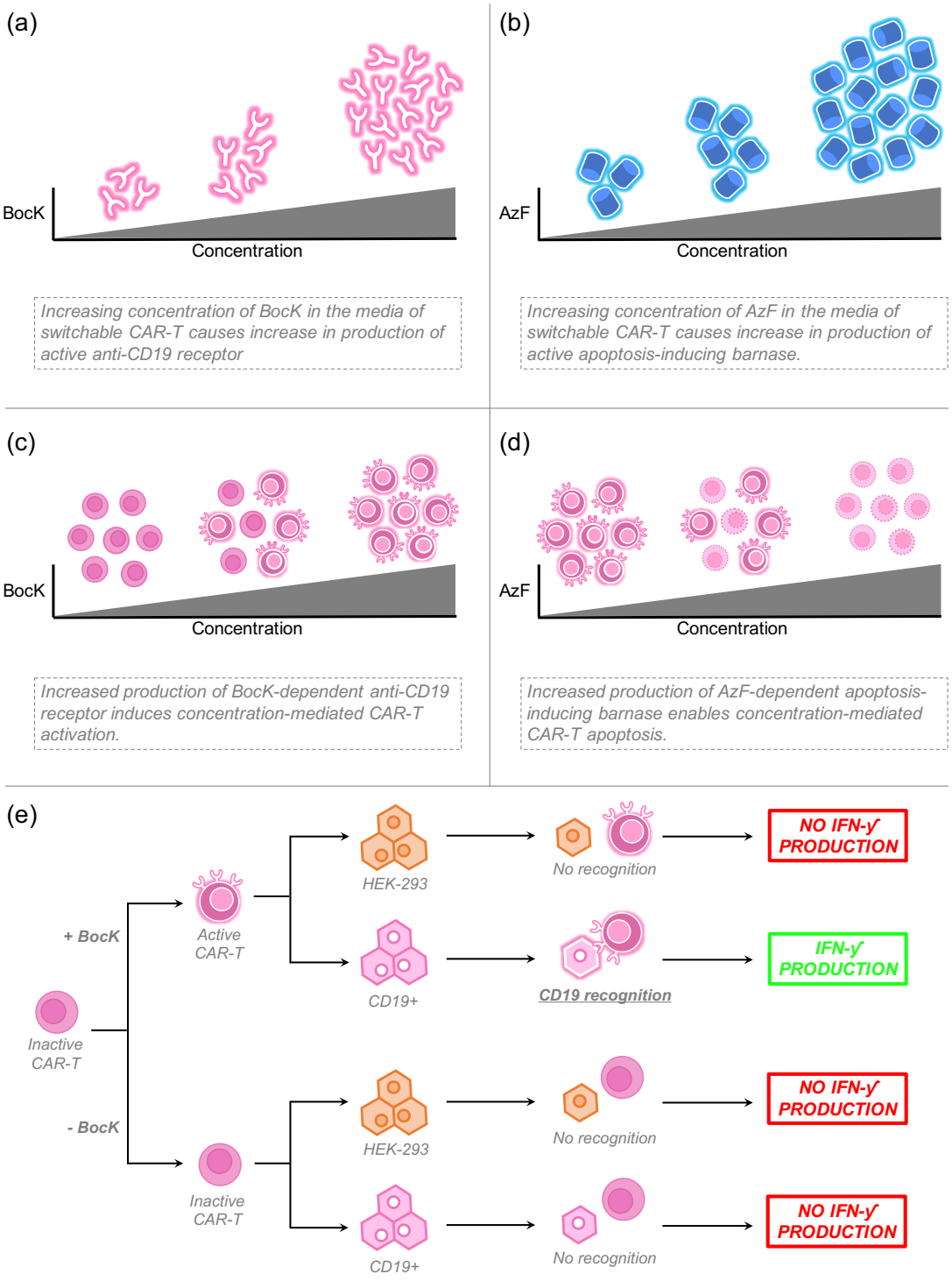

Figure 3.28: Proposed outcomes for UAA-mediated switchable CAR-T testing.
*(**a**) Concentration of BocK in the media would mediate volume of active receptor being produced by CAR-T. (**b**) Concentration of AzF in the media would mediate volume of active barnase being produced by CAR-T. (**c**) Increasing BocK concentration in media would ultimately lead to larger numbers of active CAR-T. (**d**) Increasing AzF concentration in media would ultimately lead to larger volume of CAR-T apoptosis. (**e**) Testing specificity of CAR-T; production of interferons would only be detected when CAR-T are in the presence of BocK and a CD19+ cell line.*

A positive indication of immuno-targeting is the release of cytokines, and this is a frequently analysed output of immune responses for CAR-T designs.[229, 285, 297-299, 415] Interferon gamma (IFN-γ) is a commonly measured cytokine to represent immune responses, and there are ample detection kits available commercially to measure its concentration under various conditions to a high sensitivity. To analyse the efficiency of the CAR-T on switch and simultaneously their selectivity to CD19+ cells, four basal conditions would be tested (**Figure 3.28e**). HEK293 and a CD19+ cell line would be treated with a titred range of BocK concentrations in the presence or absence of the genetically modified CAR-T. It is predicted that only when the CAR-T cells are in the presence of CD19+ cells and supplemented with a sufficient concentration of BocK, that a spike in IFN-Y would be detected (**Table 3.3**). This would confirm that the BocK is facilitating the translation of the anti-CD19 receptor, and that the receptor is functional and selective to CD19 antigens. As 1 mM concentrations of unnatural amino acid was sufficient for effective output during the split GFP experimental procedures, it is predicted that this would be a sufficient concentration to induce a substantial immune response and IFN-y output. If, however, this is not observed or the output is lower than expected, it could be due to the general incorporation efficiency of the CAR-T cell line. BocK concentrations have been previously used at 5 mM in mammalian cellular studies,[384] therefore concentrations of BocK up to 5 mM would predictably not produce an unwanted cytotoxic effect. BocK incorporation could also be confirmed via western blot, where the receptor can be tagged with a non-interruptive peptide tag, such as Myc, FLAG, or His.

Table 3.3: IFN-γ production is expected to correlate with BocK concentration and presence of CD19+ cells due to BocK-dependent production of active CAR-T.

	CAR-T + CD19+ Cells				CAR-T + HEK293			
BocK	-	+	++	+++	-	+	++	+++
Active CAR-T	-	+	++	+++	-	+	++	+++
CD19+ Cells	+	+	+	+	-	-	-	-
HEK293	-	-	-	-	+	+	+	+
IFN-γ	-	+	++	+++	-	-	-	-

3.6 Conclusions

Controlling the activity of the immune system to specifically target cancer cells is an exciting upcoming field of cancer research. The approach holds great potential for negating the requirement for using drugs and other non-selective approaches, which often are accompanied by undesirable side effects and toxicities. However, despite great advances in reprogramming the immune system to target and destroy cancerous tumours, there remains an additional unexpected obstacle that is overreaction of the immune response. This immune hyper-reaction leads to a surge in inflammatory cytokines, which ultimately can lead to irreversible organ damage, and potential fatality. In light of this, more recent research has focussed on approaches to control the activation of CAR-T in order to reduce the over-reaction side-effects they entail, with a prominent focus on mammalian cell logic gates.

This aim of this chapter was to investigate a non-toxic approach to developing mammalian cell logic gates that can in-turn be translated into a switchable CAR-T design; an approach obtainable by genetic code expansion. The data sets obtained in this chapter have expanded the understanding and applicability of genetic code expansion in mammalian cells. They have demonstrated the feasibility of using quadruplet decoding in a mammalian system with read-through comparable to that of amber decoding. Further, the incorporation of the UAAs used here could further be optimised via multiplication of tRNA copy numbers in a single plasmid, which similarly can improve their efficiency when both incorporating their respective amino acids into a single protein. Further studies proved that they can effectively be exploited as simple molecular switches for easily obtainable mammalian cell logic gates. The inability to translate these findings into a clinical setting regarding CAR-T cell control was unfortunate, however the general principles and applicability of the system is clear from the fluorescent reporter analysis. If the temporal control of CAR-T cells by unnatural amino acid incorporation is as successful as presumed, this new technique could potentially revolutionise

cancer immunotherapy tactics, enabling spatiotemporal control of CAR-T anti-cancer activities, while providing a potentially lifesaving kill switch if cytokine production remains dangerously high in a patient.

3.7 Chapter 3 Detailed Methods

3.7.1 Culture and maintenance of HEK293 cells

HEK293 cells were obtained from ECACC (ECACC General Collection, #85120602) and routinely tested for mycoplasma infection. Cells were maintained in T75 flasks at 37 °C in a 5% CO_2 atmosphere in DMEM (Fisher Scientific, #11574516) supplemented with 10% (v/v) FBS (Fisher Scientific, #11573397). They were maintained at a sub-confluent monolayer, and split at 80-85% confluency. For splitting, cells were washed with PBS, trypsinized in 1 mL of trypsin (Fisher Scientific, #11560626) and 200 µL of the 1000 µL trypsin cell suspension is re-suspended in 12 mL fresh DMEM containing 10% (v/v) FBS in a new T75 flask.

3.7.2 Transfection of HEK293 cells and imaging

HEK293 cells were plated at a $1x10^6$ cells per well of a 24 well plate (Corning, #10380932) in DMEM (Fisher Scientific, #11574516) supplemented with 10% (v/v) FBS (Fisher Scientific, #11573397) and maintained at 37 °C in a 5% CO_2 atmosphere for 24 h or until 90% confluent. For transfection per well, 1.5 µL Lipofectamine 2000 (Life Technologies, #10696343) was suspended in 50 µL OPTIMEM (Fisher Scientific, #11058021), and incubated for 10 min at room temperature. 500 ng of plasmid is diluted into 50 µL OPTIMEM and mixed with the lipofectamine-OPTIMEM solution to a final volume of 100 µL. The solution was incubated for 30 minutes at room temperature after which media was exchanged for fresh DMEM/10% v/v FBS, and supplemented with 100 mM stock of either BocK (Fluorochem, #078520), AzF (Bachem), or both when appropriate, to final working concentrations of 1 mM. Plasmid-lipofectamine solution was then added drop-wise to the well, and the plate incubated at 37 °C in a 5% CO_2 atmosphere for 48 h. Cells were imaged using Zeiss AxioCam MRm microscope camera and ZEN (version 2.3) computer imaging programme. All images were taken at 40x magnification, and representative regions of the entire well was captured. GFP fluorescence was detected with

Zeiss FSet 38 green fluorescence filter (excitation 470/40 and emission 525/50), with a constant exposure of 550 ms per image.

3.7.3 Western blotting

After imaging, media was removed from wells and cells washed twice with 1x PBS. 50 µL of RIPA Buffer (Sigma, #R0278) containing 1% v/v protease inhibitor cocktail (Sigma-Aldrich, #P8340) was added dropwise to the centre of the well and plate incubated on ice for 10 minutes. Cells were then scraped from the surface of the well, and all contents transferred to a 1.5 mL Eppendorf tube. Lysates were pelleted (20,000 g, 10 min, 4 °C) and supernatant (45 µL) added to 15 µL NuPAGE™ LDS Sample Buffer (Invitrogen, #NP0007). Samples were heated (95 °C, 5 min) and loaded onto a Novex™ WedgeWell™ 4-20% Tris-Glycine 1.0 mm Mini Protein Gel (Invitrogen, #XP04205BOX) for electrophoresis. The gel was imaged on a ChemiDoc XRS + (Bio-Rad) and transferred to a nitrocellulose membrane using a Trans-Blot Turbo Transfer System (Bio-Rad). The membrane was stained with Ponceau S to confirm protein transfer, blocked with PBST (0.05% [v/v] Tween 20 in PBS) containing 5% (w/v) milk powder at 16 °C for 1 h, and then incubated (4 °C, overnight) with primary mouse anti-eGFP antibody (Thermo Fisher, #MA1-952, 1:500 [v/v] dilution). The membrane was then washed three times (10 mL PBST, 5 min per wash). All subsequent washing steps used this procedure. Membranes were incubated in secondary anti-mouse antibody (Thermo Fisher, #32430, 1:1000 [v/v] dilution) for 1 h at 16°C, and then washed. The signal was developed by addition of Clarity Max™ Western ECL Substrate (Bio-Rad, #1705062). After imaging on a Bio-Rad ChemiDoc XRS + system, the membrane was washed 5 times (10 mL PBST, 5 min per wash) and then incubated (4 °C, overnight) with either mouse anti-GADPH antibody (Thermo Fisher, #MA5-15738, 1:500 [v/v] dilution) or mouse anti-FLAG (Sigma, #F3165, 1:500 [v/v] dilution) before being incubated with the secondary anti-mouse antibody and processed again for imaging as described above. Band quantification was conducted using ImageLab software (Biorad, version 6.0).

3.7.4 Plasmid and primer library

All plasmid stocks were generated and maintained via transformation of chemically competent One Shot™ Stbl3™ *E. coli* cells (for detailed protocols of cloning procedures used such as Gibson Assembly, T4 ligation, PCR etc. see section ***6.3 Molecular Cloning***).

Table 3.4. A list of all plasmids used and generated for this study; denoting the plasmid ID, genes carried and antibiotic resistance (AR) for bacterial propagation.

Plasmid ID	Plasmid description	AR
Plasmid 1	Pyl $tRNA_{CUA(U25C)}$	Kan
Plasmid 2	4xPyl $tRNA_{CUA(U25C)}$-PylRS-$eGFP_{(150\text{-}TAG)}$	Amp
Plasmid 3	Pyl $tRNA_{CUA(U25C)}$-PylRS-$eGFP_{(150\text{-}TAG)}$	Amp
Plasmid 4	pCAG-eGFP	Amp
Plasmid 5	$eGFP_{(150\text{-}TAGA)}$	Amp
Plasmid 6	$eGFP_{(150\text{-}CTAG)}$	Amp
Plasmid 7	$eGFP_{(150\text{-}AGGA)}$	Amp
Plasmid 8	$eGFP_{(150\text{-}TAGT)}$	Amp
Plasmid 9	$eGFP_{(150\text{-}TAGC)}$	Amp
Plasmid 10	$eGFP_{(150\text{-}TAGG)}$	Amp
Plasmid 11	Pyl $tRNA_{CUA(U25C)}$-PylRS-$eGFP_{(150\text{-}TAGA)}$	Amp
Plasmid 12	Pyl $tRNA_{CUA(U25C)}$-PylRS-$eGFP_{(150\text{-}CTAG)}$	Amp
Plasmid 13	Pyl $tRNA_{CUA(U25C)}$-PylRS-$eGFP_{(150\text{-}AGGA)}$	Amp
Plasmid 14	Pyl $tRNA_{CUA(U25C)}$-PylRS-$eGFP_{(150\text{-}TAGT)}$	Amp
Plasmid 15	Pyl $tRNA_{CUA(U25C)}$-PylRS-$eGFP_{(150\text{-}TAGC)}$	Amp
Plasmid 16	Pyl $tRNA_{CUA(U25C)}$-PylRS-$eGFP_{(150\text{-}TAGG)}$	Amp
Plasmid 17	Pyl $tRNA_{UCUA}$	Kan
Plasmid 18	Pyl $tRNA_{UCUA(Ev1)}$	Kan
Plasmid 19	Pyl $tRNA_{UCUA(Ev2)}$	Kan

Plasmid 20	Pyl $tRNA_{CUAG}$	Kan
Plasmid 21	Pyl $tRNA_{CUAG(Ev1)}$	Kan
Plasmid 22	Pyl $tRNA_{UCCU}$	Kan
Plasmid 23	Pyl $tRNA_{UCCU(Ev1)}$	Kan
Plasmid 24	Pyl $tRNA_{UCCU(Ev2)}$	Kan
Plasmid 25	Pyl $tRNA_{ACUA}$	Kan
Plasmid 26	Pyl $tRNA_{GCUA}$	Kan
Plasmid 27	Pyl $tRNA_{CCUA}$	Kan
Plasmid 28	Pyl $tRNA_{UCUA}$-PylRS-$eGFP_{(150\text{-}TAGA)}$	Amp
Plasmid 29	Pyl $tRNA_{UCUA(Ev1)}$-PylRS-$eGFP_{(150\text{-}TAGA)}$	Amp
Plasmid 30	Pyl $tRNA_{UCUA(Ev2)}$-PylRS-$eGFP_{(150\text{-}TAGA)}$	Amp
Plasmid 31	Pyl $tRNA_{CUAG}$-PylRS-$eGFP_{(150\text{-}CTAG)}$	Amp
Plasmid 32	Pyl $tRNA_{CUAG(Ev1)}$-PylRS-$eGFP_{(150\text{-}CTAG)}$	Amp
Plasmid 33	Pyl $tRNA_{UCCU}$-PylRS-$eGFP_{(150\text{-}AGGA)}$	Amp
Plasmid 34	Pyl $tRNA_{UCCU(Ev1)}$-PylRS-$eGFP_{(150\text{-}AGGA)}$	Amp
Plasmid 35	Pyl $tRNA_{UCCU(Ev2)}$-PylRS-$eGFP_{(150\text{-}AGGA)}$	Amp
Plasmid 36	Pyl $tRNA_{ACUA}$-PylRS-$eGFP_{(150\text{-}TAGT)}$	Amp
Plasmid 37	Pyl $tRNA_{GCUA}$-PylRS-$eGFP_{(150\text{-}TAGC)}$	Amp
Plasmid 38	Pyl $tRNA_{CCUA}$-PylRS-$eGFP_{(150\text{-}TAGG)}$	Amp
Plasmid 39	(U6-Tyr $tRNA_{CUA}$)x2(H1-Tyr $tRNA_{CUA}$)x2 TyrRS*-$eGFP_{(40\text{-}TAG)}$	Amp
Plasmid 40	Tyr $tRNA_{CUA}$-PylRS-$eGFP_{(150\text{-}TAG)}$	Amp
Plasmid 41	Tyr $tRNA_{CUA}$-TyrRS*-$eGFP_{(150\text{-}TAG)}$	Amp
Plasmid 42	(Pyl $tRNA_{UCCU\ (Ev2)}$)x4-PylRS-$eGFP_{(150\text{-}AGGA)}$	Amp
Plasmid 43	(Tyr $tRNA_{CUA}$)x4-TyrRS*-$eGFP_{(150\text{-}TAG)}$	Amp
Plasmid 44	eRF1(E55D)	Amp
Plasmid 45	$eGFP_{(40\text{-}TAG\text{-}150\text{-}AGGA)}$	Amp
Plasmid 46	Pyl $tRNA_{UCCU(Ev2)}$-PylRS-$eGFP_{(40\text{-}TAG\text{-}150\text{-}AGGA)}$	Amp
Plasmid 47	Tyr $tRNA_{CUA}$-TyrRS*	Amp

Plasmid 48	(Pyl $tRNA_{UCCU(Ev2)}$)x4-PylRS-$eGFP_{(40\text{-}TAG\text{-}150\text{-}AGGA)}$	Amp
Plasmid 49	(Tyrl $tRNA_{CUA}$)x4-TyrRS*-$eGFP_{(40\text{-}TAG\text{-}150\text{-}AGGA)}$	Amp
Plasmid 50	mCherry	Amp
Plasmid 51	mCherry-P2A-sGFP(1-10)	Amp
Plasmid 52	sGFP(11)	Amp
Plasmid 53	mCherry-P2A-sGFP(11)	Amp
Plasmid 54	mCherry-P2A-TAG-sGFP(1-10)	Amp
Plasmid 55	(Tyr $tRNA_{CUA}$)x4-TyrRS*-mCherry-P2A-TAG-sGFP(1-10)	Amp
Plasmid 56	(Pyl $tRNA_{UCCU(Ev2)}$)x4-PylRS-mCherry-P2A-AGGA-sGFP(11)	Amp
Plasmid 57	(Tyr $tRNA_{CUA}$)x4-TyrRS*-sGFP(1-10)-P2A-TAG-sGFP(11)	Amp

Table 3.5: List of all primers used for plasmid cloning procedures; denoting the primer ID and sequence (5' – 3')

Primer No.	Primer sequence (5'-3')
Primer 1	GGGGGGATACGGGGAAAAGGCCTAAAAACCGCACTTGTCCGGAAAC
Primer 2	GGTCAGGGCTGGGGCAGAGGCTTGCACAGGGGCAGACATG
Primer 3	ATCATGGCTGATAAGCAGAAGAAC
Primer 4	CGTTCTTCTGCTTATCAGCCATGATATAGACTCTAGTGGCTGTTGTAGTTGTACTCCAGCTTG
Primer 5	CGTTCTTCTGCTTATCAGCCATGATATAGACCTAGGTGGCTGTTGTAGTTGTACTCCAGCTTG
Primer 6	CGTTCTTCTGCTTATCAGCCATGATATAGACTCCTGTGGCTGTTGTAGTTGTACTCCAGCTTG
Primer 7	CGTTCTTCTGCTTATCAGCCATGATATAGACACTAGTGGCTGTTGTAGTTGTACTCCAGCTTG
Primer 8	CGTTCTTCTGCTTATCAGCCATGATATAGACGCTAGTGGCTGTTGTAGTTGTACTCCAGCTTG
Primer 9	CGTTCTTCTGCTTATCAGCCATGATATAGACCCTAGTGGCTGTTGTAGTTGTACTCCAGCTTG
Primer 10	TTCGATCTACATGATCAGGTTTCCGGTG
Primer 11	ACCTGATCATGTAGATCGAATGGACTTCTAAATCCGTTCAGCCGGGTTAGATTCC
Primer 12	ACCTGATCATGTAGATCGAATGGGCTTCTAATCTCGTTCAGCCGGGTTAGATTCC
Primer 13	ACCTGATCATGTAGATCGAATGGGCTTCTAATCCGCTTCAGCCGGGTTAGATTCC
Primer 14	ACCTGATCATGTAGATCGAATGGACTCTAGAATCCGTTCAGCCGGGTTAGATTCC

Primer 15	ACCTGATCATGTAGATCGAATGGCCTCTAGAACCCGTTCAGCCGGGTTAGATTCC
Primer 16	ACCTGATCATGTAGATCGAATGGACTTCCTAATCCGTTCAGCCGGGTTAGATTCC
Primer 17	ACCTGATCATGTAGATCGAATCCTCTTCCTAATAGGTTCAGCCGGGTTAGATTCC
Primer 18	ACCTGATCATGTAGATCGAAGGGGCTTCCTATCCGCTTCAGCCGGGTTAGATTCC
Primer 19	ACCTGATCATGTAGATCGAATGGACTACTAAATCCGTTCAGCCGGGTTAGATTCC
Primer 20	ACCTGATCATGTAGATCGAATGGACTGCTAAATCCGTTCAGCCGGGTTAGATTCC
Primer 21	ACCTGATCATGTAGATCGAATGGACTCCTAAATCCGTTCAGCCGGGTTAGATTCC
Primer 22	GAAAAGGAGGCCTACATGCAAATATTAAAAAATGGTGGGGGAAGGATTCGAACCTTC
Primer 23	ACCGGAGCGATCGCAACCGGTCGGGCAGGAAGAGGGCCTATTTCCCAT
Primer 24	ACTTACGCTTGCCACCATGGCTAGCGACTACAAGGACGACGACGACAAGGCAAGCAGTAAC TTGATTAAACAATTGCAAGAG
Primer 25	TCCACCACACTGGACTAGTGGATCCTTATCATTAAACGGGCCCTTTCCAGCAAATC
Primer 26	GGGGGGATACGGGGAAAAGGCCTCTTAAGAAAAACCGCACTTGTC
Primer 27	GTAAACGGCCACAAGTTCGTCGATTGGGCAGGAAGAGGGCCTATTTC
Primer 28	TCGACGAACTTGTGGCCGTTTACCCTCTTAAGAAAAACCGCACTTGTC
Primer 29	CTGGTGGAGAACTTGCCGAATTGGGCAGGAAGAGGGCCTATTTC
Primer 30	TTCGGCAAGTTCTCCACCAGCCTCTTAAGAAAAACCGCACTTGTC
Primer 31	AGTGCGGTTTTTCTTAAGAGGTTGGGCAGGAAGAGGGCCTATTTC
Primer 32	GGATACGGGGAAAAGGAGGCCTACATGC
Primer 33	GTAAACGGCCACAAGTTCGTCGATTGGGCAGGAAGAGGGCCTATTTC
Primer 34	TCGACGAACTTGTGGCCGTTTACCATGCAAATATTAAAAAATGGTGGGGGAAG
Primer 35	CTGGTGGAGAACTTGCCGAATTGGGCAGGAAGAGGGCCTATTTC
Primer 36	AATTCGGCAAGTTCTCCACCAGACATGCAAATATTAAAAAATGGTGGGGGAAG
Primer 37	TTTTAATATTTGCATGTAGGGGGCAGGAAGAGGGCCTATTTC
Primer 38	AGGGTCAGCTTGCCCTAGGTGGCATCG
Primer 39	TCGGCATGGACGAGCTGTACAAGCATCATCACCATCACCACTAAGCTGCCTATCAGAAG
Primer 40	ATGCCACCTAGGGCAAGCTGACCCTGAAGTTC
Primer 41	TTGTACAGCTCGTCCATGCCGAGAG

Primer 42	AGAACCCTGGACCTGGACAAAAG TCGTAGTCCAAAGGAGAAGAACTGTTTACCGGTGTTG
Primer 43	TCCCCATAATTTTTGGCAGAGGGAAAAAGATCTC
Primer 44	GAGAACCCTGGACCTGGACAAAAGTCGAGGACGTGAC CACATGGTCCTTCATG
Primer 45	TTTTTGGCAGAGGGAAA AAGATCTCACATG
Primer 46	TTCAGCCTGCTGAAACAGGCTGGCGACGTGGAAGAGAACCCTGGACCTGGACAAAA GTCGTAGCGTGACCACATGGTCCTTCATG
Primer 47	TTTTTGGCAGAGGGAAAAAGATCTCACATG
Primer 48	TGTCTCATCATTTTGGCAAAGAATTCATGTCCAAAGGAGAAGAACTGTTTACC
Primer 49	TTCTCTTCCACGTCGCCAGCCTGTTTCAGCAGGCTGAAATTGGTGGCGCCTCCAGACGCTTT TTCATTTGGATCTTTGCTCAGGACTGTTTG

3.7.5 Detailed cloning procedures for each plasmid

Plasmid 1: Pyl tRNA$_{CUA(U25C)}$

This plasmid was commandeered from our existing laboratory plasmid library. The plasmid was originally purchased via ThermoFisher GeneArt.

Plasmid 2: 4xPyl tRNA$_{CUA(U25C)}$-PylRS-eGFP(150TAG)

This plasmid was commandeered from our existing laboratory; it was previously developed by Suzuki et al., supervised by Dr Yu-Hsuan Tsai and Prof Anthony C F Perry.[388]

Plasmid 3: Pyl tRNACUA$_{(U25C)}$-PylRS-eGFP$_{(150-TAG)}$

This plasmid was cloned via Gibson Assembly of two fragments. **Plasmid 2** was cut with the dual cutter restriction enzyme Eco147i, and the vector (8418 bp) isolated via TAE agarose gel electrophoresis and purified using gel digestion. The new insert was generated via PCR of **Plasmid 2** using **Primer 1** and **Primer 2**. The PCR product (1606 bp) was isolated via TAE agarose gel electrophoresis and purified using gel digestion. The vector and insert were combined using Gibson assembly, propagated with Stbl3 and confirmed via sanger sequencing.

Plasmid 4: pCAG-eGFP

This plasmid was commandeered from our existing laboratory plasmid library. It was developed by Prof Anthony C F Perry,[423] and donated to the group for a previous collaborative project supervised by Dr Yu-Hsuan Tsai and Prof Anthony C F Perry.[388]

Plasmid 5: eGFP$_{(150\text{-}TAGA)}$

This plasmid was cloned by PCR mutagenesis of **Plasmid 4** using **Primer 3** and **Primer 4**. The template **Plasmid 4** was removed from the reaction mixture via DpnI restriction enzyme digest and the product (5537 bp) was then isolated via TAE agarose gel electrophoresis and purified by gel digestion. The plasmid DNA was propagated with Stbl3 and confirmed via sanger sequencing.

Plasmid 6: eGFP$_{(150\text{-}CTAG)}$

This plasmid was cloned by PCR mutagenesis of **Plasmid 4** using **Primer 3** and **Primer 5**. The template **Plasmid 4** was removed from the reaction mixture via DpnI restriction enzyme digest and the product (5537 bp) was then isolated via TAE agarose gel electrophoresis and purified by gel digestion. The plasmid DNA was propagated with Stbl3 and confirmed via sanger sequencing.

Plasmid 7: eGFP$_{(150\text{-}AGGA)}$

This plasmid was cloned by PCR mutagenesis of **Plasmid 4** using **Primer 3** and **Primer 6**. The template **Plasmid 4** was removed from the reaction mixture via DpnI restriction enzyme digest and the product (5537 bp) was then isolated via TAE agarose gel electrophoresis and purified by gel digestion. The plasmid DNA was propagated with Stbl3 and confirmed via sanger sequencing.

Plasmid 8: eGFP$_{(150\text{-}TAGT)}$

This plasmid was cloned by PCR mutagenesis of **Plasmid 4** using **Primer 3** and **Primer 7**. The template **Plasmid 4** was removed from the reaction mixture

via DpnI restriction enzyme digest and the product (5537 bp) was then isolated via TAE agarose gel electrophoresis and purified by gel digestion. The plasmid DNA was propagated with Stbl3 and confirmed via sanger sequencing.

Plasmid 9: eGFP$_{(150\text{-}TAGC)}$

This plasmid was cloned by PCR mutagenesis of **Plasmid 4** using **Primer 3** and **Primer 8**. The template **Plasmid 4** was removed from the reaction mixture via DpnI restriction enzyme digest and the product (5537 bp) was then isolated via TAE agarose gel electrophoresis and purified by gel digestion. The plasmid DNA was propagated with Stbl3 and confirmed via sanger sequencing.

Plasmid 10: eGFP$_{(150\text{-}TAGG)}$

This plasmid was cloned by PCR mutagenesis of **Plasmid 4** using **Primer 3** and **Primer 9**. The template **Plasmid 4** was removed from the reaction mixture via DpnI restriction enzyme digest and the product (5537 bp) was then isolated via TAE agarose gel electrophoresis and purified by gel digestion. The plasmid DNA was propagated with Stbl3 and confirmed via sanger sequencing.

Plasmid 11: Pyl tRNA$_{CUA(U25C)}$-PylRS-eGFP$_{(150\text{-}TAGA)}$

This plasmid was cloned via T4 ligation. The vector plasmid **Plasmid 3** was cut with the restriction enzymes BglII and XbaI, isolated via TAE agarose gel electrophoresis (9019 bp) and purified via gel digestion. The insert was generated from restriction digestion of **Plasmid 5** using BglII and XbaI, isolated by TAE agarose gel electrophoresis (909 bp) and purified by gel digestion. The vector and insert fragments were ligated by T4 ligation, propagated with Stbl3 and confirmed via sanger sequencing.

Plasmid 12: Pyl tRNA$_{CUA(U25C)}$-PylRS-eGFP$_{(150\text{-}CTAG)}$

This plasmid was cloned via T4 ligation. The vector plasmid **Plasmid 3** was cut with the restriction enzymes BglII and XbaI, isolated via TAE agarose gel

electrophoresis (9019 bp) and purified via gel digestion. The insert was generated from restriction digestion of **Plasmid 6** using BglII and XbaI, isolated by TAE agarose gel electrophoresis (909 bp) and purified by gel digestion. The vector and insert fragments were ligated by T4 ligation, propagated with Stbl3 and confirmed via sanger sequencing.

Plasmid 13: Pyl tRNA$_{CUA(U25C)}$-PylRS-eGFP$_{(150\text{-}AGGA)}$

This plasmid was cloned via T4 ligation. The vector plasmid **Plasmid 3** was cut with the restriction enzymes BglII and XbaI, isolated via TAE agarose gel electrophoresis (9019 bp) and purified via gel digestion. The insert was generated from restriction digestion of **Plasmid 7** using BglII and XbaI, isolated by TAE agarose gel electrophoresis (909 bp) and purified by gel digestion. The vector and insert fragments were ligated by T4 ligation, propagated with Stbl3 and confirmed via sanger sequencing.

Plasmid 14: Pyl tRNA$_{CUA(U25C)}$-PylRS-eGFP$_{(150\text{-}TAGT)}$

This plasmid was cloned via T4 ligation. The vector plasmid **Plasmid 3** was cut with the restriction enzymes BglII and XbaI, isolated via TAE agarose gel electrophoresis (9019 bp) and purified via gel digestion. The insert was generated from restriction digestion of **Plasmid 8** using BglII and XbaI, isolated by TAE agarose gel electrophoresis (909 bp) and purified by gel digestion. The vector and insert fragments were ligated by T4 ligation, propagated with Stbl3 and confirmed via sanger sequencing.

Plasmid 15: Pyl tRNA$_{CUA(U25C)}$-PylRS-eGFP$_{(150\text{-}TAGC)}$

This plasmid was cloned via T4 ligation. The vector plasmid **Plasmid 3** was cut with the restriction enzymes BglII and XbaI, isolated via TAE agarose gel electrophoresis (9019 bp) and purified via gel digestion. The insert was generated from restriction digestion of **Plasmid 9** using BglII and XbaI, isolated by TAE agarose gel electrophoresis (909 bp) and purified by gel

digestion. The vector and insert fragments were ligated by T4 ligation, propagated with Stbl3 and confirmed via sanger sequencing.

Plasmid 16: Pyl tRNA$_{CUA(U25C)}$-PylRS-eGFP$_{(150\text{-}TAGT)}$

This plasmid was cloned via T4 ligation. The vector plasmid **Plasmid 3** was cut with the restriction enzymes BglII and XbaI, isolated via TAE agarose gel electrophoresis (9019 bp) and purified via gel digestion. The insert was generated from restriction digestion of **Plasmid 10** using BglII and XbaI, isolated by TAE agarose gel electrophoresis (909 bp) and purified by gel digestion. The vector and insert fragments were ligated by T4 ligation, propagated with Stbl3 and confirmed via sanger sequencing.

Plasmid 17: Pyl tRNA$_{(UCUA)}$

This plasmid was cloned by PCR mutagenesis of **Plasmid 1** using **Primer 10** and **Primer 11**. The template **Plasmid 1** was removed from the reaction mixture via DpnI restriction enzyme digest and the product (3881 bp) was then isolated via TAE agarose gel electrophoresis and purified by gel digestion. The plasmid DNA was propagated with Stbl3 and confirmed via sanger sequencing.

Plasmid 18: Pyl tRNA$_{(UCUA)Ev1}$

This plasmid was cloned by PCR mutagenesis of **Plasmid 1** using **Primer 10** and **Primer 12**. The template **Plasmid 1** was removed from the reaction mixture via DpnI restriction enzyme digest and the product (3881 bp) was then isolated via TAE agarose gel electrophoresis and purified by gel digestion. The plasmid DNA was propagated with Stbl3 and confirmed via sanger sequencing.

Plasmid 19: Pyl tRNA$_{(UCUA)Ev2}$

This plasmid was cloned by PCR mutagenesis of **Plasmid 1** using **Primer 10** and **Primer 13**. The template **Plasmid 1** was removed from the reaction mixture via DpnI restriction enzyme digest and the product (3881 bp) was then isolated via TAE agarose gel electrophoresis and purified by gel digestion. The plasmid DNA was propagated with Stbl3 and confirmed via sanger sequencing.

Plasmid 20: Pyl tRNA$_{(CUAG)}$

This plasmid was cloned by PCR mutagenesis of **Plasmid 1** using **Primer 10** and **Primer 14**. The template **Plasmid 1** was removed from the reaction mixture via DpnI restriction enzyme digest and the product (3881 bp) was then isolated via TAE agarose gel electrophoresis and purified by gel digestion. The plasmid DNA was propagated with Stbl3 and confirmed via sanger sequencing.

Plasmid 21: Pyl tRNA$_{(CUAG)Ev1}$

This plasmid was cloned by PCR mutagenesis of **Plasmid 1** using **Primer 10** and **Primer 15**. The template **Plasmid 1** was removed from the reaction mixture via DpnI restriction enzyme digest and the product (3881 bp) was then isolated via TAE agarose gel electrophoresis and purified by gel digestion. The plasmid DNA was propagated with Stbl3 and confirmed via sanger sequencing.

Plasmid 22: Pyl tRNA$_{(UCCU)}$

This plasmid was cloned by PCR mutagenesis of **Plasmid 1** using **Primer 10** and **Primer 16**. The template **Plasmid 1** was removed from the reaction mixture via DpnI restriction enzyme digest and the product (3881 bp) was then isolated via TAE agarose gel electrophoresis and purified by gel digestion. The plasmid DNA was propagated with Stbl3 and confirmed via sanger sequencing.

Plasmid 23: Pyl tRNA$_{(UCCU)Ev1}$

This plasmid was cloned by PCR mutagenesis of **Plasmid 1** using **Primer 10** and **Primer 17**. The template **Plasmid 1** was removed from the reaction mixture via DpnI restriction enzyme digest and the product (3881 bp) was then isolated via TAE agarose gel electrophoresis and purified by gel digestion. The plasmid DNA was propagated with Stbl3 and confirmed via sanger sequencing.

Plasmid 24: Pyl tRNA$_{(UCCU)Ev2}$

This plasmid was cloned by PCR mutagenesis of **Plasmid 1** using **Primer 10** and **Primer 18**. The template **Plasmid 1** was removed from the reaction mixture via DpnI restriction enzyme digest and the product (3881 bp) was then isolated via TAE agarose gel electrophoresis and purified by gel digestion. The plasmid DNA was propagated with Stbl3 and confirmed via sanger sequencing.

Plasmid 25: Pyl tRNA$_{(ACUA)}$

This plasmid was cloned by PCR mutagenesis of **Plasmid 1** using **Primer 10** and **Primer 19**. The template **Plasmid 1** was removed from the reaction mixture via DpnI restriction enzyme digest and the product (3881 bp) was then isolated via TAE agarose gel electrophoresis and purified by gel digestion. The plasmid DNA was propagated with Stbl3 and confirmed via sanger sequencing.

Plasmid 26: Pyl tRNA$_{(GCUA)}$

This plasmid was cloned by PCR mutagenesis of **Plasmid 1** using **Primer 10** and **Primer 20**. The template **Plasmid 1** was removed from the reaction mixture via DpnI restriction enzyme digest and the product (3881 bp) was then isolated via TAE agarose gel electrophoresis and purified by gel digestion. The plasmid DNA was propagated with Stbl3 and confirmed via sanger sequencing.

Plasmid 27: Pyl tRNA$_{(CCUA)}$

This plasmid was cloned by PCR mutagenesis of **Plasmid 1** using **Primer 10** and **Primer 21**. The template **Plasmid 1** was removed from the reaction mixture via DpnI restriction enzyme digest and the product (3881 bp) was then isolated via TAE agarose gel electrophoresis and purified by gel digestion. The plasmid DNA was propagated with Stbl3 and confirmed via sanger sequencing.

Plasmid 28: Pyl tRNA$_{UCUA}$-PylRS-eGFP$_{(150\text{-}TAGA)}$

This plasmid was cloned via T4 ligation. The vector plasmid **Plasmid 11** was cut with the restriction enzymes Eco147i and AgeI, isolated via TAE agarose gel electrophoresis (9579 bp) and purified via gel digestion. The insert was generated from restriction digestion of **Plasmid 17** using Eco147i and AgeI, isolated by TAE agarose gel electrophoresis (348 bp) and purified by gel digestion. The vector and insert fragments were ligated by T4 ligation, propagated with Stbl3 and confirmed via sanger sequencing.

Plasmid 29: Pyl tRNA$_{UCUA(Ev1)}$-PylRS-eGFP$_{(150\text{-}TAGA)}$

This plasmid was cloned via T4 ligation. The vector plasmid **Plasmid 11** was cut with the restriction enzymes Eco147i and AgeI, isolated via TAE agarose gel electrophoresis (9579 bp) and purified via gel digestion. The insert was generated from restriction digestion of **Plasmid 18** using Eco147i and AgeI, isolated by TAE agarose gel electrophoresis (348 bp) and purified by gel digestion. The vector and insert fragments were ligated by T4 ligation, propagated with Stbl3 and confirmed via sanger sequencing.

Plasmid 30: Pyl tRNA$_{UCUA(Ev2)}$-PylRS-eGFP$_{(150\text{-}TAGA)}$

This plasmid was cloned via T4 ligation. The vector plasmid **Plasmid 11** was cut with the restriction enzymes Eco147i and AgeI, isolated via TAE agarose gel electrophoresis (9579 bp) and purified via gel digestion. The insert was generated from restriction digestion of **Plasmid 19** using Eco147i and AgeI,

isolated by TAE agarose gel electrophoresis (348 bp) and purified by gel digestion. The vector and insert fragments were ligated by T4 ligation, propagated with Stbl3 and confirmed via sanger sequencing.

Plasmid 31: Pyl $tRNA_{CUAG}$-PylRS-$eGFP_{(150\text{-}CUAG)}$

This plasmid was cloned via T4 ligation. The vector plasmid **Plasmid 12** was cut with the restriction enzymes Eco147i and AgeI, isolated via TAE agarose gel electrophoresis (9579 bp) and purified via gel digestion. The insert was generated from restriction digestion of **Plasmid 20** using Eco147i and AgeI, isolated by TAE agarose gel electrophoresis (348 bp) and purified by gel digestion. The vector and insert fragments were ligated by T4 ligation, propagated with Stbl3 and confirmed via sanger sequencing.

Plasmid 32: Pyl $tRNA_{CUAG(Ev1)}$-PylRS-$eGFP_{(150\text{-}CUAG)}$

This plasmid was cloned via T4 ligation. The vector plasmid **Plasmid 11** was cut with the restriction enzymes Eco147i and AgeI, isolated via TAE agarose gel electrophoresis (9579 bp) and purified via gel digestion. The insert was generated from restriction digestion of **Plasmid 21** using Eco147i and AgeI, isolated by TAE agarose gel electrophoresis (348 bp) and purified by gel digestion. The vector and insert fragments were ligated by T4 ligation, propagated with Stbl3 and confirmed via sanger sequencing.

Plasmid 33: Pyl $tRNA_{UCCU}$-PylRS-$eGFP_{(150\text{-}AGGA)}$

This plasmid was cloned via T4 ligation. The vector plasmid **Plasmid 13** was cut with the restriction enzymes Eco147i and AgeI, isolated via TAE agarose gel electrophoresis (9579 bp) and purified via gel digestion. The insert was generated from restriction digestion of **Plasmid 22** using Eco147i and AgeI, isolated by TAE agarose gel electrophoresis (348 bp) and purified by gel digestion. The vector and insert fragments were ligated by T4 ligation, propagated with Stbl3 and confirmed via sanger sequencing.

Plasmid 34: Pyl $tRNA_{UCCU(Ev1)}$-PylRS-$eGFP_{(150\text{-}AGGA)}$

This plasmid was cloned via T4 ligation. The vector plasmid **Plasmid 13** was cut with the restriction enzymes Eco147i and AgeI, isolated via TAE agarose gel electrophoresis (9579 bp) and purified via gel digestion. The insert was generated from restriction digestion of **Plasmid 23** using Eco147i and AgeI, isolated by TAE agarose gel electrophoresis (348 bp) and purified by gel digestion. The vector and insert fragments were ligated by T4 ligation, propagated with Stbl3 and confirmed via sanger sequencing.

Plasmid 35: Pyl $tRNA_{UCCU(Ev2)}$-PylRS-$eGFP_{(150\text{-}AGGA)}$

This plasmid was cloned via T4 ligation. The vector plasmid **Plasmid 13** was cut with the restriction enzymes Eco147i and AgeI, isolated via TAE agarose gel electrophoresis (9579 bp) and purified via gel digestion. The insert was generated from restriction digestion of **Plasmid 24** using Eco147i and AgeI, isolated by TAE agarose gel electrophoresis (348 bp) and purified by gel digestion. The vector and insert fragments were ligated by T4 ligation, propagated with Stbl3 and confirmed via sanger sequencing.

Plasmid 36: Pyl $tRNA_{ACUA}$-PylRS-$eGFP_{(150\text{-}TAGT)}$

This plasmid was cloned via T4 ligation. The vector plasmid **Plasmid 14** was cut with the restriction enzymes Eco147i and AgeI, isolated via TAE agarose gel electrophoresis (9579 bp) and purified via gel digestion. The insert was generated from restriction digestion of **Plasmid 25** using Eco147i and AgeI, isolated by TAE agarose gel electrophoresis (348 bp) and purified by gel digestion. The vector and insert fragments were ligated by T4 ligation, propagated with Stbl3 and confirmed via sanger sequencing.

Plasmid 37: Pyl $tRNA_{GCUA}$-PylRS-$eGFP_{(150\text{-}TAGC)}$

This plasmid was cloned via T4 ligation. The vector plasmid **Plasmid 15** was cut with the restriction enzymes Eco147i and AgeI, isolated via TAE agarose gel electrophoresis (9579 bp) and purified via gel digestion. The insert was

generated from restriction digestion of **Plasmid 26** using Eco147i and AgeI, isolated by TAE agarose gel electrophoresis (348 bp) and purified by gel digestion. The vector and insert fragments were ligated by T4 ligation, propagated with Stbl3 and confirmed via sanger sequencing.

Plasmid 38: Pyl $tRNA_{CCUA}$-PylRS-$eGFP_{(150\text{-}TAGG)}$

This plasmid was cloned via T4 ligation. The vector plasmid **Plasmid 16** was cut with the restriction enzymes Eco147i and AgeI, isolated via TAE agarose gel electrophoresis (9579 bp) and purified via gel digestion. The insert was generated from restriction digestion of **Plasmid 27** using Eco147i and AgeI, isolated by TAE agarose gel electrophoresis (348 bp) and purified by gel digestion. The vector and insert fragments were ligated by T4 ligation, propagated with Stbl3 and confirmed via sanger sequencing.

Plasmid 39: (U6-Tyr $tRNA_{CUA}$)x2(H1-Tyr $tRNA_{CUA}$)x2 TyrRS-$eGFP_{(40\text{-}TAG)}$*

This plasmid was a gift from Peter Schultz (Addgene plasmid #50831; http://n2t.net/addgene:50831; RRID:Addgene_50831).

Plasmid 40: Tyr $tRNA_{CUA}$-PylRS-$eGFP_{(150\text{-}TAG)}$

This plasmid was cloned via Gibson Assembly of two fragments. **Plasmid 3** was cut with the restriction enzymes Eco147i and AgeI, and the vector (9579 bp) isolated via TAE agarose gel electrophoresis and purified using gel digestion. The new insert was generated via PCR of **Plasmid 39** using **Primer 22** and **Primer 23**. The PCR product (407 bp) was isolated via TAE agarose gel electrophoresis and purified using gel digestion. The vector and insert were combined using Gibson assembly, propagated with Stbl3 and confirmed via sanger sequencing.

Plasmid 41: Tyr tRNA$_{CUA}$-TyrRS*-eGFP$_{(150\text{-}TAG)}$

This plasmid was cloned via Gibson Assembly of two fragments. **Plasmid 40** was cut with the restriction enzymes NheI and BamHI, and the vector (8529 bp) isolated via TAE agarose gel electrophoresis and purified using gel digestion. The new insert was generated via PCR of **Plasmid 39** using **Primer 24** and **Primer 25**. The PCR product (407 bp) was isolated via TAE agarose gel electrophoresis and purified using gel digestion. The vector and insert were combined using Gibson assembly, propagated with Stbl3 and confirmed via sanger sequencing.

Plasmid 42: (Pyl tRNA$_{UCCU\ (Ev2)}$)x4-PylRS-eGFP$_{(150\text{-}TAG)}$

This plasmid was cloned via 4-piece Gibson Assembly. For the vector, **Plasmid 35** was linearised with Eco147i restriction enzyme. To ensure the blunt ends did not spontaneously re-ligate, within the restriction digest reaction mixture, Thermosensitive Alkaline Phosphotase (TAP) was added to remove 5' and 3' phosphate groups and prevent re-ligation. The linearised vector product (9935 bp) was isolated via TAE agarose gel electrophoresis and purified using gel digestion. The three inserts were generated via PCR of **Plasmid 35** using three distinctive pairs of primers; **Primer 26** and **Primer 27** (398 bp), **Primer 28** and **Primer 29** (398 bp), and **Primer 30** and **Primer 31** (396 bp). The PCR products were isolated via TAE agarose gel electrophoresis and purified using gel digestion. The vector and inserts were combined using Gibson assembly, propagated with Stbl3 and confirmed via sanger sequencing.

Plasmid 43: (Tyr tRNA$_{CUA}$)x4-TyrRS*-eGFP$_{(150\text{-}TAG)}$

This plasmid was cloned via 4-piece Gibson Assembly. For the vector, **Plasmid 41** was linearised with Eco147i restriction enzyme. To ensure the blunt ends did not spontaneously re-ligate, within the restriction digest reaction mixture, Thermosensitive Alkaline Phosphotase (TAP) was added to remove 5' and 3' phosphate groups and prevent re-ligation. The linearised vector product (9865 bp) was isolated via TAE agarose gel electrophoresis and

purified using gel digestion. The three inserts were generated via PCR of **Plasmid 41** using three distinctive pairs of primers; **Primer 32** and **Primer 33** (406 bp), **Primer 34** and **Primer 35** (403 bp), and **Primer 36** and **Primer 37** (401 bp). The PCR products were isolated via TAE agarose gel electrophoresis and purified using gel digestion. The vector and inserts were combined using Gibson assembly, propagated with Stbl3 and confirmed via sanger sequencing.

Plasmid 44: eRF1(E55D)

This plasmid was commandeered from our existing laboratory plasmid library. It was a kind gift from Prof Jason Chin.[406]

Plasmid 45: eGFP$_{(40\text{-}TAG\text{-}150\text{-}AGGA)}$

This plasmid was cloned via 2 piece Gibson assembly. Vector was generated by PCR of **Plasmid 7** using **Primer 38** and **Primer 39** (4952 bp), isolated via TAE agarose gel electrophoresis and purified using gel digestion. The insert was made by PCR of **Plasmid 7** using **Primer 40** and **Primer 41** (608 bp), isolated via TAE agarose gel electrophoresis and purified using gel digestion. The vector and insert were combined using Gibson assembly, propagated with Stbl3 and confirmed via sanger sequencing.

Plasmid 46: Pyl tRNA$_{UCCU(Ev2)}$-PylRS-eGFP$_{(40\text{-}TAG\text{-}150\text{-}AGGA)}$

This plasmid was cloned via T4 ligation. The vector was generated by restriction digest of **Plasmid 35** using restriction enzymes BglII and EcoRI, and the fragment (9122 bp) isolated via TAE agarose gel electrophoresis and purified using gel digestion. Insert was created by restriction digest of **Plasmid 45** using BglII and EcoRI, isolated via TAE agarose gel electrophoresis and purified using gel digestion. The vector and insert fragments were ligated by T4 ligation, propagated with Stbl3 and confirmed via sanger sequencing.

Plasmid 47: Tyr $tRNA_{CUA}$-TyrRS*

This plasmid was cloned via T4 ligation. **Plasmid 41** was digested with the dual cutter restriction enzyme EcoRI and larger fragment (9133 bp) isolated via TAE agarose gel electrophoresis and purified using gel digestion. The DNA was re-ligated via T4 ligation, propagated with Stbl3 and confirmed via restriction digest.

Plasmid 48: (Pyl $tRNA_{UCCU(Ev2)}$)x4-PylRS-eGFP$_{(40\text{-}TAG\text{-}150\text{-}AGGA)}$

This plasmid was cloned via T4 ligation. The vector was generated by restriction digest of **Plasmid 42** using restriction enzymes BglII and XbaI, and the fragment (10134 bp) isolated via TAE agarose gel electrophoresis and purified using gel digestion. Insert was created by restriction digest of **Plasmid 42** using BglII and XbaI, isolated via TAE agarose gel electrophoresis and purified using gel digestion. The vector and insert fragments were ligated by T4 ligation, propagated with Stbl3 and confirmed via sanger sequencing.

Plasmid 49: (Tyr $tRNA_{CUA}$)x4-TyrRS*-eGFP$_{(40\text{-}TAG\text{-}150\text{-}AGGA)}$

This plasmid was cloned via T4 ligation. The vector was generated by restriction digest of **Plasmid 43** using restriction enzymes BglII and XbaI, and the fragment (10134 bp) isolated via TAE agarose gel electrophoresis and purified using gel digestion. Insert was created by restriction digest of **Plasmid 43** using BglII and XbaI, isolated via TAE agarose gel electrophoresis and purified using gel digestion. The vector and insert fragments were ligated by T4 ligation, propagated with Stbl3 and confirmed via sanger sequencing.

Plasmid 50: mCherry

This plasmid was commandeered from our existing laboratory plasmid library, originally constructed from pCAG mCherry.

Plasmid 51: mCherry-P2A-sGFP(1-10):

This plasmid was cloned by Gibson Assembly. For the Vector, **Plasmid 50** was cut using restriction enzymes BsrGI and BglII (5412 bp) and the vector fragment isolated via TAE agarose electrophoresis and gel digestion. This vector fragment was Gibson assembled with a gene strings fragment ordered from GeneArt (ThermoFisher) encoding C-terminal residues of mCherry leading to a P2A linker and sGFP(1-10) (the purchased fragment included complementary overlap sequences 5' and 3' to facilitate Gibson assembly). DNA was propagated with Stbl3 and confirmed via sanger sequencing.

Plasmid 52: sGFP(11):

This plasmid was purchased from GeneArt (ThermoFisher) with the order ID 19AC5DLP.

Plasmid 53: mCherry-P2A-sGFP(11):

This plasmid was generated by T4 ligation. **Plasmid 51** was cut with MluI and BglII and the fragment (5415 bp) isolated via TAE agarose gel electrophoresis and purified using gel digestion. The insert was obtained by digestion of **Plasmid 52** with MluI and BglII and the fragment (529 bp) isolated via TAE agarose gel electrophoresis and purified using gel digestion. Vector and insert were ligated via T4 ligation, propagated with Stbl3 and confirmed via sanger sequencing.

Plasmid 54: mCherry-P2A-TAG-sGFP(1-10):

This plasmid was made by Gibson Assembly. The vector was generated by restriction digest of **Plasmid** 51 with enzymes PshAI and BglII, and the fragment (5419 bp) isolated via TAE agarose gel electrophoresis and purified using gel digestion. The insert was produced by PCR of **Plasmid 51** with **Primer 42** and **Primer 43**, and the fragment (703 bp) isolated via TAE agarose gel electrophoresis and purified using gel digestion. The vector and insert were

combined using Gibson assembly, propagated with Stbl3 and confirmed via sanger sequencing.

Plasmid 55: (Tyr $tRNA_{CUA}$)x4-TyrRS*-mCherry-P2A-TAG-sGFP(1-10):

This plasmid was cloned via T4 ligation. The vector was generated by restriction digestion of **Plasmid 43** using BglII and XbaI, and the fragment (10134 bp) isolated via TAE agarose gel electrophoresis and purified using gel digestion. The insert was made by restriction digest of **Plasmid 54** with BglII and XbaI and the fragment (1538 bp) isolated via TAE agarose gel electrophoresis and purified using gel digestion. The vector and insert were combined using T4 ligation, propagated with Stbl3 and confirmed via sanger sequencing.

Plasmid 56: (Pyl $tRNA_{UCCU(Ev2)}$)x4-PylRS-mCherry-P2A-AGGA-sGFP(11):

This plasmid was formed via 3 piece T4 ligation. The vector was generated by restriction digest of **Plasmid 42** with XbaI and BglII, and the fragment (10134 bp) isolated via TAE agarose gel electrophoresis and purified using gel digestion. The first insert was made by restriction digest of **Plasmid 51** with PshAI and XbaI, and fragment (893 bp) isolated via TAE agarose gel electrophoresis and purified using gel digestion. The second insert was made via PCR of **Plasmid 53** using **Primer 44** and **Primer 45**, and the fragment (498 bp) isolated via TAE agarose gel electrophoresis and purified using gel digestion prior to digestion with restriction enzymes PshAI and BglII to generate sticky ends. All three fragments were ligated together by T4 ligation, propagated with Stbl3 and confirmed via sanger sequencing.

Plasmid 57: (Tyr $tRNA_{CUA}$)x4-TyrRS*-sGFP(1-10)-P2A-TAG-sGFP(11):

This plasmid was formed by 3 piece Gibson Assembly. The vector was made by restriction digest of **Plasmid 43** with XbaI and BglII, and the fragment (10134 bp) isolated via TAE agarose gel electrophoresis and purified using gel digestion. The first insert was made by PCR of **Plasmid 53** with **Primer 46**

and **Primer 47**, and the fragment (530 bp) isolated via TAE agarose gel electrophoresis and purified using gel digestion. The second insert was made by PCR of **Plasmid 51** with **Primer 48** and **Primer 49**, and the fragment (727 bp) isolated via TAE agarose gel electrophoresis and purified using gel digestion. The three DNA fragments were combined via Gibson Assembly, propagated with Stbl3 and confirmed via sanger sequencing.

CHAPTER 4:
Conclusions and Future Work

4.1 Conclusions

The desire to develop a new age of cancer therapies that possess a heightened selectivity towards cancer cells continues to dominate nearly all aspects of cancer drug development. Although conventional chemotherapeutics have significantly improved the survival outcome of cancer patients over the past century,[56, 59, 60, 73] their infliction of adverse toxicities and side effects leaves the field of oncology in increasing need of more suitable treatment options. Two opposing fields of oncological research are the use of molecular vehicles to deliver cancer therapeutics more favourably to tumours, or the training of the immune system to destroy the cancer cells directly.[68, 133, 194] Both approaches carry advantages and disadvantages, but pose probable solutions to alleviating side effects and toxicities. The aim of this project was to investigate both fields, and discern whether new approaches can be generated for both; contributing knowledge and insight into each field in the conquest to discover a new generation of selective cancer therapeutics.

4.1.1 Cyanine dyes as drug delivery vehicles

The desire for targeted delivery of chemotherapeutics to cancer cells has been present for as long as the desire to treat cancers. Treatments of all shapes and sizes are under development within the scientific community, achieving an ever-expanding knowledge of how cancer cells work, and more importantly, how they can be better-treated and overcome. Increasing the selectivity of therapies can establish a higher drug-concentration within the microenvironment of a tumour, which in-turn leads to a higher rate of eradication.[56, 101, 121, 194] Similarly, the use of fluorescent entities to track the movements and localisation of new drugs has been vastly rewarding to the community, enabling an extended understanding of how a new drug potentially functions.[424, 425] The research in **Chapter 2** proposes an additional approach that combines the use of fluorescent imaging with the treatment of cancers. By conjugating mitochondrial toxic drugs to fluorescent mitochondrial-homing

cyanine dyes **Cy3** and **Cy5**, the toxicity and specificity of them was significantly increased.

The studies performed characterised the mitochondrial-homing capacity of simple cyanine dyes **Cy3** and **Cy5**. The compounds detailed can effectively localise at the mitochondria at relatively low concentrations, and **Cy3**, **Cy5** and the conjugated form **Cy3-Cy5** are not dependent on endocytic pathways to enter a cell, or similarly the presence of serum within the cellular media. **Cy3-Cy5-R8** was generated and tested to analyse whether the addition of a CPP can alter the pathway in which the dyes enter a cell, and moreover to test previously reported behaviours of cyanine dyes in cell entry when conjugated to a CPP entity. The dyes were found to be dependent on the mitochondrial membrane potential, and conjugation of simple cyanine dyes **Cy3** or **Cy5** to mitochondrial toxins dramatically increased the toxicity of a cytotoxic peptide (**KLA**), small molecule drug (**Cip**) and a metallocomplex drug (**CPT**). Strong evidence was additionally gathered to suggest that **Cy3-Cy5-R8** adapts its mode of cell entry; indicating an endocytosis-dependence at lower concentrations, while surpassing an undetermined concentration threshold influences direct membrane transduction. The dyes do not irreversibly bind to the mitochondria, but their targeted staining behaviours can be restored when MMP is re-established.

The data sets in this chapter contribute widely to the field and provide the first extensive categorisation of the behaviours of simple cyanine dyes in a single cell line (HeLa). When put in context with the pre-existing literature, some findings were in line with previous studies. An example of this consistency is the clear positive correlation between construct fluorescence intensity and concentration of treatment. Previous literature commonly used a concentration of 10 μM to obtain the clearest fluorescent output for confocal imaging,[291, 342, 344, 355] and it was found here also that 10 μM provided the most informative imaging conditions. Many other results are counteractions to what has previously been described however, but these could be related to

inconsistencies in experimental conditions, such as variations in the cells used (mesenchymal stem cells, macrophages, or canine kidney cells), and crucially differences in construct design (inclusion of additional ring structures, or tethering to esters and use of succinamide).[291, 337, 339, 342]

An important dataset however that doesn't entirely fit with the literature is the behaviours of **Cy3-Cy5-R8**. For example, **Cy3-Cy5-R8** was shown to successfully stain the mitochondria of HeLa cells. These results are a counteraction of *Ross et al.*'s findings which stated that cell penetrating peptides are incapable of crossing the mitochondrial membrane, regardless of conjugation to a lipophilic cation.[344] Indeed, the study performed by *Ross et al.* was conducted using CPPs Tat (HIV-1 derivative), and Penetratin (Antennapedia homo-protein derivative) which have relatively similar amino acid sequences compared to R8 and nearly identical charged states.[354] However, using TPP (triphenolphosphonium) as a lipophilic cation is a notable discrepancy. Comparing this to the findings reported in **Chapter 2**, there remains the suggestion that the results cannot be directly compared due to the difference in the lipophilic cation employed. Nevertheless, the results of **Cy3-Cy5-R8** demonstrate that the statement made by *Ross et al.* is not transferrable across all conditions or constructs, and therefore this statement has been proven inaccurate. As a result, the ability of these conjugates to penetrate the mitochondria should therefore be determined on a case by case basis as varying combinations can clearly alter the end result. Additionally, another report concluded that **Cy5** conjugation alone to R8 is not capable of tracking to the mitochondria.[342] However, this was conducted using a single dye (**Cy5**), and therefore it could be possible that **Cy3-Cy5-R8**'s higher charge given the inclusion of **Cy3** potentially permits mitochondrial delivery.

Serum proteins have also been shown to hinder the efficiencies of CPP molecules,[354, 357] mostly linked to the presence of serum albumin and enzymes. This is supportive of the findings with **Cy3-Cy5-R8** treatment in the presence of FBS, as a distinct decrease in staining ability was observed which

is suggested to be due to non-specific interactions between the conjugate and serum proteins present. Conversely, an interesting murine study using Cy7-derivatives as cancer targeting entities suggested albumin as a critical component for cancer cell retention which counteracts the findings reported here. Nevertheless, the structures of the molecules used in the report carried many discrepancies compared to the molecules in this study, and the authors deemed the presence of a Cl residue responsible for the interaction with albumin;[359] a residue that is not included in the structures used here. Moreover, an explanation for the specific interactions of serum with R8 and not the other dye molecules remain unclear as all are positively charged. However, it is theorised that the proposed interactions with serum proteins may be dependent on the charged arginine residues on **Cy3-Cy5-R8** specifically, which would explain the serum only effecting the CPP conjugate.

With regards to the **Cy3-*drug*** conjugates, the drugs **KLA**, **Cip** and **CPT** were chosen as they represent three important classes of drugs in clinical application, and the molecular targets of all these drugs are believed to be the mitochondria.[345-351] Across all three **Cy3-*drug*** conjugates, an increase in toxicity was observed when covalently conjugated to **Cy3**, with **Cy3-KLA** presenting the best results with a 1000-fold improvement in EC_{50} when compared to **KLA** alone. Moreover, the **Cy3-*drug*** conjugates were all shown to be more toxic in cancer cells than non-cancer cells when comparing their toxicities in HeLa to HEK293. The EC_{50} value of **Cy3-KLA** is significantly lower ($p > 0.01$) in HeLa (4.0 μM) compared to HEK293 (11.1 μM). Furthermore, a 10-fold increase in EC_{50} (and therefore potency) was observed with **Cy3-CPT** (0.8 μM vs 11.1 μM) while a 2-fold increase was observed for **Cy3-Cip** (3.9 μM vs 6.7 μM). Their selectivity observed here is likely derived from the MMP being more negative in cancer cells compared to non-cancer cells.[34, 168, 300] However, it needs to be considered that the cell lines used here are immortalised so cannot be considered as a clear representation of how the conjugates would behave in an *in vivo* model. A natural mammalian system carries a plethora of additional complexities that cannot be assessed *in vitro*;

therefore, testing these conjugates *in vivo* is crucial to ascertain whether the promising results obtained here are transferable to a clinical setting.

Although the results regarding the drug conjugates show a clear toxicity to cancer cells, there was still a marked toxicity in the non-cancerous cell line HEK293, illustrating a lower than ideal selectivity. In order to translate these findings into a clinical setting, it would be necessary to test them on a wider range of cancer and non-cancer cell lines, alongside a range of primary cancer and non-cancer cells. These results will be required to determine whether the results found here can be converted into a clinical setting.

The selectivity of the compounds could possibly be improved via addition of a receptor-targeting entity to specifically bind to cancer cell surface markers, however this approach is complex and lengthy with no promise of success. The conjugation to a receptor-targeting molecule will make the compound much larger, likely more complex to create, and risks the retention of molecular stability. Moreover, in targeting receptors or surface proteins, a release-mechanism will also be required to facilitate drug conjugate release into the cell once the membrane has been targeted. This cell-homing moiety may also restrict the efficiency of cyanine dye entry into the cell, bringing the risk of a reduced toxicity or efficacy. Alternatively, in light of the ongoing research which involves stimulus-responsive nanoparticles, the combination of these with the drug conjugates could also prove fruitful. As mentioned in **Chapter 1**, the development of nanoparticles that respond to environmental stimuli such as the acidic pH of tumour microenvironments is a growing movement in the community.[120, 122] If a pH-sensitive nanoparticle that can transport **Cy3-KLA** or **Cy5-KLA** to the tumour microenvironment can be ascertained, then the subsequent degradation of the nanoparticle and release of the drug into the tumour microenvironment would theoretically be very effective, as the nanoparticle facilitates the release of the drug only in the vicinity of cancer cells, while the dye can then enable the delivery of the toxic peptide to the cancer mitochondria. This method would theoretically alleviate much of the

non-selective activity observed, and may additionally improve the potency of **Cy3-KLA**.

In summary, there are many hurdles that remain to be addressed before these findings can potentially be transferred into a therapeutic setting, however the results so far are promising. The next stage of research will need to focus on improving specificity, whilst not detrimentally damaging the toxicities or efficacies of the constructs.

4.1.2 Genetic code expansion as therapeutic switches

The development of chemotherapeutics that can be selectively activated is a field of research with expanding interest, especially in the context of immunotherapies.[285, 297, 299] Although great progress has been made in the generation of switchable CAR-T cells, there remains to be limitations to each one's use; be it a lack of control, the presence of only one available switch function, or even the use of drugs as switch molecules which carry their own toxicities.[285, 296-299] It is of increasing importance to generate a logic operating CAR-T system that is functional, has dual operation (ON and OFF) and doesn't require any additional molecules that can bring adverse side effects and toxicities in their own right. The research presented in **Chapter 3** demonstrates a logical solution to the problem, via the adaptation of genetic code expansion.

Through the project, many findings were inconsistent with the current presentation in the literature. For example, in the quest to identify an aaRS/tRNA pair that can incorporate the unnatural amino acid BocK, a range of tRNA mutants previously described to function in *E. coli* were tested. In contrast to the observations in *E. coli* where all 11 quadruplet Pyl tRNA variants were functional,[341, 381, 382] only five led to BocK-dependent production of eGFP. Importantly, there was negligible eGFP production with either Pyl $tRNA_{UCUA}$ or Pyl $tRNA_{UCUA(Ev2)}$, which have previously been shown to function in HEK293T cells with 5 mM BocK.[384] Nonetheless, it is possible that

deviations in the cell line tested (HEK293 vs HEK293T) and concentration of BocK used (1 mM vs 5 mM) could be responsible for this discrepancy. It was also evident from the two CUAG- and three AGGA-decoding variants that the nucleic acid sequence in the anticodon stem loop has significant influence on the incorporation, where base mutations can either improve or reduce the efficiency of BocK incorporation. Importantly, as seen in *E. coli*, neither fluorescence nor eGFP was detectable in the absence of BocK, demonstrating that the functional Pyl tRNA variants remained orthogonal in mammalian cells.

Another important finding that was different to that described in the literature was regarding the orthogonal TyrRS*/tRNA set. This pair has a range of substrates including OMeY and AzF.[409, 410] The observations by *Italia et al.* saw that TyrRS* mediated incorporation of OMeY was stronger than AzF,[410] however the opposite was observed in this case. This deviation in the favoured substrate of TyrRS*/tRNA is not entirely clear, but it could be related to difference in the cell type used for the analysis. Namely, *Italia et al.* performed these experiments in *E. coli*, whereas these studies were performed in the mammalian cell line HEK293. As a result, this discrepancy is likely down to a lack of comparability between *E. coli*-based and mammalian-cell-based genetic code expansion capabilities, which had already been demonstrated with the incomparable incorporation abilities of the quadruplet Pyl tRNA variants when used in *E. coli* or HEK293 respectively.

A previous research article discussed the use of a mutated eukaryotic release factor (eRF1) to increase the incorporation efficiency of aaRS/tRNA for amber suppression.[406] Testing this eRF1 mutant with the aaRS/tRNA pairs used in **Chapter 3** showed no significant improvement however, as there was no significant alteration in eGFP fluorescence observed between cells in the presence or absence of eRF1(E55D). Again, these results cannot be directly compared to the paper that reported this variant, as they used a PylRS mutant for amber incorporation, and they had not tested a Tyr variant which may influence the transferability.

In an attempt to improve the incorporation efficiency of the aaRS/tRNA pairs, an increase in tRNA copy number was examined. For both pairs, a marked increase in fluorescent eGFP was detected when multiple copies of tRNA were used, exhibiting an average improvement in eGFP production ranging from 2.5- to 6.5-fold. Unlike some of the other experiments performed which exhibited a lack of continuity with the existing literature, this data conversely is in line with other genetic code expansion methods. Previous studies have commonly used tRNA cassettes (which carry increased copy numbers of the tRNA gene), and the method has widely been shown to improve the final reporter output.[377, 381, 383, 385, 408, 409]

Building on the results collected through these preliminary studies, the aaRS/tRNA pairs tested were transferred into a mammalian cell logic gate design. The engineering of mammalian cell logic gates has revolutionized synthetic biology, enabling the development of sensors, diagnostics and therapeutics.[286, 389-392] The employment of environmental or synthetic switches is a fast developing next-generation technique for intricate cellular phenotype control, with exponential biotechnological and biomedical applications.[233, 299, 393-396] Here, AND and OR logic operations were developed through a combination of PylRS/$tRNA_{UCCU(Ev2)}$, TyrRS*/$tRNA_{CUA}$ and a split GFP reporter. Logic gates with an AND operation require the presence of both inputs to achieve the desired output.[414] Owing to this, a double-plasmid model was generated whereby GFP fluorescence can only be achieved upon concurrent incorporation of AzF and BocK. Upon testing in HEK293, GFP fluorescence could only be detected when cells were incubated in the presence of both AzF and BocK, and GFP fluorescence was observed to be of a relatively high level, demonstrating a reasonably high efficiency of the system. Similar efficiencies were also obtained with the OR logic operation. Logic gates with an OR operation require the presence of either inputs to achieve the desired output,[414] and indeed GFP fluorescence could be detected when cells were incubated with either or both AzF and BocK.

Combining all the data sets presented in **Chapter 3**, it is plausible that these genetic code expansion mediated logic gates can be transferred into a switchable CAR-T model. As a whole, CAR-T are an emerging therapy in cancer treatment which have shown impressive cancer-destructive capabilities.[74, 226, 283, 293] However, there is currently a shortfall in the ability to control CAR-T cells once they are introduced to a patient. Patients may experience undesirable side effects; including the common occurrence of cytokine storms which can be fatal.[281, 282, 284, 295] Resultantly, it is crucial in this line of research to develop CAR-T that can be intrinsically controlled, and the adaptation of unnatural amino acid incorporation as orthogonal and innate molecular switches could subsequently permit titrated and temporal control of CAR-T activity. Researches have already began developing switchable CAR-T models, however these studies primarily focus on engineering a single switch; be it activation, inactivation, or cell destruction.[54, 226, 296-299] With this in mind, the proposed ON/OFF CAR-T model could be invaluable to the research field. If it works, the method would provide oncologists with a heightened and intricate level of control over the immunotherapeutic intensity, while harbouring a kill switch if CAR-T are seen to cause adverse toxicity in the patient. Moreover, if the therapeutic output is lower than expected at 1 mM concentration of BocK, the amount of BocK can be increased, as concentrations have been previously used at 5 mM in mammalian cellular studies,[384] therefore it is plausible that concentrations up-to and including 5 mM would be tolerated without causing adverse effects.

In summary, the research shown in **Chapter 3** considerably contributes to the fields of genetic code expansion, mammalian cell logic circuits, and can potentially contribute substantially to the field of CAR-T based immunotherapies. If the temporal control of CAR-T cells by unnatural amino acid incorporation is as successful as presumed, this new technique could revolutionise cancer immunotherapy tactics, enabling spatiotemporal control of CAR-T anti-cancer activities, while providing a potentially lifesaving kill switch if cytokine production remains dangerously high in a patient.

4.1.3 Future work and closing remarks

Although the research in this series of work is built of preliminary studies, they nevertheless shine a light on two new and exciting approaches to opposing areas of targeted cancer treatments. To develop them further many obstacles still remain to be overcome, such as the requirement for a more-targeted tumour delivery system for **Cy3-*drug*** conjugates, and for the developed genetic code expansion logic gates to be transferred into a CAR-T model. As a whole, the fields of organelle-targeted drug delivery or switchable CAR-T immunotherapies both hold the potential to revolutionise the field of targeted cancer therapeutics.[53, 71, 101, 120, 131, 133, 168, 194, 226] Conversely, however, both approaches bring pros and cons which cannot be directly compared. For example, although targeted drug delivery is typically less selective and doesn't have life-long impact like immunological methods, these treatments are commonly easier to develop, and much more economically viable.[51, 52, 64, 246] On the other hand, immunotherapies with CAR-T are a highly specialised field which shows great promise in tumour-selectivity that is yet to be obtained with targeted drugs, however this highly specialised technique unfortunately requires a substantial amount of expertise and resources, which resultantly means treatment can cost anything up to £500,000 for a single treatment.[51, 52, 64, 246] Owing to this, it is currently difficult to discern which therapeutic approach will become the more-widely available option in decades to come, but nevertheless both show great potential to substantially contribute in the quest to develop new and improved targeted cancer therapeutics.

CHAPTER 5:
References

1. M. Malumbres and M. Barbacid, 2009. Cell cycle, CDKs and cancer: a changing paradigm. *Nat. Rev. Cancer*, **9**, 153-166.
2. K. A. Schafer, 1998. The Cell Cycle: A Review. *Vet. Pathol.*, **35**, 461-478.
3. K. Vermeulen, D. R. Van Bockstaele and Z. N. Berneman, 2003. The cell cycle: a review of regulation, deregulation and therapeutic targets in cancer. *Cell Prolif.*, **36**, 131-149.
4. J. Kalucka, R. Missiaen, M. Georgiadou, S. Schoors, C. Lange, K. De Bock, M. Dewerchin and P. Carmeliet, 2015. Metabolic control of the cell cycle. *Cell Cycle*, **14**, 3379-3388.
5. H. Ohkura, 2015. Meiosis: an overview of key differences from mitosis. *Cold Spring Harb. Perspect. Biol.*, **7**, DOI: 10.1101/cshperspect.a015859.
6. Y. Budirahardja and P. Gönczy, 2009. Coupling the cell cycle to development. *Development*, **136**, 2861-2872.
7. P. Kaldis and H. E. Richardson, 2012. When cell cycle meets development. *Development*, **139**, 225-131.
8. J. G. Carlton, H. Jones and U. S. Eggert, 2020. Membrane and organelle dynamics during cell division. *Nat. Rev. Mol. Cell Biol.*, **21**, 151-166.
9. J. P. Matson and J. G. Cook, 2017. Cell cycle proliferation decisions: the impact of single cell analyses. *FEBS J.*, **284**, 362-375.
10. J. W. Shay and W. E. Wright, 2000. Hayflick, his limit, and cellular ageing. *Nat. Rev. Mol. Cell Biol.*, **1**, 72-76.
11. K. Collins, T. Jacks and N. P. Pavletich, 1997. The cell cycle and cancer. *Proc. Nat. Acad. Sci.*, **94**, 2776-2782.
12. D. Hanahan and R. A. Weinberg, 2000. The Hallmarks of Cancer. *Cell*, **100**, 57-70.
13. J. Cicenas, E. Zalyte, A. Bairoch and P. Gaudet, 2018. Kinases and Cancer. *Cancers*, **10**, 63-70.
14. H. A. Idikio, 2011. Human cancer classification: a systems biology- based model integrating morphology, cancer stem cells, proteomics, and genomics. *J. Cancer*, **2**, 107-115.
15. A. Patel, 2020. Benign vs Malignant Tumors. *JAMA Oncol.*, **6**, 1488-1499.

16. M. S. D'Arcy, 2019. Cell death: a review of the major forms of apoptosis, necrosis and autophagy. *Cell Biol. Int.*, **43**, 582-592.

17. S. Elmore, 2007. Apoptosis: a review of programmed cell death. *Toxicol. Pathol.*, **35**, 495-516.

18. L. Galluzzi, I. Vitale, S. A. Aaronson, J. M. Abrams, D. Adam, P. Agostinis, E. S. Alnemri, L. Altucci, I. Amelio, D. W. Andrews, M. Annicchiarico-Petruzzelli, A. V. Antonov, E. Arama, E. H. Baehrecke, N. A. Barlev, N. G. Bazan, F. Bernassola, M. J. M. Bertrand, K. Bianchi, M. V. Blagosklonny, K. Blomgren, C. Borner, P. Boya, C. Brenner, M. Campanella, E. Candi, D. Carmona-Gutierrez, F. Cecconi, F. K. M. Chan, N. S. Chandel, E. H. Cheng, J. E. Chipuk, J. A. Cidlowski, A. Ciechanover, G. M. Cohen, M. Conrad, J. R. Cubillos-Ruiz, P. E. Czabotar, V. D'Angiolella, T. M. Dawson, V. L. Dawson, V. De Laurenzi, R. De Maria, K.-M. Debatin, R. J. DeBerardinis, M. Deshmukh, N. Di Daniele, F. Di Virgilio, V. M. Dixit, S. J. Dixon, C. S. Duckett, B. D. Dynlacht, W. S. El-Deiry, J. W. Elrod, G. M. Fimia, S. Fulda, A. J. García-Sáez, A. D. Garg, C. Garrido, E. Gavathiotis, P. Golstein, E. Gottlieb, D. R. Green, L. A. Greene, H. Gronemeyer, A. Gross, G. Hajnoczky, J. M. Hardwick, I. S. Harris, M. O. Hengartner, C. Hetz, H. Ichijo, M. Jäättelä, B. Joseph, P. J. Jost, P. P. Juin, W. J. Kaiser, M. Karin, T. Kaufmann, O. Kepp, A. Kimchi, R. N. Kitsis, D. J. Klionsky, R. A. Knight, S. Kumar, S. W. Lee, J. J. Lemasters, B. Levine, A. Linkermann, S. A. Lipton, R. A. Lockshin, C. López-Otín, S. W. Lowe, T. Luedde, E. Lugli, M. MacFarlane, F. Madeo, M. Malewicz, W. Malorni, G. Manic, J.-C. Marine, S. J. Martin, J.-C. Martinou, J. P. Medema, P. Mehlen, P. Meier, S. Melino, E. A. Miao, J. D. Molkentin, U. M. Moll, C. Muñoz-Pinedo, S. Nagata, G. Nuñez, A. Oberst, M. Oren, M. Overholtzer, M. Pagano, T. Panaretakis, M. Pasparakis, J. M. Penninger, D. M. Pereira, S. Pervaiz, M. E. Peter, M. Piacentini, P. Pinton, J. H. M. Prehn, H. Puthalakath, G. A. Rabinovich, M. Rehm, R. Rizzuto, C. M. P. Rodrigues, D. C. Rubinsztein, T. Rudel, K. M. Ryan, E. Sayan, L. Scorrano, F. Shao, Y. Shi, J. Silke, H.-U. Simon, A. Sistigu, B. R. Stockwell, A. Strasser, G. Szabadkai, S. W. G. Tait, D. Tang, N. Tavernarakis, A. Thorburn, Y. Tsujimoto, B. Turk, T. Vanden Berghe, P. Vandenabeele, M. G. Vander Heiden, A. Villunger, H. W. Virgin, K. H. Vousden, D. Vucic, E. F. Wagner, H. Walczak,

D. Wallach, Y. Wang, J. A. Wells, W. Wood, J. Yuan, Z. Zakeri, B. Zhivotovsky, L. Zitvogel, G. Melino and G. Kroemer, 2018. Molecular mechanisms of cell death: recommendations of the Nomenclature Committee on Cell Death 2018. *Cell Death Differ.*, **25**, 486-541.

19. R. Singh, A. Letai and K. Sarosiek, 2019. Regulation of apoptosis in health and disease: the balancing act of BCL-2 family proteins. *Nat. Rev. Mol. Cell Biol.*, **20**, 175-193.
20. M. Suzanne and H. Steller, 2013. Shaping organisms with apoptosis. *Cell Death Differ.*, **20**, 669-675.
21. T. Ozaki and A. Nakagawara, 2011. Role of p53 in Cell Death and Human Cancers. *Cancers*, **3**, 994-1013.
22. I. Chowdhury, B. Tharakan and G. K. Bhat, 2006. Current concepts in apoptosis: the physiological suicide program revisited. *Cell. Mol. Biol. Lett.*, **11**, 506-525.
23. M. Schwartz Stephen, 1998. Cell Death and the Caspase Cascade. *Circulation*, **97**, 227-229.
24. J. S. Armstrong, 2007. Mitochondrial medicine: pharmacological targeting of mitochondria in disease. *Brit. J. Pharmacol.*, **151**, 1154-1165.
25. F. Mantovani, L. Collavin and G. Del Sal, 2019. Mutant p53 as a guardian of the cancer cell. *Cell Death Differ.*, **26**, 199-212.
26. H. J. Oh, J. M. Bae, X. Wen, S. Jung, Y. Kim, K. J. Kim, N.-Y. Cho, J. H. Kim, S.-W. Han, T.-Y. Kim and G. H. Kang, 2019. p53 expression status is associated with cancer-specific survival in stage III and high-risk stage II colorectal cancer patients treated with oxaliplatin-based adjuvant chemotherapy. *Brit. J. Cancer*, **120**, 797-805.
27. S. Tandon, C. Tudur-Smith, R. D. Riley, M. T. Boyd and T. M. Jones, 2010. A systematic review of p53 as a prognostic factor of survival in squamous cell carcinoma of the four main anatomical subsites of the head and neck. *Cancer Epidemiol. Biomark. Prev.*, **19**, 574-587.
28. K. H. Vousden and C. Prives, 2005. P53 and Prognosis: New Insights and Further Complexity. *Cell*, **120**, 7-10.
29. J. Bi, T.-A. Ichu, C. Zanca, H. Yang, W. Zhang, Y. Gu, S. Chowdhry, A. Reed, S. Ikegami, K. M. Turner, W. Zhang, G. R. Villa, S. Wu, O. Quehenberger, W. H. Yong, H. I.

Kornblum, J. N. Rich, T. F. Cloughesy, W. K. Cavenee, F. B. Furnari, B. F. Cravatt and P. S. Mischel, 2019. Oncogene Amplification in Growth Factor Signaling Pathways Renders Cancers Dependent on Membrane Lipid Remodeling. *Cell Metab.*, **30**, 525-538.

30. M. Niepel, M. Hafner, E. A. Pace, M. Chung, D. H. Chai, L. Zhou, J. L. Muhlich, B. Schoeberl and P. K. Sorger, 2014. Analysis of growth factor signaling in genetically diverse breast cancer lines. *BMC Biol.*, **12**, 20-29.

31. E. C. Woodhouse, R. F. Chuaqui and L. A. Liotta, 1997. General mechanisms of metastasis. *Cancer*, **80**, 1529-1537.

32. R. Sever and J. S. Brugge, 2015. Signal transduction in cancer. *Cold Spring Harb. Perspect. Med.*, **5**, DOI: 10.1101/cshperspect.a006098.

33. B. Mansoori, A. Mohammadi, S. Davudian, S. Shirjang and B. Baradaran, 2017. The Different Mechanisms of Cancer Drug Resistance: A Brief Review. *Adv. Pharm. Bull.*, **7**, 339-348.

34. P. E. Porporato, N. Filigheddu, J. M. B.-S. Pedro, G. Kroemer and L. Galluzzi, 2018. Mitochondrial metabolism and cancer. *Cell Res.*, **28**, 265-280.

35. H. Zahreddine and K. L. B. Borden, 2013. Mechanisms and insights into drug resistance in cancer. *Front. Pharmacol.*, **4**, 28-34.

36. R. Lugano, M. Ramachandran and A. Dimberg, 2020. Tumor angiogenesis: causes, consequences, challenges and opportunities. *Cell Mol. Life Sci.*, **77**, 1745-1770.

37. N. Nishida, H. Yano, T. Nishida, T. Kamura and M. Kojiro, 2006. Angiogenesis in cancer. *Vasc. Health Risk Manag.*, **2**, 213-219.

38. M. Rajabi and S. A. Mousa, 2017. The Role of Angiogenesis in Cancer Treatment. *Biomedicines*, **5**, 34-47.

39. J. Fares, M. Y. Fares, H. H. Khachfe, H. A. Salhab and Y. Fares, 2020. Molecular principles of metastasis: a hallmark of cancer revisited. *Signal Transduct. Target. Ther.*, **5**, 28-35.

40. L. M. E. Janssen, E. E. Ramsay, C. D. Logsdon and W. W. Overwijk, 2017. The immune system in cancer metastasis: friend or foe? *J. Immunother. Cancer.*, **5**, 79-87.

41. I. Poschke, D. Mougiakakos and R. Kiessling, 2011. Camouflage and sabotage: tumor escape from the immune system. *Cancer Immunol. Immunother.*, **60**, 1161-1171.

42. D. S. Vinay, E. P. Ryan, G. Pawelec, W. H. Talib, J. Stagg, E. Elkord, T. Lichtor, W. K. Decker, R. L. Whelan, H. M. C. S. Kumara, E. Signori, K. Honoki, A. G. Georgakilas, A. Amin, W. G. Helferich, C. S. Boosani, G. Guha, M. R. Ciriolo, S. Chen, S. I. Mohammed, A. S. Azmi, W. N. Keith, A. Bilsland, D. Bhakta, D. Halicka, H. Fujii, K. Aquilano, S. S. Ashraf, S. Nowsheen, X. Yang, B. K. Choi and B. S. Kwon, 2015. Immune evasion in cancer: Mechanistic basis and therapeutic strategies. *Semin. Cancer Biol.*, **35**, 185-198.

43. L. Borthwick, 2007. Telomeres lengthen during early embryonic development. *Nat. Rep. Stem Cells*, **20**, 15-30.

44. L. Liu, S. M. Bailey, M. Okuka, P. Muñoz, C. Li, L. Zhou, C. Wu, E. Czerwiec, L. Sandler, A. Seyfang, M. A. Blasco and D. L. Keefe, 2007. Telomere lengthening early in development. *Nat. Cell Biol.*, **9**, 1436-1441.

45. M. P. Mattson and W. Klapper, 2001. Emerging roles for telomerase in neuronal development and apoptosis. *J. Neurosci. Res.*, **63**, 1-9.

46. C. B. Harley, 2008. Telomerase and cancer therapeutics. *Nat. Rev. Cancer*, **8**, 167-179.

47. M. A. Jafri, S. A. Ansari, M. H. Alqahtani and J. W. Shay, 2016. Roles of telomeres and telomerase in cancer, and advances in telomerase-targeted therapies. *Genome Med.*, **8**, 69-75.

48. Z. K. Otrock, R. A. R. Mahfouz, J. A. Makarem and A. I. Shamseddine, 2007. Understanding the biology of angiogenesis: Review of the most important molecular mechanisms. *Blood Cell. Mol. Dis.*, **39**, 212-220.

49. H. Sung, J. Ferlay, R. L. Siegel, M. Laversanne, I. Soerjomataram, A. Jemal and F. Bray, 2021. Global cancer statistics 2020: GLOBOCAN estimates of incidence and mortality worldwide for 36 cancers in 185 countries. *CA: Cancer J. Clin.*, **7**, 209-249.

50. A. Rehemtulla, 2010. Dinosaurs and ancient civilizations: reflections on the treatment of cancer. *Neoplasia*, **12**, 957-968.

51. E. Dolgin, 2018. Bringing down the cost of cancer treatment. *Nature*, **555**, 26-29.

52. M. Schlueter, K. Chan, R. Lasry and M. Price, 2020. The cost of cancer - A comparative analysis of the direct medical costs of cancer and other major chronic diseases in Europe. *PLoS One*, **15**, DOI: 10.1371/journal.pone.0241354.

53. K. S. Bhullar, N. O. Lagarón, E. M. McGowan, I. Parmar, A. Jha, B. P. Hubbard and H. P. V. Rupasinghe, 2018. Kinase-targeted cancer therapies: progress, challenges and future directions. *Mol. Cancer*, **17**, 48-68.

54. M. Liu and F. Guo, 2018. Recent updates on cancer immunotherapy. *Precis. Clin. Med.*, **1**, 65-74.

55. D. J. Benjamin, 2014. The efficacy of surgical treatment of cancer – 20years later. *Med. Hypotheses*, **82**, 412-420.

56. L. Falzone, S. Salomone and M. Libra, 2018. Evolution of Cancer Pharmacological Treatments at the Turn of the Third Millennium. *Front. Pharmacol.*, **9**, 1300-1317.

57. R. Baskar, K. A. Lee, R. Yeo and K.-W. Yeoh, 2012. Cancer and radiation therapy: current advances and future directions. *Int. J. Med. Sci.*, **9**, 193-199.

58. H. H. W. Chen and M. T. Kuo, 2017. Improving radiotherapy in cancer treatment: Promises and challenges. *Oncotarget*, **8**, 62742-62758.

59. V. T. DeVita and E. Chu, 2008. A History of Cancer Chemotherapy. *Cancer Res.*, **68**, 8643-8653.

60. D. Galmarini, C. M. Galmarini and F. C. Galmarini, 2012. Cancer chemotherapy: A critical analysis of its 60 years of history. *Crit. Rev. Oncol. Hemat.*, **84**, 181-199.

61. A. Castaño, U. Roy and O. D. Schärer, 2017. *Methods Enzymol.*, ed. B. F. Eichman, Academic Press, , **591**, 415-431.

62. R. Ralhan and J. Kaur, 2007. Alkylating agents and cancer therapy. *Expert Opin. Ther. Pat.*, **17**, 1061-1075.

63. D. S. Shewach and R. D. Kuchta, 2009. Introduction to cancer chemotherapeutics. *Chem. Rev.*, **109**, 2859-2861.

64. M. Glatzer, C. M. Panje, C. Sirén, N. Cihoric and P. M. Putora, 2020. Decision Criteria in Oncology. *Oncology*, **98**, 370-378.

65. D. Stacey, L. Paquet and R. Samant, 2010. Exploring cancer treatment decision-making by patients: a descriptive study. *Curr. Oncol.*, **17**, 85-93.

66. S. K. Vinod and E. Hau, 2020. Radiotherapy treatment for lung cancer: Current status and future directions. *Respirology*, **25**, 61-71.

67. S. Chakraborty and T. Rahman, 2012. The difficulties in cancer treatment. *Ecancermedicalscience*, **6**, DOI: 10.3332/ecancer.2012.ed3316.

68. J. Zugazagoitia, C. Guedes, S. Ponce, I. Ferrer, S. Molina-Pinelo and L. Paz-Ares, 2016. Current Challenges in Cancer Treatment. *Clin. Ther.*, **38**, 1551-1566.

69. K. Nurgali, R. T. Jagoe and R. Abalo, 2018. Editorial: Adverse Effects of Cancer Chemotherapy: Anything New to Improve Tolerance and Reduce Sequelae? *Front. Pharmacol.*, **9**, 245-251.

70. S. Salas-Vega, E. Shearer and E. Mossialos, 2020. Relationship between costs and clinical benefits of new cancer medicines in Australia, France, the UK, and the US. *Soc. Sci. Med.*, **258**, DOI: 10.1016/j.socscimed.2020.113042.

71. A. Ahmad, S. Uddin and M. Steinhoff, 2020. CAR-T Cell Therapies: An Overview of Clinical Studies Supporting Their Approved Use against Acute Lymphoblastic Leukemia and Large B-Cell Lymphomas. *Int. J. Mol. Sci.*, **21**, 3906.

72. R. Andersen, M. C. W. Westergaard, J. W. Kjeldsen, A. Müller, N. W. Pedersen, S. R. Hadrup, Ö. Met, B. Seliger, B. Kromann-Andersen, T. Hasselager, M. Donia and I. M. Svane, 2018. T-cell Responses in the Microenvironment of Primary Renal Cell Carcinoma-Implications for Adoptive Cell Therapy. *Cancer Immunol. Res.*, **6**, 222-235.

73. P. Dobosz and T. Dzieciątkowski, 2019. The Intriguing History of Cancer Immunotherapy. *Front. Immunol.*, **10**, 2965-2965.

74. K. Esfahani, L. Roudaia, N. Buhlaiga, S. V. Del Rincon, N. Papneja and W. H. Miller, Jr., 2020. A review of cancer immunotherapy: from the past, to the present, to the future. *Curr. Oncol.*, **27**, 87-97.

75. H. Gonzalez, C. Hagerling and Z. Werb, 2018. Roles of the immune system in cancer: from tumor initiation to metastatic progression. *Genes Dev.*, **32**, 1267-1284.

76. J. Blagih, M. D. Buck and K. H. Vousden, 2020. p53, cancer and the immune response. *J. Cell Sci.*, **133**, DOI: 10.1242/jcs.237453.

77. D. Hao, L. Wang and L.-j. Di, 2016. Distinct mutation accumulation rates among tissues determine the variation in cancer risk. *Sci. Rep.*, **6**, 19458-19467.

78. M. Lynch, 2010. Evolution of the mutation rate. *Trends in genetics*, **26**, 345-352.

79. K. O. Alfarouk, C.-M. Stock, S. Taylor, M. Walsh, A. K. Muddathir, D. Verduzco, A. H. H. Bashir, O. Y. Mohammed, G. O. Elhassan, S. Harguindey, S. J. Reshkin, M. E. Ibrahim and C. Rauch, 2015. Resistance to cancer chemotherapy: failure in drug response from ADME to P-gp. *Cancer Cell Int.*, **15**, 71.

80. A. S. Choudhari, P. C. Mandave, M. Deshpande, P. Ranjekar and O. Prakash, 2019. Phytochemicals in Cancer Treatment: From Preclinical Studies to Clinical Practice. *Front. Pharmacol.*, **10**, 1614-1631.

81. A. G. Desai, G. N. Qazi, R. K. Ganju, M. El-Tamer, J. Singh, A. K. Saxena, Y. S. Bedi, S. C. Taneja and H. K. Bhat, 2008. Medicinal plants and cancer chemoprevention. *Curr. Drug Metab.*, **9**, 581-591.

82. P. Garcia-Oliveira, P. Otero, A. G. Pereira, F. Chamorro, M. Carpena, J. Echave, M. Fraga-Corral, J. Simal-Gandara and M. A. Prieto, 2021. Status and Challenges of Plant-Anticancer Compounds in Cancer Treatment. *Pharmaceuticals*, **14**, DOI: 10.3390/ph14020157.

83. M. Greenwell and P. K. S. M. Rahman, 2015. Medicinal Plants: Their Use in Anticancer Treatment. *Int. J. Pharm. Sci. Res.*, **6**, 4103-4112.

84. G. M. Cragg, D. Kingston and D. Newman, 2005. Anticancer agents from natural products, *CRC Press*, Boca Raton, 2nd Edition.

85. A. D. Kinghorn, Y.-W. Chin and S. M. Swanson, 2009. Discovery of natural product anticancer agents from

biodiverse organisms. *Curr. Opin. Drug. Discov. Devel.*, **12**, 189-196.

86. D. J. Newman, G. M. Cragg, S. Holbeck and E. A. Sausville, 2002. Natural products and derivatives as leads to cell cycle pathway targets in cancer chemotherapy. *Curr. Cancer Drug Targets*, **2**, 279-308.

87. J. Iqbal, B. A. Abbasi, T. Mahmood, S. Kanwal, B. Ali, S. A. Shah and A. T. Khalil, 2017. Plant-derived anticancer agents: A green anticancer approach. *Asian Pac. J. of Trop. Biomed.*, **7**, 1129-1150.

88. Y. Gao, S. A. Snyder, J. N. Smith and Y. C. Chen, 2016. Anticancer properties of baicalein: a review. *Med. Chem. Res.*, **25**, 1515-1523.

89. J. Dou, Z. Wang, L. Ma, B. Peng, K. Mao, C. Li, M. Su, C. Zhou and G. Peng, 2018. Baicalein and baicalin inhibit colon cancer using two distinct fashions of apoptosis and senescence. *Oncotarget*, **9**, 20089-20102.

90. S. C. Gupta, S. Patchva and B. B. Aggarwal, 2013. Therapeutic roles of curcumin: lessons learned from clinical trials. *AAPS J.*, **15**, 195-218.

91. H. Hatcher, R. Planalp, J. Cho, F. M. Torti and S. V. Torti, 2008. Curcumin: from ancient medicine to current clinical trials. *Cellular Mol. Life Sci.*, **65**, 1631-1652.

92. C. H. Hsu and A. L. Cheng, 2007. Clinical studies with curcumin. *Adv. Exp. Med. Biol.*, **595**, 471-480.

93. B. Salehi, Z. Stojanović-Radić, J. Matejić, M. Sharifi-Rad, N. V. Anil Kumar, N. Martins and J. Sharifi-Rad, 2019. The therapeutic potential of curcumin: A review of clinical trials. *Eur. J. Med. Chem.*, **163**, 527-545.

94. S. Hu, R. Zhao, Y. Liu, J. Chen, Z. Zheng and S. Wang, 2019. Preventive and Therapeutic Roles of Berberine in Gastrointestinal Cancers. *Biomed. Res. Int.*, **2019**, DOI: 10.1155/2019/6831520.

95. H. Wang, C. Zhu, Y. Ying, L. Luo, D. Huang and Z. Luo, 2017. Metformin and berberine, two versatile drugs in treatment of common metabolic diseases. *Oncotarget*, **9**, 10135-10146.

96. Y. Wang, Y. Liu, X. Du, H. Ma and J. Yao, 2020. The Anti-Cancer Mechanisms of Berberine: A Review. *Cancer Manag. Res.*, **12**, 695-702.

97. O. Kucuk, F. H. Sarkar, W. Sakr, Z. Djuric, M. N. Pollak, F. Khachik, Y. W. Li, M. Banerjee, D. Grignon, J. S. Bertram, J. D. Crissman, E. J. Pontes and D. P. Wood, Jr., 2001. Phase II randomized clinical trial of lycopene supplementation before radical prostatectomy. *Cancer Epidemiol. Biomark. Prev.*, **10**, 861-878.

98. N. B. Kumar, K. Besterman-Dahan, L. Kang, J. Pow-Sang, P. Xu, K. Allen, D. Riccardi and J. P. Krischer, 2008. Results of a Randomized Clinical Trial of the Action of Several Doses of Lycopene in Localized Prostate Cancer: Administration Prior to Radical Prostatectomy. *Clin. Med. Urol.*, **1**, 1-14.

99. R. Epelbaum, M. Schaffer, B. Vizel, V. Badmaev and G. Bar-Sela, 2010. Curcumin and Gemcitabine in Patients With Advanced Pancreatic Cancer. *Nutr. Cancer*, **62**, 1137-1141.

100. S. Lev-Ari, A. Vexler, A. Starr, M. Ashkenazy-Voghera, J. Greif, D. Aderka and R. Ben-Yosef, 2007. Curcumin Augments Gemcitabine Cytotoxic Effect on Pancreatic Adenocarcinoma Cell Lines. *Cancer Investig.*, **25**, 411-418.

101. M. Kumar, R. Nagpal, R. Hemalatha, V. Verma, A. Kumar, S. Singh, F. Marotta, S. Jain and H. Yadav, 2012. Targeted cancer therapies: the future of cancer treatment. *Acta Biomed.*, **83**, 220-233.

102. J. A. Endicott, M. E. M. Noble and L. N. Johnson, 2012. The Structural Basis for Control of Eukaryotic Protein Kinases. *Annu. Rev. Biochem.*, **81**, 587-613.

103. P. Cohen, 2002. Protein kinases — the major drug targets of the twenty-first century? *Nat. Rev. Drug Discov.*, **1**, 309-315.

104. S. R. Hubbard and J. H. Till, 2000. Protein Tyrosine Kinase Structure and Function. *Annu. Rev. Biochem.*, **69**, 373-398.

105. M. A. Lemmon and J. Schlessinger, 2010. Cell signaling by receptor tyrosine kinases. *Cell*, **141**, 1117-1134.

106. Z. Du and C. M. Lovly, 2018. Mechanisms of receptor tyrosine kinase activation in cancer. *Mol. Cancer*, **17**, 58-67.

107. D. S. Metibemu, O. A. Akinloye, A. J. Akamo, D. A. Ojo, O. T. Okeowo and I. O. Omotuyi, 2019. Exploring receptor tyrosine kinases-inhibitors in Cancer treatments. *Egypt J. Med. Hum. Genet.*, **20**, 35-46.

108. E. K. Greuber, P. Smith-Pearson, J. Wang and A. M. Pendergast, 2013. Role of ABL family kinases in cancer: from

leukaemia to solid tumours. *Nature reviews. Cancer*, **13**, 559-571.

109. A. Quintás-Cardama and J. Cortes, 2009. Molecular biology of bcr-abl1-positive chronic myeloid leukemia. *Blood*, **113**, 1619-1630.
110. R. Ren, 2005. Mechanisms of BCR–ABL in the pathogenesis of chronic myelogenous leukaemia. *Nat. Rev. Cancer*, **5**, 172-183.
111. N. Iqbal and N. Iqbal, 2014. Imatinib: a breakthrough of targeted therapy in cancer. *Chemother. Res. Pract.*, **2014**, 357027-357041.
112. G. Marcucci, D. Perrotti and M. A. Caligiuri, 2003. Understanding the Molecular Basis of Imatinib Mesylate Therapy in Chronic Myelogenous Leukemia and the Related Mechanisms of Resistance. *Clin. Cancer Res.*, **9**, 1248-1263.
113. R. Bitencourt, I. Zalcberg and I. D. Louro, 2011. Imatinib resistance: a review of alternative inhibitors in chronic myeloid leukemia. *Rev. Bras. Hematol. Hemoter.*, **33**, 470-475.
114. D. Bixby and M. Talpaz, 2011. Seeking the causes and solutions to imatinib-resistance in chronic myeloid leukemia. *Leukemia*, **25**, 7-22.
115. M. Hoemberger, W. Pitsawong and D. Kern, 2020. Cumulative mechanism of several major imatinib-resistant mutations in Abl kinase. *Proc. Nat. Acad. Sci.*, **117**, 19221-19229.
116. X. An, A. K. Tiwari, Y. Sun, P. R. Ding, C. R. Ashby, Jr. and Z. S. Chen, 2010. BCR-ABL tyrosine kinase inhibitors in the treatment of Philadelphia chromosome positive chronic myeloid leukemia: a review. *Leuk. Res.*, **34**, 1255-1268.
117. F. Rossari, F. Minutolo and E. Orciuolo, 2018. Past, present, and future of Bcr-Abl inhibitors: from chemical development to clinical efficacy. *J. Hematol. Oncol.*, **11**, 84-93.
118. F. Yu and W. Bender, 2001. The mechanism of tamoxifen in breast cancer prevention. *Breast Cancer Res.*, **3**, 74-85.
119. K. Novak, 2004. Conference report--protein kinase inhibitors in cancer treatment: mixing and matching? Highlights of the keystone symposium on protein kinases and cancer;

February 24-29, 2004; Lake Tahoe, California. *Medscape Gen. Med.*, **6**, 25-25.

120. B. Aslan, B. Ozpolat, A. K. Sood and G. Lopez-Berestein, 2013. Nanotechnology in cancer therapy. *J. Drug. Target.*, **21**, 904-913.
121. W. H. Gmeiner and S. Ghosh, 2015. Nanotechnology for cancer treatment. *Nanotechnol. Rev.*, **3**, 111-122.
122. N. R. Jabir, S. Tabrez, G. M. Ashraf, S. Shakil, G. A. Damanhouri and M. A. Kamal, 2012. Nanotechnology-based approaches in anticancer research. *Int. J. Nanomed.*, **7**, 4391-4408.
123. A. M. Merlot, D. S. Kalinowski and D. R. Richardson, 2014. Unraveling the mysteries of serum albumin—more than just a serum protein. *Front. Physiol.*, **5**, DOI: 10.3389/fphys.2014.00299.
124. K. Yamasaki, V. T. Chuang, T. Maruyama and M. Otagiri, 2013. Albumin-drug interaction and its clinical implication. *Biochim. Biophys. Acta*, **1830**, 5435-5443.
125. F. Kratz, 2008. Albumin as a drug carrier: Design of prodrugs, drug conjugates and nanoparticles. *J. Control. Release*, **132**, 171-183.
126. A. Wall, K. Nicholls, M. B. Caspersen, S. Skrivergaard, K. A. Howard, K. Karu, V. Chudasama and J. R. Baker, 2019. Optimised approach to albumin–drug conjugates using monobromomaleimide-C-2 linkers. *Organic Biomol. Chem.*, **17**, 7870-7873.
127. J. Gong, J. Yan, C. Forscher and A. Hendifar, 2018. Aldoxorubicin: a tumor-targeted doxorubicin conjugate for relapsed or refractory soft tissue sarcomas. *Drug Des. Devel. Ther.*, **12**, 777-786.
128. E. N. Hoogenboezem and C. L. Duvall, 2018. Harnessing albumin as a carrier for cancer therapies. *Adv. Drug. Deliv. Rev.*, **130**, 73-89.
129. J. Yang, Q. Lv, W. Wei, Z. Yang, J. Dong, R. Zhang, Q. Kan, Z. He and Y. Xu, 2018. Bioresponsive albumin-conjugated paclitaxel prodrugs for cancer therapy. *Drug Deliv.*, **25**, 807-814.
130. D. G. Levitt and M. D. Levitt, 2016. Human serum albumin homeostasis: a new look at the roles of synthesis,

catabolism, renal and gastrointestinal excretion, and the clinical value of serum albumin measurements. *Int. J. Gen. Med.*, **9**, 229-255.

131. N. M. Sakhrani and H. Padh, 2013. Organelle targeting: third level of drug targeting. *Drug Des. Devel. Ther.*, **7**, 585-599.
132. P. Gao, W. Pan, N. Li and B. Tang, 2019. Boosting Cancer Therapy with Organelle-Targeted Nanomaterials. *ACS Appl. Mater. Inter.*, **11**, 26529-26558.
133. O. C. Ubah and H. M. Wallace, 2014. Cancer therapy: Targeting mitochondria and other sub-cellular organelles. *Curr. Pharm. Des.*, **20**, 201-222.
134. D. Wlodkowic, J. Skommer, D. McGuinness, C. Hillier and Z. Darzynkiewicz, 2009. ER-Golgi network--a future target for anti-cancer therapy. *Leukemia Res.*, **33**, 1440-1447.
135. D. Mohr, S. Frey, T. Fischer, T. Güttler and D. Görlich, 2009. Characterisation of the passive permeability barrier of nuclear pore complexes. *EMBO J.*, **28**, 2541-2553.
136. L. Pan, Q. He, J. Liu, Y. Chen, M. Ma, L. Zhang and J. Shi, 2012. Nuclear-Targeted Drug Delivery of TAT Peptide-Conjugated Monodisperse Mesoporous Silica Nanoparticles. *J. Am. Chem. Soc.*, **134**, 5722-5725.
137. L. Pan, J. Liu, Q. He and J. Shi, 2014. MSN-Mediated Sequential Vascular-to-Cell Nuclear-Targeted Drug Delivery for Efficient Tumor Regression. *Adv. Mater.*, **26**, 6742-6748.
138. N. Li, Q. Sun, Z. Yu, X. Gao, W. Pan, X. Wan and B. Tang, 2018. Nuclear-Targeted Photothermal Therapy Prevents Cancer Recurrence with Near-Infrared Triggered Copper Sulfide Nanoparticles. *ACS Nano*, **12**, 5197-5206.
139. L. Pan, J. Liu and J. Shi, 2017. Nuclear-Targeting Gold Nanorods for Extremely Low NIR Activated Photothermal Therapy. *ACS Appl. Mater. Inter.*, **9**, 15952-15961.
140. S. Chatterjee and T. F. Burns, 2017. Targeting Heat Shock Proteins in Cancer: A Promising Therapeutic Approach. *Int. J. Mol. Sci.*, **18**, 1978 - 1917.
141. B. J. Lang, M. E. Guerrero-Giménez, T. L. Prince, A. Ackerman, C. Bonorino and S. K. Calderwood, 2019. Heat Shock Proteins Are Essential Components in Transformation and Tumor Progression: Cancer Cell Intrinsic Pathways and Beyond. *Int. J. Mol. Sci.*, **20**, 4507-4517.

142. Y. Mosesson, G. B. Mills and Y. Yarden, 2008. Derailed endocytosis: an emerging feature of cancer. *Nat. Rev. Cancer*, **8**, 835-850.

143. C. C. Scott, F. Vacca and J. Gruenberg, 2014. Endosome maturation, transport and functions. *Semin. Cell Dev. Biol.*, **31**, 2-10.

144. A. Ballabio and J. S. Bonifacino, 2020. Lysosomes as dynamic regulators of cell and organismal homeostasis. *Nat. Rev. Mol. Cell Biol.*, **21**, 101-118.

145. B. Zhitomirsky and Y. G. Assaraf, 2016. Lysosomes as mediators of drug resistance in cancer. *Drug Resist. Updat.*, **24**, 23-33.

146. C. Fennelly and R. K. Amaravadi, 2017. Lysosomal Biology in Cancer. *Methods Mol. Biol.*, **1594**, 293-308.

147. T. Kirkegaard and M. Jäättelä, 2009. Lysosomal involvement in cell death and cancer. *BBA Mol. Cell. Res.*, **1793**, 746-754.

148. T. Tang, Z.-y. Yang, D. Wang, X.-y. Yang, J. Wang, L. Li, Q. Wen, L. Gao, X.-w. Bian and S.-c. Yu, 2020. The role of lysosomes in cancer development and progression. *Cell Biosci.*, **10**, 131-138.

149. C. E. Chwieralski, T. Welte and F. Bühling, 2006. Cathepsin-regulated apoptosis. *Apoptosis*, **11**, 143-149.

150. M. A. G. De Castro, G. Bunt and F. S. Wouters, 2016. Cathepsin B launches an apoptotic exit effort upon cell death-associated disruption of lysosomes. *Cell Death Discov.*, **2**, 10.1038/cddis.2016.1076.

151. W.-L. Liu, D. Liu, K. Cheng, Y.-J. Liu, S. Xing, P.-D. Chi, X.-H. Liu, N. Xue, Y.-Z. Lai, L. Guo and G. Zhang, 2016. Evaluating the diagnostic and prognostic value of circulating cathepsin S in gastric cancer. *Oncotarget*, **7**, 28124-28138.

152. G. Tan, Q. Liu, X. Tang, T. Kang, Y. Li, J. Lu, X. Zhao and F. Tang, 2016. Diagnostic values of serum cathepsin B and D in patients with nasopharyngeal carcinoma. *BMC Cancer*, **16**, 241-149.

153. V. Vetvicka and M. Fusek, 2013. Cathepsin D: Autoantibody profiling as a diagnostic marker for cancers. *World J. Clin. Oncol.*, **4**, 1-3.

154. J. Nylandsted, M. Gyrd-Hansen, A. Danielewicz, N. Fehrenbacher, U. Lademann, M. Høyer-Hansen, E. Weber, G. Multhoff, M. Rohde and M. Jäättelä, 2004. Heat shock protein 70 promotes cell survival by inhibiting lysosomal membrane permeabilization. *J. Exp. Med.*, **200**, 425-435.

155. N. H. Petersen, T. Kirkegaard, O. D. Olsen and M. Jäättelä, 2010. Connecting Hsp70, sphingolipid metabolism and lysosomal stability. *Cell Cycle*, **9**, 2305-2309.

156. X. Guan, Z. Liu, Z. Zhao, X. Zhang, S. Tao, B. Yuan, J. Zhang, D. Wang, Q. Liu and Y. Ding, 2019. Emerging roles of low-density lipoprotein in the development and treatment of breast cancer. *Lipids Health Dis.*, **18**, 137-151.

157. Z. Roslan, M. Muhamad, L. Selvaratnam and S. Ab-Rahim, 2019. The Roles of Low-Density Lipoprotein Receptor-Related Proteins 5, 6, and 8 in Cancer: A Review. *J. Oncol.*, **2019**, DOI: 10.1155/2019/4536302.

158. S. Huang and Y. Wang, 2017. Golgi structure formation, function, and post-translational modifications in mammalian cells. *F1000Res.*, **6**, 2050-2071.

159. B. V. Howley, L. A. Link, S. Grelet, M. El-Sabban and P. H. Howe, 2018. A CREB3-regulated ER–Golgi trafficking signature promotes metastatic progression in breast cancer. *Oncogene*, **37**, 1308-1325.

160. C. Luchsinger, M. Aguilar, P. V. Burgos, P. Ehrenfeld and G. A. Mardones, 2018. Functional disruption of the Golgi apparatus protein ARF1 sensitizes MDA-MB-231 breast cancer cells to the antitumor drugs Actinomycin D and Vinblastine through ERK and AKT signaling. *PLoS One*, **13**, DOI: 10.1371/journal.pone.0195401.

161. S. Banerjee, A. Dixit, R. N. Shridharan, A. A. Karande and A. R. Chakravarty, 2014. Endoplasmic reticulum targeted chemotherapeutics: the remarkable photo-cytotoxicity of an oxovanadium(iv) vitamin-B6 complex in visible light. *Chem. Comm.*, **50**, 5590-5592.

162. F. Xue, Y. Wen, P. Wei, Y. Gao, Z. Zhou, S. Xiao and T. Yi, 2017. A smart drug: a pH-responsive photothermal ablation agent for Golgi apparatus activated cancer therapy. *Chem. Comm.*, **53**, 6424-6427.

163. J. E. Rothman, 2010. The future of Golgi research. *Mol. Biol. Cell*, **21**, 3776-3780.

164. A. Vitale and E. Pedrazzini, 2017. Endoplasmic reticulum and Golgi apparatus: old friends, novel intimate relationships. *J. Exp. Bot.*, **68**, 3283-3285.

165. D. C. Chan, 2006. Mitochondria: Dynamic Organelles in Disease, Aging, and Development. *Cell*, **125**, 1241-1252.

166. N. S. Chandel, 2014. Mitochondria as signaling organelles. *BMC Biol.*, **12**, 34-41.

167. J. R. Friedman and J. Nunnari, 2014. Mitochondrial form and function. *Nature*, **505**, 335-343.

168. S. Fulda, L. Galluzzi and G. Kroemer, 2010. Targeting mitochondria for cancer therapy. *Nat. Rev. Drug Discov.*, **9**, 447-464.

169. M. D. P. S. Idelchik, U. Begley, T. J. Begley and J. A. Melendez, 2017. Mitochondrial ROS control of cancer. *Semin. Cancer Biol.*, **47**, 57-66.

170. M. Davidescu, L. Macchioni, G. Scaramozzino, M. Cristina Marchetti, G. Migliorati, R. Vitale, A. Corcelli, R. Roberti, E. Castigli and L. Corazzi, 2015. The energy blockers bromopyruvate and lonidamine lead GL15 glioblastoma cells to death by different p53-dependent routes. *Sci. Rep.*, **5**, DOI: 10.1038/srep14343

171. D. DeWaal, V. Nogueira, A. R. Terry, K. C. Patra, S.-M. Jeon, G. Guzman, J. Au, C. P. Long, M. R. Antoniewicz and N. Hay, 2018. Hexokinase-2 depletion inhibits glycolysis and induces oxidative phosphorylation in hepatocellular carcinoma and sensitizes to metformin. *Nat. Comm.*, **9**, 446-460.

172. K. Nath, L. Guo, B. Nancolas, D. S. Nelson, A. A. Shestov, S.-C. Lee, J. Roman, R. Zhou, D. B. Leeper, A. P. Halestrap, I. A. Blair and J. D. Glickson, 2016. Mechanism of antineoplastic activity of lonidamine. *Biochim. Biophys. Acta*, **1866**, 151-162.

173. A. S. Belzacq, C. El Hamel, H. L. Vieira, I. Cohen, D. Haouzi, D. Métivier, P. Marchetti, C. Brenner and G. Kroemer, 2001. Adenine nucleotide translocator mediates the mitochondrial membrane permeabilization induced by lonidamine, arsenite and CD437. *Oncogene*, **20**, 7579-7587.

174. S. Gupta, G. E. N. Kass, E. Szegezdi and B. Joseph, 2009. The mitochondrial death pathway: a promising therapeutic target in diseases. *J. Cell Mol. Med.*, **13**, 1004-1033.

175. M. De Lena, V. Lorusso, A. Latorre, G. Fanizza, G. Gargano, L. Caporusso, M. Guida, A. Catino, E. Crucitta, D. Sambiasi and A. Mazzei, 2001. Paclitaxel, cisplatin and lonidamine in advanced ovarian cancer. A phase II study. *Eur. J. Cancer*, **37**, 364-378.

176. D. A. Eiznhamer and Z. Q. Xu, 2004. Betulinic acid: a promising anticancer candidate. *IDrugs*, **7**, 359-373.

177. S. Fulda and K. M. Debatin, 2000. Betulinic acid induces apoptosis through a direct effect on mitochondria in neuroectodermal tumors. *Med. Pediatr. Oncol.*, **35**, 616-628.

178. F. B. Mullauer, J. H. Kessler and J. P. Medema, 2009. Betulinic acid induces cytochrome c release and apoptosis in a Bax/Bak-independent, permeability transition pore dependent fashion. *Apoptosis*, **14**, 191-202.

179. S. Fulda, C. Friesen, M. Los, C. Scaffidi, W. Mier, M. Benedict, G. Nuñez, P. H. Krammer, M. E. Peter and K. M. Debatin, 1997. Betulinic acid triggers CD95 (APO-1/Fas)-and p53-independent apoptosis via activation of caspases in neuroectodermal tumors. *Cancer Res.*, **57**, 4956-4964.

180. A. S. Don, O. Kisker, P. Dilda, N. Donoghue, X. Zhao, S. Decollogne, B. Creighton, E. Flynn, J. Folkman and P. J. Hogg, 2003. A peptide trivalent arsenical inhibits tumor angiogenesis by perturbing mitochondrial function in angiogenic endothelial cells. *Cancer Cell*, **3**, 497-509.

181. P. J. Dilda, S. Decollogne, L. Weerakoon, M. D. Norris, M. Haber, J. D. Allen and P. J. Hogg, 2009. Optimization of the Antitumor Efficacy of a Synthetic Mitochondrial Toxin by Increasing the Residence Time in the Cytosol. *J. Med. Chem.*, **52**, 6209-6216.

182. D. Park, J. Chiu, G. G. Perrone, P. J. Dilda and P. J. Hogg, 2012. The tumour metabolism inhibitors GSAO and PENAO react with cysteines 57 and 257 of mitochondrial adenine nucleotide translocase. *Cancer Cell Int.*, **12**, 11-18.

183. J. Alexandre, C. Nicco, C. Chéreau, A. Laurent, B. Weill, F. Goldwasser and F. Batteux, 2006. Improvement of the therapeutic index of anticancer drugs by the superoxide dismutase mimic mangafodipir. *J. Natl. Cancer Inst.*, **98**, 236-244.

184. J. L. Cleveland and M. B. Kastan, 2000. A radical approach to treatment. *Nature*, **407**, 309-311.

185. D. Matei, J. Schilder, G. Sutton, S. Perkins, T. Breen, C. Quon and C. Sidor, 2009. Activity of 2 methoxyestradiol (Panzem NCD) in advanced, platinum-resistant ovarian cancer and primary peritoneal carcinomatosis: a Hoosier Oncology Group trial. *Gynecol. Oncol.*, **115**, 90-96.

186. A. J. Tevaarwerk, K. D. Holen, D. B. Alberti, C. Sidor, J. Arnott, C. Quon, G. Wilding and G. Liu, 2009. Phase I trial of 2-methoxyestradiol NanoCrystal dispersion in advanced solid malignancies. *Clin. Cancer. Res.*, **15**, 1460-1465.

187. L. Wood, M. R. Leese, B. Leblond, L. W. Woo, D. Ganeshapillai, A. Purohit, M. J. Reed, B. V. Potter and G. Packham, 2001. Inhibition of superoxide dismutase by 2-methoxyoestradiol analogues and oestrogen derivatives: structure-activity relationships. *Anticancer Drug Des.*, **16**, 209-215.

188. D. B. Zorov, E. Kobrinsky, M. Juhaszova and S. J. Sollott, 2004. Examining intracellular organelle function using fluorescent probes: from animalcules to quantum dots. *Circ. Res.*, **95**, 239-252.

189. I. Bohovych and O. Khalimonchuk, 2016. Sending Out an SOS: Mitochondria as a Signaling Hub. *Front. Cell. Dev. Biol.*, **4**, DOI: 10.3389/fcell.2016.00109.

190. K. L. Hertweck and S. Dasgupta, 2017. The Landscape of mtDNA Modifications in Cancer: A Tale of Two Cities. *Front. Oncol.*, **7**, 262-273.

191. M. T. Jeena, S. Kim, S. Jin and J.-H. Ryu, 2020. Recent Progress in Mitochondria-Targeted Drug and Drug-Free Agents for Cancer Therapy. *Cancers*, **12**, DOI: 10.3390/cancers12010004.

192. S. S. Sabharwal and P. T. Schumacker, 2014. Mitochondrial ROS in cancer: initiators, amplifiers or an Achilles' heel? *Nature reviews. Cancer*, **14**, 709-721.

193. S. E. Weinberg and N. S. Chandel, 2015. Targeting mitochondria metabolism for cancer therapy. *Nat. Chem. Biol.*, **11**, 9-15.

194. C. Sawyers, 2004. Targeted cancer therapy. *Nature*, **432**, 294-297.

195. M. R. Atashzar, R. Baharlou, J. Karami, H. Abdollahi, R. Rezaei, F. Pourramezan and S. H. Zoljalali Moghaddam,

2020. Cancer stem cells: A review from origin to therapeutic implications. *J. Cell. Physiol.*, **235**, 790-803.

196. R. B. Moharil, A. Dive, S. Khandekar and A. Bodhade, 2017. Cancer stem cells: An insight. *J. Oral. Maxillofac. Pathol.*, **21**, 463-478.

197. R. Bhatia, M. Holtz, N. Niu, R. Gray, D. S. Snyder, C. L. Sawyers, D. A. Arber, M. L. Slovak and S. J. Forman, 2003. Persistence of malignant hematopoietic progenitors in chronic myelogenous leukemia patients in complete cytogenetic remission following imatinib mesylate treatment. *Blood*, **101**, 4701-4707.

198. S. Chu, H. Xu, N. P. Shah, D. S. Snyder, S. J. Forman, C. L. Sawyers and R. Bhatia, 2005. Detection of BCR-ABL kinase mutations in CD34+ cells from chronic myelogenous leukemia patients in complete cytogenetic remission on imatinib mesylate treatment. *Blood*, **105**, 2093-2098.

199. S. M. Graham, H. G. Jørgensen, E. Allan, C. Pearson, M. J. Alcorn, L. Richmond and T. L. Holyoake, 2002. Primitive, quiescent, Philadelphia-positive stem cells from patients with chronic myeloid leukemia are insensitive to STI571 in vitro. *Blood*, **99**, 319-325.

200. S. A. Rosenberg, 2004. Shedding light on immunotherapy for cancer. *N. Engl. J. Med.*, **350**, 1461-1463.

201. H. Hurwitz, L. Fehrenbacher, W. Novotny, T. Cartwright, J. Hainsworth, W. Heim, J. Berlin, A. Baron, S. Griffing, E. Holmgren, N. Ferrara, G. Fyfe, B. Rogers, R. Ross and F. Kabbinavar, 2004. Bevacizumab plus irinotecan, fluorouracil, and leucovorin for metastatic colorectal cancer. *N. Engl. J. Med.*, **350**, 2335-2342.

202. G. Valabrega, F. Montemurro and M. Aglietta, 2007. Trastuzumab: mechanism of action, resistance and future perspectives in HER2-overexpressing breast cancer. *Ann. Oncol.*, **18**, 977-984.

203. N. Iqbal and N. Iqbal, 2014. Human Epidermal Growth Factor Receptor 2 (HER2) in Cancers: Overexpression and Therapeutic Implications. *Mol. Biol. Int.*, **2014**, 852748-852761.

204. A. Osterborg, C. Karlsson, J. Lundin, E. Kimby and H. Mellstedt, 2006. Strategies in the management of alemtuzumab-related side effects. *Semin. Oncol.*, **33**, 29-35.

205. M. Los, J. M. Roodhart and E. E. Voest, 2007. Target practice: lessons from phase III trials with bevacizumab and vatalanib in the treatment of advanced colorectal cancer. *Oncologist*, **12**, 443-450.

206. G. Altan-Bonnet and R. Mukherjee, 2019. Cytokine-mediated communication: a quantitative appraisal of immune complexity. *Nat. Rev. Immunol.*, **19**, 205-217.

207. P. Berraondo, M. F. Sanmamed, M. C. Ochoa, I. Etxeberria, M. A. Aznar, J. L. Pérez-Gracia, M. E. Rodríguez-Ruiz, M. Ponz-Sarvise, E. Castañón and I. Melero, 2019. Cytokines in clinical cancer immunotherapy. *Brit. J. Cancer*, **120**, 6-15.

208. S. Lee and K. Margolin, 2011. Cytokines in cancer immunotherapy. *Cancers*, **3**, 3856-3893.

209. K. Gadó, G. Domján, H. Hegyesi and A. Falus, 2000. Role of INTERLEUKIN-6 in the pathogenesis of multiple myeloma. *Cell Biol. Int.*, **24**, 195-209.

210. J. P. Dutcher, D. J. Schwartzentruber, H. L. Kaufman, S. S. Agarwala, A. A. Tarhini, J. N. Lowder and M. B. Atkins, 2014. High dose interleukin-2 (Aldesleukin) - expert consensus on best management practices-2014. *J. Immunother. Cancer.*, **2**, 26-38.

211. F. P. Ognibene, S. A. Rosenberg, M. Lotze, J. Skibber, M. M. Parker, J. H. Shelhamer and J. E. Parrillo, 1988. Interleukin-2 administration causes reversible hemodynamic changes and left ventricular dysfunction similar to those seen in septic shock. *Chest*, **94**, 750-754.

212. K. Margolin, M. B. Atkins, J. P. Dutcher, M. S. Ernstoff, J. W. Smith, 2nd, J. I. Clark, J. Baar, J. Sosman, J. Weber, C. Lathia, J. Brunetti, F. Cihon and B. Schwartz, 2007. Phase I trial of BAY 50-4798, an interleukin-2-specific agonist in advanced melanoma and renal cancer. *Clin. Cancer Res.*, **13**, 3312-3319.

213. L. Matthews, S. Chapman, M. S. Ramchandani, H. C. Lane, R. T. Davey, Jr. and I. Sereti, 2004. BAY 50-4798, a novel, high-affinity receptor-specific recombinant interleukin-2 analog, induces dose-dependent increases in CD25 expression and proliferation among unstimulated, human peripheral blood mononuclear cells in vitro. *Clin. Immunol.*, **113**, 248-255.

214. P. De Paoli, 2001. Immunological effects of interleukin-2 therapy in human immunodeficiency virus-positive subjects. *Clin. Diagn. Lab. Immunol.*, **8**, 671-677.

215. T. Jiang, C. Zhou and S. Ren, 2016. Role of IL-2 in cancer immunotherapy. *Oncoimmunology*, **5**, DOI: 10.1080/2162402X.2162016.1163462.

216. S. A. Rosenberg, M. T. Lotze, J. C. Yang, W. M. Linehan, C. Seipp, S. Calabro, S. E. Karp, R. M. Sherry, S. Steinberg and D. E. White, 1989. Combination therapy with interleukin-2 and alpha-interferon for the treatment of patients with advanced cancer. *J. Clin. Oncol.*, **7**, 1863-1874.

217. R. Jalah, V. Patel, V. Kulkarni, M. Rosati, C. Alicea, B. Ganneru, A. von Gegerfelt, W. Huang, Y. Guan, K. E. Broderick, N. Y. Sardesai, C. LaBranche, D. C. Montefiori, G. N. Pavlakis and B. K. Felber, 2012. IL-12 DNA as molecular vaccine adjuvant increases the cytotoxic T cell responses and breadth of humoral immune responses in SIV DNA vaccinated macaques. *Hum. Vaccin. Immunother.*, **8**, 1620-1629.

218. W. Lasek, R. Zagożdżon and M. Jakobisiak, 2014. Interleukin 12: still a promising candidate for tumor immunotherapy? *Cancer Immunol. Immunother.*, **63**, 419-435.

219. J. E. Portielje, J. W. Gratama, H. H. van Ojik, G. Stoter and W. H. Kruit, 2003. IL-12: a promising adjuvant for cancer vaccination. *Cancer Immunol. Immunother.*, **52**, 133-144.

220. T. T. Hecht, D. L. Longo and L. A. Matis, 1983. The relationship between immune interferon production and proliferation in antigen-specific, MHC-restricted T cell lines and clones. *J. Immunol.*, **131**, 1049-1055.

221. L. Galluzzi, E. Vacchelli, J.-M. Bravo-San Pedro, A. Buqué, L. Senovilla, E. E. Baracco, N. Bloy, F. Castoldi, J.-P. Abastado, P. Agostinis, R. N. Apte, F. Aranda, M. Ayyoub, P. Beckhove, J.-Y. Blay, L. Bracci, A. Caignard, C. Castelli, F. Cavallo, E. Celis, V. Cerundolo, A. Clayton, M. P. Colombo, L. Coussens, M. V. Dhodapkar, A. M. Eggermont, D. T. Fearon, W. H. Fridman, J. Fučíková, D. I. Gabrilovich, J. Galon, A. Garg, F. Ghiringhelli, G. Giaccone, E. Gilboa, S. Gnjatic, A. Hoos, A. Hosmalin, D. Jäger, P. Kalinski, K. Kärre, O. Kepp, R. Kiessling, J. M. Kirkwood, E. Klein, A. Knuth, C. E. Lewis, R. Liblau, M. T. Lotze, E. Lugli, J.-P. Mach, F.

Mattei, D. Mavilio, I. Melero, C. J. Melief, E. A. Mittendorf, L. Moretta, A. Odunsi, H. Okada, A. K. Palucka, M. E. Peter, K. J. Pienta, A. Porgador, G. C. Prendergast, G. A. Rabinovich, N. P. Restifo, N. Rizvi, C. Sautès-Fridman, H. Schreiber, B. Seliger, H. Shiku, B. Silva-Santos, M. J. Smyth, D. E. Speiser, R. Spisek, P. K. Srivastava, J. E. Talmadge, E. Tartour, S. H. Van Der Burg, B. J. Van Den Eynde, R. Vile, H. Wagner, J. S. Weber, T. L. Whiteside, J. D. Wolchok, L. Zitvogel, W. Zou and G. Kroemer, 2014. Classification of current anticancer immunotherapies. *Oncotarget*, **5**, 12472-12508.

222. A. Kudrin, 2012. Overview of cancer vaccines: considerations for development. *Hum. Vaccin. Immunother.*, **8**, 1335-1353.

223. A. Eisenberger, B. M. Elliott and H. L. Kaufman, 2006. Viral vaccines for cancer immunotherapy. *Hematol. Oncol. Clin. North. Am.*, **20**, 661-687.

224. S. T. Khan, J. Montroy, N. Forbes, D. Bastin, M. A. Kennedy, J.-S. Diallo, N. Kekre, D. A. Fergusson, M. Lalu and R. C. Auer, 2020. Safety and efficacy of autologous tumour cell vaccines as a cancer therapeutic to treat solid tumours and haematological malignancies: a meta-analysis protocol for two systematic reviews. *BMJ Open*, **10**, DOI: 10.1002/hon.2875.

225. F. Akram, H. Ikram Ul, Z. Ahmed, H. Khan and M. S. Ali, 2020. CRISPR-Cas9, A Promising Therapeutic Tool for Cancer Therapy: A Review. *Protein Pept. Lett.*, **27**, 931-944.

226. H. Almåsbak, T. Aarvak and M. C. Vemuri, 2016. CAR T Cell Therapy: A Game Changer in Cancer Treatment. *J. Immunol. Res.*, **2016**, 5474602.

227. S. K. Das, M. E. Menezes, S. Bhatia, X. Y. Wang, L. Emdad, D. Sarkar and P. B. Fisher, 2015. Gene Therapies for Cancer: Strategies, Challenges and Successes. *J. Cell. Physiol.*, **230**, 259-271.

228. L. A. Johnson, R. A. Morgan, M. E. Dudley, L. Cassard, J. C. Yang, M. S. Hughes, U. S. Kammula, R. E. Royal, R. M. Sherry, J. R. Wunderlich, C. C. Lee, N. P. Restifo, S. L. Schwarz, A. P. Cogdill, R. J. Bishop, H. Kim, C. C. Brewer, S. F. Rudy, C. VanWaes, J. L. Davis, A. Mathur, R. T. Ripley, D. A. Nathan, C. M. Laurencot and S. A. Rosenberg, 2009. Gene therapy with human and mouse T-cell receptors

mediates cancer regression and targets normal tissues expressing cognate antigen. *Blood*, **114**, 535-546.

229. A. N. Miliotou and L. C. Papadopoulou, 2018. CAR T-cell Therapy: A New Era in Cancer Immunotherapy. *Curr. Pharm. Biotechnol.*, **19**, 5-18.

230. K. Kawane, K. Motani and S. Nagata, 2014. DNA degradation and its defects. *Cold Spring Harb. Perspect. Biol.*, **6**, DOI: 10.1101/cshperspect.a016394.

231. J. M. Lee, T. J. Yoon and Y. S. Cho, 2013. Recent developments in nanoparticle-based siRNA delivery for cancer therapy. *Biomed. Res. Int.*, **2013**, DOI: 10.1155/2013/782041.

232. D. C. Luther, Y. W. Lee, H. Nagaraj, F. Scaletti and V. M. Rotello, 2018. Delivery approaches for CRISPR/Cas9 therapeutics in vivo: advances and challenges. *Expert Opin. Drug. Deliv.*, **15**, 905-913.

233. B. Zetsche, S. E. Volz and F. Zhang, 2015. A split-Cas9 architecture for inducible genome editing and transcription modulation. *Nat. Biotechnol.*, **33**, 139-142.

234. L. E. Dow, J. Fisher, K. P. O'Rourke, A. Muley, E. R. Kastenhuber, G. Livshits, D. F. Tschaharganeh, N. D. Socci and S. W. Lowe, 2015. Inducible in vivo genome editing with CRISPR-Cas9. *Nat. Biotechnol.*, **33**, 390-394.

235. J. Weltner, D. Balboa, S. Katayama, M. Bespalov, K. Krjutškov, E.-M. Jouhilahti, R. Trokovic, J. Kere and T. Otonkoski, 2018. Human pluripotent reprogramming with CRISPR activators. *Nat. Comm.*, **9**, 2643-2655.

236. F. Kreppel and C. Hagedorn, 2021. Capsid and Genome Modification Strategies to Reduce the Immunogenicity of Adenoviral Vectors. *Int. J. Mol. Sci.*, **22**, DOI: 10.3390/ijms22052417.

237. B. Everts and H. G. van der Poel, 2005. Replication-selective oncolytic viruses in the treatment of cancer. *Cancer Gene Ther.*, **12**, 141-161.

238. J. K. Chan and P. Y. Lam, 2013. Human mesenchymal stem cells and their paracrine factors for the treatment of brain tumors. *Cancer Gene Ther.*, **20**, 539-543.

239. M. Studeny, F. C. Marini, R. E. Champlin, C. Zompetta, I. J. Fidler and M. Andreeff, 2002. Bone marrow-derived

mesenchymal stem cells as vehicles for interferon-beta delivery into tumors. *Cancer Res.*, **62**, 3603-3608.

240. P. Dent, A. Yacoub, H. A. Hamed, M. A. Park, R. Dash, S. K. Bhutia, D. Sarkar, P. Gupta, L. Emdad, I. V. Lebedeva, M. Sauane, Z.-Z. Su, M. Rahmani, W. C. Broaddus, H. F. Young, M. Lesniak, S. Grant, D. T. Curiel and P. B. Fisher, 2010. MDA-7/IL-24 as a cancer therapeutic: from bench to bedside. *Anti-Cancer Drug.*, **21**, 725-731.
241. P. B. Fisher, 2005. Is mda-7/IL-24 a “Magic Bullet” for Cancer? *Cancer Res.*, **65**, 10128-10138.
242. I. V. Lebedeva, M. Sauane, R. V. Gopalkrishnan, D. Sarkar, Z.-z. Su, P. Gupta, J. Nemunaitis, C. Cunningham, A. Yacoub, P. Dent and P. B. Fisher, 2005. mda-7/IL-24: Exploiting Cancer's Achilles' Heel. *Mol. Ther.*, **11**, 4-18.
243. A. K. Pradhan, P. Bhoopathi, S. Talukdar, D. Scheunemann, D. Sarkar, W. K. Cavenee, S. K. Das, L. Emdad and P. B. Fisher, 2019. MDA-7/IL-24 regulates the miRNA processing enzyme DICER through downregulation of MITF. *Proc. Nat. Acad. Sci.*, **116**, 5687-5693.
244. A. K. Pradhan, S. Talukdar, P. Bhoopathi, X.-N. Shen, L. Emdad, S. K. Das, D. Sarkar and P. B. Fisher, 2017. mda-7/IL-24 Mediates Cancer Cell–Specific Death via Regulation of miR-221 and the Beclin-1 Axis. *Cancer Res.*, **77**, 949.
245. M. E. Menezes, S. Bhatia, P. Bhoopathi, S. K. Das, L. Emdad, S. Dasgupta, P. Dent, X.-Y. Wang, D. Sarkar and P. B. Fisher, 2014. MDA-7/IL-24: multifunctional cancer killing cytokine. *Adv. Exp. Med. Biol.*, **818**, 127-153.
246. O. L. Aiyegbusi, K. Macpherson, L. Elston, S. Myles, J. Washington, N. Sungum, M. Briggs, P. N. Newsome and M. J. Calvert, 2020. Patient and public perspectives on cell and gene therapies: a systematic review. *Nat. Comm.*, **11**, 6265.
247. M. W. Rohaan, S. Wilgenhof and J. Haanen, 2019. Adoptive cellular therapies: the current landscape. *Virchows Arch.*, **474**, 449-461.
248. M. G. Morvan and L. L. Lanier, 2016. NK cells and cancer: you can teach innate cells new tricks. *Nat. Rev. Cancer*, **16**, 7-19.
249. C. G. Clemente, M. C. Mihm, Jr., R. Bufalino, S. Zurrida, P. Collini and N. Cascinelli, 1996. Prognostic value of tumor

infiltrating lymphocytes in the vertical growth phase of primary cutaneous melanoma. *Cancer*, **77**, 1303-1310.

250. A. L. Burton, B. A. Roach, M. P. Mays, A. F. Chen, B. A. Ginter, A. M. Vierling, C. R. Scoggins, R. C. Martin, A. J. Stromberg, L. Hagendoorn and K. M. McMasters, 2011. Prognostic significance of tumor infiltrating lymphocytes in melanoma. *Am. Surg.*, **77**, 188-192.

251. P. J. Spiess, J. C. Yang and S. A. Rosenberg, 1987. In vivo antitumor activity of tumor-infiltrating lymphocytes expanded in recombinant interleukin-2. *J. Natl. Cancer Inst.*, **79**, 1067-1075.

252. R. Andersen, M. Donia, E. Ellebaek, T. H. Borch, P. Kongsted, T. Z. Iversen, L. R. Hölmich, H. W. Hendel, Ö. Met, M. H. Andersen, P. Thor Straten and I. M. Svane, 2016. Long-Lasting Complete Responses in Patients with Metastatic Melanoma after Adoptive Cell Therapy with Tumor-Infiltrating Lymphocytes and an Attenuated IL2 Regimen. *Clin. Cancer Res.*, **22**, 3734-3745.

253. R. Ben-Avi, R. Farhi, A. Ben-Nun, M. Gorodner, E. Greenberg, G. Markel, J. Schachter, O. Itzhaki and M. J. Besser, 2018. Establishment of adoptive cell therapy with tumor infiltrating lymphocytes for non-small cell lung cancer patients. *Cancer Immunol. Immunother.*, **67**, 1221-1230.

254. M. J. Besser, R. Shapira-Frommer, O. Itzhaki, A. J. Treves, D. B. Zippel, D. Levy, A. Kubi, N. Shoshani, D. Zikich, Y. Ohayon, D. Ohayon, B. Shalmon, G. Markel, R. Yerushalmi, S. Apter, A. Ben-Nun, E. Ben-Ami, A. Shimoni, A. Nagler and J. Schachter, 2013. Adoptive transfer of tumor-infiltrating lymphocytes in patients with metastatic melanoma: intent-to-treat analysis and efficacy after failure to prior immunotherapies. *Clin. Cancer Res.*, **19**, 4792-4800.

255. H. J. Lee, Y. A. Kim, C. K. Sim, S. H. Heo, I. H. Song, H. S. Park, S. Y. Park, W. S. Bang, I. A. Park, M. Lee, J. H. Lee, Y. S. Cho, S. Chang, J. Jung, J. Kim, S. B. Lee, S. Y. Kim, M. S. Lee and G. Gong, 2017. Expansion of tumor-infiltrating lymphocytes and their potential for application as adoptive cell transfer therapy in human breast cancer. *Oncotarget*, **8**, 113345-113359.

256. S. A. Rosenberg, J. C. Yang, R. M. Sherry, U. S. Kammula, M. S. Hughes, G. Q. Phan, D. E. Citrin, N. P. Restifo, P. F.

Robbins, J. R. Wunderlich, K. E. Morton, C. M. Laurencot, S. M. Steinberg, D. E. White and M. E. Dudley, 2011. Durable complete responses in heavily pretreated patients with metastatic melanoma using T-cell transfer immunotherapy. *Clin. Cancer Res.*, **17**, 4550-4557.

257. S. Stevanović, L. M. Draper, M. M. Langhan, T. E. Campbell, M. L. Kwong, J. R. Wunderlich, M. E. Dudley, J. C. Yang, R. M. Sherry, U. S. Kammula, N. P. Restifo, S. A. Rosenberg and C. S. Hinrichs, 2015. Complete regression of metastatic cervical cancer after treatment with human papillomavirus-targeted tumor-infiltrating T cells. *J. Clin. Oncol.*, **33**, 1543-1550.

258. K. Fujita, H. Ikarashi, K. Takakuwa, S. Kodama, A. Tokunaga, T. Takahashi and K. Tanaka, 1995. Prolonged disease-free period in patients with advanced epithelial ovarian cancer after adoptive transfer of tumor-infiltrating lymphocytes. *Clin. Cancer Res.*, **1**, 501-507.

259. M. Hall, H. Liu, M. Malafa, B. Centeno, P. J. Hodul, J. Pimiento, S. Pilon-Thomas and A. A. Sarnaik, 2016. Expansion of tumor-infiltrating lymphocytes (TIL) from human pancreatic tumors. *J. Immunother. Cancer*, **4**, 61-71.

260. S. Turcotte, A. Gros, K. Hogan, E. Tran, C. S. Hinrichs, J. R. Wunderlich, M. E. Dudley and S. A. Rosenberg, 2013. Phenotype and function of T cells infiltrating visceral metastases from gastrointestinal cancers and melanoma: implications for adoptive cell transfer therapy. *J. Immunol.*, **191**, 2217-2225.

261. S. Turcotte, A. Gros, E. Tran, C. C. Lee, J. R. Wunderlich, P. F. Robbins and S. A. Rosenberg, 2014. Tumor-reactive CD8+ T cells in metastatic gastrointestinal cancer refractory to chemotherapy. *Clin. Cancer Res.*, **20**, 331-343.

262. F. Garrido, F. Ruiz-Cabello and N. Aptsiauri, 2017. Rejection versus escape: the tumor MHC dilemma. *Cancer Immunol. Immunother.*, **66**, 259-271.

263. C. Barrow, J. Browning, D. MacGregor, I. D. Davis, S. Sturrock, A. A. Jungbluth and J. Cebon, 2006. Tumor antigen expression in melanoma varies according to antigen and stage. *Clin. Cancer Res.*, **12**, 764-771.

264. Y. T. Chen, E. Stockert, A. Jungbluth, S. Tsang, K. A. Coplan, M. J. Scanlan and L. J. Old, 1996. Serological analysis of

Melan-A(MART-1), a melanocyte-specific protein homogeneously expressed in human melanomas. *Proc. Natl. Acad. Sci.*, **93**, 5915-5919.

265. A. A. Jungbluth, C. R. Antonescu, K. J. Busam, K. Iversen, D. Kolb, K. Coplan, Y. T. Chen, E. Stockert, M. Ladanyi and L. J. Old, 2001. Monophasic and biphasic synovial sarcomas abundantly express cancer/testis antigen NY-ESO-1 but not MAGE-A1 or CT7. *Int. J. Cancer*, **94**, 252-256.

266. S. M. Oba-Shinjo, O. L. Caballero, A. A. Jungbluth, S. Rosemberg, L. J. Old, A. J. Simpson and S. K. Marie, 2008. Cancer-testis (CT) antigen expression in medulloblastoma. *Cancer Immun.*, **8**, 7-14.

267. K. Odunsi, A. A. Jungbluth, E. Stockert, F. Qian, S. Gnjatic, J. Tammela, M. Intengan, A. Beck, B. Keitz, D. Santiago, B. Williamson, M. J. Scanlan, G. Ritter, Y. T. Chen, D. Driscoll, A. Sood, S. Lele and L. J. Old, 2003. NY-ESO-1 and LAGE-1 cancer-testis antigens are potential targets for immunotherapy in epithelial ovarian cancer. *Cancer Res.*, **63**, 6076-6083.

268. G. Gross, T. Waks and Z. Eshhar, 1989. Expression of immunoglobulin-T-cell receptor chimeric molecules as functional receptors with antibody-type specificity. *Proc. Natl. Acad. Sci.*, **86**, 10024-10028.

269. Y. Kuwana, Y. Asakura, N. Utsunomiya, M. Nakanishi, Y. Arata, S. Itoh, F. Nagase and Y. Kurosawa, 1987. Expression of chimeric receptor composed of immunoglobulin-derived V regions and T-cell receptor-derived C regions. *Biochem. Biophys. Res. Commun.*, **149**, 960-968.

270. R. J. Brentjens, J. B. Latouche, E. Santos, F. Marti, M. C. Gong, C. Lyddane, P. D. King, S. Larson, M. Weiss, I. Rivière and M. Sadelain, 2003. Eradication of systemic B-cell tumors by genetically targeted human T lymphocytes co-stimulated by CD80 and interleukin-15. *Nat. Med.*, **9**, 279-286.

271. R. J. Brentjens, I. Rivière, J. H. Park, M. L. Davila, X. Wang, J. Stefanski, C. Taylor, R. Yeh, S. Bartido, O. Borquez-Ojeda, M. Olszewska, Y. Bernal, H. Pegram, M. Przybylowski, D. Hollyman, Y. Usachenko, D. Pirraglia, J. Hosey, E. Santos, E. Halton, P. Maslak, D. Scheinberg, J. Jurcic, M. Heaney, G. Heller, M. Frattini and M. Sadelain, 2011. Safety and persistence of adoptively transferred autologous CD19-

targeted T cells in patients with relapsed or chemotherapy refractory B-cell leukemias. *Blood*, **118**, 4817-4828.

272. S. Ghorashian, M. Pule and P. Amrolia, 2015. CD19 chimeric antigen receptor T cell therapy for haematological malignancies. *Br. J. Haematol.*, **169**, 463-478.

273. S. A. Grupp, M. Kalos, D. Barrett, R. Aplenc, D. L. Porter, S. R. Rheingold, D. T. Teachey, A. Chew, B. Hauck, J. F. Wright, M. C. Milone, B. L. Levine and C. H. June, 2013. Chimeric Antigen Receptor–Modified T Cells for Acute Lymphoid Leukemia. *New Eng. J. Med.*, **368**, 1509-1518.

274. D. L. Porter, B. L. Levine, M. Kalos, A. Bagg and C. H. June, 2011. Chimeric antigen receptor-modified T cells in chronic lymphoid leukemia. *New Eng. J. Med.*, **365**, 725-733.

275. A. Hombach, A. Wieczarkowiecz, T. Marquardt, C. Heuser, L. Usai, C. Pohl, B. Seliger and H. Abken, 2001. Tumor-specific T cell activation by recombinant immunoreceptors: CD3 zeta signaling and CD28 costimulation are simultaneously required for efficient IL-2 secretion and can be integrated into one combined CD28/CD3 zeta signaling receptor molecule. *J. Immunol.*, **167**, 6123-6131.

276. C. Imai, K. Mihara, M. Andreansky, I. C. Nicholson, C. H. Pui, T. L. Geiger and D. Campana, 2004. Chimeric receptors with 4-1BB signaling capacity provoke potent cytotoxicity against acute lymphoblastic leukemia. *Leukemia*, **18**, 676-684.

277. J. Maher, R. J. Brentjens, G. Gunset, I. Rivière and M. Sadelain, 2002. Human T-lymphocyte cytotoxicity and proliferation directed by a single chimeric TCRzeta /CD28 receptor. *Nat. Biotechnol.*, **20**, 70-75.

278. H. J. Pegram, J. C. Lee, E. G. Hayman, G. H. Imperato, T. F. Tedder, M. Sadelain and R. J. Brentjens, 2012. Tumor-targeted T cells modified to secrete IL-12 eradicate systemic tumors without need for prior conditioning. *Blood*, **119**, 4133-4141.

279. M. Sadelain, 2017. CD19 CAR T Cells. *Cell*, **171**, 1471-1479.

280. M. T. Stephan, V. Ponomarev, R. J. Brentjens, A. H. Chang, K. V. Dobrenkov, G. Heller and M. Sadelain, 2007. T cell-encoded CD80 and 4-1BBL induce auto- and transcostimulation, resulting in potent tumor rejection. *Nat. Med.*, **13**, 1440-1449.

281. J. C. Fitzgerald, S. L. Weiss, S. L. Maude, D. M. Barrett, S. F. Lacey, J. J. Melenhorst, P. Shaw, R. A. Berg, C. H. June, D. L. Porter, N. V. Frey, S. A. Grupp and D. T. Teachey, 2017. Cytokine Release Syndrome After Chimeric Antigen Receptor T Cell Therapy for Acute Lymphoblastic Leukemia. *Crit. Care Med.*, **45**, 124-131.

282. H. Murthy, M. Iqbal, J. C. Chavez and M. A. Kharfan-Dabaja, 2019. Cytokine Release Syndrome: Current Perspectives. *Immunotargets Ther.*, **8**, 43-52.

283. S. Feins, W. Kong, E. F. Williams, M. C. Milone and J. A. Fraietta, 2019. An introduction to chimeric antigen receptor (CAR) T-cell immunotherapy for human cancer. *Am. J. Hematol.*, **94**, 3-9.

284. S. L. Maude, D. Barrett, D. T. Teachey and S. A. Grupp, 2014. Managing cytokine release syndrome associated with novel T cell-engaging therapies. *Cancer J.*, **20**, 119-122.

285. N. G. Minutolo, E. E. Hollander and D. J. Powell, 2019. The Emergence of Universal Immune Receptor T Cell Therapy for Cancer. *Front. Oncol.*, **9**, DOI: 10.3389/fonc.2019.00176.

286. L. Scheller and M. Fussenegger, 2019. From synthetic biology to human therapy: engineered mammalian cells. *Curr Opin. Biotechnol.*, **58**, 108-116.

287. B. Chazotte, 2011. Labeling mitochondria with MitoTracker dyes. *Cold Spring Harb. Protoc.*, **2011**, 990-202.

288. E. B. Gökerküçük, M. Tramier and G. Bertolin, 2020. Imaging Mitochondrial Functions: from Fluorescent Dyes to Genetically-Encoded Sensors. *Genes*, **11**, 125-134.

289. R. Lincoln, L. E. Greene, W. Zhang, S. Louisia and G. Cosa, 2017. Mitochondria Alkylation and Cellular Trafficking Mapped with a Lipophilic BODIPY–Acrolein Fluorogenic Probe. *J. Am. Chem. Soc.*, **139**, 16273-16281.

290. Y. Liu, J. Zhou, L. Wang, X. Hu, X. Liu, M. Liu, Z. Cao, D. Shangguan and W. Tan, 2016. A Cyanine Dye to Probe Mitophagy: Simultaneous Detection of Mitochondria and Autolysosomes in Live Cells. *J. Am. Chem. Soc.*, **138**, 12368-12374.

291. S. Lorenz, S. Tomcin and V. Mailänder, 2011. Staining of mitochondria with Cy5-labeled oligonucleotides for long-term microscopy studies. *Microsc. Microanal.*, **17**, 440-445.

292. S. W. Perry, J. P. Norman, J. Barbieri, E. B. Brown and H. A. Gelbard, 2011. Mitochondrial membrane potential probes and the proton gradient: a practical usage guide. *BioTechniques*, **50**, 98-115.

293. M. M. Boyiadzis, M. V. Dhodapkar, R. J. Brentjens, J. N. Kochenderfer, S. S. Neelapu, M. V. Maus, D. L. Porter, D. G. Maloney, S. A. Grupp, C. L. Mackall, C. H. June and M. R. Bishop, 2018. Chimeric antigen receptor (CAR) T therapies for the treatment of hematologic malignancies: clinical perspective and significance. *J. Immunother. Cancer.*, **6**, 137-149.

294. B. Liu, Y. Song and D. Liu, 2017. Clinical trials of CAR-T cells in China. *J. Hematol. Oncol.*, **10**, 166-178.

295. R. Q. Le, L. Li, W. Yuan, S. S. Shord, L. Nie, B. A. Habtemariam, D. Przepiorka, A. T. Farrell and R. Pazdur, 2018. FDA Approval Summary: Tocilizumab for Treatment of Chimeric Antigen Receptor T Cell-Induced Severe or Life-Threatening Cytokine Release Syndrome. *The oncologist*, **23**, 943-947.

296. L. J. B. Brandt, M. B. Barnkob, Y. S. Michaels, J. Heiselberg and T. Barington, 2020. Emerging Approaches for Regulation and Control of CAR T Cells: A Mini Review. *Front. Immunol.*, **11**, DOI: 10.3389/fimmu.2020.00326.

297. D. Liu, J. Zhao and Y. Song, 2019. Engineering switchable and programmable universal CARs for CAR T therapy. *J. Hematol. Oncol.*, **12**, 69-75.

298. X. Liu, J. Wen, H. Yi, X. Hou, Y. Yin, G. Ye, X. Wu and X. Jiang, 2020. Split chimeric antigen receptor-modified T cells targeting glypican-3 suppress hepatocellular carcinoma growth with reduced cytokine release. *Ther. Adv. Med. Oncol.*, **12**, DOI: 10.1177/1758835920910347.

299. C. Y. Wu, K. T. Roybal, E. M. Puchner, J. Onuffer and W. A. Lim, 2015. Remote control of therapeutic T cells through a small molecule-gated chimeric receptor. *Science*, **350**, DOI: 10.1126/science.aab4077.

300. M. P. Murphy and R. C. Hartley, 2018. Mitochondria as a therapeutic target for common pathologies. *Nat. Rev. Drug Discov.*, **17**, 865-886.

301. L. D. Osellame, T. S. Blacker and M. R. Duchen, 2012. Cellular and molecular mechanisms of mitochondrial

function. *Best Pract. Res. Clin. Endocrinol. Metab.*, **26**, 711-723.

302. L. B. Sullivan and N. S. Chandel, 2014. Mitochondrial reactive oxygen species and cancer. *Cancer Metab.*, **2**, 17-24.
303. M. W. Gray, 2012. Mitochondrial evolution. *Cold Spring Harb. Perspect. Biol.*, **4**, DOI: 10.1101/cshperspect.a011403.
304. D. J. Pagliarini and J. Rutter, 2013. Hallmarks of a new era in mitochondrial biochemistry. *Genes Dev.*, **27**, 2615-2627.
305. W. F. Martin, S. Garg and V. Zimorski, 2015. Endosymbiotic theories for eukaryote origin. *Philos. Trans. R. Soc. Lond. B, Biol. Sci.*, **370**, DOI: 10.1098/rstb.2014.0330.
306. T. D. Fox, 2012. Mitochondrial protein synthesis, import, and assembly. *Genetics*, **192**, 1203-1234.
307. P. Mishra and D. C. Chan, 2014. Mitochondrial dynamics and inheritance during cell division, development and disease. *Nat. Rev. Mol. Cell Biol.*, **15**, 634-646.
308. M. Giacomello, A. Pyakurel, C. Glytsou and L. Scorrano, 2020. The cell biology of mitochondrial membrane dynamics. *Nat. Rev. Mol. Cell Biol.*, **21**, 204-224.
309. H. Alshaabi, M. Heininger and B. Cunniff, 2019. Dynamic regulation of subcellular mitochondrial position for localized metabolite levels. *J. Biochem.*, **167**, 109-117.
310. R. Z. Zhao, S. Jiang, L. Zhang and Z. B. Yu, 2019. Mitochondrial electron transport chain, ROS generation and uncoupling (Review). *Int. J. Mol. Med.*, **44**, 3-15.
311. D. Ben-Shachar, 2002. Mitochondrial dysfunction in schizophrenia: a possible linkage to dopamine. *J. Neurochem.*, **83**, 1241-1251.
312. S. Prabakaran, J. E. Swatton, M. M. Ryan, S. J. Huffaker, J.-J. Huang, J. L. Griffin, M. Wayland, T. Freeman, F. Dudbridge, K. S. Lilley, N. A. Karp, S. Hester, D. Tkachev, M. L. Mimmack, R. H. Yolken, M. J. Webster, E. F. Torrey and S. Bahn, 2004. Mitochondrial dysfunction in schizophrenia: evidence for compromised brain metabolism and oxidative stress. *Mol. Psychiatr.*, **9**, 684-697.
313. A. Rajasekaran, G. Venkatasubramanian, M. Berk and M. Debnath, 2015. Mitochondrial dysfunction in schizophrenia:

Pathways, mechanisms and implications. *Neurosci. Biobehav. Rev.*, **48**, 10-21.

314. I. S. Al-Gadi, R. H. Haas, M. J. Falk, A. Goldstein and S. E. McCormack, 2018. Endocrine Disorders in Primary Mitochondrial Disease. *J. Endocr. Soc.*, **2**, 361-373.
315. J. Chow, J. Rahman, J. C. Achermann, M. T. Dattani and S. Rahman, 2017. Mitochondrial disease and endocrine dysfunction. *Nat. Rev. Endocrinol.*, **13**, 92-104.
316. A. M. Schaefer, M. Walker, D. M. Turnbull and R. W. Taylor, 2013. Endocrine disorders in mitochondrial disease. *Mol. Cell Endocrinol.*, **379**, 2-11.
317. M. Laura, T. Eva, A.-M. Paloma, Q. Iván, N. Ángel and S. Reinaldo Sousa dos, 2018. Mitochondria as target of endocrine-disrupting chemicals: implications for type 2 diabetes. *J. Endocrinol.*, **239**, 27-45.
318. S. Arun, L. Liu and G. Donmez, 2016. Mitochondrial Biology and Neurological Diseases. *Curr. Neuropharmacol.*, **14**, 143-154.
319. I. P. De Castro, L. M. Martins and R. Tufi, 2010. Mitochondrial quality control and neurological disease: an emerging connection. *Expert Rev. Mol. Med.*, **12**, DOI: 10.1017/S1462399410001456.
320. R. McFarland, R. W. Taylor and D. M. Turnbull, 2010. A neurological perspective on mitochondrial disease. *Lancet Neurol.*, **9**, 829-840.
321. P. Norat, S. Soldozy, J. D. Sokolowski, C. M. Gorick, J. S. Kumar, Y. Chae, K. Yağmurlu, F. Prada, M. Walker, M. R. Levitt, R. J. Price, P. Tvrdik and M. Y. S. Kalani, 2020. Mitochondrial dysfunction in neurological disorders: Exploring mitochondrial transplantation. *NPJ Regen. Med.*, **5**, 22-32.
322. J. P. Burgstaller, I. G. Johnston and J. Poulton, 2015. Mitochondrial DNA disease and developmental implications for reproductive strategies. *Mol. Hum. Reprod.*, **21**, 11-22.
323. M. J. Falk, 2010. Neurodevelopmental manifestations of mitochondrial disease. *J. Dev. Behav. Pediatr.*, **31**, 610-621.
324. L. E. Gyllenhammer, S. Entringer, C. Buss and P. D. Wadhwa, 2020. Developmental programming of mitochondrial biology: a conceptual framework and review.

Proc. Royal Soc. B. Biol. Sci., **287**, DOI: 10.1098/rspb.2019.2713.

325. M. Al-Enezi, H. Al-Saleh and M. Nasser, 2008. Mitochondrial disorders with significant ophthalmic manifestations. *Middle East Afr. J. Ophthalmol.*, **15**, 81-86.

326. P. Yu-Wai-Man and N. J. Newman, 2017. Inherited eye-related disorders due to mitochondrial dysfunction. *Hum. Mol. Genet.*, **26**, 12-20.

327. D. M. Niyazov, S. G. Kahler and R. E. Frye, 2016. Primary Mitochondrial Disease and Secondary Mitochondrial Dysfunction: Importance of Distinction for Diagnosis and Treatment. *Mol. Syndromol.*, **7**, 122-137.

328. J. Zielonka, J. Joseph, A. Sikora, M. Hardy, O. Ouari, J. Vasquez-Vivar, G. Cheng, M. Lopez and B. Kalyanaraman, 2017. Mitochondria-Targeted Triphenylphosphonium-Based Compounds: Syntheses, Mechanisms of Action, and Therapeutic and Diagnostic Applications. *Chem. Rev.*, **117**, 10043-10120.

329. S. Biswas, N. S. Dodwadkar, P. P. Deshpande and V. P. Torchilin, 2012. Liposomes loaded with paclitaxel and modified with novel triphenylphosphonium-PEG-PE conjugate possess low toxicity, target mitochondria and demonstrate enhanced antitumor effects in vitro and in vivo. *J. Control. Release*, **159**, 393-402.

330. X. Han, R. Su, X. Huang, Y. Wang, X. Kuang, S. Zhou and H. Liu, 2019. Triphenylphosphonium-modified mitochondria-targeted paclitaxel nanocrystals for overcoming multidrug resistance. *Asian J. Pharm. Sci.*, **14**, 569-580.

331. R. A. J. Smith, R. C. Hartley, H. M. Cochemé and M. P. Murphy, 2012. Mitochondrial pharmacology. *Trends Pharmacol. Sci.*, **33**, 341-352.

332. E. J. Gane, F. Weilert, D. W. Orr, G. F. Keogh, M. Gibson, M. M. Lockhart, C. M. Frampton, K. M. Taylor, R. A. Smith and M. P. Murphy, 2010. The mitochondria-targeted anti-oxidant mitoquinone decreases liver damage in a phase II study of hepatitis C patients. *Liver Int.*, **30**, 1019-1026.

333. B. J. Snow, F. L. Rolfe, M. M. Lockhart, C. M. Frampton, J. D. O'Sullivan, V. Fung, R. A. Smith, M. P. Murphy and K. M. Taylor, 2010. A double-blind, placebo-controlled study to assess the mitochondria-targeted antioxidant MitoQ as a

disease-modifying therapy in Parkinson's disease. *Mov. Disord.*, **25**, 1670-1674.

334. M. Takeuchi and T. Ozawa, 2007. Methods for imaging and analyses of intracellular organelles using fluorescent and luminescent proteins. *Anal. Sci.*, **23**, 25-29.

335. H. Zhu, J. Fan, J. Du and X. Peng, 2016. Fluorescent Probes for Sensing and Imaging within Specific Cellular Organelles. *Acc. Chem. Res.*, **49**, 2115-2126.

336. J. F. Buckman, H. Hernández, G. J. Kress, T. V. Votyakova, S. Pal and I. J. Reynolds, 2001. MitoTracker labeling in primary neuronal and astrocytic cultures: influence of mitochondrial membrane potential and oxidants. *J. Neurosci. Meth.*, **104**, 165-176.

337. X. Jia, Q. Chen, Y. Yang, Y. Tang, R. Wang, Y. Xu, W. Zhu and X. Qian, 2016. FRET-Based Mito-Specific Fluorescent Probe for Ratiometric Detection and Imaging of Endogenous Peroxynitrite: Dyad of Cy3 and Cy5. *J. Am. Chem. Soc.*, **138**, 10778-10781.

338. Y. Yamaguchi, Y. Matsubara, T. Ochi, T. Wakamiya and Z.-i. Yoshida, 2008. How the π Conjugation Length Affects the Fluorescence Emission Efficiency. *J. Am. Chem. Soc.*, **130**, 13867-13869.

339. A. K. Kenworthy, 2001. Imaging protein-protein interactions using fluorescence resonance energy transfer microscopy. *Methods*, **24**, 289-296.

340. D. Shrestha, A. Jenei, P. Nagy, G. Vereb and J. Szöllősi, 2015. Understanding FRET as a research tool for cellular studies. *Int. J. Mol. Sci.*, **16**, 6718-6756.

341. K. Wang, A. Sachdeva, D. J. Cox, N. M. Wilf, K. Lang, S. Wallace, R. A. Mehl and J. W. Chin, 2014. Optimized orthogonal translation of unnatural amino acids enables spontaneous protein double-labelling and FRET. *Nat. Chem.*, **6**, 393-403.

342. N. Chuard, K. Fujisawa, P. Morelli, J. Saarbach, N. Winssinger, P. Metrangolo, G. Resnati, N. Sakai and S. Matile, 2016. Activation of Cell-Penetrating Peptides with Ionpair−π Interactions and Fluorophiles. *J. Am. Chem. Soc.*, **138**, 11264-11271.

343. J. R. Masters, 2002. HeLa cells 50 years on: the good, the bad and the ugly. *Nat. Rev. Cancer.*, **2**, 315-319.

344. M. F. Ross, A. Filipovska, R. A. Smith, M. J. Gait and M. P. Murphy, 2004. Cell-penetrating peptides do not cross mitochondrial membranes even when conjugated to a lipophilic cation: evidence against direct passage through phospholipid bilayers. *Biochem. J.*, **383**, 457-468.

345. B. Law, L. Quinti, Y. Choi, R. Weissleder and C.-H. Tung, 2006. A mitochondrial targeted fusion peptide exhibits remarkable cytotoxicity. *Mol. Cancer Ther.*, **5**, 1944-1962.

346. J. C. Mai, Z. Mi, S. H. Kim, B. Ng and P. D. Robbins, 2001. A proapoptotic peptide for the treatment of solid tumors. *Cancer Res.*, **61**, 7709-7012.

347. J. Azéma, B. Guidetti, J. Dewelle, B. Le Calve, T. Mijatovic, A. Korolyov, J. Vaysse, M. Malet-Martino, R. Martino and R. Kiss, 2009. 7-((4-Substituted)piperazin-1-yl) derivatives of ciprofloxacin: synthesis and in vitro biological evaluation as potential antitumor agents. *Bioorg. Med. Chem.*, **17**, 5396-5407.

348. A. Hangas, K. Aasumets, N. J. Kekäläinen, M. Paloheinä, J. L. Pohjoismäki, J. M. Gerhold and S. Goffart, 2018. Ciprofloxacin impairs mitochondrial DNA replication initiation through inhibition of Topoisomerase 2. *Nucleic Acids Res.*, **46**, 9625-9636.

349. S. Kalghatgi, C. S. Spina, J. C. Costello, M. Liesa, J. R. Morones-Ramirez, S. Slomovic, A. Molina, O. S. Shirihai and J. J. Collins, 2013. Bactericidal antibiotics induce mitochondrial dysfunction and oxidative damage in Mammalian cells. *Sci. Transl. Med.*, **5**, 192-215.

350. J. W. Lawrence, D. C. Claire, V. Weissig and T. C. Rowe, 1996. Delayed cytotoxicity and cleavage of mitochondrial DNA in ciprofloxacin-treated mammalian cells. *Mol. Pharmacol.*, **50**, 1178-1189.

351. V. Reshetnikov, S. Daum, C. Janko, W. Karawacka, R. Tietze, C. Alexiou, S. Paryzhak, T. Dumych, R. Bilyy, P. Tripal, B. Schmid, R. Palmisano and A. Mokhir, 2018. ROS-Responsive N-Alkylaminoferrocenes for Cancer-Cell-Specific Targeting of Mitochondria. *Angew. Chem. Int. Ed. Engl.*, **57**, 11943-11946.

352. T. Hallap, S. Nagy, U. Jaakma, A. Johannisson and H. Rodriguez-Martinez, 2005. Mitochondrial activity of frozen-thawed spermatozoa assessed by MitoTracker Deep Red 633. *Theriogenology*, **63**, 2311-2322.

353. K. W. Dunn, M. M. Kamocka and J. H. McDonald, 2011. A practical guide to evaluating colocalization in biological microscopy. *Am. J. Physiol. Cell. Physiol.*, **300**, 723-742.

354. H. Derakhshankhah and S. Jafari, 2018. Cell penetrating peptides: A concise review with emphasis on biomedical applications. *Biomed. Pharmacother.*, **108**, 1090-1096.

355. S. Tomcin, G. Baier, K. Landfester and V. Mailänder, 2014. Pharmacokinetics on a microscale: visualizing Cy5-labeled oligonucleotide release from poly(n-butylcyanoacrylate) nanocapsules in cells. *Int. J. Nanomedicine*, **9**, 5471-5489.

356. C. Y. Fang, C. C. Wu, C. L. Fang, W. Y. Chen and C. L. Chen, 2017. Long-term growth comparison studies of FBS and FBS alternatives in six head and neck cell lines. *PLoS One*, **12**, DOI: 10.1371/journal.pone.0178960.

357. H. He, L. Sun, J. Ye, E. Liu, S. Chen, Q. Liang, M. C. Shin and V. C. Yang, 2016. Enzyme-triggered, cell penetrating peptide-mediated delivery of anti-tumor agents. *J. Control Release*, **240**, 67-76.

358. R. Patel, N. Maurya, M. u. d. Parray, N. Farooq, A. Siddique, K. L. Verma and N. Dohare, 2018. Esterase activity and conformational changes of bovine serum albumin toward interaction with mephedrone: Spectroscopic and computational studies. *J. Mol. Recognit.*, **31**, DOI: 10.1002/jmr.2734.

359. S. M. Usama, G. K. Park, S. Nomura, Y. Baek, H. S. Choi and K. Burgess, 2020. Role of Albumin in Accumulation and Persistence of Tumor-Seeking Cyanine Dyes. *Bioconjugate Chem.*, **31**, 248-259.

360. P. H. Weigel and J. A. Oka, 1981. Temperature dependence of endocytosis mediated by the asialoglycoprotein receptor in isolated rat hepatocytes. Evidence for two potentially rate-limiting steps. *J. Biol. Chem.*, **256**, 2615-2617.

361. C.-C. Chang, M. Wu and F. Yuan, 2014. Role of specific endocytic pathways in electrotransfection of cells. *Mol. Ther. Methods Clin. Dev.*, **1**, DOI: 10.1038/mtm.2014.1058.

362. G. Gottlieb, 1998. Normally occurring environmental and behavioral influences on gene activity: from central dogma to probabilistic epigenesis. *Psychol. Rev.*, **105**, 792-802.

363. T. Schneider-Poetsch and M. Yoshida, 2018. Along the Central Dogma—Controlling Gene Expression with Small Molecules. *Annu. Rev. Biochem.*, **87**, 391-420.

364. K. H. Khan, 2013. Gene expression in Mammalian cells and its applications. *Adv. Pharm. Bull.*, **3**, 257-263.

365. B. G. Vértessy and J. Tóth, 2009. Keeping uracil out of DNA: physiological role, structure and catalytic mechanism of dUTPases. *Acc. Chem. Res.*, **42**, 97-106.

366. D. N. Wilson and J. H. Doudna Cate, 2012. The structure and function of the eukaryotic ribosome. *Cold Spring Harb. Perspect. Biol.*, **4**, DOI: 10.1101/cshperspect.a011536.

367. P. B. Moore and T. A. Steitz, 2011. The roles of RNA in the synthesis of protein. *Cold Spring Harb. Perspect. Biol.*, **3**, DOI: 10.1101/cshperspect.a003780.

368. S. V. Kyriacou and M. P. Deutscher, 2008. An important role for the multienzyme aminoacyl-tRNA synthetase complex in mammalian translation and cell growth. *Mol. Cell*, **29**, 419-427.

369. D. A. Dougherty, 2000. Unnatural amino acids as probes of protein structure and function. *Curr. Opin. Chem. Biol.*, **4**, 645-652.

370. J. C. Jackson, S. P. Duffy, K. R. Hess and R. A. Mehl, 2006. Improving Nature's Enzyme Active Site with Genetically Encoded Unnatural Amino Acids. *J. Am. Chem. Soc.*, **128**, 11124-11127.

371. K. Lang and J. W. Chin, 2014. Cellular Incorporation of Unnatural Amino Acids and Bioorthogonal Labeling of Proteins. *Chem. Rev.*, **114**, 4764-4806.

372. A. R. Nödling, L. A. Spear, T. L. Williams, L. Y. P. Luk and Y.-H. Tsai, 2019. Using genetically incorporated unnatural amino acids to control protein functions in mammalian cells. *Essays Biochem.*, **63**, 237-266.

373. J. W. Chin, 2017. Expanding and reprogramming the genetic code. *Nature*, **550**, 53-60.

374. A. Dumas, L. Lercher, C. D. Spicer and B. G. Davis, 2015. Designing logical codon reassignment - Expanding the chemistry in biology. *Chem. Sci.*, **6**, 50-69.

375. Y. Huang and T. Liu, 2018. Therapeutic applications of genetic code expansion. *Synth. Syst. Biotechnol.*, **3**, 150-158.

376. Y. Kato, 2019. Translational Control using an Expanded Genetic Code. *Int. J. Mol. Sci.*, **20**, 887-896.

377. P. Neumann-Staubitz and H. Neumann, 2016. The use of unnatural amino acids to study and engineer protein function. *Curr. Opin. Struc. Biol.*, **38**, 119-128.

378. E. Trotta, 2016. Selective forces and mutational biases drive stop codon usage in the human genome: a comparison with sense codon usage. *BMC Genom.*, **17**, 366-369.

379. B. Meineke, J. Heimgartner, L. Lafranchi and S. J. Elsasser, 2018. Methanomethylophilus alvus Mx1201 Provides Basis for Mutual Orthogonal Pyrrolysyl tRNA/Aminoacyl-tRNA Synthetase Pairs in Mammalian Cells. *ACS Chem. Biol.*, **13**, 3087-3096.

380. H. Xiao, A. Chatterjee, S. H. Choi, K. M. Bajjuri, S. C. Sinha and P. G. Schultz, 2013. Genetic incorporation of multiple unnatural amino acids into proteins in mammalian cells. *Angew. Chem. Int. Ed.*, **52**, 14080-14083.

381. W. Niu, P. G. Schultz and J. Guo, 2013. An Expanded Genetic Code in Mammalian Cells with a Functional Quadruplet Codon. *ACS Chem. Biol.*, **8**, 1640-1645.

382. N. Wang, X. Shang, R. Cerny, W. Niu and J. Guo, 2016. Systematic Evolution and Study of UAGN Decoding tRNAs in a Genomically Recoded Bacteria. *Sci. Rep.*, **6**, 21898-21910.

383. Y. Chen, J. Ma, W. Lu, M. Tian, M. Thauvin, C. Yuan, M. Volovitch, Q. Wang, J. Holst, M. Liu, S. Vriz, S. Ye, L. Wang and D. Li, 2017. Heritable expansion of the genetic code in mouse and zebrafish. *Cell Res.*, **27**, 294-297.

384. Y. Chen, Y. Wan, N. Wang, Z. Yuan, W. Niu, Q. Li and J. Guo, 2018. Controlling the Replication of a Genomically Recoded HIV-1 with a Functional Quadruplet Codon in Mammalian Cells. *ACS Synth. Biol.*, **7**, 1612-1617.

385. S. Han, A. Yang, S. Lee, H. W. Lee, C. B. Park and H. S. Park, 2017. Expanding the genetic code of Mus musculus. *Nat. Comm.*, **8**, 14568-14577.

386. T. P. Krogager, R. J. Ernst, T. S. Elliott, L. Calo, V. Beranek, E. Ciabatti, M. G. Spillantini, M. Tripodi, M. H. Hastings and J. W. Chin, 2018. Labeling and identifying cell-specific proteomes in the mouse brain. *Nat. Biotechnol.*, **36**, 156-159.

387. J. Liu, J. Hemphill, S. Samanta, M. Tsang and A. Deiters, 2017. Genetic Code Expansion in Zebrafish Embryos and Its Application to Optical Control of Cell Signaling. *J. Am. Chem. Soc.*, **139**, 9100-9103.

388. T. Suzuki, M. Asami, S. G. Patel, L. Y. P. Luk, Y.-H. Tsai and A. C. F. Perry, 2018. Switchable genome editing via genetic code expansion. *Sci. Rep.*, **8**, 10051-10067.

389. W. Brown, J. Liu and A. Deiters, 2018. Genetic Code Expansion in Animals. *ACS Chem. Biol.*, **13**, 2375-2386.

390. T. Kitada, B. DiAndreth, B. Teague and R. Weiss, 2018. Programming gene and engineered-cell therapies with synthetic biology. *Science*, **359**, DOI: 10.1126/science.aad1067.

391. V. Singh, 2014. Recent advances and opportunities in synthetic logic gates engineering in living cells. *Syst. Synth. Biol.*, **8**, 271-282.

392. W. Zhou, T. Šmidlehner and R. Jerala, 2020. Synthetic biology principles for the design of protein with novel structures and functions. *FEBS Lett.*, **594**, 2199-2212.

393. L. Cuthbertson and J. R. Nodwell, 2013. The TetR family of regulators. *Microbiol. Mol. Biol. Rev.*, **77**, 440-475.

394. T. Fink, J. Lonzarić, A. Praznik, T. Plaper, E. Merljak, K. Leben, N. Jerala, T. Lebar, Ž. Strmšek, F. Lapenta, M. Benčina and R. Jerala, 2019. Design of fast proteolysis-based signaling and logic circuits in mammalian cells. *Nat. Chem. Biol.*, **15**, 115-122.

395. D. P. Nguyen, Y. Miyaoka, L. A. Gilbert, S. J. Mayerl, B. H. Lee, J. S. Weissman, B. R. Conklin and J. A. Wells, 2016. Ligand-binding domains of nuclear receptors facilitate tight control of split CRISPR activity. *Nat. Comm.*, **7**, DOI: 10.1038/ncomms12009.

396. B. Ross, S. Mehta and J. Zhang, 2016. Molecular tools for acute spatiotemporal manipulation of signal transduction. *Curr. Opin. Chem. Biol.*, **34**, 135-142.

397. N. Soheili, M. Eshghi, M. Emadi-Baygi, S. A. Mirzaei, R. Heidari and M. Hosseinzadeh, 2020. Design and evaluation of biological gate circuits and their therapeutic applications in a model of multidrug resistant cancers. *Biotechnol. Lett.*, **42**, 1419-1429.

398. A. D. Barlow, M. L. Nicholson and T. P. Herbert, 2013. Evidence for Rapamycin Toxicity in Pancreatic β-Cells and a Review of the Underlying Molecular Mechanisms. *Diabetes*, **62**, 2674-2682.

399. A. D. Barlow, J. Xie, C. E. Moore, S. C. Campbell, J. A. M. Shaw, M. L. Nicholson and T. P. Herbert, 2012. Rapamycin toxicity in MIN6 cells and rat and human islets is mediated by the inhibition of mTOR complex 2 (mTORC2). *Diabetologia*, **55**, 1355-1365.

400. S. Melnikov, K. Manakongtreecheep and D. Söll, 2018. Revising the Structural Diversity of Ribosomal Proteins Across the Three Domains of Life. *Mol. Biol. Evol.*, **35**, 1588-1598.

401. L. S. Lambeth, R. J. Moore, M. Muralitharan, B. P. Dalrymple, S. McWilliam and T. J. Doran, 2005. Characterisation and application of a bovine U6 promoter for expression of short hairpin RNAs. *BMC Biotechnol.*, **5**, 13-21.

402. L. Nie, M. Das Thakur, Y. Wang, Q. Su, Y. Zhao and Y. Feng, 2010. Regulation of U6 promoter activity by transcriptional interference in viral vector-based RNAi. *Genom. Proteom. Bioinf.*, **8**, 170-179.

403. Y. Cao, M. Portela, J. Janikiewicz, J. Doig and C. M. Abbott, 2014. Characterisation of translation elongation factor eEF1B subunit expression in mammalian cells and tissues and co-localisation with eEF1A2. *PLoS One*, **9**, DOI: 10.1371/journal.pone.0114117.

404. Y. Nitta, S. Kawamoto, C. Halbert, A. Iwata, A. Dusty Miller, J.-i. Miyazaki and M. D. Allen, 2005. A CMV-actin-globin hybrid promoter improves adeno-associated viral vector gene expression in the arterial wall in vivo. *J. Gene Med.*, **7**, 1348-1355.

405. N. Aloush, T. Schvartz, A. I. König, S. Cohen, E. Brozgol, B. Tam, D. Nachmias, O. Ben-David, Y. Garini, N. Elia and E. Arbely, 2018. Live Cell Imaging of Bioorthogonally Labelled Proteins Generated With a Single Pyrrolysine tRNA Gene. *Sci. Rep.*, **8**, 14527.

406. W. H. Schmied, S. J. Elsässer, C. Uttamapinant and J. W. Chin, 2014. Efficient multisite unnatural amino acid incorporation in mammalian cells via optimized pyrrolysyl tRNA synthetase/tRNA expression and engineered eRF1. *J. Am. Chem. Soc.*, **136**, 15577-15583.

407. R. Serfling, C. Lorenz, M. Etzel, G. Schicht, T. Böttke, M. Mörl and I. Coin, 2018. Designer tRNAs for efficient incorporation of non-canonical amino acids by the pyrrolysine system in mammalian cells. *Nucleic Acids Res.*, **46**, 1-10.

408. T. Mukai, T. Kobayashi, N. Hino, T. Yanagisawa, K. Sakamoto and S. Yokoyama, 2008. Adding l-lysine derivatives to the genetic code of mammalian cells with engineered pyrrolysyl-tRNA synthetases. *Biochem. Biophys. Res. Commun.*, **371**, 818-822.

409. A. Chatterjee, H. Xiao, M. Bollong, H. W. Ai and P. G. Schultz, 2013. Efficient viral delivery system for unnatural amino acid mutagenesis in mammalian cells. *Proc. Natl. Acad. Sci.*, **110**, 11803-11808.

410. J. S. Italia, C. Latour, C. J. J. Wrobel and A. Chatterjee, 2018. Resurrecting the Bacterial Tyrosyl-tRNA Synthetase/tRNA Pair for Expanding the Genetic Code of Both E. coli and Eukaryotes. *Cell Chem. Biol.*, **25**, 1304-1312.

411. S. Cabantous, T. C. Terwilliger and G. S. Waldo, 2005. Protein tagging and detection with engineered self-assembling fragments of green fluorescent protein. *Nat. Biotechnol.*, **23**, 102-107.

412. D. Kamiyama, S. Sekine, B. Barsi-Rhyne, J. Hu, B. Chen, L. A. Gilbert, H. Ishikawa, M. D. Leonetti, W. F. Marshall, J. S. Weissman and B. Huang, 2016. Versatile protein tagging in cells with split fluorescent protein. *Nat. Comm.*, **7**, 11046-11063.

413. J. H. Kim, S. R. Lee, L. H. Li, H. J. Park, J. H. Park, K. Y. Lee, M. K. Kim, B. A. Shin and S. Y. Choi, 2011. High cleavage efficiency of a 2A peptide derived from porcine teschovirus-1

in human cell lines, zebrafish and mice. *PLoS One*, **6**, DOI: 10.1371/journal.pone.0018556.

414. S. Erbas-Cakmak, S. Kolemen, A. C. Sedgwick, T. Gunnlaugsson, T. D. James, J. Yoon and E. U. Akkaya, 2018. Molecular logic gates: the past, present and future. *Chem. Soc. Rev.*, **47**, 2221-2250.

415. J. Zhao, Y. Song and D. Liu, 2019. Clinical trials of dual-target CAR T cells, donor-derived CAR T cells, and universal CAR T cells for acute lymphoid leukemia. *J. Hematol. Oncol.*, **12**, 17-21.

416. K. Wang, G. Wei and D. Liu, 2012. CD19: a biomarker for B cell development, lymphoma diagnosis and therapy. *Exp. Hematol. Oncol.*, **1**, 36-41.

417. E. Edelweiss, T. G. Balandin, J. L. Ivanova, G. V. Lutsenko, O. G. Leonova, V. I. Popenko, A. M. Sapozhnikov and S. M. Deyev, 2008. Barnase as a new therapeutic agent triggering apoptosis in human cancer cells. *PLoS One*, **3**, DOI: 10.1371/journal.pone.0002434.

418. H. E. Gouvarchin Ghaleh, M. Bolandian, R. Dorostkar, A. Jafari and M. F. Pour, 2020. Concise review on optimized methods in production and transduction of lentiviral vectors in order to facilitate immunotherapy and gene therapy. *Biomed. Pharmacother.*, **128**, 110276-111289.

419. B. Schutte, R. Nuydens, H. Geerts and F. Ramaekers, 1998. Annexin V binding assay as a tool to measure apoptosis in differentiated neuronal cells. *J. Neurosci. Methods*, **86**, 63-69.

420. L. Duprez, N. Takahashi, F. Van Hauwermeiren, B. Vandendriessche, V. Goossens, T. Vanden Berghe, W. Declercq, C. Libert, A. Cauwels and P. Vandenabeele, 2011. RIP Kinase-Dependent Necrosis Drives Lethal Systemic Inflammatory Response Syndrome. *Immunity*, **35**, 908-918.

421. G. Bergamaschi, V. Perfetti, L. Tonon, A. Novella, C. Lucotti, M. Danova, M. J. Glennie, G. Merlini and M. Cazzola, 1996. Saporin, a ribosome-inactivating protein used to prepare immunotoxins, induces cell death via apoptosis. *Br. J. Haematol.*, **93**, 789-794.

422. D. Sikriwal, P. Ghosh and J. K. Batra, 2008. Ribosome inactivating protein saporin induces apoptosis through

mitochondrial cascade, independent of translation inhibition. *Int. J. Biochem. Cell. Biol.*, **40**, 2880-2888.

423. A. C. Perry, T. Wakayama, H. Kishikawa, T. Kasai, M. Okabe, Y. Toyoda and R. Yanagimachi, 1999. Mammalian transgenesis by intracytoplasmic sperm injection. *Science*, **284**, 1180-1183.

424. M. Gao, F. Yu, C. Lv, J. Choo and L. Chen, 2017. Fluorescent chemical probes for accurate tumor diagnosis and targeting therapy. *Chem. Soc. Rev.*, **46**, 2237-2271.

425. N. S. H. Motlagh, P. Parvin, F. Ghasemi and F. Atyabi, 2016. Fluorescence properties of several chemotherapy drugs: doxorubicin, paclitaxel and bleomycin. *Biomed. Opt. Express*, **7**, 2400-2406.

CHAPTER 6:
General Materials and Methods

6.1 Materials

6.1.1 Bacterial work materials

Table 6.1: List of materials for bacterial experiments

Materials	Manufacturer	Catalogue Number
Agar Powder	Fisher Scientific	10572775
Ampicillin	Thermo Scientific	11593027
$CaCl_2$	Fisher Scientific	10478590
EDTA	Sigma Aldrich (Merck)	ED-100G
FastAP enzyme kit	VWR	EF0651
Gene Ruler 1kbp Plus	Thermo Scientific	SM1331
Gibson Assembly Kit	New England Biolabs	E5520
Glacial Acetic Acid	Fisher Scientific	10371411
Glycerol	Fisher Scientific	10336040
Guanidine thiocyanate	Fluorochem	M01833-500G
Kanamycin	Fisher Scientific	10134924
KCl	Fisher Scientific	10735874
KH_2PO_4	Sigma Aldrich (Merck)	7778770
KOAc	Fisher Scientific	11437797
$MnCl_2$	Fisher Scientific	10552991
MOPS	Fisher Scientific	11419733
NaCl	Fisher Scientific	10316943
Na_2HPO_4	Sigma Aldrich (Merck)	7558794
NEB HiFi DNA assembly	New England Biolabs	E2621S
One Shot™ Stbl3™	Invitrogen	C737303
PrimeSTAR™	Takara	R045A
QiaPrep Mini Kit	Qiagen	27106

Restriction Enzymes	Thermo Scientific	N/A
SybrSAFE™	Invitrogen	S33102
Tris-base	Fisher Scientific	15506017
Tris-HCl	Sigma Aldrich (Merck)	BP153-500
Tryptone	Fisher Scientific	10301783
T4 Ligase Kit	Thermo Scientific	EL0014
Yeast Extract	Fisher Scientific	15169323

6.1.2 Mammalian cell work materials

Table 6.2: List of materials for mammalian experiments

Materials	Manufacturer	Cat. Number
Anti-eGFP Antibody	Thermo Scientific	MA1-952
Anti-FLAG Antibody	Sigma Aldrich (Merck)	F1804
Anti-GAPDH Antibody	Thermo Scientific	MA5-15738
Anti-Mouse Antibody	Thermo Scientific	32430
AzF	Sigma Aldrich (Merck)	909564
BocK	Fluorochem	078520
BSA	Fisher Scientific	11493823
CCCP	Fisher Scientific	10175140
Cell Titre Blue	Promega	G8081
Clarity MAX™	Biorad	1705062
Confocal dishes	Mattek	P35G1510C
DMEM GlutaMAX™	Gibco	11574516
DMSO	Fisher Scientific	10103483
FBS	Fisher Scientific	11573397
HEK293	ECACC	85120602

HeLa	ATCC	CCL-2
Hoechst	Invitrogen	H3569
Lipofectamine	Life Technologies	10696343
MitoTracker	Invitrogen	M7514
Mr Frosty™	Thermo Scientific	5100-0001
Nitrocellulose Membrane 0.2 µm	Biorad	1704156
Novex™ WedgeWell™	Invitrogen	XP04205BOX
NuPAGE™ LDS Buffer	Invitrogen	NP0007
OMeY	Alfa Aesar	H63096
OptiMEM	Gibco	11058021
Protease Inhibitor	Sigma Aldrich (Merck)	P8340
RIPA Buffer	Sigma Aldrich (Merck)	R0278
RPMI	Gibco	11835030
Skimmed Milk Powder	Sigma Aldrich (Merck)	70166-500G
Trypsin	Fisher Scientific	11560626
Tween 20	Fisher Scientific	10301783
T25 Flask	Corning	430639
T75 Flask	Corning	430641U
24 well plates	Corning	10380932
96 well plate black	Corning	10357891

6.2 Bacteria culture: buffers and mediums

6.2.1 Luria-Burtani (LB) liquid medium

Per 1 L of LB liquid medium prepared, tryptone (10.0 g), yeast extract (5.0 g) and NaCl (10.0 g) were dissolved in 800 mL deionised water (dH_2O) before the volume was made up to 1 L with dH_2O. The solution was autoclaved for sterilisation and stored at room temperature.

6.2.2 Luria-Burtani (LB) solid medium

Per 1 L of solid LB medium, tryptone (10.0 g), yeast extract (5.0 g), NaCl (10.0 g) and agar powder (15 g) were dissolved in 800 mL deionised water (dH2O) before the volume was made up to 1 L with dH_2O. The solution was autoclaved for sterilisation and stored at room temperature.

6.2.3 Sterile antibiotic stock solutions

1000x antibiotic stock solution were made by dissolving ampicillin in dH_2O at 100 mg/mL, or kanamycin in dH_2O at 50 mg/mL. All antibiotic stocks were filter sterilised under an open flame, aliquoted into sterile 1.5 mL Eppendorf tubes and stored at -20 ºC.

6.2.4 Competent cell preparation buffer 1 (B1)

200 mL of B1 buffer was prepared by dissolving 0.589 g KOAc, 1.259 g $MnCl_2$, 1.49g KCl and 0.222 g $CaCl_2$ in 100 mL dH_2O and pH adjusted accordingly to 5.8. 30 mL (15% v/v) glycerol was then added and total volume made up to 200 mL with dH_2O. Total buffer working concentration was 30 mM KOAc, 50 mM $MnCl_2$, 100 mM KCl and 10 mM $CaCl_2$. Buffer was filter sterilised under an open flame into sterile falcon tubes and stored at -20 ºC.

6.2.5 Competent cell preparation buffer 2 (B2)

200 mL of B2 buffer was prepared by dissolving 0.418 g MOPS, 1.66 g $CaCl_2$ and 0.149 g KCl in 100 mL dH_2O and pH adjusted accordingly to 7.0. 30 mL (15% v/v) glycerol was then added and total volume made up to 200 mL with dH_2O. Total buffer working concentration was 10 mM MOPS, 75 mM $CaCl_2$ and 10 mM KCl. Buffer was filter sterilised under an open flame into sterile falcon tubes and stored at 4 ºC.

6.3 Molecular cloning

6.3.1 Preparation of chemically competent Stbl3 cell stocks

Chemically competent Stbl3 stocks were generated from One Shot™ Stbl3™ *E. coli* cells obtained from ThermoFisher. A bacterial stab was spread on a sterile LB agar plate and incubated at 37 ºC for 16 hours. A bacterial starter culture was generated by isolating a single colony from the plate and suspending it in 5 mL LB media in a sterile falcon tube. The starter culture was incubated at 37 ºC for 16 hours overnight with constant shaking at 180 RPM. 200 mL of sterile LB in a conical flask was induced with 1 mL of the starter culture and incubated at 37 ºC with constant shaking until the culture reached an OD within the range of 0.6 – 0.7. The flask was then removed from the incubator and chilled to 4 ºC for 30 minutes to suspend the cell growth phase. Culture was split into 50 mL falcon tubes and centrifuged at 1000 g for 30 minutes at constant temperature of 4 ºC. supernatant was removed under an open flame and pellets were re-suspended in 30 mL of buffer B1 and incubated at 4 ºC for 1 hour. Cultures were then centrifuged again at 1000 g for 30 minutes at constant temperature of 4 ºC. Supernatant was then removed and pellets re-suspended in 5 mL of buffer B2. Under an open flame, the 5-mL suspension was split into sterile Eppendorf 1.5 mL tubes as 50 µL aliquots, snap frozen in liquid nitrogen and stored at -80 ºC until required.

6.3.2 Transformation of chemically competent Stbl3 cells

The following procedure accounts for the propagation of a single plasmid, where “plasmid DNA” denotes a previously purified plasmid, or a new clone generated via PCR, T4 Ligation or Gibson Assembly respectively (see section ***6.3.4***, ***6.3.7*** or ***6.3.8*** for the appropriate cloning protocols). A single 50 µL aliquot of Stbl3 was thawed on ice. An appropriate volume of plasmid DNA was added and gently mixed into the aliquot (volume added allowing for 10 – 20 ng total plasmid DNA) and incubated on ice for 30 minutes. The suspension was heat-shocked in a pre-heated water bath at 42 ºC for 45 seconds prior to

chilling on ice for 2 minutes. Under an open flame using sterile technique, 1 mL LB liquid media was added to the aliquot and gently mixed to achieve an even suspension. The culture was then recovered, where it is incubated at 37 ºC for 1 hour at constant shaking at 400 g. After recovery, the sample was centrifuged at 20,000 g for 2 minutes to form a pellet, and under an open flame 900 µL of supernatant removed and the pellet re-suspended in the remaining supernatant (approximately 100 µL). Continuing under an open flame, 50 µL of the suspension was plated on a pre-prepared agar plate containing a 1x antibiotic concentration (derived from the respective 1000x stock solution) corresponding to the plasmid DNA's antibiotic resistance gene. The suspension was evenly spread across the plate and allowed to dry for approximately 5 minutes under sterile conditions, before incubation in an oven set to 37 ºC for 16 hours to permit growth of bacterial colonies.

6.3.3 Plasmid DNA purification via spin column extraction

A bacterial starter culture was generated by isolating a single colony from a plate (as described in section **6.3.2**) and suspending it in 5 mL LB media in a sterile falcon tube. The starter culture was incubated at 37 ºC for 16 hours overnight with constant shaking. The resulting culture was centrifuged at 1000 g for 20 minutes at 4 ºC to form a bacterial pellet. Following the manufacturers protocol, the supernatant was removed and pellet re-suspended in 250 µL of buffer P1. 250 µL buffer P2 was subsequently added and the mixture shaken to obtain a coherent blue and viscous solution. 350 µL of buffer N3 was then added and shaken to neutralise any blue colouring and obtain a distinctive white precipitate. The contents were transferred to a 1.5 mL Eppendorf tube and centrifuged at 20,000 g for 20 minutes to facilitate debris pelleting. Supernatant was carefully aspirated and added to a QIAGEN miniprep spin column. Resulting supernatant was run through the column via centrifugation at 20,000 g for 1 minute and flow-through in the collection tube discarded. The column was washed with 500 µL PB buffer, centrifuged for 1 minute at 20,000 g and flow-through discarded, washed with 750 µL PE buffer by centrifuging for 1 minute at 20,000 g and flow-through discarded. The collection column was removed and placed in a 1.5 mL Eppendorf tube and 50 µL EB buffer

added. The column was incubated with EB buffer for 2 minutes at room temperature before centrifuging for 1 minute at 20,000 g. Column was subsequently discarded and plasmid DNA concentration measured with a Nano-drop before storage at -20 ºC.

6.3.4 DNA amplification via polymerase chain reaction (PCR)

All PCR reactions were performed using PrimeSTAR HS DNA polymerase following the manufacturers protocol. DNA fragments were generated using the ***general*** 3-step protocol, however if this was unsuccessful a ***ramp-up*** 3-step protocol was used (**Figure 6.1**).

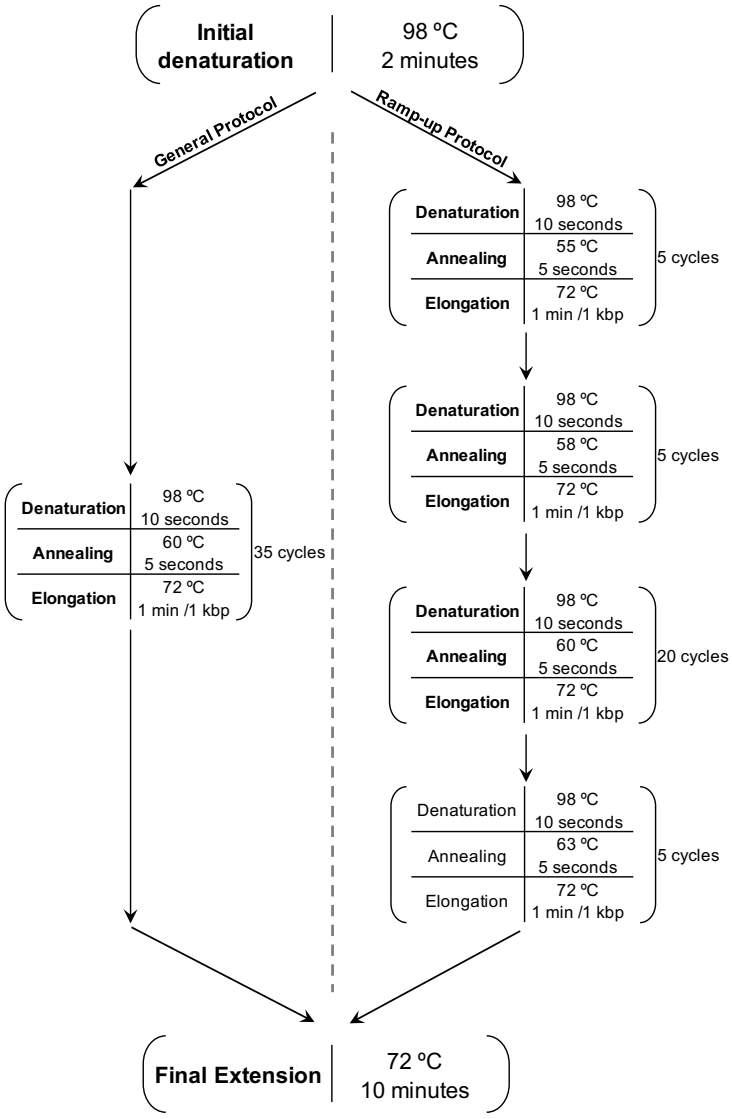

Figure 6.1: General and Ramp-up protocols undertaken for PCR amplification

6.3.5 DNA purification via TAE agarose electrophoresis

DNA fragment purification was used to isolate fragments generated by PCR or restriction enzyme digestion (see sections ***6.3.4*** and ***6.3.6*** respectively for the appropriate protocols). A 1 L 50x stock of TAE buffer was prepared by mixing 242 g Tris-base, 57.1 mL glacial acetic acid and 10 mL 0.5 mM EDTA solution (pH 8.0) into dH_2O. 1 L working stock of 1x TAE buffer was made by diluting 20 mL 50x TAE into 980 mL dH_2O. Agarose gels were made by suspending 1 g agarose powder in 100 mL 1x TAE buffer and heated to boiling using a microwave). 5 µL SYBR Safe dye was then added and mixed to obtain an even to suspension prior to pouring the solution into a gel casting tray and left at RT for 30 minutes to set. Gels were submerged in 1x TAE buffer in a gel tank and Gene ruler 1kb plus DNA ladder was loaded to one well as a reference marker. FastDigest Green loading dye buffer (10x) was added to DNA samples (1 µL/10 µL) and they were loaded to the appropriate wells. Gel was run at constant voltage of 120 V for 35 minutes to obtain clear DNA fragment separation, then imaged using a Chemi-Doc gel imager. Bands of interest were cut from the gel using a scalpel knife and transferred to a 1.5 mL Eppendorf tube and weighed. The gel slices were dissolved in QG buffer (20 mM Tris-HCl, 5.5 M guanidine thiocyanate, pH 6.6) (300 µL QG per 100 µg gel) and incubated at 50 ºC for 10 minutes to dissolve gel. The solution was transferred to a Qiagen miniprep spin column, and centrifuged for 1 minute at 20,000 g. Flow through was discarded, and the column washed with 750 µL PE buffer by centrifugation at 20,000 g for 1 minute. The column was transferred to a new 1.5 mL Eppendorf tube and 50 µL EB buffer was added before centrifuging at 20,000 g for 1 minute to elute DNA into the Eppendorf. DNA concentrations were then measured via nanodrop and stored at -20 ºC.

6.3.6 DNA digestion via restriction enzyme reaction

Restriction enzyme digestions were performed following the manufacturers protocol. Reaction mixtures consisted of 1000 ng DNA, 1 µL 10x FastDigest Green Buffer, FastDigest restriction enzymes (total volume 1 µL) and dH_2O to achieve a total volume of 10 µL. Where a TAP reaction is required to prevent blunt ends re-ligating during T4 ligation (see section ***6.3.7*** for T4 ligation

protocol), 1 µL alkaline phosphatase is added to the reaction mixture. Reactions were incubated at 37 ºC for 1 hour to achieve complete digestion and ran on an agarose gel for fragment separation and purification (see section ***6.3.5*** for agarose electrophoresis).

6.3.7 DNA fragment T4 ligation

T4 ligation was performed following the manufacturers protocol. DNA fragments required for T4 ligation were added to a PCR tube at a 3:1 vector to insert ratio. 2 µL T4 Ligase buffer was added along with 1 µL T4 Ligase. Reaction was made up to 20 µL with dH_2O and incubated at RT for 20 minutes. Reaction mixture was then directly transformed into chemically competent Stbl3 cells (see section ***6.3.2***).

6.3.8 DNA fragment Gibson assembly

Gibson assembly was performed with NEB HiFi DNA assembly master mix following the manufacturers protocol. DNA fragments were mixed to a total volume of 5 µL at a 3:1 vector to insert ratio. 5 µL NEB HiFi DNA assembly master mix was added and mixed thoroughly, before incubation at 50 ºC for 1 hour. The resulting reaction mixture could then be directly transformed into chemically competent Stbl3 cells (see section ***6.3.2***).

6.4 Mammalian cell culture

6.4.1 Buffers and growth mediums

All cell lines were continuously maintained in Dulbecco's modified eagle medium (DMEM) supplemented with 10% v/v foetal bovine serum (FBS).

6.4.2 Cell-line start-up

A 1 mL aliquot of frozen cell stocks was part thawed at 37 ºC for 3 minutes until a small ice cube remained. The aliquot was then mixed with 4 mL of growth medium (DMEM 10% v/v FBS) in a 15-mL falcon tube prior to centrifugation at 400 g for 5 minutes to facilitate cell pellet formation. Supernatant was then discarded from the pellet and cell pellet gently re-suspended in fresh 5 mL growth medium. The cell suspension was then transferred to a T25 flask and cultured at 37 ºC, 5% CO_2 atmosphere for 48 hours. Media was changed as necessary every 48-72 hours until the cells formed a uniform monolayer at a confluency of 80-85%. Once at this confluency, cells lines were maintained and passaged (as detailed in section ***6.4.3***).

6.4.3 Maintenance and passage

All cell lines were maintained in DMEM (10% v/v FBS) and passaged when a monolayer confluency of 80-85% is established. For cell passage, media is removed from the flask and cells gently washed with PBS to remove any residual media and dead cells. PBS wash was then removed, and 1 mL trypsin added to the flask and incubated at 37 ºC, 5% CO_2 atmosphere for 3-5 minutes to allow cells to detach from the flask surface. Once detached, 1 mL of DMEM (10% FBS) was added to the flask to deactivate the trypsin, and the solution gently pipetted to obtain an even suspension. The suspension was centrifuged at 400 g for 5 minutes in a 15-mL falcon tube to form a cell pellet. The resulting supernatant was removed gently from the falcon tube to ensure the cell pellet

was not disturbed, and the pellet re-suspended in 1 mL fresh DMEM (10% FBS). Of the 1 mL cellular suspension, 200 µL was taken and added to a new T25 cell culture flask and suspended in 4.8 mL fresh DMEM (10% FBS) to obtain a 1/5 dilution. The new T25 flask culture was subsequently incubated at 37 ºC, 5% CO_2 atmosphere and the passage procedure repeated as required whenever the culture reached a confluency of 80-85%.

6.4.4 Generating frozen cell stocks

For frozen stock generation, the passage protocol detailed in ***6.4.3*** was undertaken but cells are instead transferred into a T75 cell culture flask (total volume 10 mL DMEM (10% FBS)). The relevant cell line was grown in the T75 flask until a confluency of 90-95% is established, and during this growth period the media was exchanged as required to maintain cell health. Once at the target confluency, media was removed and cells washed with PBS to remove any residual media and cell debris. 2 mL of trypsin was then added and the flask incubated at 37 ºC, 5% CO_2 atmosphere for 3-5 minutes to allow cells to detach from the flask surface. Once detached, 2 mL of DMEM (10% FBS) was added to the flask to deactivate the trypsin, and the solution gently pipetted to obtain an even cell suspension. The resulting suspension was transferred to a 15-mL falcon tube and centrifuged at 400 g for 5 minutes to facilitate cell pellet formation. The supernatant was removed gently from the falcon tube to ensure the cell pellet is not disturbed, and the pellet evenly re-suspended in 5 mL of FBS (10% v/v DMSO). The subsequent 5-mL solution was then quickly split into five cryogenic tubes to generate five 1 mL aliquots. The samples were then transferred into a specialised cooling container (Mr Frosty™, ThermoFisher, #10110051) before storage in a -80 ºC freezer. The container facilitates gradual temperature reduction of 1 ºC per minute, ensuring cell stock preservation. After 48 hours, the aliquots were removed from the container and stored in a -80 ºC freezer until required.

CHAPTER 7:
Appendix

7.1 Gene sequences

Table A1: Table of gene sequences used throughout Chapter 3

Gene Name	DNA sequence 5' to 3'
Ampicillin resistance	ATGAGTATTCAACATTTCCGTGTCGCCCTTATTCCCTTTTT TGCGGCATTTTGCCTTCCTGTTTTTGCTCACCCAGAAACG CTGGTGAAAGTAAAAGATGCTGAAGATCAGTTGGGTGCAC GAGTGGGTTACATCGAACTGGATCTCAACAGCGGTAAGAT CCTTGAGAGTTTTCGCCCCGAAGAACGTTTTCCAATGATG AGCACTTTTAAAGTTCTGCTATGTGGCGCGGTATTATCCC GTATTGACGCCGGGCAAGAGCAACTCGGTCGCCGCATAC ACTATTCTCAGAATGACTTGGTTGAGTACTCACCAGTCACA GAAAAGCATCTTACGGATGGCATGACAGTAAGAGAATTAT GCAGTGCTGCCATAACCATGAGTGATAACACTGCGGCCAA CTTACTTCTGACAACGATCGGAGGACCGAAGGAGCTAACC GCTTTTTTGCACAACATGGGGGATCATGTAACTCGCCTTG ATCGTTGGGAACCGGAGCTGAATGAAGCCATACCAAACG ACGAGCGTGACACCACGATGCCTGTAGCAATGGCAACAA CGTTGCGCAAACTATTAACTGGCGAACTACTTACTCTAGC TTCCCGGCAACAATTAATAGACTGGATGGAGGCGGATAAA GTTGCAGGACCACTTCTGCGCTCGGCCCTTCCGGCTGGC TGGTTTATTGCTGATAAATCTGGAGCCGGTGAGCGTGGGT CTCGCGGTATCATTGCAGCACTGGGGCCAGATGGTAAGC CCTCCCGTATCGTAGTTATCTACACGACGGGGAGTCAGG CAACTATGGATGAACGAAATAGACAGATCGCTGAGATAGG TGCCTCACTGATTAAGCATTGGTAA
CAG	GACATTGATTATTGACTAGTTATTAATAGTAATCAATTACG GGGTCATTAGTTCATAGCCCATATATGGAGTTCCGCGTTA CATAACTTACGGTAAATGGCCCGCCTGGCTGACCGCCCA ACGACCCCCGCCCATTGACGTCAATAATGACGTATGTTCC CATAGTAACGCCAATAGGGACTTTCCATTGACGTCAATGG GTGGAgTATTTACGGTAAACTGCCCACTTGGCAGTACATC AAGTGTATCATATGCCAAGTACGCCCCCTATTGACGTCAA TGACGGTAAATGGCCCGCCTGGCATTATGCCCAGTACATG ACCTTATGGGACTTTCCTACTTGGCAGTACATCTACGTATT AGTCATCGCTATTACCATGGTCGAGGTGAGCCCCACGTTC TGCTTCACTCTCCCCATCTCCCCCCCCCTCCCCACCCCCAA TTTTGTATTTATTTATTTTTTAATTATTTTGTGCAGCGATGG GGGCGGGGGGGGGGGGGGGCGCGCGCCAGGCGGGGCG GGGCGGGGCGAGGGGCGGGGCGGGGCGAGGCGGAGAG GTGCGGCGGCAGCCAATCAGAGCGGCGCGCTCCGAAAG TTTCCTTTTATGGCGAGGCGGCGGCGGCGGCGGCCCTAT AAAAAGCGAAGCGCGCGGCGGGCGGGAGTCGCTGCGTT GCCTTCGCCCCGTGCCCCGCTCCGCGCCGCCTCGCGCC GCCCGCCCCGGCTCTGACTGACCGCGTTACTCCCACAGG TGAGCGGGCGGGACGGCCCTTCTCCTCCGGGCTGTAATT AGCGCTTGGTTTAATGACGGCTCGTTTCTTTTCTGTGGCT GCGTGAAAGCCTTAAAGGGCTCCGGGAGGGCCCTTTGTG CGGGGGGGAGCGGCTCGGGGGGTGCGTGCGTGTGTGTG

	TGCGTGGGGAGCGCCGCGTGCGGCCCGCGCTGCCCGGC GGCTGTGAGCGCTGCGGGCGCGGCGCGGGGCTTTGTGC GCTCCGCGTGTGCGCGAGGGGAGCGCGGCCGGGGGCG GTGCCCCGCGGTGCGGGGGGGCTGCGAGGGGAACAAAG GCTGCGTGCGGGGTGTGTGCGTGGGGGGGTGAGCAGGG GGTGTGGGCGCGGCGGTCGGGCTGTAACCCCCCCCTGC ACCCCCCTCCCCGAGTTGCTGAGCACGGCCCGGCTTCGG GTGCGGGGCTCCGTACGGGGCGTGGCGCGGGGCTCGCC GTGCCGGGCGGGGGGTGGCGGCAGGTGGGGGTGCCGG GCGGGGCGGGGCCGCCTCGGGCCGGGGAGGGCTCGGG GGAGGGGCGCGGCGGCCCCCGGAGCGCCGGCGGCTGT CGAGGCGCGGCGAGCCGCAGCCATTGCCTTTTATGGTAA TCGTGCGAGAGGGCGCAGGGACTTCCTTTGTCCCAAATC TGTGCGGAGCCGAAATCTGGGAGGCGCCGCCGCACCCC CTCTAGCGGGCGCGGGGCGAAGCGGTGCGGCGCCGGCA GGAAGGAAATGGGCGGGGAGGGCCTTCGTGCGTCGCCG CGCCGCCGTCCCCTTCTCCCTCTCCAGCCTCGGGGCTGT CCGCGGGGGGACGGCTGCCTTCGGGGGGGACGGGGCA GGGCGGGGTTCGGCTTCTGGCGTGTGACCGGCGGCTCT AGAGCCTCTGCTAACCATGTTCATGCCTTCTTCTTTTTCCT ACAG
EF1	GGGCAGAGCGCACATCGCCCACAGTCCCCGAGAAGTTGG GGGGAGGGGTCGGCAATTGAACGGGTGCCTAGAGAAGG TGGCGCGGGGTAAACTGGGAAAGTGATGTCGTGTACTGG CTCCGCCTTTTTCCCGAGGGTGGGGGAGAACCGTATATAA GTGCAGTAGTCGCCGTGAACGTTCTTTTTCGCAACGGGTT TGCCGCCAGAACACAG
eGFP	ATGGTGAGCAAGGGCGAGGAGCTGTTCACCGGGGTGGT GCCCATCCTGGTCGAGCTGGACGGCGACGTAAACGGCCA CAAGTTCAGCGTGTCCGGCGAGGGCGAGGGCGATGCCA CCTACGGCAAGCTGACCCTGAAGTTCATCTGCACCACCG GCAAGCTGCCCGTGCCCTGGCCCACCCTCGTGACCACCC TGACCTACGGCGTGCAGTGCTTCAGCCGCTACCCCGACC ACATGAAGCAGCACGACTTCTTCAAGTCCGCCATGCCCGA AGGCTACGTCCAGGAGCGCACCATCTTCTTCAAGGACGA CGGCAACTACAAGACCCGCGCCGAGGTGAAGTTCGAGGG CGACACCCTGGTGAACCGCATCGAGCTGAAGGGCATCGA CTTCAAGGAGGACGGCAACATCCTGGGGCACAAGCTGGA GTACAACTACAACAGCCACAACGTCTATATCATGGCCGAC AAGCAGAAGAACGGCATCAAGGTGAACTTCAAGATCCGC CACAACATCGAGGACGGCAGCGTGCAGCTCGCCGACCAC TACCAGCAGAACACCCCCATCGGCGACGGCCCCGTGCTG CTGCCCGACAACCACTACCTGAGCACCCAGTCCGCCCTG AGCAAAGACCCCAACGAGAAGCGCGATCACATGGTCCTG CTGGAGTTCGTGACCGCCGCCGGGATCACTCTCGGCATG GACGAGCTGTACAAGTAA
eGFP(TAG)	ATGGTGAGCAAGGGCGAGGAGCTGTTCACCGGGGTGGT GCCCATCCTGGTCGAGCTGGACGGCGACGTAAACGGCCA CAAGTTCAGCGTGTCCGGCGAGGGCGAGGGCGATGCCA CCTACGGCAAGCTGACCCTGAAGTTCATCTGCACCACCG GCAAGCTGCCCGTGCCCTGGCCCACCCTCGTGACCACCC TGACCTACGGCGTGCAGTGCTTCAGCCGCTACCCCGACC

	ACATGAAGCAGCACGACTTCTTCAAGTCCGCCATGCCCGA AGGCTACGTCCAGGAGCGCACCATCTTCTTCAAGGACGA CGGCAACTACAAGACCCGCGCCGAGGTGAAGTTCGAGGG CGACACCCTGGTGAACCGCATCGAGCTGAAGGGCATCGA CTTCAAGGAGGACGGCAACATCCTGGGGCACAAGCTGGA GTACAACTACAACAGCCAC**TAG**GTCTATATCATGGCCGAC AAGCAGAAGAACGGCATCAAGGTGAACTTCAAGATCCGC CACAACATCGAGGACGGCAGCGTGCAGCTCGCCGACCAC TACCAGCAGAACACCCCCATCGGCGACGGCCCCGTGCTG CTGCCCGACAACCACTACCTGAGCACCCAGTCCGCCCTG AGCAAAGACCCCAACGAGAAGCGCGATCACATGGTCCTG CTGGAGTTCGTGACCGCCGCCGGGATCACTCTCGGCATG GACGAGCTGTACAAGTAA
eGFP(TAGA)	ATGGTGAGCAAGGGCGAGGAGCTGTTCACCGGGGTGGT GCCCATCCTGGTCGAGCTGGACGGCGACGTAAACGGCCA CAAGTTCAGCGTGTCCGGCGAGGGCGAGGGCGATGCCA CCTACGGCAAGCTGACCCTGAAGTTCATCTGCACCACCG GCAAGCTGCCCGTGCCCTGGCCCACCCTCGTGACCACCC TGACCTACGGCGTGCAGTGCTTCAGCCGCTACCCCGACC ACATGAAGCAGCACGACTTCTTCAAGTCCGCCATGCCCGA AGGCTACGTCCAGGAGCGCACCATCTTCTTCAAGGACGA CGGCAACTACAAGACCCGCGCCGAGGTGAAGTTCGAGGG CGACACCCTGGTGAACCGCATCGAGCTGAAGGGCATCGA CTTCAAGGAGGACGGCAACATCCTGGGGCACAAGCTGGA GTACAACTACAACAGCCAC**TAGA**GTCTATATCATGGC**T**GA **T**AAGCAGAAGAACGGCATCAAGGTGAACTTCAAGATCCGC CACAACATCGAGGACGGCAGCGTGCAGCTCGCCGACCAC TACCAGCAGAACACCCCCATCGGCGACGGCCCCGTGCTG CTGCCCGACAACCACTACCTGAGCACCCAGTCCGCCCTG AGCAAAGACCCCAACGAGAAGCGCGATCACATGGTCCTG CTGGAGTTCGTGACCGCCGCCGGGATCACTCTCGGCATG GACGAGCTGTACAAGTAA
eGFP(TAGC)	ATGGTGAGCAAGGGCGAGGAGCTGTTCACCGGGGTGGT GCCCATCCTGGTCGAGCTGGACGGCGACGTAAACGGCCA CAAGTTCAGCGTGTCCGGCGAGGGCGAGGGCGATGCCA CCTACGGCAAGCTGACCCTGAAGTTCATCTGCACCACCG GCAAGCTGCCCGTGCCCTGGCCCACCCTCGTGACCACCC TGACCTACGGCGTGCAGTGCTTCAGCCGCTACCCCGACC ACATGAAGCAGCACGACTTCTTCAAGTCCGCCATGCCCGA AGGCTACGTCCAGGAGCGCACCATCTTCTTCAAGGACGA CGGCAACTACAAGACCCGCGCCGAGGTGAAGTTCGAGGG CGACACCCTGGTGAACCGCATCGAGCTGAAGGGCATCGA CTTCAAGGAGGACGGCAACATCCTGGGGCACAAGCTGGA GTACAACTACAACAGCCAC**TAGC**GTCTATATCATGGC**T**GA **T**AAGCAGAAGAACGGCATCAAGGTGAACTTCAAGATCCGC CACAACATCGAGGACGGCAGCGTGCAGCTCGCCGACCAC TACCAGCAGAACACCCCCATCGGCGACGGCCCCGTGCTG CTGCCCGACAACCACTACCTGAGCACCCAGTCCGCCCTG AGCAAAGACCCCAACGAGAAGCGCGATCACATGGTCCTG CTGGAGTTCGTGACCGCCGCCGGGATCACTCTCGGCATG GACGAGCTGTACAAGTAA

eGFP(TAGG)	ATGGTGAGCAAGGGCGAGGAGCTGTTCACCGGGGTGGT GCCCATCCTGGTCGAGCTGGACGGCGACGTAAACGGCCA CAAGTTCAGCGTGTCCGGCGAGGGCGAGGGCGATGCCA CCTACGGCAAGCTGACCCTGAAGTTCATCTGCACCACCG GCAAGCTGCCCGTGCCCTGGCCCACCCTCGTGACCACCC TGACCTACGGCGTGCAGTGCTTCAGCCGCTACCCCGACC ACATGAAGCAGCACGACTTCTTCAAGTCCGCCATGCCCGA AGGCTACGTCCAGGAGCGCACCATCTTCTTCAAGGACGA CGGCAACTACAAGACCCGCGCCGAGGTGAAGTTCGAGGG CGACACCCTGGTGAACCGCATCGAGCTGAAGGGCATCGA CTTCAAGGAGGACGGCAACATCCTGGGGCACAAGCTGGA GTACAACTACAACAGCCAC**TAGG**GTCTATATCATGGC**T**GA **T**AAGCAGAAGAACGGCATCAAGGTGAACTTCAAGATCCGC CACAACATCGAGGACGGCAGCGTGCAGCTCGCCGACCAC TACCAGCAGAACACCCCCATCGGCGACGGCCCCGTGCTG CTGCCCGACAACCACTACCTGAGCACCCAGTCCGCCCTG AGCAAAGACCCCAACGAGAAGCGCGATCACATGGTCCTG CTGGAGTTCGTGACCGCCGCCGGGATCACTCTCGGCATG GACGAGCTGTACAAGTAA
eGFP(TAGT)	ATGGTGAGCAAGGGCGAGGAGCTGTTCACCGGGGTGGT GCCCATCCTGGTCGAGCTGGACGGCGACGTAAACGGCCA CAAGTTCAGCGTGTCCGGCGAGGGCGAGGGCGATGCCA CCTACGGCAAGCTGACCCTGAAGTTCATCTGCACCACCG GCAAGCTGCCCGTGCCCTGGCCCACCCTCGTGACCACCC TGACCTACGGCGTGCAGTGCTTCAGCCGCTACCCCGACC ACATGAAGCAGCACGACTTCTTCAAGTCCGCCATGCCCGA AGGCTACGTCCAGGAGCGCACCATCTTCTTCAAGGACGA CGGCAACTACAAGACCCGCGCCGAGGTGAAGTTCGAGGG CGACACCCTGGTGAACCGCATCGAGCTGAAGGGCATCGA CTTCAAGGAGGACGGCAACATCCTGGGGCACAAGCTGGA GTACAACTACAACAGCCAC**TAGT**GTCTATATCATGGC**T**GA **T**AAGCAGAAGAACGGCATCAAGGTGAACTTCAAGATCCGC CACAACATCGAGGACGGCAGCGTGCAGCTCGCCGACCAC TACCAGCAGAACACCCCCATCGGCGACGGCCCCGTGCTG CTGCCCGACAACCACTACCTGAGCACCCAGTCCGCCCTG AGCAAAGACCCCAACGAGAAGCGCGATCACATGGTCCTG CTGGAGTTCGTGACCGCCGCCGGGATCACTCTCGGCATG GACGAGCTGTACAAGTAA
eGFP(CTAG)	ATGGTGAGCAAGGGCGAGGAGCTGTTCACCGGGGTGGT GCCCATCCTGGTCGAGCTGGACGGCGACGTAAACGGCCA CAAGTTCAGCGTGTCCGGCGAGGGCGAGGGCGATGCCA CCTACGGCAAGCTGACCCTGAAGTTCATCTGCACCACCG GCAAGCTGCCCGTGCCCTGGCCCACCCTCGTGACCACCC TGACCTACGGCGTGCAGTGCTTCAGCCGCTACCCCGACC ACATGAAGCAGCACGACTTCTTCAAGTCCGCCATGCCCGA AGGCTACGTCCAGGAGCGCACCATCTTCTTCAAGGACGA CGGCAACTACAAGACCCGCGCCGAGGTGAAGTTCGAGGG CGACACCCTGGTGAACCGCATCGAGCTGAAGGGCATCGA CTTCAAGGAGGACGGCAACATCCTGGGGCACAAGCTGGA GTACAACTACAACAGCCAC**CTAG**GTCTATATCATGGC**T**GA **T**AAGCAGAAGAACGGCATCAAGGTGAACTTCAAGATCCGC CACAACATCGAGGACGGCAGCGTGCAGCTCGCCGACCAC

	TACCAGCAGAACACCCCCATCGGCGACGGCCCCGTGCTG CTGCCCGACAACCACTACCTGAGCACCCAGTCCGCCCTG AGCAAAGACCCCAACGAGAAGCGCGATCACATGGTCCTG CTGGAGTTCGTGACCGCCGCCGGGATCACTCTCGGCATG GACGAGCTGTACAAGTAA
eGFP(AGGA)	ATGGTGAGCAAGGGCGAGGAGCTGTTCACCGGGGTGGT GCCCATCCTGGTCGAGCTGGACGGCGACGTAAACGGCCA CAAGTTCAGCGTGTCCGGCGAGGGCGAGGGCGATGCCA CCTACGGCAAGCTGACCCTGAAGTTCATCTGCACCACCG GCAAGCTGCCCGTGCCCTGGCCCACCCTCGTGACCACCC TGACCTACGGCGTGCAGTGCTTCAGCCGCTACCCCGACC ACATGAAGCAGCACGACTTCTTCAAGTCCGCCATGCCCGA AGGCTACGTCCAGGAGCGCACCATCTTCTTCAAGGACGA CGGCAACTACAAGACCCGCGCCGAGGTGAAGTTCGAGGG CGACACCCTGGTGAACCGCATCGAGCTGAAGGGCATCGA CTTCAAGGAGGACGGCAACATCCTGGGGCACAAGCTGGA GTACAACTACAACAGCCAC**AGGA**GTCTATATCATGGC**T**GA **T**AAGCAGAAGAACGGCATCAAGGTGAACTTCAAGATCCGC CACAACATCGAGGACGGCAGCGTGCAGCTCGCCGACCAC TACCAGCAGAACACCCCCATCGGCGACGGCCCCGTGCTG CTGCCCGACAACCACTACCTGAGCACCCAGTCCGCCCTG AGCAAAGACCCCAACGAGAAGCGCGATCACATGGTCCTG CTGGAGTTCGTGACCGCCGCCGGGATCACTCTCGGCATG GACGAGCTGTACAAGTAA
eGFP(TAG-AGGA)	ATGGTGAGCAAGGGCGAGGAGCTGTTCACCGGGGTGGT GCCCATCCTGGTCGAGCTGGACGGCGACGTAAACGGCCA CAAGTTCAGCGTGTCCGGCGAGGGCGAGGGCGATGCCA CC**TAG**GGCAAGCTGACCCTGAAGTTCATCTGCACCACCG GCAAGCTGCCCGTGCCCTGGCCCACCCTCGTGACCACCC TGACCTACGGCGTGCAGTGCTTCAGCCGCTACCCCGACC ACATGAAGCAGCACGACTTCTTCAAGTCCGCCATGCCCGA AGGCTACGTCCAGGAGCGCACCATCTTCTTCAAGGACGA CGGCAACTACAAGACCCGCGCCGAGGTGAAGTTCGAGGG CGACACCCTGGTGAACCGCATCGAGCTGAAGGGCATCGA CTTCAAGGAGGACGGCAACATCCTGGGGCACAAGCTGGA GTACAACTACAACAGCCAC**AGGA**GTCTATATCATGGC**T**GA **T**AAGCAGAAGAACGGCATCAAGGTGAACTTCAAGATCCGC CACAACATCGAGGACGGCAGCGTGCAGCTCGCCGACCAC TACCAGCAGAACACCCCCATCGGCGACGGCCCCGTGCTG CTGCCCGACAACCACTACCTGAGCACCCAGTCCGCCCTG AGCAAAGACCCCAACGAGAAGCGCGATCACATGGTCCTG CTGGAGTTCGTGACCGCCGCCGGGATCACTCTCGGCATG GACGAGCTGTACAAGCATCATCACCATCACCACTAA
ERF1(E55D)	GCCGATGATCCAAGCGCCGCAGACCGCAATGTTGAGATC TGGAAGATAAAAAAGCTGATAAAGAGCTTGGAGGCCGCAC GGGGCAACGGCACGTCCATGATATCCCTCATTATCCCACC AAAGGATCAGATCAGCCGTGTGGCGAAGATGTTGGCGGA TGA**T**TTCGGAACGGCCAGTAACATTAAAAGTCGCGTGAAC CGGCTGTCGGTCTTGGGCGCCATCACTTCCGTGCAGCAA CGTCTGAAACTGTACAACAAAGTCCCACCCAACGGTTTGG TCGTCTACTGCGGTACGATAGTTACCGAGGAAGGAAAGG AGAAGAAAGTGAATATTGATTTCGAACCATTTAAACCGATA

	AACACTAGCTTGTACTTGTGCGACAATAAGTTTCATACAGA GGCACTCACGGCCCTGCTGAGCGACGACTCGAAATTCGG ATTCATTGTCATTGATGGAAGTGGAGCGCTGTTCGGCACG CTGCAGGGTAACACGCGCGAGGTCTTGCACAAATTCACC GTGGACTTGCCCAAAAAGCATGGCCGTGGTGGCCAGAGC GCCCTCAGGTTTGCGCGGCTGCGCATGGAGAAGCGCCAT AACTACGTGCGCAAGGTCGCAGAGACGGCTGTGCAGCTG TTCATCTCGGGTGATAAGGTAAATGTCGCGGGACTGGTGC TCGCCGGCAGCGCGGACTTCAAAACCGAGCTGAGTCAGT CCGACATGTTCGATCAGCGTCTGCAGTCGAAGGTACTGAA GCTCGTCGACATTAGCTACGGCGGCGAGAACGGCTTCAA TCAGGCCATCGAACTGAGTACCGAAGTCCTCAGTAACGTA AAGTTTATTCAGGAAAAAAAGTTGATTGGACGCTACTTTGA TGAAATAAGCCAAGATACGGGCAAATACTGTTTTGGCGTC GAGGATACTCTGAAAGCGCTCGAGATGGGAGCAGTGGAA ATACTCATCGTATATGAAAATCTCGATATAATGCGCTATGT ACTGCATTGCCAAGGAACAGAAGAGGAGAAAATTCTCTAC CTCACCCCGGAGCAAGAGAAGGACAAGAGCCATTTTACA GACAAGGAGACGGGCCAAGAGCACGAGCTCATTGAGTCG ATGCCCTTGCTCGAATGGTTTGCCAACAACTACAAGAAGT TCGGCGCGACCCTGGAAATTGTCACGGATAAATCGCAGG AGGGCAGCCAGTTTGTGAAGGGCTTCGGTGGCATCGGCG GCATCCTCCGCTACCGGGTGGATTTCCAAGGCATGGAATA TCAAGGTGGAGATGATGAATTCTTCGATTTGGATGATTACT AATGATAG
Kanamycin resistance	ATGATTGAACAGGATGGCCTGCATGCGGGTAGCCCGGCA GCGTGGGTGGAACGTCTGTTTGGCTATGATTGGGCGCAG CAGACCATTGGCTGCTCTGATGCGGCGGTGTTTCGTCTGA GCGCGCAGGGTCGTCCGGTGCTGTTTGTGAAAACCGATC TGAGCGGTGCGCTGAACGAGCTGCAGGATGAAGCGGCG CGTCTGAGCTGGCTGGCCACCACCGGTGTTCCGTGTGCG GCGGTGCTGGATGTGGTGACCGAAGCGGGCCGTGATTG GCTGCTGCTGGGCGAAGTGCCGGGTCAGGATCTGCTGTC TAGCCATCTGGCGCCGGCAGAAAAAGTGAGCATTATGGC GGATGCCATGCGTCGTCTGCATACCCTGGACCCGGCGAC CTGTCCGTTTGATCATCAGGCGAAACATCGTATTGAACGT GCGCGTACCCGTATGGAAGCGGGCCTGGTGGATCAGGAT GATCTGGATGAAGAACATCAGGGCCTGGCACCGGCAGAG CTGTTTGCGCGTCTGAAAGCGAGCATGCCGGATGGCGAA GATCTGGTGGTGACCCATGGTGATGCGTGCCTGCCGAAC ATTATGGTGGAAAATGGCCGTTTTAGCGGCTTTATTGATTG CGGCCGTCTGGGCGTGGCGGATCGTTATCAGGATATTGC GCTGGCCACCCGTGATATTGCGGAAGAACTGGGCGGCGA ATGGGCGGATCGTTTTCTGGTGCTGTATGGCATTGCGGCA CCGGATAGCCAGCGTATTGCGTTTTATCGTCTGCTGGATG AATTTTTCTAATAA
Pyl $tRNA_{ACUA}$	GGAAACCTGATCATGTAGATCGAATGGACT**ACTA**AATCCG TTCAGCCGGGTTAGATTCCCGGGGTTTCCG
Pyl $tRNA_{CCUA}$	GGAAACCTGATCATGTAGATCGAATGGACT**CCTA**AATCCG TTCAGCCGGGTTAGATTCCCGGGGTTTCCG

Pyl $tRNA_{GCUA}$	GGAAACCTGATCATGTAGATCGAATGGACTGCTAAATCCG TTCAGCCGGGTTAGATTCCCGGGGTTTCCG
Pyl $tRNA_{UCUA}$	GGAAACCTGATCATGTAGATCGAATGGACTTCTAAATCCG TTCAGCCGGGTTAGATTCCCGGGGTTTCCG
Pyl $tRNA_{UCUA(Ev1)}$	GGAAACCTGATCATGTAGATCGAATGGGCTTCTAATCCTG TTCAGCCGGGTTAGATTCCCGGGGTTTCCG
Pyl $tRNA_{UCUA(Ev2)}$	GGAAACCTGATCATGTAGATCGAATGGGCTTCTAATCTCG TTCAGCCGGGTTAGATTCCCGGGGTTTCCG
Pyl $tRNA_{CUAG}$	GGAAACCTGATCATGTAGATCGAATGGACTCTAGAATCCG TTCAGCCGGGTTAGATTCCCGGGGTTTCCG
Pyl $tRNA_{CUAG(Ev1)}$	GGAAACCTGATCATGTAGATCGAATGGCCTCTAGAATCCG TTCAGCCGGGTTAGATTCCCGGGGTTTCCG
Pyl $tRNA_{UCCU}$	GGAAACCTGATCATGTAGATCGAATGGACTTCCTAATCCG TTCAGCCGGGTTAGATTCCCGGGGTTTCCG
Pyl $tRNA_{UCCU(Ev1)}$	GGAAACCTGATCATGTAGATCGAATCCTCTTCCTAATAGG TTCAGCCGGGTTAGATTCCCGGGGTTTCCG
Pyl $tRNA_{UCCU(Ev2)}$	GGAAACCTGATCATGTAGATCGAAGGGGCTTCCTATCCGC TTCAGCCGGGTTAGATTCCCGGGGTTTCCG
mCherry-P2A-sGFP(1-10)	ATGGTGAGCAAGGGCGAGGAGGATAACATGGCCATCATC AAGGAGTTCATGCGCTTCAAGGTGCACATGGAGGGCTCC GTGAACGGCCACGAGTTCGAGATCGAGGGCGAGGGCGA GGGCCGCCCCTACGAGGGCACCCAGACCGCCAAGCTGA AGGTGACCAAGGGTGGCCCCCTGCCCTTCGCCTGGGACA TCCTGTCCCCTCAGTTCATGTACGGCTCCAAGGCCTACGT GAAGCACCCCGCCGACATCCCCGACTACTTGAAGCTGTC CTTCCCCGAGGGCTTCAAGTGGGAGCGCGTGATGAACTT CGAGGACGGCGGCGTGGTGACCGTGACCCAGGACTCCT CCCTGCAGGACGGCGAGTTCATCTACAAGGTGAAGCTGC GCGGCACCAACTTCCCCTCCGACGGCCCCGTAATGCAGA AGAAGACCATGGGCTGGGAGGCCTCCTCCGAGCGGATGT ACCCCGAGGACGGCGCCCTGAAGGGCGAGATCAAGCAG AGGCTGAAGCTGAAGGACGGCGGCCACTACGACGCTGAG GTCAAGACCACCTACAAGGCCAAGAAGCCCGTGCAGCTG CCCGGCGCCTACAACGTCAACATCAAGTTGGACATCACCT CCCACAACGAGGACTACACCATCGTGGAACAGTACGAAC GCGCCGAGGGCCGCCACTCCACCGGCGGCATGGACGAG CTGTACGCGTCTGGAGGCGCCACCAATTTCAGCCTGCTG AAACAGGCTGGCGACGTGGAAGAGAACCCTGGACCTGGA CAAAAGTCGATGTCCAAAGGAGAAGAACTGTTTACCGGTG TTGTGCCAATTTTGGTTGAACTCGATGGTGATGTCAACGG ACATAAGTTCTCAGTGAGAGGCGAAGGAGAAGGTGACGC CACCATTGGAAAATTGACTCTTAAATTCATCTGTACTACTG GTAAACTTCCTGTACCATGGCCGACTCTCGTAACAACGCT TACGTACGGAGTTCAGTGCTTTTCGAGATACCCAGACCAT

	ATGAAAAGACATGACTTTTTTAAGTCGGCTATGCCTGAAG GTTACGTGCAAGAAAGAACAATTTCGTTCAAAGATGATGG AAAATATAAAACTAGAGCAGTTGTTAAATTTGAAGGAGATA CTTTGGTTAACCGCATTGAACTGAAAGGAACAGATTTTAAA GAAGATGGTAATATTCTTGGACACAAACTCGAATACAATTT TAATAGTCATAACGTATACATCACTGCTGATAAGCAAAAGA ACGGAATTAAAGCGAATTTCACAGTACGCCATAATGTAGA AGATGGCAGTGTTCAACTTGCCGACCATTACCAACAAAAC ACCCCTATTGGAGACGGTCCGGTACTTCTTCCTGATAATC ACTACCTCTCAACACAAACAGTCCTGAGCAAAGATCCAAA TGAAAAATGA
mCherry-P2A-TAG-sGFP(1-10)	ATGGTGAGCAAGGGCGAGGAGGATAACATGGCCATCATC AAGGAGTTCATGCGCTTCAAGGTGCACATGGAGGGCTCC GTGAACGGCCACGAGTTCGAGATCGAGGGCGAGGGCGA GGGCCGCCCCTACGAGGGCACCCAGACCGCCAAGCTGA AGGTGACCAAGGGTGGCCCCCTGCCCTTCGCCTGGGACA TCCTGTCCCCTCAGTTCATGTACGGCTCCAAGGCCTACGT GAAGCACCCCGCCGACATCCCCGACTACTTGAAGCTGTC CTTCCCCGAGGGCTTCAAGTGGGAGCGCGTGATGAACTT CGAGGACGGCGGCGTGGTGACCGTGACCCAGGACTCCT CCCTGCAGGACGGCGAGTTCATCTACAAGGTGAAGCTGC GCGGCACCAACTTCCCCTCCGACGGCCCCGTAATGCAGA AGAAGACCATGGGCTGGGAGGCCTCCTCCGAGCGGATGT ACCCCGAGGACGGCGCCCTGAAGGGCGAGATCAAGCAG AGGCTGAAGCTGAAGGACGGCGGCCACTACGACGCTGAG GTCAAGACCACCTACAAGGCCAAGAAGCCCGTGCAGCTG CCCGGCGCCTACAACGTCAACATCAAGTTGGACATCACCT CCCACAACGAGGACTACACCATCGTGGAACAGTACGAAC GCGCCGAGGGCCGCCACTCCACCGGCGGCATGGACGAG CTGTACGCGTCTGGAGGCGCCACCAATTTCAGCCTGCTG AAACAGGCTGGCGACGTGGAAGAGAACCCTGGACCTGGA CAAAAGTCG**TAG**TCCAAAGGAGAAGAACTGTTTACCGGTG TTGTGCCAATTTTGGTTGAACTCGATGGTGATGTCAACGG ACATAAGTTCTCAGTGAGAGGCGAAGGAGAAGGTGACGC CACCATTGGAAAATTGACTCTTAAATTCATCTGTACTACTG GTAAACTTCCTGTACCATGGCCGACTCTCGTAACAACGCT TACGTACGGAGTTCAGTGCTTTTCGAGATACCCAGACCAT ATGAAAAGACATGACTTTTTTAAGTCGGCTATGCCTGAAG GTTACGTGCAAGAAAGAACAATTTCGTTCAAAGATGATGG AAAATATAAAACTAGAGCAGTTGTTAAATTTGAAGGAGATA CTTTGGTTAACCGCATTGAACTGAAAGGAACAGATTTTAAA GAAGATGGTAATATTCTTGGACACAAACTCGAATACAATTT TAATAGTCATAACGTATACATCACTGCTGATAAGCAAAAGA ACGGAATTAAAGCGAATTTCACAGTACGCCATAATGTAGA AGATGGCAGTGTTCAACTTGCCGACCATTACCAACAAAAC ACCCCTATTGGAGACGGTCCGGTACTTCTTCCTGATAATC ACTACCTCTCAACACAAACAGTCCTGAGCAAAGATCCAAA TGAAAAATGA
mCherry-P2A-sGFP(11)	ATGGTGAGCAAGGGCGAGGAGGATAACATGGCCATCATC AAGGAGTTCATGCGCTTCAAGGTGCACATGGAGGGCTCC GTGAACGGCCACGAGTTCGAGATCGAGGGCGAGGGCGA GGGCCGCCCCTACGAGGGCACCCAGACCGCCAAGCTGA AGGTGACCAAGGGTGGCCCCCTGCCCTTCGCCTGGGACA

	TCCTGTCCCCTCAGTTCATGTACGGCTCCAAGGCCTACGT GAAGCACCCCGCCGACATCCCCGACTACTTGAAGCTGTC CTTCCCCGAGGGCTTCAAGTGGGAGCGCGTGATGAACTT CGAGGACGGCGGCGTGGTGACCGTGACCCAGGACTCCT CCCTGCAGGACGGCGAGTTCATCTACAAGGTGAAGCTGC GCGGCACCAACTTCCCCTCCGACGGCCCCGTAATGCAGA AGAAGACCATGGGCTGGGAGGCCTCCTCCGAGCGGATGT ACCCCGAGGACGGCGCCCTGAAGGGCGAGATCAAGCAG AGGCTGAAGCTGAAGGACGGCGGCCACTACGACGCTGAG GTCAAGACCACCTACAAGGCCAAGAAGCCCGTGCAGCTG CCCGGCGCCTACAACGTCAACATCAAGTTGGACATCACCT CCCACAACGAGGACTACACCATCGTGGAACAGTACGAAC GCGCCGAGGGCCGCCACTCCACCGGCGGCATGGACGAG CTGTACGCGTCTGGAGGCGCCACCAATTTCAGCCTGCTG AAACAGGCTGGCGACGTGGAAGAGAACCCTGGACCTGGA CAAAAGTCGATGCGTGACCACATGGTCCTTCATGAGTATG TAAATGCTGCTGGGATTACAGGTGGCTCTGGAGGTAGAG ATCATATGGTTCTCCACGAATACGTTAACGCCGCAGGCAT CACTGGCGGTAGTGGAGGACGCGACCATATGGTACTACA TGAATATGTCAATGCAGCCGGAATAACCGGAGGGTCCGG AGGCCGGGATCACATGGTGCTGCATGAGTATGTGAACGC GGCGGGTATAACTGGTGGGTCGGGCGGACGAGACCATAT GGTGCTTCACGAATACGTAAACGCAGCTGGCATTACTGGC GGATCAGGTGGCAGGGATCACATGGTACTCCATGAGTAC GTGAACGCTGCTGGAATCACAGGCGGTAGCGGCGGTCG GGACCATATGGTCCTGCACGAATATGTCAATGCTGCCGGT ATCACCGGCGGCAAATTCATGTGA
mCherry-P2A-AGGA-sGFP(11)	ATGGTGAGCAAGGGCGAGGAGGATAACATGGCCATCATC AAGGAGTTCATGCGCTTCAAGGTGCACATGGAGGGCTCC GTGAACGGCCACGAGTTCGAGATCGAGGGCGAGGGCGA GGGCCGCCCCTACGAGGGCACCCAGACCGCCAAGCTGA AGGTGACCAAGGGTGGCCCCCTGCCCTTCGCCTGGGACA TCCTGTCCCCTCAGTTCATGTACGGCTCCAAGGCCTACGT GAAGCACCCCGCCGACATCCCCGACTACTTGAAGCTGTC CTTCCCCGAGGGCTTCAAGTGGGAGCGCGTGATGAACTT CGAGGACGGCGGCGTGGTGACCGTGACCCAGGACTCCT CCCTGCAGGACGGCGAGTTCATCTACAAGGTGAAGCTGC GCGGCACCAACTTCCCCTCCGACGGCCCCGTAATGCAGA AGAAGACCATGGGCTGGGAGGCCTCCTCCGAGCGGATGT ACCCCGAGGACGGCGCCCTGAAGGGCGAGATCAAGCAG AGGCTGAAGCTGAAGGACGGCGGCCACTACGACGCTGAG GTCAAGACCACCTACAAGGCCAAGAAGCCCGTGCAGCTG CCCGGCGCCTACAACGTCAACATCAAGTTGGACATCACCT CCCACAACGAGGACTACACCATCGTGGAACAGTACGAAC GCGCCGAGGGCCGCCACTCCACCGGCGGCATGGACGAG CTGTACGCGTCTGGAGGCGCCACCAATTTCAGCCTGCTG AAACAGGCTGGCGACGTGGAAGAGAACCCTGGACCTGGA CAAAAGTCG**AGGA**CGTGACCACATGGTCCTTCATGAGTAT GTAAATGCTGCTGGGATTACAGGTGGCTCTGGAGGTAGA GATCATATGGTTCTCCACGAATACGTTAACGCCGCAGGCA TCACTGGCGGTAGTGGAGGACGCGACCATATGGTACTAC ATGAATATGTCAATGCAGCCGGAATAACCGGAGGGTCCG GAGGCCGGGATCACATGGTGCTGCATGAGTATGTGAACG CGGCGGGTATAACTGGTGGGTCGGGCGGACGAGACCATA

	TGGTGCTTCACGAATACGTAAACGCAGCTGGCATTACTGG CGGATCAGGTGGCAGGGATCACATGGTACTCCATGAGTA CGTGAACGCTGCTGGAATCACAGGCGGTAGCGGCGGTCG GGACCATATGGTCCTGCACGAATATGTCAATGCTGCCGGT ATCACCGGCGGCAAATTCATGTGA
Pyl tRNA$_{UCCU(Ev2)}$ x4	GAGGGCCTATTTCCCATGATTCCTTCATATTTGCATATACG ATACAAGGCTGTTAGAGAGATAATTAGAATTAATTTGACTG TAAACACAAAGATATTAGTACAAAATACGTGACGTAGAAAG TAATAATTTCTTGGGTAGTTTGCAGTTTTAAAATTATGTTTT AAAATGGACTATCATATGCTTACCGTAACTTGAAAGTATTT CGATTTCTTGGCTTTATATATCTTGTGGAAAGGACGAAACA CCGGAAACCTGATCATGTAGATCGAAGGGGCT**TCCT**ATCC GCTTCAGCCGGGTTAGATTCCCGGGGTTTCCGGACAAGT GCGGTTTTTCTTAAGAGGTTGGGCAGGAAGAGGGCCTATT TCCCATGATTCCTTCATATTTGCATATACGATACAAGGCTG TTAGAGAGATAATTAGAATTAATTTGACTGTAAACACAAAG ATATTAGTACAAAATACGTGACGTAGAAAGTAATAATTTCT TGGGTAGTTTGCAGTTTTAAAATTATGTTTTAAAATGGACT ATCATATGCTTACCGTAACTTGAAAGTATTTCGATTTCTTG GCTTTATATATCTTGTGGAAAGGACGAAACACCGGAAACC TGATCATGTAGATCGAAGGGGCT**TCCT**ATCCGCTTCAGCC GGGTTAGATTCCCGGGGTTTCCGGACAAGTGCGGTTTTTC TTAAGAGGctggtggagaacttgccgaaTTGGGCAGGAAGAGGGC CTATTTCCCATGATTCCTTCATATTTGCATATACGATACAA GGCTGTTAGAGAGATAATTAGAATTAATTTGACTGTAAACA CAAAGATATTAGTACAAAATACGTGACGTAGAAAGTAATAA TTTCTTGGGTAGTTTGCAGTTTTAAAATTATGTTTTAAAATG GACTATCATATGCTTACCGTAACTTGAAAGTATTTCGATTT CTTGGCTTTATATATCTTGTGGAAAGGACGAAACACCGGA AACCTGATCATGTAGATCGAAGGGGCT**TCCT**ATCCGCTTC AGCCGGGTTAGATTCCCGGGGTTTCCGGACAAGTGCGGT TTTTCTTAAGAGGGTAAACGGCCACAAGTTCGTCGATTGG GCAGGAAGAGGGCCTATTTCCCATGATTCCTTCATATTTG CATATACGATACAAGGCTGTTAGAGAGATAATTAGAATTAA TTTGACTGTAAACACAAAGATATTAGTACAAAATACGTGAC GTAGAAAGTAATAATTTCTTGGGTAGTTTGCAGTTTTAAAA TTATGTTTTAAAATGGACTATCATATGCTTACCGTAACTTG AAAGTATTTCGATTTCTTGGCTTTATATATCTTGTGGAAAG GACGAAACACCGGAAACCTGATCATGTAGATCGAAGGGG CT**TCCT**ATCCGCTTCAGCCGGGTTAGATTCCCGGGGTTTC CG
PylRS	GACAAGAAGCCCCTGAACACCCTGATCAGCGCCACAGGA CTGTGGATGTCCAGAACCGGCACCATCCACAAGATCAAG CACCACGAGGTGTCCCGGTCCAAAATCTACATCGAGATG GCCTGCGGCGATCACCTGGTCGTCAACAACAGCAGAAGC AGCCGGACAGCCAGAGCCCTGCGGCACCACAAGTACAGA AAGACCTGCAAGCGGTGCAGAGTGTCCGACGAGGACCTG AACAAGTTCCTGACCAAGGCCAACGAGGACCAGACCAGC GTGAAAGTGAAGGTGGTGTCCGCCCCCACCCGGACCAAG AAAGCCATGCCCAAGAGCGTGGCCAGAGCCCCCAAGCCC CTGGAAAACACCGAAGCCGCTCAGGCCCAGCCCAGCGGC AGCAAGTTCAGCCCCGCCATCCCCGTGTCTACCCAGGAA AGCGTCAGCGTCCCCGCCAGCGTGTCCACCAGCATCTCT

	AGCATCTCAACCGGCGCCACAGCTTCTGCCCTGGTCAAG GGCAACACCAACCCCATCACCAGCATGTCTGCCCCTGTG CAAGCCTCTGCCCCAGCCCTGACCAAGTCCCAGACCGAC CGGCTGGAAGTGCTCCTGAACCCCAAGGACGAGATCAGC CTGAACAGCGGCAAGCCCTTCCGGGAGCTGGAAAGCGAG CTGCTGAGCCGGCGGAAGAAGGACCTCCAGCAAATCTAC GCCGAGGAACGGGAGAACTACCTGGGCAAGCTGGAAAGA GAGATCACCCGGTTCTTCGTGGACCGGGGCTTCCTGGAA ATCAAGAGCCCCATCCTGATCCCCCTGGAGTACATCGAGC GGATGGGCATCGACAACGACACCGAGCTGAGCAAGCAGA TTTTCCGGGTGGACAAGAACTTCTGCCTGCGGCCCATGCT GGCCCCCAACCTGTACAACTACCTGCGGAAACTGGATCG CGCTCTGCCCGACCCCATCAAGATTTTCGAGATCGGCCC CTGCTACCGGAAAGAGAGCGACGGCAAAGAGCACCTGGA AGAGTTTACAATGCTGAACTTTTGCCAGATGGGCAGCGGC TGCACCAGAGAGAACCTGGAATCCATCATCACCGACTTTC TGAACCACCTGGGGATCGACTTCAAGATCGTGGGCGACA GCTGCATGGTGTACGGCGACACCCTGGACGTGATGCACG GCGACCTGGAACTGTCTAGCGCCGTCGTGGGACCCATCC CTCTGGACCGGGAGTGGGGCATCGATAAGCCCTGGATCG GAGCCGGCTTCGGCCTGGAACGGCTGCTGAAAGTCAAGC ACGACTTTAAGAACATCAAGCGGGCTGCCAGAAGCGAGA GCTACTACAACGGCATCAGCACCAACCTGTGA
sGFP(1-10)-P2A-TAG-sGFP(11)	ATGTCCAAAGGAGAAGAACTGTTTACCGGTGTTGTGCCAA TTTTGGTTGAACTCGATGGTGATGTCAACGGACATAAGTT CTCAGTGAGAGGCGAAGGAGAAGGTGACGCCACCATTGG AAAATTGACTCTTAAATTCATCTGTACTACTGGTAAACTTC CTGTACCATGGCCGACTCTCGTAACAACGCTTACGTACGG AGTTCAGTGCTTTTCGAGATACCCAGACCATATGAAAAGA CATGACTTTTTTAAGTCGGCTATGCCTGAAGGTTACGTGC AAGAAAGAACAATTTCGTTCAAAGATGATGGAAAATATAAA ACTAGAGCAGTTGTTAAATTTGAAGGAGATACTTTGGTTAA CCGCATTGAACTGAAAGGAACAGATTTTAAAGAAGATGGT AATATTCTTGGACACAAACTCGAATACAATTTTAATAGTCA TAACGTATACATCACTGCTGATAAGCAAAAGAACGGAATTA AAGCGAATTTCACAGTACGCCATAATGTAGAAGATGGCAG TGTTCAACTTGCCGACCATTACCAACAAAACACCCCTATTG GAGACGGTCCGGTACTTCTTCCTGATAATCACTACCTCTC AACACAAACAGTCCTGAGCAAAGATCCAAATGAAAAAGCG TCTGGAGGCGCCACCAATTTCAGCCTGCTGAAACAGGCT GGCGACGTGGAAGAGAACCCTGGACCTGGACAAAAGTCG **TAG**CGTGACCACATGGTCCTTCATGAGTATGTAAATGCTG CTGGGATTACAGGTGGCTCTGGAGGTAGAGATCATATGGT TCTCCACGAATACGTTAACGCCGCAGGCATCACTGGCGG TAGTGGAGGACGCGACCATATGGTACTACATGAATATGTC AATGCAGCCGGAATAACCGGAGGGTCCGGAGGCCGGGA TCACATGGTGCTGCATGAGTATGTGAACGCGGCGGGTAT AACTGGTGGGTCGGGCGGACGAGACCATATGGTGCTTCA CGAATACGTAAACGCAGCTGGCATTACTGGCGGATCAGG TGGCAGGGATCACATGGTACTCCATGAGTACGTGAACGCT GCTGGAATCACAGGCGGTAGCGGCGGTCGGGACCATATG GTCCTGCACGAATATGTCAATGCTGCCGGTATCACCGGC GGCAAATTCATGTGA

Tyr $tRNA_{CUA}$	GGTGGGGTTCCCGAGCGGCCAAAGGGAGCAGACT**CTA**AA TCTGCCGTCACAGACTTCGAAGGTTCGAATCCTTCCCCCA CCA
Tyr $tRNA_{CUA}$ x4	GAGGGCCTATTTCCCATGATTCCTTCATATTTGCATATACG ATACAAGGCTGTTAGAGAGATAATTAGAATTAATTTGACTG TAAACACAAAGATATTAGTACAAAATACGTGACGTAGAAAG TAATAATTTCTTGGGTAGTTTGCAGTTTTAAAATTATGTTTT AAAATGGACTATCATATGCTTACCGTAACTTGAAAGTATTT CGATTTCTTGGCTTTATATATCTTGTGGAAAGGACGAAACA CCGGTGGGGTTCCCGAGCGGCCAAAGGGAGCAGACT**CT** **A**AATCTGCCGTCACAGACTTCGAAGGTTCGAATCCTTCCC CCACCATTTTTTAATATTTGCATGTAGGGGGCAGGAAGAG GGCCTATTTCCCATGATTCCTTCATATTTGCATATACGATA CAAGGCTGTTAGAGAGATAATTAGAATTAATTTGACTGTAA ACACAAAGATATTAGTACAAAATACGTGACGTAGAAAGTAA TAATTTCTTGGGTAGTTTGCAGTTTTAAAATTATGTTTTAAA ATGGACTATCATATGCTTACCGTAACTTGAAAGTATTTCGA TTTCTTGGCTTTATATATCTTGTGGAAAGGACGAAACACCG GTGGGGTTCCCGAGCGGCCAAAGGGAGCAGACT**CTA**AAT CTGCCGTCACAGACTTCGAAGGTTCGAATCCTTCCCCCAC CATTTTTTAATATTTGCATGTCTGGTGGAGAACTTGCCGAA TTGGGCAGGAAGAGGGCCTATTTCCCATGATTCCTTCATA TTTGCATATACGATACAAGGCTGTTAGAGAGATAATTAGAA TTAATTTGACTGTAAACACAAAGATATTAGTACAAAATACG TGACGTAGAAAGTAATAATTTCTTGGGTAGTTTGCAGTTTT AAAATTATGTTTTAAAATGGACTATCATATGCTTACCGTAA CTTGAAAGTATTTCGATTTCTTGGCTTTATATATCTTGTGG AAAGGACGAAACACCGGTGGGGTTCCCGAGCGGCCAAAG GGAGCAGACT**CTA**AATCTGCCGTCACAGACTTCGAAGGTT CGAATCCTTCCCCCACCATTTTTTAATATTTGCATGGTAAA CGGCCACAAGTTCGTCGATTGGGCAGGAAGAGGGCCTAT TTCCCATGATTCCTTCATATTTGCATATACGATACAAGGCT GTTAGAGAGATAATTAGAATTAATTTGACTGTAAACACAAA GATATTAGTACAAAATACGTGACGTAGAAAGTAATAATTTC TTGGGTAGTTTGCAGTTTTAAAATTATGTTTTAAAATGGAC TATCATATGCTTACCGTAACTTGAAAGTATTTCGATTTCTT GGCTTTATATATCTTGTGGAAAGGACGAAACACCGGTGGG GTTCCCGAGCGGCCAAAGGGAGCAGACT**CTA**AATCTGCC GTCACAGACTTCGAAGGTTCGAATCCTTCCCCCACCA
TyrRS*	GGCAAGCAGTAACTTGATTAAACAATTGCAAGAGCGGGG GCTGGTAGCCCAGGTGACGGACGAGGAAGCGTTAGCAGA GCGACTGGCGCAAGGCCCGATCGCACTC**GTG**TGTGGCTT CGATCCTACCGCTGACAGCTTGCATTTGGGGCATCTTGTT CCATTGTTATGCCTGAAACGCTTCCAGCAGGCGGGCCAC AAGCCGGTTGCGCTGGTAGGCGGCGCGACGGGTCTGATT GGCGACCCGAGCTTCAAAGCTGCCGAGCGTAAGCTGAAC ACCGAAGAAACTGTTCAGGAGTGGGTGGACAAAATCCGTA AGCAGGTTGCCCCGTTCCTCGATTTCGACTGTGGAGAAAA CTCTGCTATCGCGGCCAATAATTATGACTGGTTCGGCAAT ATGAATGTGCTGACCTTCCTGCGCGATATTGGCAAACACT TCTCCGTTAACCAGATGATCAACAAAGAAGCGGTTAAGCA GCGTCTCAACCGTGAAGATCAGGGGATTTCGTTCACTGAG

	TTTTCCTACAACCTGCTGCAGGGTTAT**AGTATG**GCCTGTT TGAACAAACAGTACGGTGTGGTGCTGCAAATTGGTGGTTC TGACCAGTGGGGTAACATCACTTCTGGTATCGACCTGACC CGTCGTCTGCATCAGAATCAGGTGTTTGGCCTGACCGTTC CGCTGATCACTAAAGCAGATGGCACCAAATTTGGTAAAAC TGAAGGCGGCGCAGTCTGGTTGGATCCGAAGAAAACCAG CCCGTACAAATTCTACCAGTTCTGGATCAACACTGCG**CGT** GCCGACGTTTACCGCTTCCTGAAGTTCTTCACCTTTATGA GCATTGAAGAGATCAACGCCCTGGAAGAAGAAGATAAAAA CAGCGGTAAAGCACCGCGCGCCCAGTATGTACTGGCGGA GCAGGTGACTCGTCTGGTTCACGGTGAAGAAGGTTTACA GGCGGCAAAACGTATTACCGAATGCCTGTTCAGCGGTTCT TTGAGTGCGCTGAGTGAAGCGGACTTCGAACAGCTGGCG CAGGACGGCGTACCGATGGTTGAGATGGAAAAGGGCGCA GACCTGATGCAGGCACTGGTCGATTCTGAACTGCAACCTT CCCGTGGTCAGGCACGTAAAACTATCGCCTCCAATGCCAT CACCATTAACGGTGAAAAACAGTCCGATCCTGAATACTTC TTTAAAGAAGAAGATCGTCTGTTTGGTCGTTTTACCTTACT GCGTCGCGGTAAAAAGAATTACTGTCTGATTTGCTGGAAA GGGCCCGTTTAA
U6	GAGGGCCTATTTCCCATGATTCCTTCATATTTGCATATACG ATACAAGGCTGTTAGAGAGATAATTAGAATTAATTTGACTG TAAACACAAAGATATTAGTACAAAATACGTGACGTAGAAAG TAATAATTTCTTGGGTAGTTTGCAGTTTTAAAATTATGTTTT AAAATGGACTATCATATGCTTACCGTAACTTGAAAGTATTT CGATTTCTTGGCTTTATATATCTTGTGGAAAGGAC

Mutations; *codons*; *anticodons*; *linkers*.